'CLICK' CHEMISTRY IN COORDINATION AND SUPRAMOLECULAR CHEMICAL APPLICATIONS

By Baljinder Singh Uppal

A Thesis Submitted in Partial Fulfilment of the Requirements

for the

Degree of Doctor of Philosophy

Department of Chemical and Biological Sciences

The University of Huddersfield

November 2012

AKNOWLEGEMENTS

First and foremost, I would like to thank Dr. Paul Elliott for giving me the opportunity to carry out this work, and his continued support and guidance throughout this project. I would also like to thank the University of Huddersfield for the funding of this doctorate and for the last eight years of my life here at Huddersfield, as an undergraduate student, and now a postgraduate. I have fond memories that I shall take with me wherever I go and whatever I do in the future.

I would also like to thank the following people within the Department of Chemical and Biological Sciences for their support and help with understanding specific aspects of my research; Professor Craig Rice for x-ray crystallography, Dr. Neil McLay for NMR and mass spectrometry, Somaia Kamouka and Paul Elliott for DFT calculations and Dr. Kate Wilson for help with the electrochemistry. I would also like to thank Professor Mike Ward at the University of Sheffield for allowing us use his instrumentation.

I also thank the entire office crew who made my time in Huddersfield so enjoyable. I will miss the fun we have had mostly at each other's expense!!

The biggest thank you of all goes to my parents Kulwant and Rashpal, for all their support they have provided both financially and emotionally since I started school. Without their support none of my recent achievements would have been possible.

Finally I would like to thank my wife Tanveer and the rest of my family and friends for their support over recent years.

ABSTRACT

The term “click chemistry” was first coined by Sharpless and co-workers in 2001 [1] and encompasses a range of high yielding organic coupling reactions which are rapid, highly selective and proceed with good functional group tolerance. Furthermore the reaction conditions are mild and require minimal workup and product purification. The most prominent example of these reactions is the copper catalysed alkyne/azide cycloaddition (CuAAC) for the formation of 1,4-disubstituted-1,2,3-triazoles. [2, 3] CuACC has been utilised in a variety of chemical disciplines including organic synthesis, the modification of biological macromolecules [4] and in polymer and materials chemistry. [5-7] More recently this reaction has shown a growing interest from the inorganic community for the design of new ligands for transition metal complexes [8-10] and their supramolecular assemblies.[11-13]

In this thesis, I present my results on the use of the 'click' chemistry in coordination and supramolecular chemical applications.

Described in chapter 3 is the synthesis of 1,4-disubstituted-1,2,3-triazole ligands which can act as either axial monodentate ligands, through the N3 atom of the triazole ring, or as bidentate N^N donor ligands if a pyridyl substituent is incorporated into a chelate ligand framework. The photophysical effects of these ligands were investigated on rhenium tricarbonyl complexes. It was found that replacing the Cl^- ligand by the triazole stabilises the energy of the HOMO with respect to the LUMO and results in a blue shift of the emission maximum whilst changing the bidentate ligand by replacing the bipyridyl ligand by pyridine-triazole ligand elevates the LUMO with respect to the HOMO again resulting in a blue shift in luminescence.

Described in chater 4 is the synthesis of 4-azido-2,2’-bipyridyl and 4,4’-diazido-2,2’-bipyridyl ligands and the CuAAC modification thereof. 4-azido-2,2’-bipyridyl was incorporated in to [Ru(*p*-cymene)(4-azido-2,2’-bipyridyl)Cl]$^+$ type complexes. The CuAAC reaction was utilised to chemically modify the periphery

of a metal complex when an azido substituted ligand is allowed to react with a range of alkynes. Through this approach a second metal binding domain can easily be introduced upon reaction with 2-pyridyl acetylene. [Ru(*p*-cymene)(4-azido-2,2'-bipyridyl)Cl]$^{+}$ and "click" chemistry can be used as a potential tool in building metallo-supramolecular species. We have therefore made some of the first steps towards the goal of the development of a general "click" chemistry-based methodology for the construction of functional supramolecular architectures *via* azide-functionalised transition metal complexes.

Desciribed in chapter 5 is the preperation of 1,2,3-triazole bridged luminescent redox switches. Ruthenium, iridium and rhenium complexes incorporating ferrocenyl-bipyridyl ligand in which the ferrocene unit is tethered to the bipyridyl through a 1,2,3-triazole linkage were prepared. We have developed two potential luminescent switches with ferrocene tagged bipyridyl ligands containing a CuAAC derived triazole linker. The ferrocene moiety quenches the Ru/Ir based luminescent emission, presumably by electron transfer across the triazole bridge. We have demonstrated that the luminescent emission can be switched on by oxidation of the Fc moiety to Fc^{+}.

Described in chapter 6 is the synthesis and characterisation of a range of ligands, incorporating the 1,2,3-triazole moiety, which have designed to act as bridging ligands for the construction of supramolecular assemblies. We have subsequently prepared two dinuclear ruthenium and iridium complexes of the 4-pyridyl-1-(2,2'-bipyrid-4-yl)-1,2,3-triazole bridging ligand, and carried photophysical studies. We have shown that the dinuclear species exhibit greater luminescent intensities than mono-nuclear model complexes because the metal centre coordinated to the pyridine-triazole domain acts as a sensitizer for the metal centre coordinated to the bipyridyl domain through a photoinduced energy transfer mechanism. This shows that there is efficient transfer across the bridging ligand.

TABLE OF CONTENTS

LIST OF FIGURES

LIST OF TABLES

LIST OF SCHEMES

ABREVIATIONS

°	Degrees
δ	Delta (chemical shift)
Å	Angstrom
aq	Aqueous
bpy	2,2'-bipyridyl
btz	4,4-bi-1,2,3-triazol-4-yl
btzpy	2,6-bis(1,2,3-triazol-4-yl)pyridine
°C	Degrees celcius
$CDCl_3$	Dueterated chloroform
^{13}C NMR	Carbon-13 nuclear magnetic resonance
CH_3CN	Acetonitrile
cm^{-1}	Wavenumbers
COSY	Correlation Spectroscopy
Cp	Cyclopentadienyl
CuAAC	Copper catalysed azide alkyne cycloaddition
2D	2-dimensional
DCM	Dichloromethane
dfptz	4-(2,4-difluorophenyl)-1,2,3-triazole
DFT	Density functional theory
DMF	Dimethyl formamide
DMSO	Dimethyl sulfoxide

DSSC	Dye sensitized solar cell
EDTA	Ethylenediaminotetraacetic acid
ESI-MS	Electrospray ionization mass spectrometry
eV	Electronvolt
F_2ppy	2-(2,4-difluorophenyl)pyridine
FT-IR	Fourier transform infra-red
g	Grams
^{1}H NMR	Proton nuclear magnetic resonance
HOMO	Highest occupied molecular orbital
HPLC	High performance liquid chromatography
HRMS	High resolution mass spectrometry
Hz	Hertz
J	Coupling Constant
K	Kelvin
Kcal mol^{-1}	Kilocalories per molecule
LC	Ligand centred
LEEC	Light emitting electrochemical cell
LUMO	Lowest unoccupied molecular orbital
M	Molarity/Molar
mCPBA	*meta*-chloroperbenzoic acid
mg	Milligram
mmol	Millimole
MC	Metal centred

mins	Minutes
mL	Millilitre
MLCT	Metal-to-ligand charge transfer
^{1}MLCT	Singlet metal-to-ligand charge transfer
^{3}MLCT	Triplet metal-to-ligand charge transfer
MLLCT	Metal-to-ligand-to-ligand charge transfer
m/z	mass/charge
NHC	N-heterocyclic carbene
nm	Nanometer
NOESY	Nuclear Overhauser effect spectroscopy
nOe	Nuclear Overhauser effect
ns	Nanosecond
OLED	Organic light emitting diode
PLED	Polymer light emitting diode
ppm	Parts per million
ppy	2-phenylpyridine
py	Pyridine
pytz	2-(1,2,3-triazol-4-yl)pyridine
RuACC	Ruthenium catalysed azide alkyne cycloaddition
S_0	Singlet ground state
SOMO	Singly occupied molecular orbital
T_1	Lowest triplet excited state
TBTA	Tris-(benzyltriazolymethyl)amine

THF	Tetrahydrofuran
TMS	Trimethylsilyl
tpy	2,2’:6’,2’’-terpyridine
UV-vis	Ultraviolet-visible
V	Volts

1 INTRODUCTION

1.1 Introduction

The synthesis and preparation of photo- and redox-active transition metal complexes and their supramolecular architectures has become an area of intense interest. The strong interest in this area stems from the potential application of these materials for the modelling of energy transfer processes in biological photosynthesis, the development of new light harvesting photocatalysts and novel materials for solar energy conversion. Therefore reactions that enable the facile routes to modular construction of new ligands and these architectures are particularly useful in the development of such materials.

A series of such candidate coupling reactions exist and fall under the umbrella term of 'click' chemistry. [1, 3] The predominant reaction within this category is the copper catalysed azide-alkyne cycloaddition (CuAAC) reaction to form 1,2,3-triazoles.

Here, the general principles of 'click' chemistry are introduced with a focus on CuAAC and its applications in transition metal coordination chemistry.

1.2 Click Chemistry

The term "click chemistry" was first coined by Professor K. Barry Sharpless and co-workers in 2001 [1] who defined a set of stringent criteria which must be adhered to for a reaction to be considered a "click" reaction. The reaction must be efficient and high yielding, modular and wide in scope, generate few or no side products and where the derived product can easily be isolated, ideally without the use of chromatographic techniques.

Furthermore Sharpless *et al.* also discussed the criteria with regards to reaction conditions for an ideal "click" reaction; the reaction must be simple and insensitive to both oxygen and water, the starting materials must be readily available or accessible and the reaction should be carried out with no solvent or a solvent that is benign or easily removed. The product should also be stable under physiological conditions (as much of the early work focused on potential for biologically active molecules).

Therefore it can be said that the term "click" chemistry can be used to define any chemical process that is simple and efficient. Furthermore we can say that the idea of "click" chemistry is not a new type of chemistry, but it is a concept, which groups a variety of reactions which can create a wide range of complex molecules in a very efficient manner.

Although the criteria for "click" reactions are quite specific, there are a number of reactions which have been identified as good "click" reactions. These include nucleophilic substitution reactions, particularly ring opening reactions of strained

heterocyclic electrophiles such as epoxides, aziridines, aziridinium ions etc., carbonyl chemistry of the "non-aldol" type such as formation of ureas, aromatic heterocycles, oxime ethers etc., additions to carbon-carbon multiple bonds, such as epoxidation, dihydroxylation etc., Michael additions of Nu-H reactants and finally cycloaddition reactions such as 1,3-dipolar cycloaddition reactions and Diels-Alder transformations (Figure 1.1).

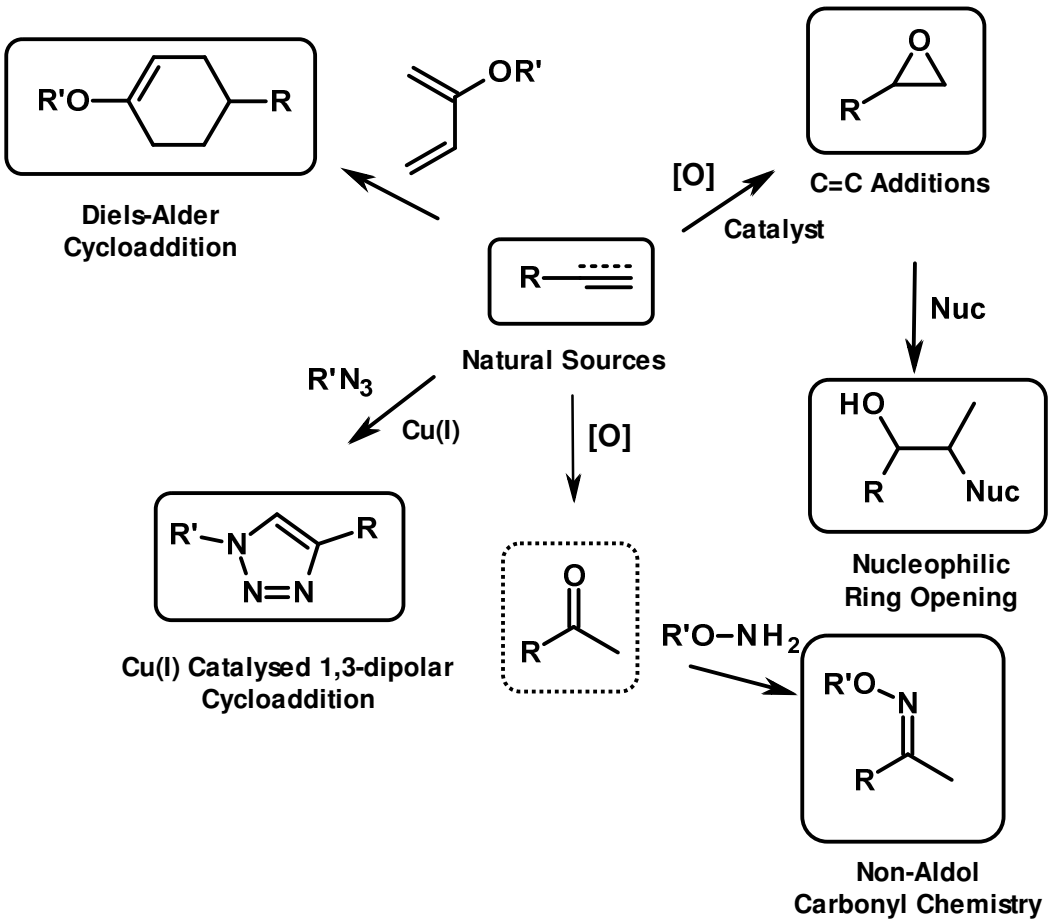

Figure 1.1 A selection of reactions which match the "click chemistry" criteria.

1.2.1 Copper catalysed azide-alkyne cycloaddition (CuAAC)

The most widely known and utilised 'click' reaction is the copper catalysed azide-alkyne cycloaddition (CuAAC) for the synthesis of 1,2,3-triazoles which occurs by the 1,3-dipolar cycloaddition of organic azides to terminal alkynes. The thermally induced [3+2] cycloaddition between alkynes and organic azides was discovered in 1893 [14] and the reaction was studied extensively in the 1960's [15, 16] by Huisgen and co-workers. This 1,2,3-triazole formation was traditionally an uncatalysed reaction which results in the formation of the two regioisomeric, 1,4- and 1,5-disubstituted-1,2,3-triazole products (Figure 1.2). The 1,4- and the 1,5-disubstituted isomers are formed in approximately a 1:1 molar ratio and furthermore when it was originally reported the experimental conditions did not satisfy the criteria of a click reaction as it required long reaction times and elevated temperatures.

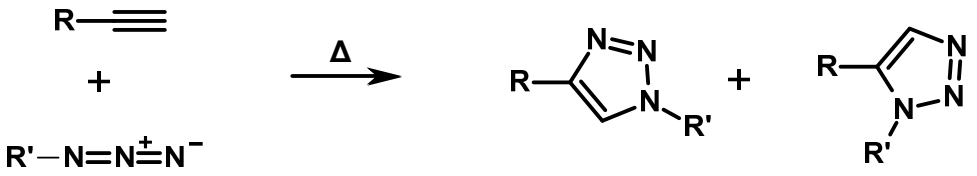

Figure 1.2 Uncatalysed 1,3-dipolar cycloaddition of organic azides to alkynes to yield 1,4- and 1,5-substituted-1,2,3-triazoles.

In 2002 the groups of Sharpless[2] and Meldal[17] independently reported a modified version of this reaction, in which they used a copper(I) catalyst, with a resultant increase in the rate of the reaction by approximately 10^7 fold and allowed the reaction to be carried out at room temperature. [18, 19] The introduction of a copper catalyst also resulted in the formation of exclusively the 1,4-disubstituted-1,2,3-triazole regioisomer in very high yields with few or no side products (Figure 1.3). Furthermore, steric or electronic factors do not have a significant effect on the reaction which is also tolerant of a wide range of functional groups. Alkyne and azide functionality can easily be incorporated into a wide range of compounds, and the use of protecting groups is not required. The reaction also proceeds efficiently in water as well as organic solvents, with almost complete conversion and selectivity for the 1,2,3-triazole product which is often easily isolable by simple filtration. The resultant 1,2,3 triazole is also a very stable moiety and is unaffected by oxidation, reduction and hydrolysis. The reaction has been utilised in many different areas of chemistry [3] and is fast becoming the synthetic method of choice in materials synthesis, [20-24] polymer synthesis, [25-28] interlocked architectures, [29-32] bioconjugation [6, 21, 33-37] and drug discovery [6, 37]

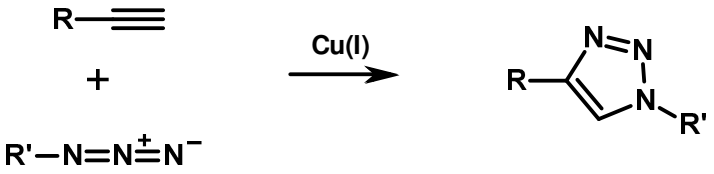

Figure 1.3 The copper catalysed azide-alkyne cycloaddition (CuAAC) resulting in the formation of exclusively the 1,4-disubstituted-1,2,3-triazole regioisomer.

1.2.1.1 General CuAAC reaction conditions

The CuAAC reaction is an extremely robust and versatile reaction therefore a vast number of successful experimental variations have been developed and a wide range of copper sources have been exploited. Sharpless and co-workers carried out their original work using $CuSO_4$ or $Cu(OAc)_2$ as the source of copper. These copper compounds were used in conjunction with sodium ascorbate as a reducing agent to generate Cu(I) *in situ* in an aqueous environment. [2] Since this original publication, alternative sources of copper have been utilised due to the specific reaction conditions, for example CuI has been shown to be a more desirable source of copper when the CuAAC reaction is carried out in organic solvents (e.g. CH_3CN, DMF, DMSO, THF). Yoo *et al.* [38] have shown that a catalytic quantity of CuI results in formation of the desired 1,4-disubstitued-1,2,3-triazole in non-aqueous conditions, however, use of a base is required (typically an N-donor base such as 2,6-lutidine) in order to promote the generation of an intermediate copper acetylide. [39] Alternative sources of copper which have been utilised in the CuAAC reaction include; metallic copper Cu(0), [40, 41] copper nano particles, [42] and copper catalysts immobilised on solid supports[43].

To date, most CuAAC syntheses are carried out at room temperature, however, when the temperature of the reaction is increased using a microwave reactor, the time required for the reaction can be drastically decreased with no detrimental effect to the desired products.[18, 44] Substrate concentrations seem not to be important on the outcome of the CuAAC reaction[3] as there have been reports using both very dilute concentrations up to neat concentrations.

CuAAC reactions to prepare triazoles with the potential for metal chelation, can result in problems with regards to isolation of the pure product due to copper coordination. For compounds which are soluble in organic solvents the most effective method of purification is liquid-liquid extraction. Washing with aqueous ammonia solution or ethylenediaminetetraacetic acid (EDTA) solution is the most commonly used method for the extraction of copper from the reaction media, in both liquid and solid phases. [12, 17, 45] Removing the copper from the reaction media has also been undertaken with the use of commercially available metal scavenger resins. [46] However, to date there have been numerous publications which have employed the CuAAC reaction to prepare multidentate products which have been isolated and in good yields. [46, 47]

The introduction of coligands in order to accelerate CuAAC reactions has also been widely studied. Although metal stabilizing ligands are not essential for the catalytic activity of Cu(I) in the CuAAC reaction, they have often been employed to enhance the rate of the reaction and to protect the Cu(I) from oxidation to Cu(II) and/or disproportionation to Cu(0) and Cu(II). [48, 49] Protecting the catalyst from oxidation is beneficial, to ensure that there is a sufficient concentration of the catalyst throughout the time scale of the reaction. Whilst carrying out early mechanistic studies Fokin *et al.* discovered that the rates of reaction for the formation of certain polyvalent products were unusually high and that these reactions seemed to be autocatalytic. They hypothesized based on their results that the resulting polytriazole products, were acting as rate-accelerating ligands for the Cu(I) catalyst. [47] On testing a range of metal stabilising ligands for a model reaction between phenyl acetylene and benzyl azide, ligands that were found to be

the best performing ligands shared a similar oligotriazole structural motif based on cycloaddition to a propargylamine core (Figure 1.4). *Tris*-(benzyltriazolymethyl)amine (TBTA) was identified as being most efficient ligand in this family for accelerating the rate of CuAAC reactions. After further comparing the rate-accelerating ability of TBTA to other polydentate ligands, Finn *et al.* concluded that *tris*-(2-benzimidazolylmethyl)amines are also promising rate accelerating ligands as they gave considerable improvements in both rate and yield. [50, 51]

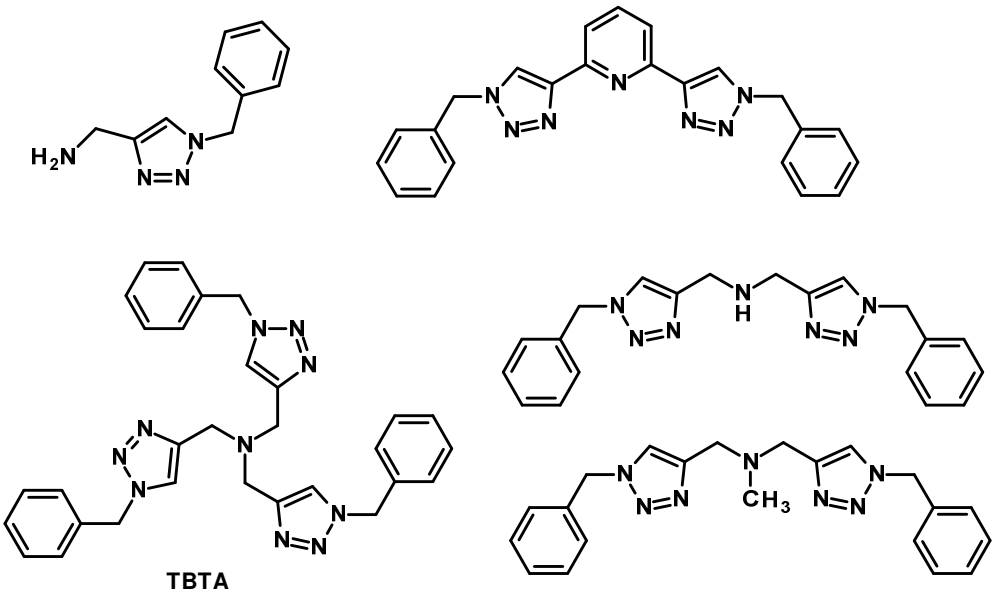

Figure 1.4 A selection of metal stabilising ligands which have been used to enhance the rate of reaction for the CuAAC reaction.

Well defined Cu(I) complexes with N-heterocyclic carbene (NHC) ligands have successfully been used as catalysts for CuAAC reactions. Díez-González *et al.* have shown that using NHC copper(I) complexes yields 1,4-disubstituted products in excellent yields[52, 53] (Figure 1.5).

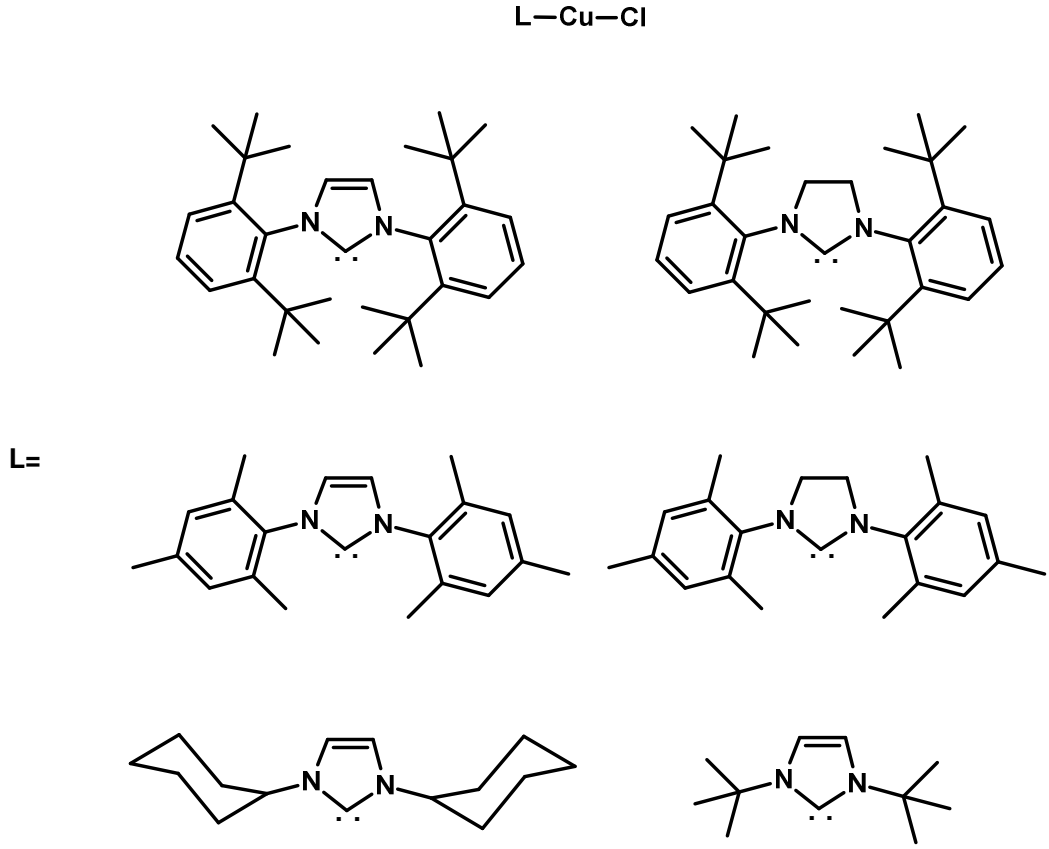

Figure 1.5 A selection of N-heterocyclic carbene complexes which have been used as catalysts for CuAAC reactions.

1.2.1.2 One-Pot CuAAC reactions

In the previously discussed methodologies pre-prepared azides and alkynes were synthesised and isolated prior to their use in CuAAC reactions. However low molecular weight azides are often thermally and shock sensitive and may detonate. In an effort to improve the efficiency, scope and safety of the CuAAC reactions a number of groups have developed one-pot CuAAC methodologies in which either the alkyne or azide reactants are generated *in situ* and reacted immediately without isolation or purification.

Crowley [11, 12] and Schubert [10, 54] have shown that organic azides can be generated *in situ* from their corresponding halides or boronic acids, and then further reacted with terminal alkynes in a one pot CuAAC reaction. Crowley and co-workers utilised the one-pot CuAAC methodology for the safe generation of benzyl-, alkyl- and aryl-substituted 2-(1H-1,2,3-triazol-4-yl)pyridine and 2,6-bis(1H-1,2,3-triazol-4-yl)pyridine ligands. Exploiting the conditions that were developed by Folkin, [55] the benzyl- and alkyl-substituted ligands were synthesised using, sodium azide and the appropriate alkyl halide.

Fletcher *et al*. have shown that trimethylsilyl (TMS) -protected alkynes can be deprotected *in situ* and then "clicked" to preformed organic azides to form bi-, tri- and quadridentate pyridyltriazole ligands in excellent yields. They have also shown that commercially available 1,4-bis(trimethylsilyl)butadiyne can be deprotected *in situ* for the convenient synthesis of 4,4'-bis-1,2,3-triazolyl ligands, without the need for preparation of unstable gaseous butadiyne (Figure 1.6). [56]

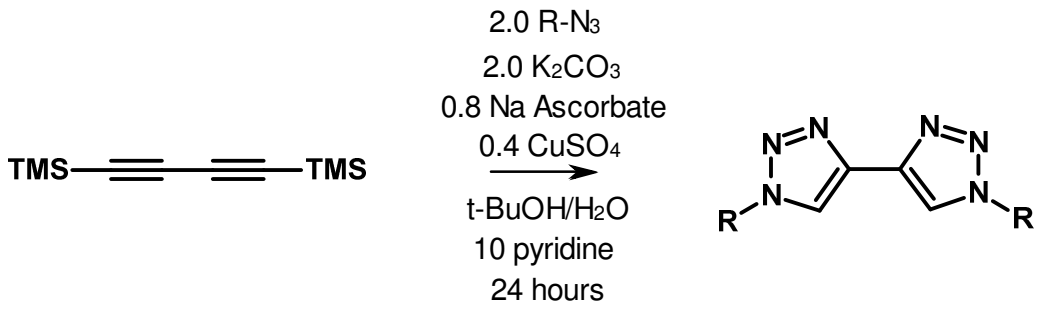

Figure 1.6 Tandem in situ deprotection of bis(trimethylsilyl)butadiyne and "click" reaction to synthesise 4,4'-bis-1,2,3-triazolyl ligands.

1.2.1.3 Mechanism for CuAAC reaction

The significant rate enhancement observed under Cu(I) catalysis with respect to the uncatalysed reaction is best explained by a stepwise cycloaddition mechanism, catalysed by a Cu(I) species which lowers the activation barrier relative to the uncatalysed reaction by as much as 11 kcal mol^{-1}. [39, 40] Mononuclear and dinuclear mechanisms have been proposed (Figure 1.7) which are first order and second order with respect to copper respectively. In both mechanisms the first step involves the formation of a copper acetylide intermediate. In the first order mechanism the acetylide formed is thought to be capable of immediately forming an acetylide-azide complex, while in the second order mechanism a second copper centre is required to activate the azide. The copper acetylide-azide complexes then undergo cyclisation and formation of a metallocycle through nucleophilic attack on the acetylide by the azide group. Finally, ring contraction occurs to yield a copper triazolide intermediate which eliminates the product triazole upon protonation (Figure 1.7).

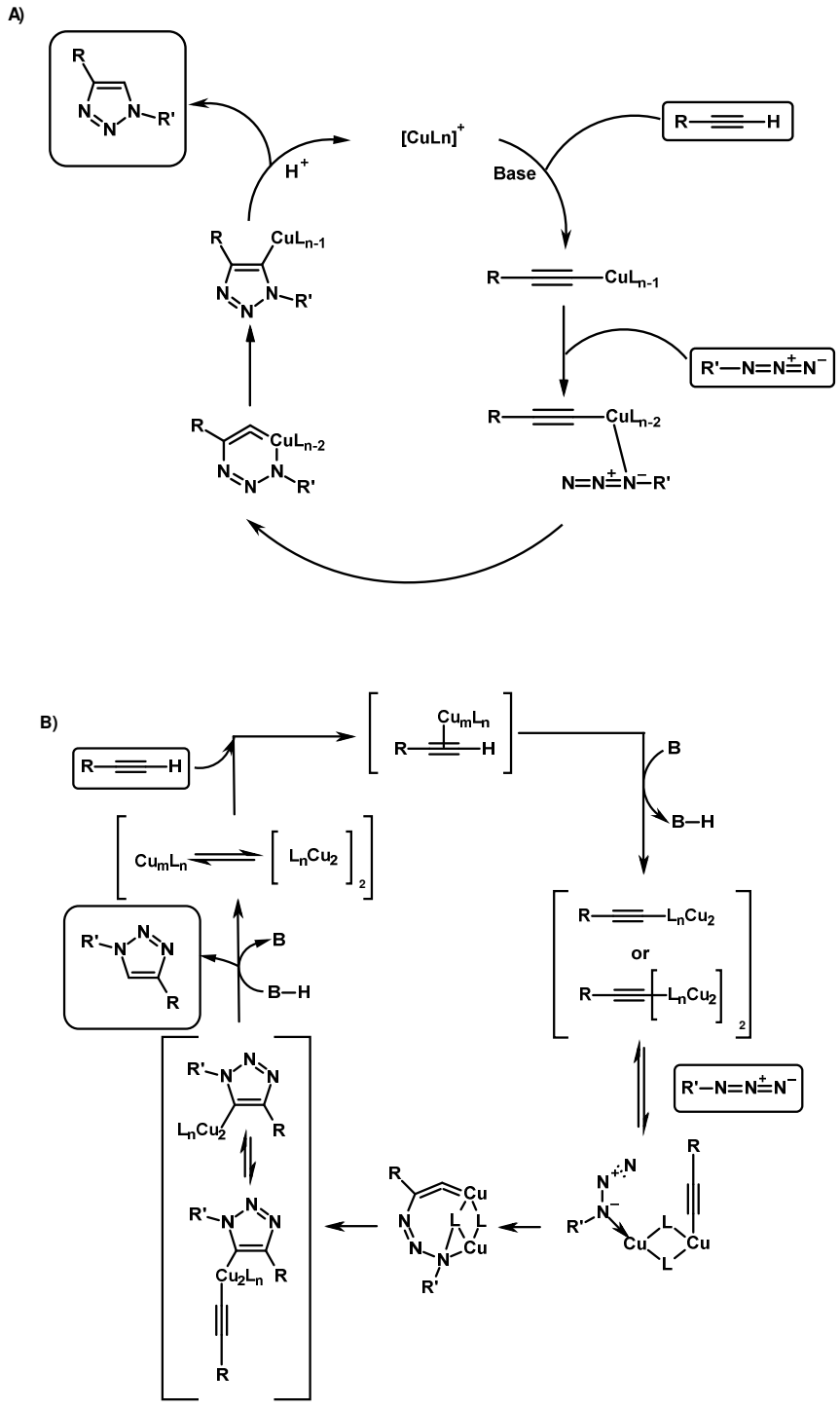

Figure 1.7 Proposed catalytic cycles for the stepwise CuAAC reaction A) First order with respect to copper; and B) second order with respect to copper.

1.2.2 Ruthenium catalysed azide-alkyne cycloaddition (RuAAC)

Fokin *et al.* [57] have shown that ruthenium pentamethylcyclopentadienyl complexes can be used as efficient catalysts for the regioselective formation of the alternative 1,5-disubstituted-1,2,3-triazole (Figure 1.6). For example [$Cp^*RuCl(PPh_3)_2$], [$Cp^*RuCl_2]_2$ and [$Cp^*RuCl(COD)$]. Whist the scope and functional group tolerance of RuAAC reaction are excellent, the reaction is more sensitive to the choice of solvent and the steric demands of the azide reactant than in CuAAC reactions. As such, it has not yet been applied as widely. [58-60]

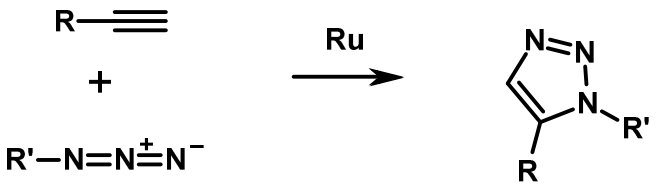

Figure 1.8 The ruthenium catalysed azide-alkyne cycloaddition (RuAAC) resulting in the formation of exclusively the 1,5-disubstituted-1,2,3-triazole regioisomer

1.3 Coordination chemistry of CuAAC derived ligands

Whilst the coordination chemistry of 1,2,4-triazoles [61-67] and the unsubstituted 1H-1,2,3-triazole [61, 67] have been extensively explored, metal complexes of 1,2,3-triazoles remained relatively unexplored until recently. The majority of reported applications of the CuAAC reaction had utilised the 1,2,3-triazole moiety as a stable linker unit for two chemical or biochemical components, with little attention being paid to the heterocycle itself. This is despite the fact that the 1,4-disubstituted-1,2,3-triazole is similar in terms of molecular dimension and planarity to amide bonds, and is expected to have similar coordination properties to substituted imidazole [37, 46, 68] for example. The 1,4-disubstitued-1,2,3-triazole moiety has enormous potential for metal coordination. [69] The triazole can act as a N-donor ligand through the more basic N3 position but coordination could also occur through the N2 atom (Figure 1.9). In addition coordination can also occur through the C5 position in anionic triazolides or mesoionic triazolylidene NHCs.

Since 2007 there has been a rapid increase in the use of 1,4-disubstitued-1,2,3-triazole as ligands derived through CuAAC reactions.

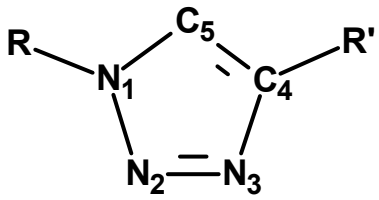

Figure 1.9 The potential metal coordination sites of 1,4-disubstitued-1,2,3-triazole ligands

The remainder of this section forms a systematic review of the use of triazole-based "click" chemistry in coordination chemistry.

1.3.1 1,4-Disubstituted-1,2,3-Triazoles as Monodentate N-Donor Ligands

Van Köten and co-workers have used the CuAAC reaction to prepare 1,4-disubstituted-1,2,3-triazoles as tuneable monodentate ligands for aryl diamine cyclometalated pincer complexes of Pd and Pt (Figure 1.10). [70] An X-ray crystal structure of a Pd complex showed that coordination to the metal occurs through the N3 atom of the triazole ring. The coordination behaviour of the triazole in the complex was studied by variable temperature ^{1}H NMR spectroscopy. These experimental observations indicate that at room temperature intermolecular triazole ligand exchange at Pd is fast on the NMR timescale while exchange for the corresponding Pt complexes is much slower throughout the temperature scale studied. In order to assess the relative coordination strength of the triazole ligand, competitive ligand exchange experiments were carried out with more common Lewis bases such as H_2O, triphenylphosphine, 1-methylimidazole, diethylsulfide, dimethylsulfoxide, aniline, acetonitrile and pyridine. The data show that the triazole ligand is a better ligand than H_2O, dimethylsulfoxide and acetonitrile, comparable in strength to aniline and a slightly weaker donor than pyridine. It was found that by varying the substituents of the triazole the relative binding strength of these ligands could be tuned.

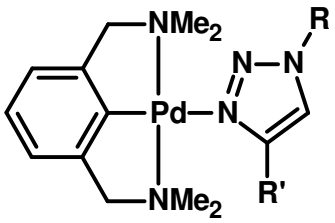

Figure 1.10 Structure of monodentate 1,4-disubstituted-1,2,3-triazoles N^C^C pincer complexes.

Following on from this work Astruc *et al.* [71] prepared three novel ligands containing either one, two or three ferrocenyl triazole moieties, starting from the corresponding azidomethylbenzene and ethynylferrocene.[71] The mono(ferrocenyltriazole) ligand was reacted with $[PdCl_2(C_6H_5CN)_2]$ to yield a *trans* bis triazole complex in which the triazole ligands are again coordinated to the metal through the N3 of the triazole position. The X-ray crystal structure is shown in Figure 1.11.

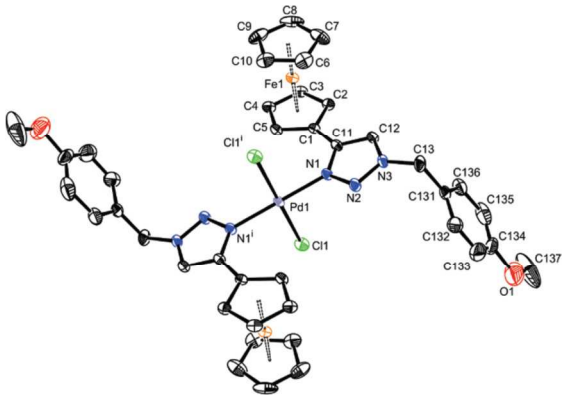

Figure 1.11 Molecular structure of trans-[$PdCl_2L_2$] (L= 1-({4-methoxylphenyl}methyl-4-ferrocenyl-1,2,3-triazole))[71]

When ^{1}H NMR spectra were recorded in d_6-dimethylsulfoxide solutions the complexes were found to exist in equilibrium with free ligand and a monotriazole solvento complex.

Crowley and co-workers have reported that di-1,4-substituted-1,2,3-triazole ligands can be used as pyridine surrogates to self-assemble coordinatively saturated, quadruply stranded helicate cages with Pd(II) ions. [13] The species are stable in both solution and solid-state as they have been fully characterised by NMR, HRMS and X-ray crystallography. X-ray crystallography again shows coordination to the metal through the more basic N3 atom of the triazole ring.

In one final example Osuka, Shinokubo and co-workers have synthesised 1,4-disubstituted-1,2,3-triazole appended Zn(II)-porphyrin complexes. NMR studies show that the complexes dimerise in solution and X-ray crystallography shows that dimerisation is driven by bridging coordination of the pendant 1,4-disubstituted-1,2,3-triazole to Zn of a second porphyrin complex. As with the other complexes of a similar type the triazole is coordinated to the metal through the N3 of the triazole. [72]

There are a number of other reported 1,4-disubstituted-1,2,3-triazole metal complexes in which monodentate coordination is assumed, however none of these compounds have been structurally characterised, and therefore it is not known whether coordination to the 1,4-disubstituted-1,2,3-triazole is through the N2 or the N3 of the 1,2,3-triazole. [72-78]

1.3.2 1,4-Disubstituted-1,2,3-Triazoles as Bridging N-Donor Ligands

Related ligands to 1,4-disubstituted-1,2,3-triazoles with neighbouring nitrogen donor atoms, such as pyrazolates and 1,2,4-triazole have been widely used as bridging ligands. Therefore it is surprising that only one report of crystallographically characterised complexes containing bridging-1,2,3-triazole ligands has appeared. Crowley and co-workers have prepared two silver complexes, which display the same dinuclear core in which the two silver ions are bridged by two 1,4-disubstituted-1,2,3-triazole units [79] (Figure 1.12).

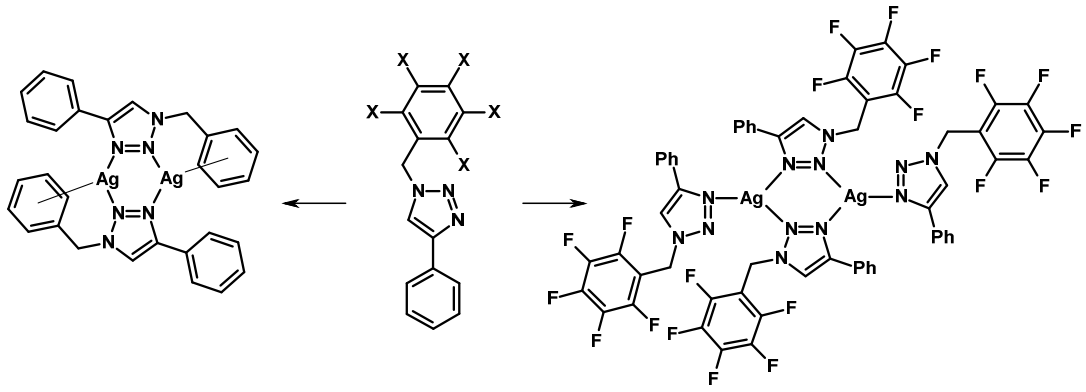

Figure 1.12 1,2,3-triazole bridged silver complex

Steel *et al.* [80] have prepared a series of ruthenium complexes in which they utilised an anionic 1,2,3-triazolate based ligand to bridge two metal centres. The new ligand was prepared by the reaction of di(pyrid-2-yl)acetylene and azidotrimethylsilane. This is not strictly "click" chemistry however it is copper catalysed. The new ligand was analysed by X-ray crystallography and it was found that in the solid state the ligand exists in a zwitterionic form. When the ligand was reacted with excess $[Ru(bpy)_2Cl_2]$ a dinuclear complex was formed

and found to exist in an approximate 1:1 ratio as two diastereoisomers (*meso* and *rac*) isomers could easily be separated using column chromatography. Reaction of the ligand with one equivalent of $[Ru(bpy)_2Cl_2]$ led to the mononuclear complex leaving one of pyridyl-triazole domains vacant. The X-ray crystal structure (Figure 1.13) of the dinuclear complex was obtained and it was noted that the plane of the dipyridyltriazolate ligand is somewhat distorted with deviation from coplainarity of the pyridyl and triazolate rings. The electronic absorption spectra and redox potentials of the complex were also measured and the mononuclear complex was more readily oxidised than $[Ru(bpy)_3]^{2+}$ and was significantly harder to reduce. The difference in the first oxidation potential and the red-shifted absorption indicates a smaller HOMO-LUMO gap than that of $[Ru(bpy)_3]^{2+}$. The two stereoisomers of the dinuclear complex both show well separated oxidation potentials indicating a strong metal-metal interaction.

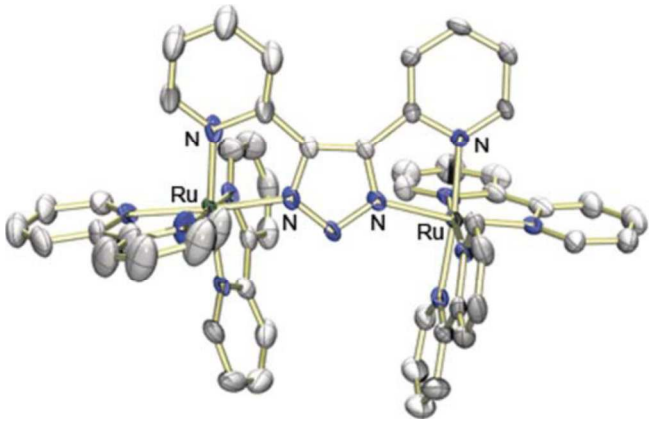

Figure 1.13 Molecular structure of $[\{Ru(bpy)_2\}_2L]^{n+}$ (L= 4,5-di(pyrid-2-yl)-1,2,3-triazolate) [80]

1.3.3 1,4-Disubstiuted-1,2,3-Triazoles as Monodentate C-Donor Ligands

The most favoured metal coordination sites of the 1,4-disubstitued-1,2,3-traizole is the N2 and N3 of the triazole ring however as discussed previously there is the potential for functionalisation at the C5 position. Due to the relatively acidic nature of the hydrogen atom at C5 it can be relatively easily be deprotonated and yield anionic 1,4-disubstituted-1,2,3-triazolide ligands. Straub and co-workers successfully isolated a copper 1,4-disubstituted-1,2,3-triazolide complex. The complex was prepared by reacting a bulky copper acetylide with azidodi-4-tolylmethane and the molecular structure of the complex was confirmed through X-ray crystallography. In this work they state that this copper complex is an isolated intermediate in the catalytic cycle of the CuAAC. [81] Furthermore they demonstrated that this copper complex showed catalytic activity for the CuAAC reaction, providing strong evidence for the role of the 1,2,3-triazolide intermediate in the catalytic mechanism. Another example of this C5 coordination of the triazole ring was demonstrated by Gray and co-workers, [82] who prepared a family of luminescent gold 1,2,3-triazolide complexes. (Figure 1.14) Excitation at 312 nm leads to dual emission, a shorter-wavelength emission peak near 383 nm and a longer-wavelength, O_2-quenchable emission near 475 nm. Time-resolved measurements at 77 K find that the emissions near 475 nm last from hundreds of microseconds to tens of milliseconds.

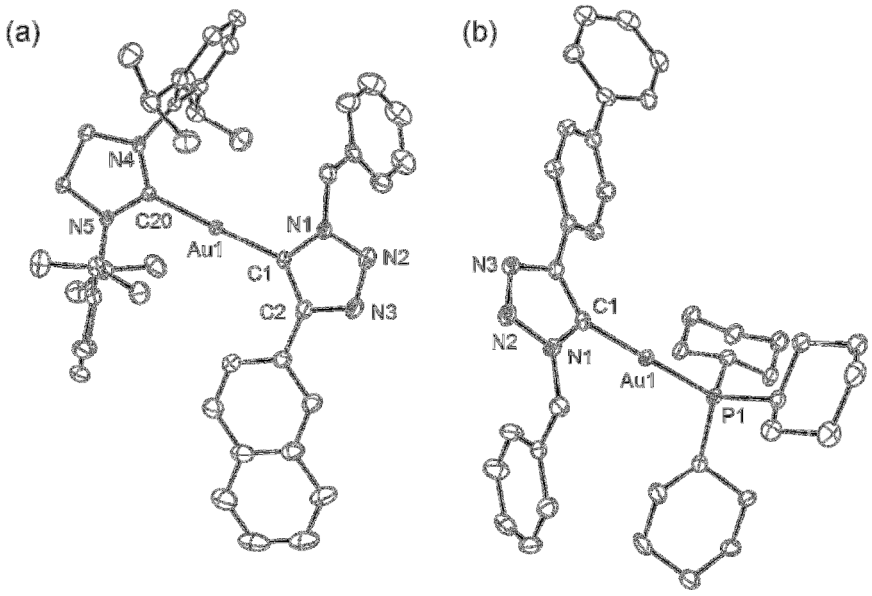

Figure 1.14 Molecular structure of luminescent gold-1,2,3-triazolide complexes[82]

Gandelman *et al.* also investigated the uses of the 1,2,3-triazole as a potential pincer ligand. [83] Here, they synthesised a range of 1,4-disubstituted-1,2,3-triazoles with donor substituents using the copper catalysed reaction, and utilised the relatively acidic C-H of the triazole for insertion by the metal in analogous fashion to more established 1,3-disubstituted phenyl based systems. Representative example ligand precurseors that were prepared by this approach included PCP-, PCN- and PCS-. The new pincer ligands demonstrate typical tridentate coordination upon reaction with late-transition metals. The molecular structure of one of the Pd complexes was determined by X-ray crystallography and it was confirmed that coordination to the metal occurs through the C5 atom of the triazole ring and through the donor groups attached at the N1 and C4 positions (Figure 1.15). The influence of these pincer ligands on catalytic activity was investigated, and the results showed that the PCP and PCN based systems are

extremely efficient catalysts for the Heck reaction, where as the PCS system has substantially lower activity.

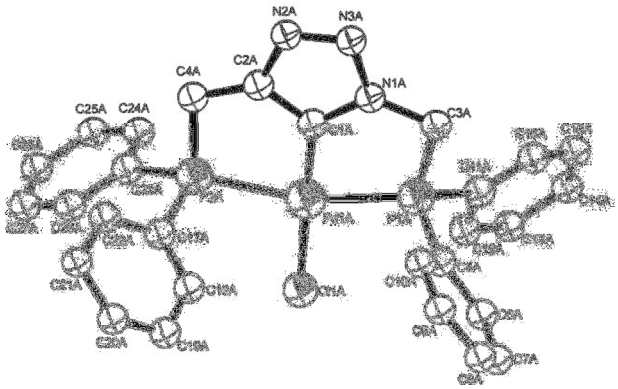

Figure 1.15 Molecular structure of palladium-1,2,3-triazolide pincer ligand complex [83]

Gandelman *et al.* [84] have used the 1,2,3-triazole to prepared a range of cationic N-donor *N*-heterocyclic nitrenium ions that are isoelectronic and isostructural to NHCs, and studied their ligand properties. Experimental and computational studies of the electronic properties of this novel type of ligand suggest that they are poor σ-donors and good π-acceptors.

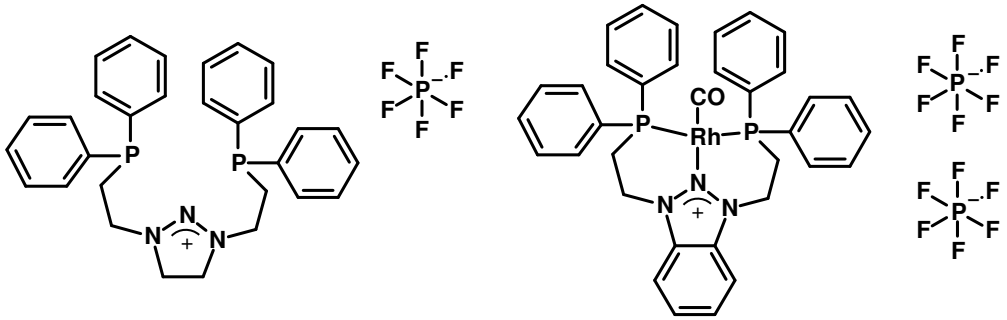

Figure 1.16 Nitrenium ions as ligands for transition metal complexes. [84]

As well as allowing access to 1,4-disubstituted-1,2,3-triazolide ligands 1,2,3-triazoles can also be easily alkylated at the N3 position to give 1,3,4-trisubstitued-1,2,3-triazolium salts. *N*-heterocyclic carbenes have become very popular ligands in late transition metal chemistry predominantly due to their good catalytic activity. [85] Recent reports have shown the use of 1,2,3-triazolium salts for the generation of 'abnormal' mesoionic *N*-heterocyclic "click" carbenes. [86] Deprotonation of the 1,3,4-trisubstitued-1,2,3-triazolium salts with Ag_2O generates the moderately stable silver 1,3,4-trisubstitued-1,2,3-triazol-5-ylidene which can then be used to synthesise a wide range (including complexes of Pd(II), [86-88] Ru(II), [89] Rh(I), [86, 87] Ir(I), [86] Cu(I) [90, 91] and Au(I) [92]) of stable metal 1,3,4-trisubstitued-1,2,3-triazolidene complexes by transmetallation. [91] [93] Infra-red stretching frequencies for iridium dicarbonyl chloride complexes show that these "click" carbenes are better donors than conventional carbenes but not as good as imidazole-5-ylidene ligands. Copper complexes of these ligands have also been utilised as catalysts for CuAAC reactions. [90, 91] X-ray crystal structures of two complexes are shown in Figure 1.17.

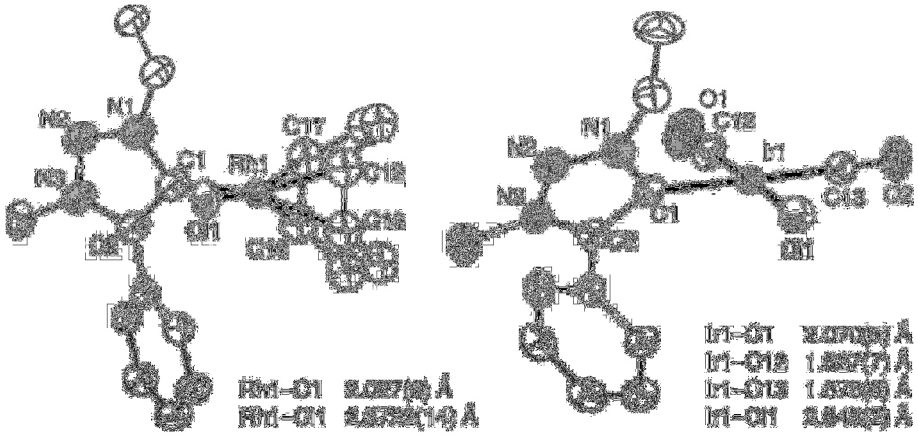

Figure 1.17 Molecular structure of 1,3,4-trisubstitued-1,2,3-triazol-5-ylidene N-heterocyclic carbenes complexes [86]

1.3.4 Bidentate N^N donor Ligands

Bidentate ligands containing 1,4-disubstituted-1,2,3-triazole ligands are by far the most widely studied CuAAC derived ligand systems. Common ligands include pyridyl-1,2,3-triazole, 2-(1-R-1H-1,2,3-triazol-4-yl)pyridine and [2-(4-R-1H-1,2,3-triazol-1-yl)methyl]pyridine frameworks (Figure 1.18).

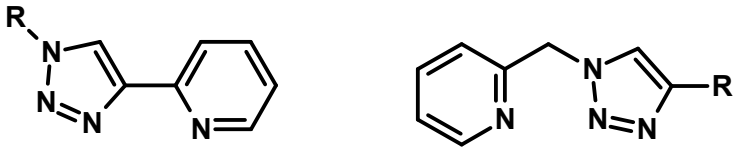

Figure 1.18 Bidentate ligands containing 1,4-disubstituted-1,2,3-triazoles 2-(1-R-1H-1,2,3-triazol-4-yl)pyridine and [2-(4-R-1H-1,2,3-triazol-1-yl)methyl]pyridine.

The 2-(1,2,3-triazol-4-yl)pyridine (pytz) type ligands have been studied as readily tuneable bpy analogues. Monofunctionalised triazole compounds incorporating pyridine can easily be synthesised by a simple CuAAC reaction of 2-ethynyl pyridine with an organic azide. Complexes of a number of metals have now been reported and include octahedral complexes of Re(I), [94-96] Tc(I), [94] Ru(II), [10, 56, 80, 97-99] Ir(III), [98, 100-102] tetrahedral complexes of Ag(I) and Cu(I) [12, 103] and some square planar complexes of Pd(II) and Pt(II). [104-108]

Over the past few decades there has been interest in complexes of bpy ligands such as $[Ru(bpy)_3]^{2+}$ and $[Re(bpy)(CO)_3Cl]$, stemming mainly from their interesting electrochemical and photophysical luminescent properties. This has therefore encouraged a number of groups to examine the optoelectronic properties

of complexes of pytz type ligands that are analogues to bpy. Obata and Yano [96] and Benoist [94, 95] have prepared several rhenium complexes using this ligand framework by refluxing a stoichiometric quantity of the corresponding ligand with $[Re(CO)_5Cl]$ in an alcoholic solvent to yield the complexes of the type $[Re(pytz)(CO)_3Cl]$ (Figure 1.19). Characterisation data indicates that exclusively the *fac* isomers of the complexes were prepared as observed for the bpy analogues. These complexes exhibit UV-visible absorption spectra with blue-shifted bands compared to those of $[Re(bpy)(CO)_3Cl]$. Absorptions were assigned as the mixed metal-to-ligand-to-ligand charge transfer (MLLCT) in nature from time-dependent density functional theory (DFT) calculations and are blue shifted due to higher energy LUMO of the pytz ligand. Similarly, a blue-shifted maximum was observed in luminescence spectra when compared to that of the complex $[Re(bpy)(CO)_3Cl]$. Luminescent lifetime measurements were also carried out on the complexes and an almost three fold increase in lifetime for the pytz complexes was observed over the bpy analogue. Benoist, Machura and co-workers have also prepared radiolabeled technetium-99 complexes of this ligand framework as potential imaging probes for nervous system receptors. [94]

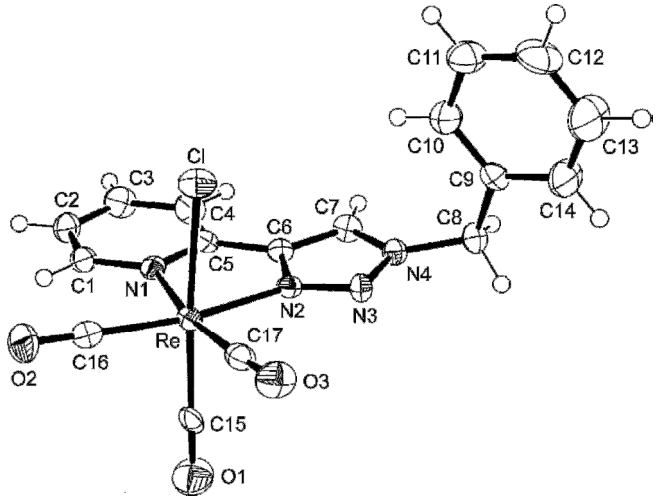

Figure 1.19 X-ray structure of [Re(pytz)(CO)$_3$Cl].[96]

Fletcher [56] and Schubert [10] have independently prepared pytz analogues of $[Ru(bpy)_3]^{2+}$ by reacting $RuCl_3.H_2O$ with three equivalents of the pytz ligand. Due to the asymmetry of the pytz ligands preparation of these homoleptic complexes results in a mixture of the *mer* and *fac* isomers which prove difficult to separate unless a bulky substituent is present at the N1 position of the triazole heterocycle. In contrast to their bpy analogues it was found that the homoleptic complexes are only modestly coloured and are not emissive. [10, 56] Schubert *et al.* also investigated mixed bpy/pytz heteroleptic complexes. [10, 80, 99] The photophysical and electrochemical properties of the series of complexes $[Ru(bpy)_{3-n}(pytz)_n]^{2+}$ (Figure 1.20) were studied and it was found as the number of pytz ligands increases in the complex a blue shift in both the MLCT band in the UV-visible absorption spectra and in the photoluminescence emission spectra are observed and also leads to quenching of emission intensity. Consistent with this, the increase in the number of pytz ligands leads to an increase in the energy of the LUMO as observed by cyclic voltammetry.

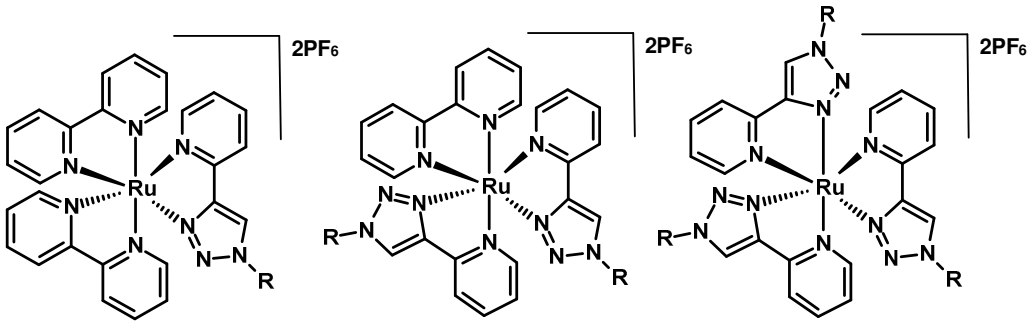

Figure 1.20 Structure of $[Ru(bpy)_2(pytz)]^{2+}$, $[Ru(bpy)(pytz)_2]^{2+}$ and $[Ru(pytz)_3]^{2+}$

Baurele, Gratzel, Zakeeruddin and co-workers have utilised the pytz ligand to prepare the heteroleptic Ru(II) complex [Ru(**L**)(dcbpy)$(NCS)_2$] (L = 2-(1-(4-hexylphenyl)-1,2,3-triazol-4-yl)pyridine) and have demonstrated its use as a sensitizer in dye-sensitized solar cells (DSSC) (Figure 1.21). [109] DSSC devices, with an acetonitrile-based I_3^-/I^- electrolyte showed a respectable power conversion efficiency of 7.8%, which is quite high taking into account the diminished light absorption properties of the complex when compared to [Ru(dcbpy)$_2(NCS)_2$] (~10 % efficiency dcbpy is 4,4'-dicarboxylic-2,2'-bipyridyl).

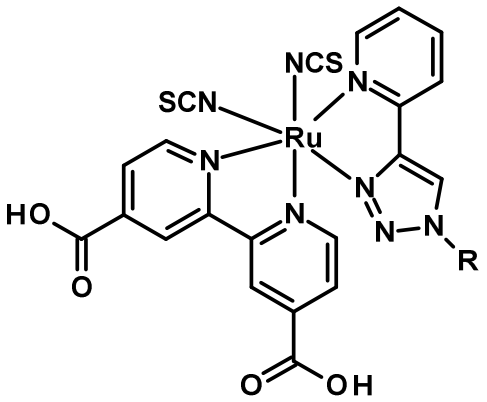

Figure 1.21 An example of 2-(1-R-1,2,3-triazol-4-yl)pyridine ligands used as sensitizers for a DSSC.

Cyclometallated Ir(III) complexes with pytz ancillary ligands have also been prepared. DeCola *et al*. have prepared complexes of the type $[Ir(ppy)_2(pytz)]^+$ and $[Ir(F_2ppy)_2(pytz)]^+$ (where ppy = 2-phenylpyridine and F_2ppy = 2-(2,4-difluorophenyl)pyridine) and examined their photophysical and electrochemical properties. [98, 100-102] These complexes displayed excellent emission quantum yields, (0.16-0.32 in degassed dichloromethane), long luminescent lifetimes, (0.53-1.3 μs) and show reversible oxidation behaviour. The authors have also shown that these complexes show electrochemiluminescence where the emission colour can be modulated from green to blue by modification of the cyclometalated ligands. [102] The same series of complexes have been used to develop light-emitting electrochemical cells (LEEC), which can be used as an alternative to the more studied prevalent organic light emitting diode (OLED) devices. The LEECs generated using the F_2ppy Ir(III) complexes display very blue emission and have drastically reduced response time, which in the past have been problematic with LEEC technology, therefore bringing practical LEECs a step closer. [101]

Another group of bidentate "click" ligands are the 4,4'-bi-1,2,3-triazolyl ligands (btz). A number of groups including our own have attempted to exploit the use of these symmetrical ligands as readily prepared bpy analogues.[56, 110, 111]

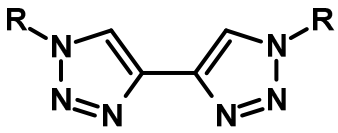

Figure 1.22 Structure of bidentate 4,4'-bis-1,2,3-triazolyl ligands.

Fletcher *et al.* [56] and Monkowius and co-workers [111] independently reported ruthenium complexes of the type $[Ru(btz)_3]^{2+}$. The optoelectronic properties of these complexes were studied and it was found that the MLCT absorption bands appear at significantly higher energy in comparison to that of $[Ru(bpy)_3]^{2+}$such that $[Ru(btz)_3]^{2+}$ is not at all strongly coloured. These homoleptic btz complexes do not display any measurable luminescent emission at room temperature. [56]

Monkowius and co-workers [111] also prepared copper and rhenium complexes of the form $[Cu(btz)L]^+$ (L= bis[2-(diphenylphosphanyl)phenyl] ether) and $[Re(btz)(CO)_3Cl]$. The UV-visible spectra of the btz complexes again revealed absorption bands which were significantly higher in energy than the analogous bpy complexes. Again, unlike their bpy analogues neither of these btz complexes are emissive in either the solid state or in solution.

The group of Elliott have prepared and characterised a family of complexes $[Ru(bpy)_{3-n}(btz)_n][PF_6]_2$ (n = 1 to 3) and investigated the resultant photophysical effects of the btz ligand across the series. [112] The experimental data reveal a blue-

shifting in the absorption bands consistent with the destabilization of the LUMO relative to the HOMO, with a very large blue-shift being observed on replacement of the final bpy ligand by btz. The data indicates that the LUMO in all the bpy-containing complexes is bpy-centred, whereas that for $[Ru(btz)_3]^{2+}$ is btz-centred. The inclusion of btz also results in blue-shifted luminescent emission for $[Ru(bpy)_2(btz)]^{2+}$, which is highly quenched compared to that of $[Ru(bpy)_3]^{2+}$. Luminescent emission for $[Ru(bpy)(btz)_2]^{2+}$ can only be observed on cooling to 77 K. These data are consistent with quenching through thermal population of ^{3}MC states from elevated ^{3}MLCT states. Theoretical studies showed that the replacement of bpy ligands by btz ligands infact leads to a fundamental change in the ordering of excited states such that the nature of the lowest energy excited state changes from MLCT in nature to MC for $[Ru(btz)_3]^{2+}$. [112]

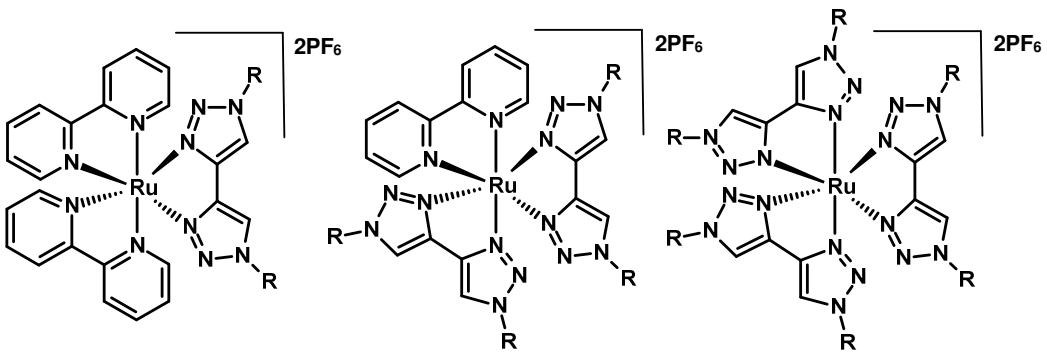

Figure 1.23 Structures of the complexes $[Ru(bpy)_2(btz)](PF_6)_2$, $[Ru(bpy)(btz)_2](PF_6)_2$ and $[Ru(btz)_3](PF_6)_2$.

The more flexible ligand [2-(1,2,3-triazol-1-yl)methyl]pyridine has also been studied. Like 2-(1,2,3-triazol-4-yl)pyridine it also behaves as an N-N bidentate ligand, chelating through the pyridyl and the triazole rings forming a six-membered chelate ring. Chelation through the coordination of the pyridyl donor forces coordination via N2 rather than the more basic N3 position. A range of complexes have been prepared and characterised using this ligand scaffold, including octahedral complexes of Cu(II), [12, 113-116] Co(II), [116] Ni(II), Ru(II), [115, 117] tetrahedral complexes of Ag(I) [12, 115] and Zn(II) and square planar complexes of Ag(I), Pd(II) and Pt(II). [104, 105, 115, 118-120] Whilst the majority of work with this ligand framework has focused on the synthetic and structural chemistry of the ligand, applications of the resulting complexes are beginning to emerge. Scrivanti *et al.* have prepared a cationic palladium allyl complex with this type of ligand (Figure 1.24) and have shown that it exhibits good activity in the Suzuki-Miyaura couplings of aryl bromides with phenyl boronic acid. [121] Brastos, Turel and co-workers have synthesised a small family of ruthenium *p*-cymene complexes and tested them for *in vitro* activity against two human cancer cell lines (Figure 1.24). [117]

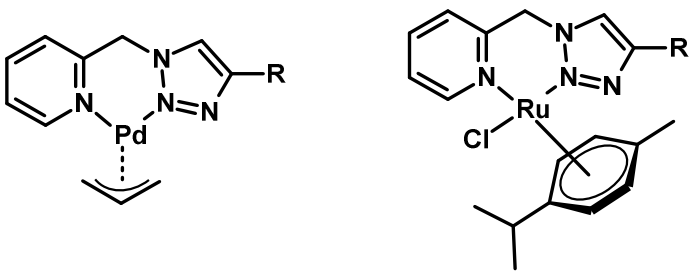

Figure 1.24 Examples of [2-(4-R-1H-1,2,3-triazol-1-yl)methyl]pyridine ligands coordination

1.3.5 Bidentate C^N donor Ligands

A number of groups have explored the use of 4-phenyl-1,2,3-triazoles [9, 100, 122, 123] as precursors for cyclometallating ligands. Schubert[9] showed that refluxing 4-phenyl-1,2,3-triazole with $IrCl_3.3H_2O$ in ethoxyethanol resulted in the formation of a biscyclometalated chloride-bridged dimer. The dimers where treated with a range of different neutral and anion bidentate ancillary ligands (e.g. bpy, acetylacetonate (acac) and picolinate (pic)) resulting in monomeric complexes (Figure 1.25) in excellent yields. [9, 100] The optical-electronic properties for the complexes were studied and it was shown that emission colour-tuning could be easily achieved through changing the ancillary ligand. Using similar conditions DeCola and co-workers have prepared and characterised iridium dimers bearing 4-(2,4-difluorophenyl)-1,2,3-triazolyl)pyridine (dfptz),[100, 124] however crystallographic analysis showed that this is not a dichloro-bridged dimer but a dimer in which one of the 1,2,3-triazole units acts as a bridging moiety. The authors were able to successfully cleave the dimer and access the monomeric complexes e.g. $[Ir(dfptz)_2(bpy)]^+$. The complexes reported showed absorption features similar to those previously reported for other $Ir(ppy)_2$ type complexes, with strong π-π^* transitions in the near UV region localised on the dfptz ligand (~260 nm) and on the triazole (~300 nm) and weaker MLCT bands at lower energies between 350-450nm. The complexes with the fluorinated phenyl ring exhibit more intense absorption bands and display intense unstructured emission bands. Polymer light-emitting diode (PLEDs) devices were fabricated with these complexes and it was found that the electroluminescent spectra for the new devices were almost identical to those of the complex in isolation, with no

emission from the host polymer matrix. This shows that efficient energy transfer from the host to the guest iridium complex occurs. Therefore, it may be possible to use these types of complexes as phosphorescent dopants in the fabrication of PLEDs.

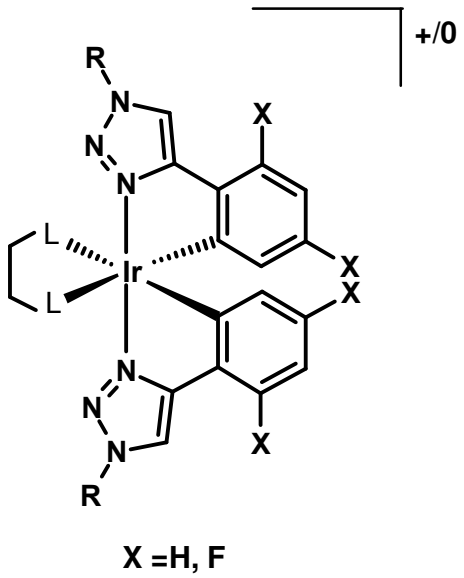

Figure 1.25 Molecular structure of $[Ir(dfptz)_2(L)]^{+/0}$ *(L = bpy, acac*$^-$*, pic*$^-$*)*

1.3.6 Miscellaneous Bidentate Ligands

Amine and phosphine substituted-1,2,3-triazole ligands have also been reported. Bidentate amine-1,2,3-triazole ligands have been used to prepare cisplatin like platinum complexes for use as potential anticancer drugs. [125] Heteroleptic copper(I) amido-1,2,3-triazole complexes have been synthesised and used to develop efficient OLEDs. Ruthenium complexes of bidentate amine-1,2,3-triazole ligands have been used as catalysts for organic reactions. [126]

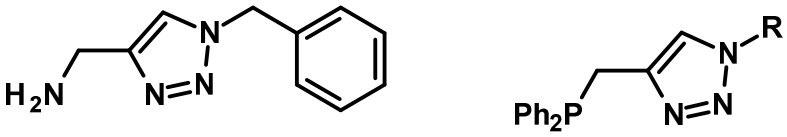

Figure 1.26 Structures of bidentate 4-aminomethyl-1,2,3-triazole and 4-(diphenylphosphinomethyl)-1,2,3-triazole ligands

Related bidentate phosphine-1,2,3-triazole ligands have also been utilised in catalysis. Van Maarseven *et al.* prepared palladium complexes of the ligand shown in Figure 1.26 and demonstrated that these complexes are effective catalysts for Suzuki coupling reactions.[127] They showed that the palladium catalyst maybe hemilabile and exist as either the monodentate complex, where only the phosphine donor is coordinated to the metal or as the bidentate complex where coordination to the metal is through both the phosphine and the triazole N3 position. Crystallographic analysis of the complex prepared from $[Pd(allyl)Cl]_2$ only showed evidence of the monodentate complexes, although the ^{1}H and ^{31}P NMR spectra suggest bidentate coordination after the complex had been treated with $AgBF_4$ to abstract the chloride ligand. After mechanistic studies it was found

that the monoligated complex is more likely to be the catalytically active complex.

1.3.7 Triazole containing Tridentate Ligands

A range of tridentate "click" ligands have been synthesised and characterised. Whilst the majority of these ligands contain two or more 1,4-disubstituted-1,2,3-triazole units, a few examples of tridentate chelators with one triazole unit have been reported.

1.3.7.1 Tridentate Ligands Containing One Triazole

Mindt and Schilibi have synthesised a family of amino acid-derived mono-1,4-disubstitued-1,2,3-triazole containing chelators for Re(I) and ^{99m}Tc(I) as potential imaging agents in PET scans. [46, 128-134] Recently the authors have developed a one-pot procedure which enable the *in situ* generation of both the ligand and the radiocomplex, further improving the synthetic efficiency. [135]

Adolfsson and co-workers have used similar ligands as chelators for rhodium and have shown that they are efficient in rhodium catalysed organic reactions. [136] Chen *et al.* have synthesised hybrid *N*-heterocyclic carbene-1,2,3-triazole tridentate ligands and successfully characterised their Ag(I), Pd(II) and Pt(II) complexes. The authors showed that the palladium complex is a highly active catalyst for the Suzuki-Miryaura cross-coupling reactions. [137]

1.3.7.2 Tridentate Ligands Containing Two Triazole Donors

Another ligand which is widely used in coordination chemistry is 2,2':6',2"-terpyridine (tpy). Several groups have employed the CuAAC reaction to prepare analogues of ligands starting from 2,6-diethynylpyridines (Figure 1.27). For the most part these ligands act as tpy-like tridentate ligands coordinating through the pyridyl and the N3 atoms of the triazole rings. Complexes of ligands of this type have been prepared for a wide range of metal ions including Fe(II), [138-140] Ru(II), [140] Cu(II), [12, 141] Zn(II), [140] Eu(III) [138, 139] and Ag(I). [12]

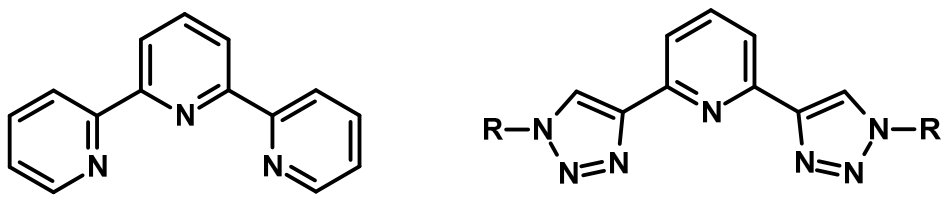

Figure 1.27 Tridentate 6-bis(1-R-1,2,3-triazol-4-yl)pyridine ligands and 2,2':6',2"-terpyridine

Flood [138] and Hecht and Limberg [139] were the first to report the synthesis of 2,6-bis(1,2,3-triazol-4-yl)pyridine based ligands (btzpy) and reported some representative coordination to Fe(II) and Eu(III) (Figure 1.27). Reacting these ligands with Cu(II), Fe(II) and Ru(II) gave octahedral complexes which were characterised by X-ray crystallography. [140] The btzpy ligand was found to be less sterically demanding than the tpy analogues and this is demonstrated in the X-ray crystal structures of each of complexes. However, it was shown that there was greater distortion from the octahedral symmetry in the ruthenium and iron complexes when compared to their analogues tpy complexes. The effects of the

coordination on the electronic structure of the complexes was investigated using UV-visible absorption spectroscopy, and it was found that upon coordination the ligand-centered π-π* (LC) band was blue-shifted by ~10nm. When the ligand was coordinated to iron it led to a red coloured complex with an intense MLCT at 443nm, whilst coordination to ruthenium led to an MLCT band at 393nm. These bands are blue shifted compared to their tpy analogues and this is attributed to the LUMO of the btzpy ligand being higher in energy than the tpy ligand.

The group of Ulrich Schubert carried out a study on the series of complexes $[Ru(tpy)_2]^{2+}$, $[Ru(tpy)(btzpy)]^{2+}$ and $[Ru(btzpy)_2]^{2+}$ (Figure 1.28).[54] Photophophysical and electrochemical properties were studied and it was found that the heteroleptic ruthenium complex exhibits an MLCT band at 432nm mid way between the two MLCT bands for the individual homoleptic btzpy and tpy complexes. Photoluminescence spectra were recorded at 77K and show a pronounced blue-shift of the emission maxima of ~20nm for the heteroleptic complex when compared to that of the homoleptic bis-terpyridine complex. No emission was detected for the homoleptic bis-btzpy complex.

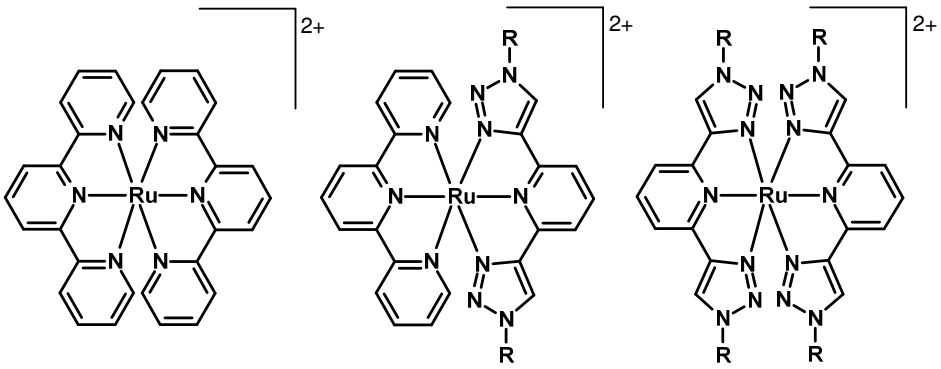

Figure 1.28 Structures of $[Ru(tpy)_2]^{2+}$, $[Ru(tpy)(btzpy)]^{2+}$ and $[Ru(btzpy)_2]^{2+}$

Chandrasekher have prepared octahedral Fe(II) complexes with tridentate ligands containing a central pyridyl donor, pyrazolyl and triazolyl donors in the 2- and 6-position. These new ligands have been termed "super-hybrid" ligands and the iron complexes have shown reversible spin crossover behaviour. [142]

Cyclometallated complexes and metallostar complexes have also been synthesised utilising these types of ligands. Obata, Kakuchi and co-workers reacted an azido functionalised polystyrene polymer with 2,6-diethynylpyridine. The resulting ligand was reacted with Ru(II) to give a four-arm metallostar architecture. [97] O'Reilly *et al.* reported a similar approach to metallostar complexes of Ru(II) and Eu(III).[143]

Yao, Zhong and co-workers have reacted [Ru(tpy)Cl_3] with the bis(triazolyl)benzene ligand to give an octahedral cycloruthenated complex. [144] The same group have also utilised the CuAAC reaction to prepare bridging ligand precursors to construct a mixed-valance system with cyclometalated ruthenium complexes [145, 146] based on, 1,3,6,8-tetrakis(1-butyl-1*H*-1,2,3-triazol-4-yl)pyrene and 3,3',5,5'-tetrakis-(1*H*-1,2,3-triazol-4-yl)biphenyl, the latter complex being shown in Figure 1.29. Electronic coupling was found to be present between mixed-valent redox centres of the one-electron-oxidised complexes. The one-electron oxidation of the complex is mainly associated with the metal center although there is substantial participation from the anionic ligand.

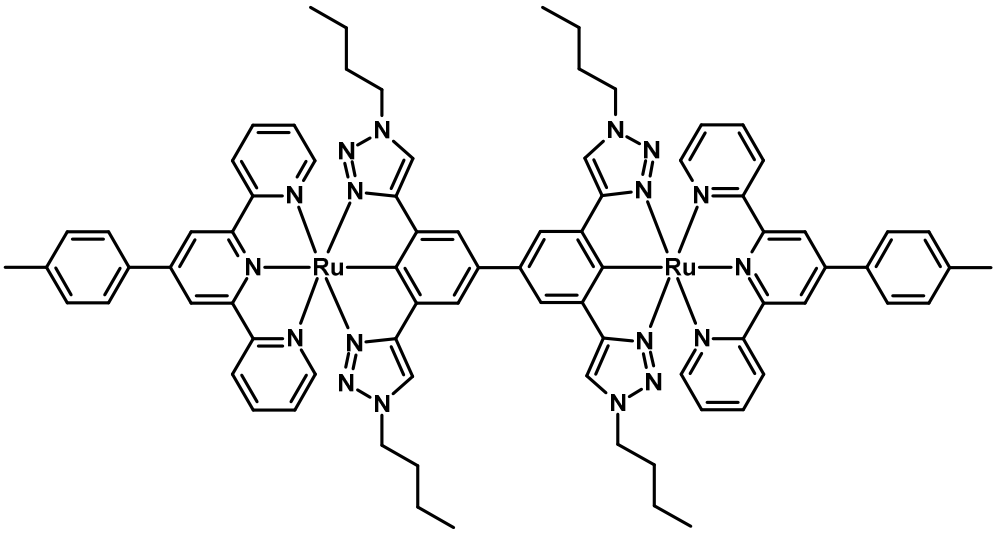

Figure 1.29 Cyclometalated ruthenium bridged complex.

Click-derived tridentate (C,N,C) carbene pincer ligands, derived from btzpy, have been utilised for the preparation of heteroleptic bis(tridentate) ruthenium complexes (Figure 1.30). [147, 148] The absorption profile of these complexes is similar to the related heteroleptic complex with the N,N,N bound ligand, however the absorption MLCT band of these carbene complexes is slightly blue-shifted with respect to that of $[Ru(tpy)_2](PF_6)_2$ complex. The room-temperature emission of the complex revealed red emission with an unstructured emission band and quantum yields similar to those for $[Ru(bpy)_3](PF_6)_2$. The excited-state lifetime of 633 ns is 2500 times longer than that for $[Ru(tpy)_2](PF_6)_2$ and is comparable to $[Ru(bpy)_3](PF_6)_2$. Bis tridentate ruthenium complexes are not usually emissive due to low lying ^{3}MC states arising from the coordination geometry deviating from an ideal octahedral geometry. The good emission properties here are due to the

strong σ-donor properties of the "click" carbene moieties that push up the energy of the ^{3}MC state.

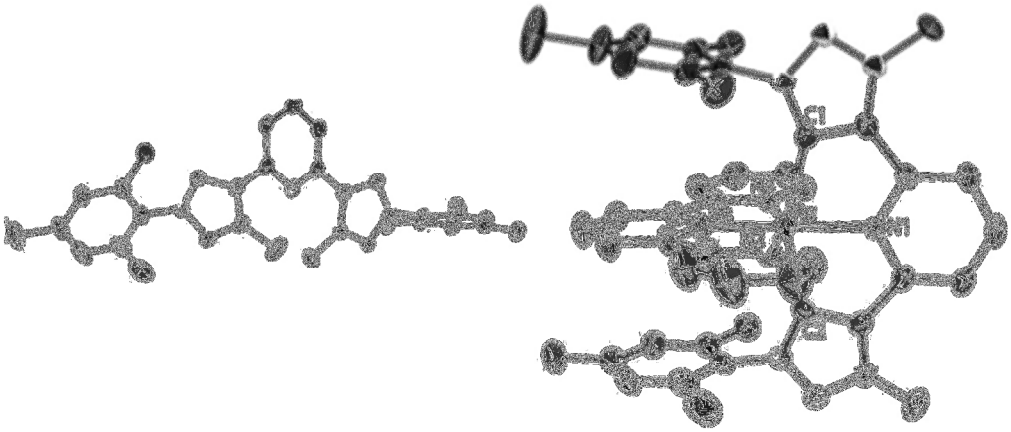

Figure 1.30 Click-derived carbene pincer ligand and heteroleptic bis(tridentate) ruthenium complex. [148]

The more flexible 2,6-bis(4-R-1,2,3-triazol-1-ylmethyl)pyridine ligands related to btzpy have also been studied (Figure 1.31). [12, 149] Crowley and co-workers explored the coordination of these types of ligands with Cu(II) and Ag(I). The silver complex was found to be polymeric in the solid state with the tetrahedral Ag(I) centres coordinated to the pyridyl and triazolyl nitrogens from one ligand along with the other two nitrogen donors from a second identical ligand resulting in a 4,4 net structure.

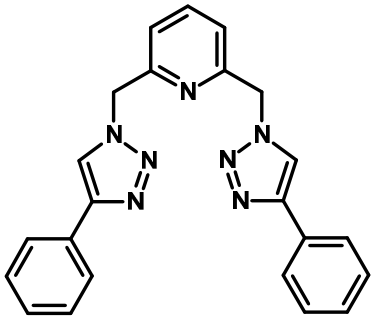

Figure 1.31 Structure of 2,6-bis(4-phenyl-1,2,3-triazol-1-ylmethyl)pyridine ligands

1.4 Peripheral "click" modification of metal complexes

As well as providing a facile route to ligand design and preparation, the CuAAC reaction also provides a versatile route to using the 1,2,3-triazole moiety as a supramolecular linking unit.

The traditional method for the preparation of metallosupramolcular materials has relied on the preparation of bridging ligands with multiple coordination sites into which metal centres can subsequently be incorporated. This methodology suffers from key disadvantages with problems in controlling the selectivity of metal binding when, for example, heterometallic complexes are required and where the bridging ligand is non-symmetric. "Expanded ligand" based approaches [150] have also been championed in which complexes are prepared and modified at their periphery in order to graft onto the complex a second binding domain.

A desirable route to such architectures would involve coupling discrete preformed complexes into supramolecular complexes under mild conditions, requiring as few steps as possible. Such an approach would require a coupling reaction that is highly efficient and high yielding and for which the required functional groups for the coupling reaction can be easily incorporated into the periphery of the metal complex components. With such a methodology in place and a library of suitably derivatised transition metal complex components available, this would allow facile access to supramolecular architectures with an extraordinary diversity of structure. The CuAAC reaction is therefore an excellent candidate for this purpose.

A few reports have appeared on the CuAAC modification of transition metal complexes with peripheral alkyne functionalities. Ren first demonstrated the peripheral modification of an alkynyl-substituted diruthenium paddlewheel complex[151, 152] whilst Wang *et al.* tethered an alkyne-substituted luminescent iridium complex to an azide functionalised polymer. [153] More recently, Sierra and co-workers reported the formation of dinuclear complexes from alkynyl substituted Fisher carbene complexes of pentacarbonylchromium(0) by CuAAC coupling with bisazide spacers including bis(azidomethyl)ferrocene.[154] Similar results have been obtained with analogous pentacarbonyltungsten(0) complexes. [155] Constable *et al*. have demonstrated the coupling of azidosugars with alkyne-functionalised bipyridyl ligands and the preparation of their ruthenium complexes.[156]

The comparable use of azido-functionalised complexes is far less developed. Azidoferrocenes have been used for the preparation of ferrocenyl triazoles which have subsequently been used as monodentate ligands for example.[157] Fallahpour has developed routes to azide derivatives of bipyridyl and terpyridyl[158-160] ligands and demonstrated the formation of an azidoterpyridyl Fe(II) complex. Attempts to prepare their ruthenium complexes led to azide reduction to the amine under the conditions used, however. Recently, Aukauloo and co-workers have utilized an azido bipyridyl ligand to prepare a chromophore tagged ligand and have shown efficient electron transfer through the triazole linker.[161] There remains, however, very little in the literature regarding the CuAAC functionalisation of complexes with coordinated azide-substituted ligands. Beyond ferrocene, the first example of CuAAC modification of an azide functionalized complex was demonstrated by

Constable and co-workers using bis(azidoterpyridyl)iron(II) where the ligand can be attached to the metal under mild conditions.[162] The iron complex was prepared by reacting the ligand in excess with $FeCl_2.4H_2O$ in EtOH at room temperature and was characterised by X-ray crystallography which showed that the ligand had been successfully coordinated to the metal with the azide remaining intact (Figure 1.32). This complex was then reacted with phenylacteylene in the presence of copper(I). IR spectroscopy revealed that the azide stretch at 2110cm^{-1} had disappeared and in the ^1H NMR a singlet resonance was observed at δ 9.35 was assigned to the triazole ring proton. The complex was characterised by X-ray crystallography which showed the successful formation of 1,2,3-triazole appended complex (Figure 1.32).

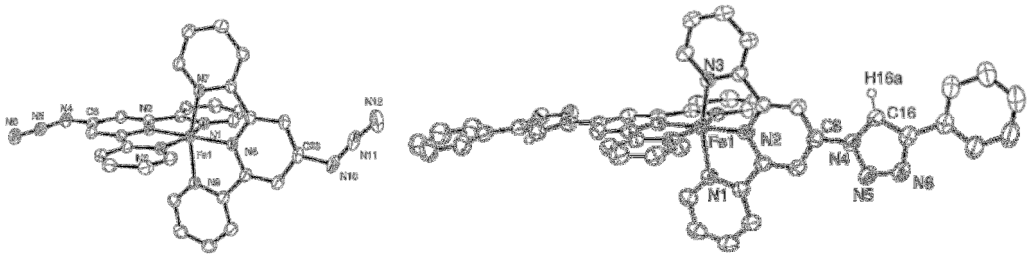

Figure 1.32 Molecular structure of bis(azidoterpyridyl)iron(II) and bis(1-phenyl-4-tpy-1,2,3-triazolyl)iron(II) complexes [162]

1.5 Summary and Overlook

The CuAAC has proven to be one of the most versatile ligation reactions available. The reaction is simple and robust and has led to many applications in many areas of chemistry and biochemistry. Despite the fact that the 1,2,3-triazoles formed in the reaction are capable of coordination through the *N2*, *N3* or *C5* to a wide range of transition metals, the potential of the CuAAC in coordination chemistry has only just begun to be fully exploited. The main advantage of the CuAAC reaction in all applications is the modular nature of the reaction and good functional group tolerance. These factors are particularly important when studying metal chelating systems, as they allow a number of potential ligands to be easily prepared in high yields with minimal synthetic effort. Another useful factor of the 1,2,3-triazole moieties, with respect to metal chelating systems is that further functionality can easily be introduced in to the N1 and C4 positions, enabling the synthesis of polydentate ligand systems, where the 1,2,3-triazole is an integral part of the metal chelator. The modular nature of the reaction provides a straightforward opportunity to systematically tune the electronic properties of the metal centre, the steric requirements of the ligand, hydrophilicity, charge and other physicochemical properties of the resulting complexes. These properties are all crucial in the preparation of metal complexes for use in catalysis, environmental and pharmaceutical applications. As the examples discussed have highlighted, the CuAAC reaction is beginning to be utilised for the preparation of ligands for a wide range of metals and applications. Given the ease with which novel chelators can be prepared and elaborated, it is anticipated that the number and diversity of applications will continue to increase.

2 EXPERIMENTAL

2.1 General

Reagents and solvents were purchased from Aldrich and Acros Organics and used as supplied, $[Re(bpy)(CO)_3Cl]$ [163], $[Re(bpy)(CO)_3(Py)](PF_6)$ [163], $[Ru(bpy)_2Cl_2]$ [164] and $[Ir(ppy)_2Cl]_2$ [165] were all prepared according to literature procedures. NMR spectra were recorded in Bruker 500 Avance and 400 AMX spectrometers, UV-visible absorption spectra recorded on a Varian Cary 300 spectrometer and luminescence spectra on a Hitachi F-4500 spectrometer (spectra were not corrected for detector response). Solution infrared spectra in dichloromethane were recorded on a Nicolet 380 FTIR spectrometer. Mass spectra were collected on a Bruker Micro-Q-TOF instrument. Luminescent lifetime measurements were carried out using an Edinburgh Instruments Mini-Tau spectrometer.

Caution: Low molecular weight azides are often thermally and shock sensitive and may detonate. Therefore, low molecular weight azides should **never** be isolated and should only be generated *in situ* in solution and used immediatly.

2.1.1 Electrochemistry

2.1.1.1 Instrumentation

Measurements were recorded using a μ-autolab potentiometer with autolab USB interface The software installed was a General Purpose Electrochemical System (GPES) with Windows 1998. Using Ag/AgCl reference electrode. The electrode potential of this electrode is +0.197 V (against the standard hydrogen electrode) and platinum wire counter electrode. Tetrabutylammonium tetrafluoroborate was employed as the electrolyte. Measured potentials were referenced against Fc/Fc^{+} redox couple.

2.2 Ligand Synthesis

2.2.1 Synthesis of 4-phenyl-1-methyl-1,2,3-triazole (1a)

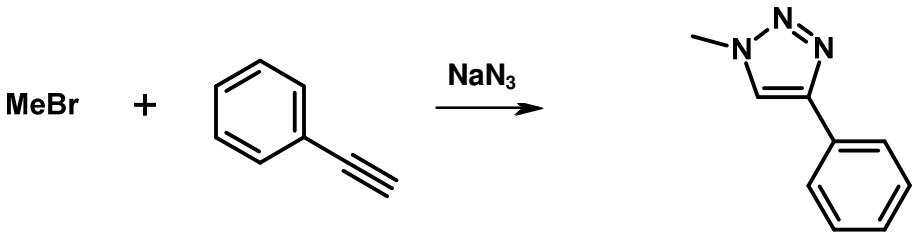

Iodomethane (3.55 mL, 11 mmol) and sodium azide (0.61 g, 9.38 mmol) were combined in dimethyl sulfoxide (15 mL) with one crystal of potassium iodide. The mixture was stirred at room temperature for two hours. The following reagents were then added to the reaction mixture in the following order: water (7 mL), phenylacetylene (1.2 mL, 11 mmol), 1M sodium ascorbate solution (1.2 mL, 1.2 mmol), copper sulfate pentahydrate (35 mg, 0.14 mmol) in water (0.3 mL), 2,6-lutidine (1.28 mL, 11 mmol). The mixture was stirred at room temperature for 12 hours. The reaction mixture was then diluted with water (25 mL) and the solid filtered and washed with water (25 mL) and dilute ammonia (25 mL). The solid was air dried and washed with petroleum ether (40-60 ^{o}C, 25 mL). (1.17 g, 67 %)

^{1}H NMR ($CDCl_3$) δ (ppm) 7.84 (d, *J* = 7.6 Hz, 2H, o-Ph); 7.77 (s, 1H, triazole CH); 7.45 (t, *J* = 7.5 Hz, 2H, m-Ph); 7.34 (tt, *J* = 7.4, 2.1 Hz, 1H, p-Ph); 4.18 (s, 3H, Me); ^{13}C NMR ($CDCl_3$) δ (ppm) 148.1; 130.6; 128.9; 128.2; 125.7; 120.6; 36.8. MS (ESI) *m*/*z* 182.1 (M + Na).

2.2.2 Synthesis of 4-phenyl-1-propyl-1,2,3-triazole (1b)

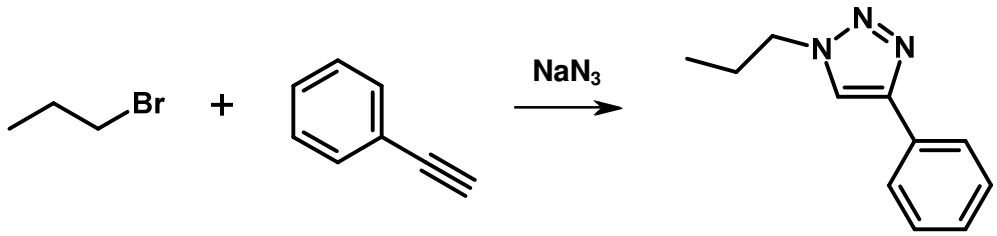

1-bromopropane (1 mL, 11 mmol) and sodium azide (0.61 g, 9.38 mmol) were combined in dimethyl sulfoxide (15 mL) with one crystal of potassium iodide. The mixture was stirred at room temperature for two hours. The following reagents were then added to the reaction mixture in the following order: water (7 mL), phenylacetylene (1.2 mL, 11 mmol), 1M sodium ascorbate solution (1.2 mL, 1.2 mmol), copper sulfate pentahydrate (35 mg, 0.14 mmol) in water (0.3 mL), 2,6-lutidine (1.28 mL, 11 mmol). The mixture was stirred at room temperature for 12 hours. The reaction mixture was then diluted with water (25 mL) and the solid filtered and washed with water (25 mL) and dilute ammonia (25 mL). The solid was air dried and washed with petroleum ether (40-60 ^{o}C, 25 mL). (1.46 g, 71%)

H NMR ($CDCl_3$) δ (ppm) 7.85 (d, J = 4.2 Hz, 2H, o-Ph); 7.77 (s, 1H, Tz); 7.44 (t, J = 7.5 Hz, 2H, m-Ph); 7.34 (t, J = 7.4 Hz, 1H, p-Ph); 4.38 (t, J = 7.2 Hz, 2H, CH_2); 1.99 (sextet, J = 7.3 Hz, 2H, CH_2); 1.00 (t, J = 7.6 Hz, 3H, Me); ^{13}C NMR ($CDCl_3$) δ (ppm) 147.8; 130.8; 128.9; 128.2; 125.8; 119.6; 52.1; 23.9; 11.2 MS (ESI) m/z 210.1 (M + Na). HRMS (ESI) calcd: 210.100169, found 210.100285.

2.2.3 Synthesis of 4-phenyl-1-benzyl-1,2,3-triazole. (1c)

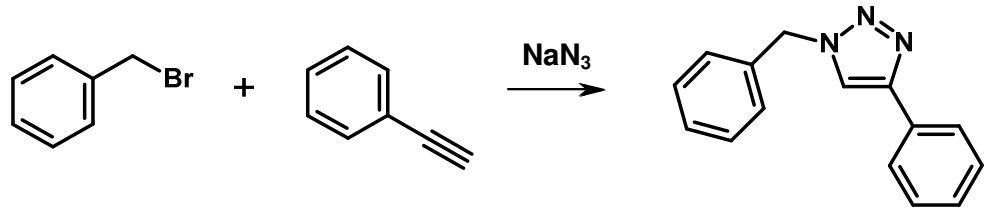

Bromomethylbenzene (0.88 mL, 11 mmol) and sodium azide (0.61 g, 9.38 mmol) were combined in dimethyl sulfoxide (15 mL) with one crystal of potassium iodide. The mixture was stirred at room temperature for two hours. The following reagents were then added to the reaction mixture in the following order: water (7 mL), phenylacetylene (1.2 mL, 11 mmol), 1M sodium ascorbate solution (1.2 mL, 1.2 mmol), copper sulfate pentahydrate (35 mg, 0.14 mmol) in water (0.3 mL), 2,6-lutidine (1.28 mL, 11 mmol). The mixture was stirred at room temperature for 12 hours. The reaction mixture was then diluted with water (25 mL) and the solid filtered and washed with water (25 mL) and dilute ammonia (25 mL). The solid was air dried and washed with petroleum ether (40-60 ^{o}C, 25 mL). (1.16 g, 45%)

^{1}H NMR ($CDCl_3$) δ (ppm) 7.82 (d, J = 7.26 Hz, 2H, o-Ph); 7.68 (s, 1H, Tz), 7.45–7.30 (m, 8H, Ar); 5.98 (s, 2H, CH_2); ^{13}C NMR ($CDCl_3$) δ (ppm) 148.3; 134.7; 130.6; 129.2; 128.9; 128.3; 128.1; 125.8; 119.6; 54.3. MS (ESI) m/z 258.1 (M + Na) HRMS (ESI) calcd: 258.100169, found: 285.099385.

2.2.4 Synthesis of 4-(*p*-tolyl)-1-propyl-1,2,3-triazole (1d)

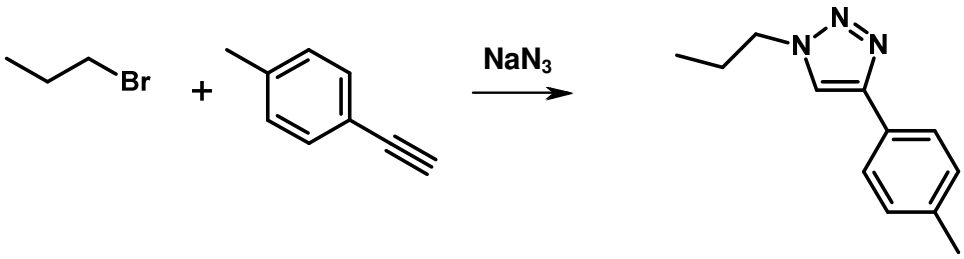

1-bromopropane (1 mL, 11 mmol) and sodium azide (0.61 g, 9.38 mmol) were combined in dimethyl sulfoxide (15 mL) with one crystal of potassium iodide. The mixture was stirred at room temperature for two hours. The following reagents were then added to the reaction mixture in the following order: water (7 mL), *p*-tolylacetylene (1.39 mL, 11 mmol), 1M sodium ascorbate solution (1.2 mL, 1.2 mmol), copper sulfate pentahydrate (35 mg, 0.14 mmol) in water (0.3 mL), 2,6-lutidine (1.28 mL, 11 mmol). The mixture was stirred at room temperature for 12 hours. The reaction mixture was then diluted with water (25 mL) and the solid filtered and washed with distilled water (25 mL) and dilute ammonia (25 mL). The solid was air dried and washed with petroleum ether (40-60 ^{o}C, 25 mL). (1.41 g, 64 %)

^{1}H NMR ($CDCl_3$) δ (ppm): 7.75 (s, 1H, Tz); 7.73 (d, J = 7.9 Hz, 2H, Ar); 7.25 (d, J = 7.9 Hz, 2H, Ar); 4.38 (t, J = 7.1Hz, 2H, CH_2); 2.40 (s, 3H, $ArCH_3$); 1.99 (sextet, J = 7.3 Hz, 2H, CH_2); 1.00 (t, J = 7.5Hz, 3H, Me); ^{13}C NMR ($CDCl_3$) δ (ppm): 147.9; 138.0; 129.6; 128.0; 125.7; 119.2; 52.1; 23.9; 21.4; 11.2 MS (ESI) m/z 224.1 (M + Na). HRMS (ESI) calcd: 224.115819, found: 224.115713.

2.2.5 Synthesis of 2,2'-bipyridyl-N-oxide [166]

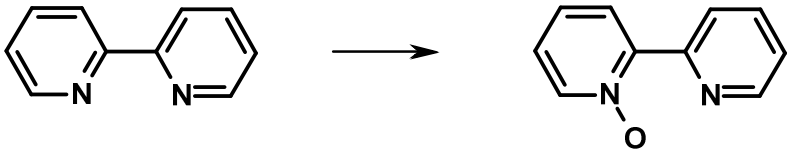

A solution of 2,2'-bipyridyl (7.00 g, 44.82 mmol) in $CHCl_3$ (25 mL), was stirred at 0 °C, for 35 min. A solution of *m*-chloroperbenzoic acid (84.5%, 9.156 g, 44.8 mmol) in $CHCl_3$ (87 mL), was then added dropwise over 80 min and the mixture allowed to stir at room temperature for 13.5 h. The solution was washed three times with portions of 5% aqueous Na_2CO_3 (500 mL), dried ($MgSO_4$), and evaporated to give an oil. To remove unreacted 2,2'-bipyridyl, the residual oil was extracted with boiling hexane. The upper hexane layer was discarded and the remaining oil dried under vacuum to give the product as a hygroscopic solid. To improve yield, the aqueous Na_2CO_3 washings were extracted with $CHCl_3$ (4 x 45 mL). The organic layer was dried ($MgSO_4$) and evaporated to provide more of the grey-brown 2,2'-bipyridyl N-oxide. (total yield 4.27 g, 55 %)

^{1}H NMR ($CDCl_3$) δ (ppm): 8.81 (dt, J = 8.2 & 1.0 Hz, 1H); 8.64 (ddd, J = 4.8 & 1.0 Hz, 1H); 8.23 (dd, J = 6.5 & 1.0 Hz, 1H); 8.08 (dd, J = 8.0 & 2.1 Hz, 1H); 7.74 (dt, J = 7.7 & 1.7 Hz, 1H); 7.31-7.24 (m, 1H); 7.19 (dt, J = 6.6 & 2.2 Hz, 1H).

2.2.6 Synthesis of 4-nitro-2,2'-bipyridyl-N-oxide [166]

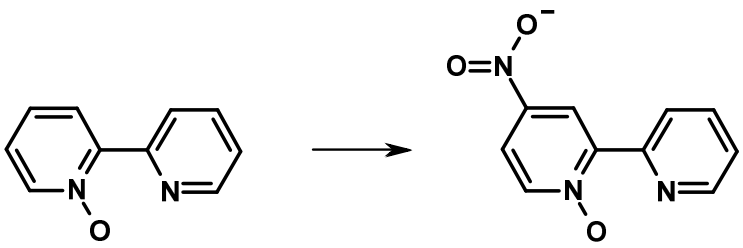

2,2'-bipyridyl-N-oxide (5.00 g, 28.7 mmol) was dissolved in concentrated sulfuric acid (20 mL), whilst in an ice bath. Fuming nitric acid (30 mL) in concentrated sulfuric acid (20mL) was added to the mixture over 20 minutes with stirring. The mixture was heated at 100 °C for 2 hours. The solution was poured onto ice and the pH was adjusted to 13 with aqueous sodium hydroxide, (25% v/v). The orange-brown precipitate was collected by filtration. The filtrate was dissolved in $CHCl_3$ and filtered to remove any 4,4'-dinitro-2,2'-bipyridyl. The $CHCl_3$ was then removed under vacuum to yield a pale yellow solid. (4.08 g, 65 %)

^{1}H NMR ($CDCl_3$) δ (ppm): 9.18 (d, J = 3.4 Hz, 1H); 8.90 (dt, J = 8.1 & 0.8 Hz, 1H); 8.81 (ddd, J = 4.8 & 0.9 Hz, 1H); 8.38 (d, J = 7.3 Hz, 1H); 8.09 (dd, J = 7.3 & 3.3 Hz, 1H); 7.90 (td, J = 7.8 & 1.7 Hz, 1H); 7.46 (ddd, J = 6.2, 4.8 & 1.22 Hz, 1H)

2.2.7 Synthesis of 4-nitro-2,2'-bipyridyl [166]

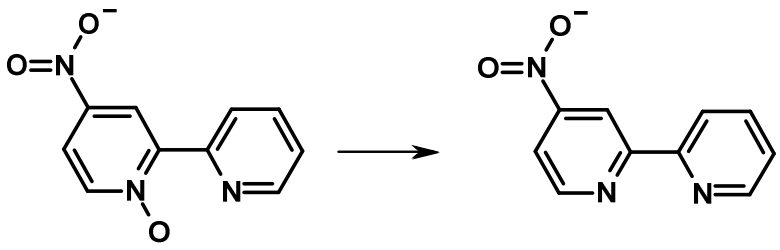

4-nitro-2,2'-bipyridyl-N-oxide (3.00 g, 13.6 mmol) was refluxed in PCl_3 (25 mL, 290 mmol) for 21 hours. The reaction mixture was poured into 200 mL of ice water. This was then basified to pH 13 with concentrated NaOH and extracted exhaustively with $CHCl_3$. The combined $CHCl_3$, layers were dried ($MgSO_4$) and evaporated to yield a pale yellow solid. (2.21 g, 80 %)

^{1}H NMR ($CDCl_3$) δ (ppm): 9.18 (d, J = 2.2 Hz, 1H); 8.97 (d, J = 5.3 Hz, 1H); 8.77 (d, J = 4.3 Hz, 1H); 8.49 (dt, J = 8.0 & 0.9 Hz, 1H); 8.04 (dd, J = 5.4 & 2.2 Hz, 1H); 7.90 (td, J = 7.6 & 1.8 Hz, 1H); 7.43 (ddd, J = 6.2, 4.9 & 1.2 Hz, 1H)

2.2.8 Synthesis of 4-azido-2,2'-bipyridyl (4a) [167]

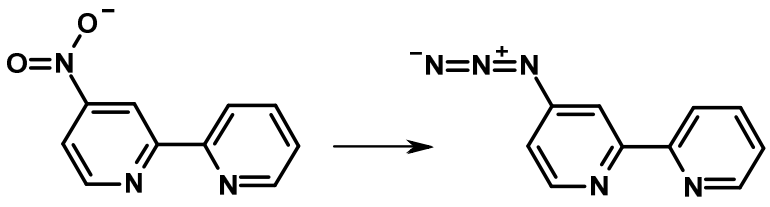

A mixture of 4-nitro-2,2'-bipyridyl (0.57 g, 0.4 mmol) and NaN_3 (1.50 g, 3.85 mmol) was heated in DMF (25 mL) for 3 hours at 100 °C. The DMF was removed by rotary evaporation and water (40 mL) was added, the mixture was extracted with DCM (3 x 50 mL) and the combined organic phase was dried over $MgSO_4$ and the solvent was removed. 4-azido-2,2'-bipyridyl was purified by column chromatography (silica gel, DCM/AcOEt 1:1) to yield a yellow solid. (0.52 g, 93.54 %)

^{1}H NMR ($CDCl_3$) δ (ppm): 8.69 (ddd, J = 4.8, 1.8 & 0.9 Hz, 1H, H-6'); 8.58 (d, J = 5.4 Hz, 1H, H-6); 8.40 (dt, J = 7.8 & 0.9 Hz, 1H, H-4'); 8.15 (d, J = 2.3 Hz, 1H, H-3); 7.83 (td, J = 7.8 & 1.8, 1H, H-5'); 7.34 (ddd, J = 7.5, 4.8 & 1.2, 1H, H-3'); 6.94 (dd, J = 5.4 & 2.3 Hz, 1H, H-5). ^{13}C NMR (CD3Cl) δ (ppm): 160.0; 155.2; 150.5; 149.8; 149.2; 137.1; 124.3; 121.3; 114.2; 111.2. MS: (ESI) m/z 220 (M+Na). HRMS: calcd: 220.059366, found: 220.058833. IR (ATR) 2115 cm-1.

2.2.9 Synthesis of 2,2'-bipyridyl-N,N'-dioxide [168]

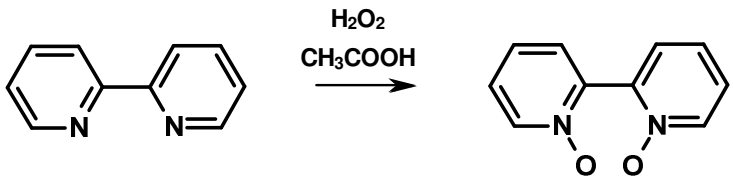

A mixture of 2,2'-bipyridyl (15.7 g, 0.1 mol), hydrogen peroxide (20.4 mL, 30%) and glacial acetic acid (120 mL) was heated at 80 °C for 3 hours. Hydrogen peroxide (15 mL, 30%) was added and the heating was continued for a further 4 hours. The pale yellow solution was allowed to cool to room temperature and slowly added to acetone (1500 mL). Upon cooling a white solid of 2,2'-bipyridyl-N,N'-dioxide precipitated and was collected by filtration and air dried. (10.87 g, 56.3 %)

^{1}H NMR (d_6-Me_2SO) δ (ppm): 8.36 (d, J = 6.4 Hz, 2H); 8.64 (dd, J = 7.8 & 1.8 Hz, 2H); 7.52 (td, J = 7.8 & 2.0 Hz, 2H); 7.42 (t, J = 7.7 Hz, 2H)

2.2.10 Synthesis of 4,4'-dinitro-2,2'-bipyridyl-N,N'-dioxide [168]

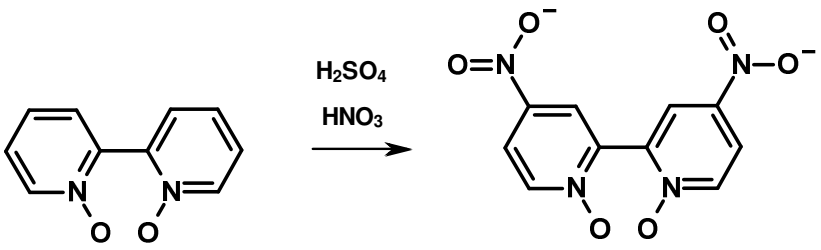

A solution of 2,2'-bipyridyl-N,N'dioxide (5.6g, 29.8mmol) in conc. H2SO4 (20mL) was cooled to 5°C and then fuming nitric acid (12mL) was added dropwise. The brown solution was heated at 120°C for 5 hours under reflux. The reaction mixture was allowed to cool to room temperature and then quenched by pouring it on to an ice-water (50% w/v) solution, which gave a pale yellow precipitate which was collected by filtration and washed several times with water and acetone, and allowed to air dry to yield a pale yellow solid as 4,4'-dinitro-2,2'-bipyridyl-N,N'-dioxide. (2.72g, 32 %)

^{1}H NMR (d_6-Me_2SO) δ (ppm): 8.70 (d, J = 3.4 Hz, 2H); 8.60 (d, J = 7.2 Hz, 2H); 8.37 (dd, J = 7.2 & 3.3 Hz, 2H)

2.2.11 Synthesis of 4,4'-dinitro-2,2'-bipyridyl [168]

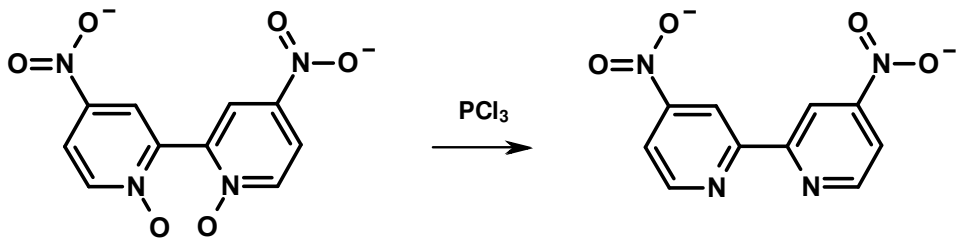

4,4'-Dinitro-2,2'-bipyridyl-N,N-dioxide (3.00 g, 10.8 mmol) was refluxed in PCl_3 (25 mL, 290 mmol) for 21 hours. The reaction was thrown into 200 mL of ice water. This was then basified to pH 13 with concentrated NaOH and extracted exhaustively with $CHCl_3$. The combined $CHCl_3$, layers were dried ($MgSO_4$) and evaporated to give a yellow solid. (2.22 g, 83 %)

^{1}H NMR ($CDCl_3$) δ (ppm): 9.24 (d, J = 2.1 Hz, 2H); 9.06 (d, J = 5.3 Hz, 2H); 8.15 (dd, J = 5.3 & 2.1 Hz, 2H).

2.2.12 Synthesis of 4,4'-dinitro-2,2'-bipyridyl (4b)

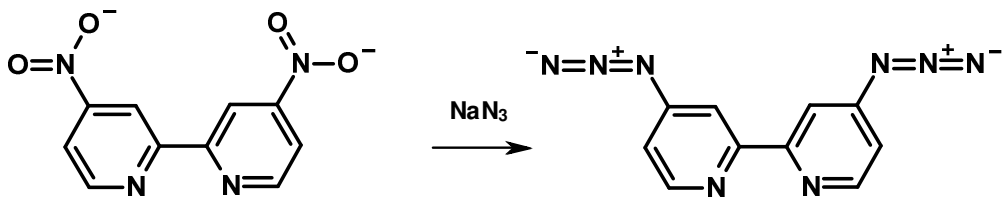

A mixture of 4,4'-dinitro-2,2'-bipyridyl (0.10 g, 0.4 mmol) and NaN_3 (0.25 g, 3.85 mmol) was heated in DMF (10 mL) for 3 hours at 100 °C. The DMF was removed by rotary evaporation and water (40 mL) was added, the mixture was extracted with dichloromethane (3 x 30 mL) and the combined organic phase was dried over $MgSO_4$ and the solvent was removed. 4,4'-diazido-2,2'-bipyridyl was purified by column chromatography (silica gel, DCM/AcOEt 1:1) to yield a yellow solid. (0.09 g, 95.0 %)

^{1}H NMR ($CDCl_3$) δ (ppm): 8.58 (d, J = 5.4 Hz, 2H, H-6); 8.14 (d, J = 2.2 Hz, 2H, H-3); 6.96 (dd, J = 5.4 & 2.2 Hz, 2H, H-5). ^{13}C NMR ($CDCl_3$) δ (ppm): 157.3; 150.8; 150.3; 114.9; 111.8; MS (ESI) m/z 261 (M+Na). HRMS calcd 261.060765; found 261.060763. IR (ATR) 2117 cm^{-1}.

2.2.13 Synthesis of 4-phenyl-1-(2,2'-bipyrid-4-yl)-1,2,3-triazole (5a)

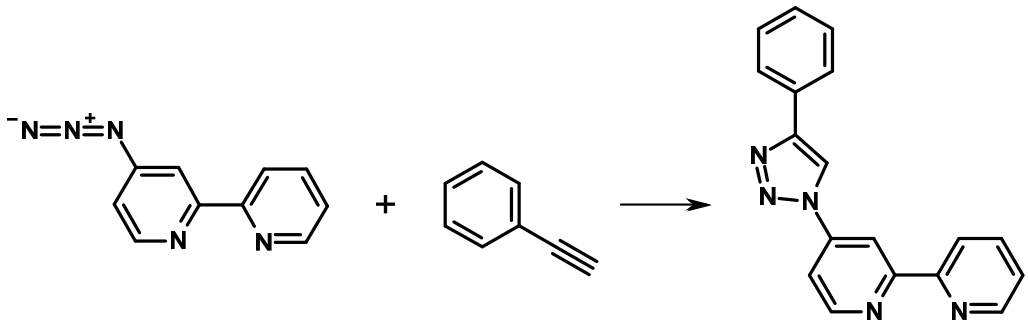

4-azido-2,2'-bipyridyl (0.5 g, 2.54 mmol) and phenylacetylene (0.39 g, 3.80 mmol) were dissolved in THF (30 mL) and water was added (30 mL). At 20 °C $CuSO_4$ (1M aqueous solution 2.54 mL) was added followed by freshly prepared sodium ascorbate solution (1M aqueous solution 5.08 mL) dropwise. The solution was allowed to stir at room temperature for 1 hour. After removing the THF under vacuum, dichloromethane (30 mL) and concentrated ammonia solution (15 mL) were added to the solution. The solution was allowed to stir for a further 30 mins. at room temperature to remove any remaining Cu(I). The organic phase was washed twice with water (30 mL) and once with brine (30 mL) and dried over $MgSO_4$. The solvent was removed under vacuum and the product was recrystallised from dichloromethane and hexane to yield a buff coloured solid. (0.58g, 76.3%)

^{1}H NMR ($CDCl_3$) δ (ppm): 8.84 (d, J = 5.3 Hz, 1H, bpy H-6); 8.75 (d, J = 2.1 Hz, 1H, bpy H-3); 8.72 (d, J = 4.5 Hz, 1H, py); 8.50 (d, J = 8.0 Hz, 1H, py); 8.48 (s, 1H, Tz); 7.99 (dd, J = 5.3 & 2.1 Hz, 1H, py(tz)); 7.94 (d, J = 7.7 Hz, 2H, Ph); 7.87 (td, J = 7.7 & 1.6 Hz, py); 7.48 (t, J = 7.7 Hz, 2H, Ph); 7.39 (m, 2H, Ph & py). ^{13}C NMR ($CDCl_3$) δ (ppm): 158.5; 154.8; 151.1; 149.3; 149.0; 144.1; 137.1; 129.8; 129.0; 128.8; 126.0; 124.5; 121.4; 116.9; 113.9; 110.2. MS (ESI) m/z 322 (M+Na). HRMS: calcd 322.106317, found 322.106153.

2.2.14 Synthesis of 4-ferrocenyl-1-(2,2'-bipyrid-4-yl)-1,2,3-triazole (5b)

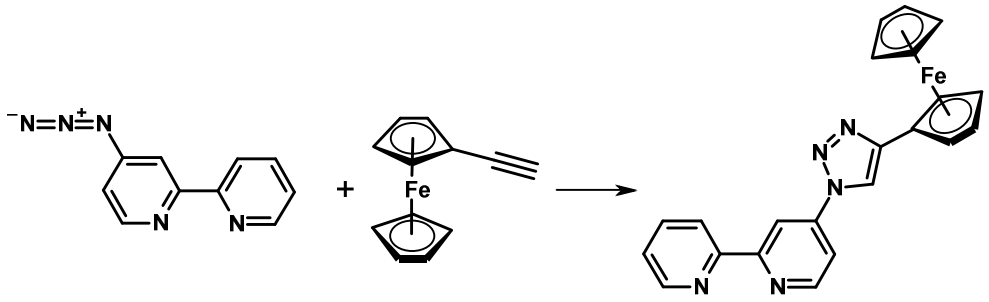

4-azido-2,2'-bipyridyl (0.10 g, 0.51 mmol) and ethynylferrocene (0.16 g, 0.76 mmol) was dissolved in THF (15 mL) and water was added (15 mL). At 20 °C was added $CuSO_4$ (1M aqueous solution 0.51 mL) was added followed by freshly prepared sodium ascorbate solution (1M aqueous solution 1.01 mL) dropwise. The solution was allowed to stir at room temperature for 1 hour. After removing the THF under vacuum, dichloromethane (30 mL) and concentrated ammonia solution (10 mL) were added to the solution. The solution was allowed to stir for a further 30 mins. at room temperature to remove any remaining Cu(I). The organic phase was washed twice with water (15 mL) and once with brine (15 mL) and dried over $MgSO_4$. The solvent was removed under vacuum and the product was recrystallised from dichloromethane and hexane to yield an orange coloured solid. (0.087 g, 42.0 %)

^{1}H NMR ($CDCl_3$) δ (ppm): 8.83 (d, J = 5.4 Hz, 1H, py(tz)); 8.74 (ddd, J = 4.7, 1.7 & 0.7 Hz, 1H, py); 8.69 (d, J = 2.0 Hz, 1H, py(tz)); 8.51 (d, J = 7.9 Hz, 1H, py); 8.18 (s, 1H, Tz); 8.01 (dd, J = 5.4 & 2.1 Hz, 1H, py(tz)); 7.89 (td, J = 7.7 & 1.7 Hz, 1H py); 7.40 (ddd, J = 7.6, 4.7 & 1.2 Hz, 1H, py); 4.82 (t, J = 1.9 Hz, 2H, C_5H_4Fe); 4.37 (t, J = 1.9 Hz, 2H, C_5H_4Fe); 4.12 (s, 5H, Cp). ^{13}C NMR ($CDCl_3$) δ (ppm): 158.4; 154.9; 151.1; 149.2; 148.5; 144.2; 137.2; 124.5; 121.5; 115.7; 113.9; 110.0; 74.3; 69.7; 69.1; 66.9. MS (ESI) m/z 430 (M+Na). HRMS: calcd: 430.072559, found: 430.073052.

2.2.15 Synthesis of 4-pyrid-2-yl-1-(2,2'-bipyrid-4-yl)-1,2,3-triazole (5c)

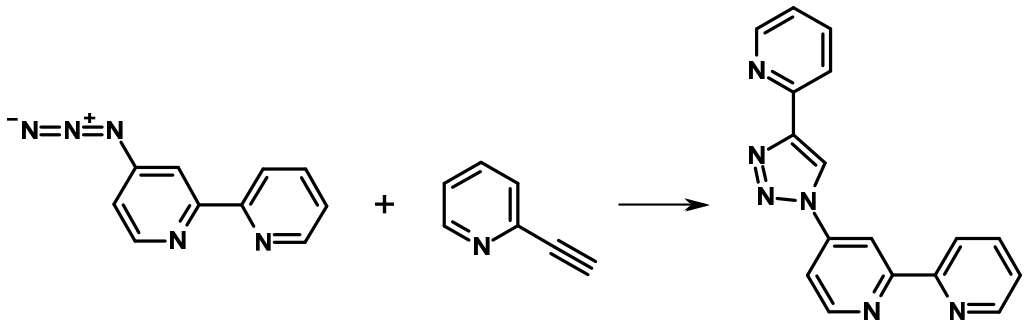

4-azido-2,2'-bipyridyl (0.25 g, 1.27 mmol) and 2-ethynylpyridine (0.196 g, 1.90 mmol) was dissolved in THF (30 mL) and water was added (30 mL). At 20 °C was added $CuSO_4$ (1M aqueous solution 1.27 mL) was added followed by freshly prepared sodium ascorbate solution (1M aqueous solution 2.54 mL) dropwise. The solution was allowed to stir at room temperature for 1 hour. After removing the THF under vacuum, dichloromethane (30 mL) and concentrated ammonia solution (15 mL) were added to the solution. The solution was allowed to stir for a further 30 mins. at room temperature to remove any remaining Cu(I). The organic phase was washed twice with water (30 mL) and once with brine (30 mL) and dried over $MgSO_4$. The solvent was removed under vacuum and the product was recrystallised from dichloromethane and hexane to yield a white coloured solid. (0.31 g, 81.4 %)

^{1}H NMR ($CDCl_3$) δ (ppm): 8.91 (s, 1H, Tz); 8.88 (d, J = 2.1 Hz, 1H, bpy py(tz)); 8.85 (d, J = 5.4 Hz, 1H, bpy py(tz)); 8.72 (ddd, J = 4.8, 1.8 & 0.8 Hz, 1H, pyA); 8.65 (ddd, J = 4.8, 1.7 & 0.8 Hz, 1H, py); 8.49 (dt, J = 8.0 & 0.8 Hz, 1H, pyA); 8.27 (dt, J = 8.0 & 0.9 Hz, 1H, pyB); 7.97 (dd, J = 5.4 & 2.2 Hz, 1H, bpy py(tz)); 7.87 (td, J = 7.8 & 1.7 Hz, 1H, pyA); 7.84 (td, J = 7.8 & 1.7 Hz, 1H, pyB); 7.38 (ddd, J = 7.5, 4.8 & 1.2 Hz, 1H, pyA); 7.30 (ddd, J = 7.7, 4.8 & 1.2 Hz, 1H, pyB). ^{13}C NMR ($CDCl_3$) δ (ppm): 158.7; 154.8; 151.1; 149.7; 149.6; 149.56; 149.4; 144.1; 137.1; 137.0; 124.5; 123.4; 121.3; 120.6; 119.6; 113.8; 110.7. MS (ESI) m/z 323 (M+Na). HRMS: calcd: 323.101566, found: 323.101593

2.2.16 Synthesis of 4-pyrid-2-yl-1-benzyl-1,2,3-triazole. (10)

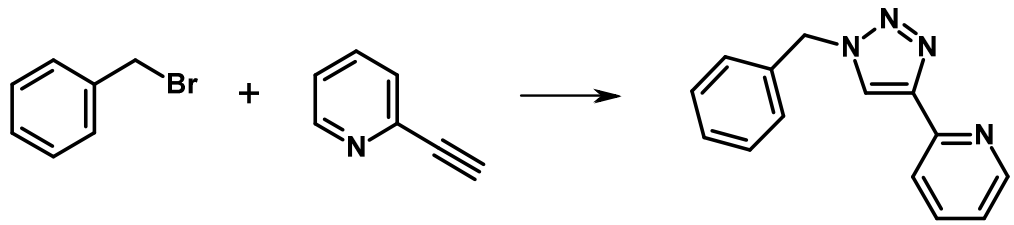

Bromomethylbenzene (0.88 mL, 11 mmol) and sodium azide (0.61 g, 9.38 mmol) were combined in dimethyl sulfoxide (15 mL) with one crystal of potassium iodide. The mixture was stirred at room temperature for two hours. The following reagents were then added to the reaction mixture in the following order: water (7 mL), 2-ethynylpyridine (1.2 mL, 11 mmol), 1M sodium ascorbate solution (1.2 mL, 1.2 mmol), copper sulfate pentahydrate (35 mg, 0.14 mmol) in water (0.3 mL), 2,6-lutidine (1.28 mL, 11 mmol). The mixture was stirred at room temperature for 12 hours. The reaction mixture was then diluted with water (25 mL) and the solid filtered and washed with water (25 mL) and dilute ammonia (25 mL). The solid was air dried and washed with petroleum ether (40-60 °C, 25 mL). (1.96 g, 75%)

^{1}H NMR (400 MHz, $CDCl_3$): δ (ppm) 8.53 (ddd, J = 4.9, 1.8 & 1.0 Hz, 1H, 6-pyH); 8.17 (dt, J = 7.9 & 1.1 Hz, 1H, 3-pyH); 8.04 (s, 1H, 5-triazole H); 7.76 (dt, J = 7.8 & 1.8 Hz, 1H, 4-pyH); 7.40–7.31 (m, 5H, PhH); 7.20 (ddd, J = 7.5, 4.9 & 1.2 Hz, 1H, 5-pyH); 5.58 (s, 2H, CH_2). ^{13}C NMR (100 MHz, $CDCl_3$): δ (ppm) 150.1; 149.2; 148.6; 136.8; 134.2; 129.1; 128.7; 128.2; 122.7; 121.7; 120.1; 54.45

2.2.17 Synthesis of di-([1-{2,2'-bipyrid-4-yl}-1,2,3-triazol-4-yl]methyl)ether (21)

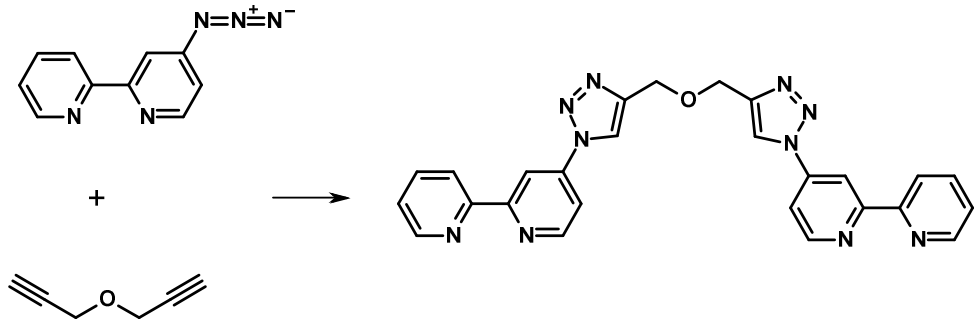

4-azido-2,2'-bipyridyl (0.25 g, 1.27 mmol) and propargyl ether (0.36 g, 3.83 mmol) was dissolved in THF (30 mL) and water was added (30 mL). At 20 °C was added $CuSO_4$ (1M aqueous solution 2.50 mL) was added followed by freshly prepared sodium ascorbate solution (1M aqueous solution 5.00 mL) dropwise. The solution was allowed to stir at room temperature for 1 hour. After removing the THF under vacuum, dichloromethane (30 mL) and concentrated ammonia solution (15 mL) were added to the solution. The solution was allowed to stir for a further 30 mins. at room temperature to remove any Cu(I) trapped as $Cu(NH_3)_6^+$ ions. The organic phase was washed twice with water (30 mL) and once with brine (30 mL) and dried over $MgSO_4$. The solvent was removed under vacuum and the product was recrystallised from dichloromethane and hexane to yield a white coloured solid. (0.97 g, 78.3 %)

^{1}H NMR ($CDCl_3$) δ (ppm): 8.83 (d, 5.5 Hz, 2H, bpy H-6); 8.76 (d, J = 2.2 Hz, 2H, bpy H-3); 8.70 (d, J = 5.1, 2H, bpy H-6'); 8.48 (d, J = 7.9 Hz, 2H, bpy H-3'); 8.35 (s, 2H, Tz); 7.92 (dd, J = 5.5 & 2.2 Hz, 2H, bpy H-5); 7.87 (td, J = 7.6 & 1.8 Hz, 2H, bpy H-4'); 7.37 (dd, J = 4.7 & 1.0 Hz, 2H, bpy H-5'); 4.91 (s, 4H, Tz-*CH2*-O); ^{13}C NMR ($CDCl_3$) δ (ppm): 158.7; 155.0; 151.3; 149.5; 146.4; 144.3; 137.2; 124.6; 121.5; 120.7; 114.2; 110.8; 63.9 MS (ESI) *m/z* 511.2 (M + Na) HRMS (ESI) calcd: 511.171376, found: 511.171819.

2.2.18 Synthesis of 1,4-bis-({4-(pyrid-2-yl)-1,2,3-triazol-1-yl}methyl)benzene (22)

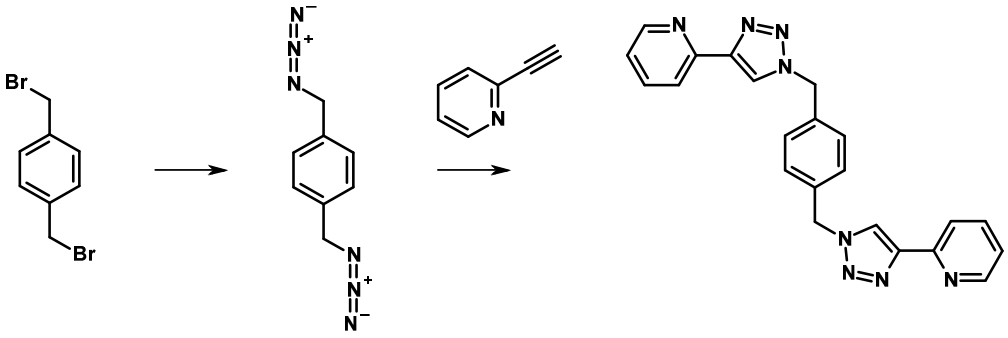

1,4-dibromomethylbenzene (0.25 g, 0.947 mmol) and sodium azide (0.125 g, 1.92 mmol) were combined in dimethyl sulfoxide (10 mL). The mixture was stirred at room temperature for two hours. The following reagents were then added to the reaction mixture in the following order: water (4.7 mL), pyridyl acetylene (0.41 g, 3.98 mmol), $CuSO_4$ (1M aqueous solution 2.50 mL), sodium ascorbate solution (1M aqueous solution 3.98 mL), and 2,6-lutidine (0.3 mL). The mixture was stirred at room temperature for 12 hours. The reaction mixture was then diluted with water (25 mL) and the solid filtered and washed with water (25 mL) and dilute ammonia (25 mL) and the product was recrystallised from dichloromethane and hexane to yield a white coloured solid. (0.32 g, 86.8 %)

^{1}H NMR ($CDCl_3$) δ (ppm): 8.46 (d, 4.8 Hz, 2H, py H-6); 8.10 (d, J = 7.5 Hz, 2H, py H-3); 7.99 (s, 2H, Tz); 7.70 (td, J = 7.7 & 1.7 Hz, 2H, py H-4); 7.20 (s, 4H, benzyl); 7.15 (dd, J = 4.8 & 1.0 Hz, 2H, py H-5); 5.52 (s, 4H, CH_2-Benzyl); ^{13}C NMR ($CDCl_3$) δ (ppm): 150.1; 149.4; 136.9; 135.3; 129.0; 122.9; 122.0; 120.3; 53.9 MS (ESI) *m/z* 417.2 (M + Na) HRMS (ESI) calcd: 417.154664, found: 417.154751.

2.2.19 Synthesis of 1,3,5-tris-({4-(pyrid-2-yl)-1,2,3-triazol-1-yl}methyl)benzene (23)

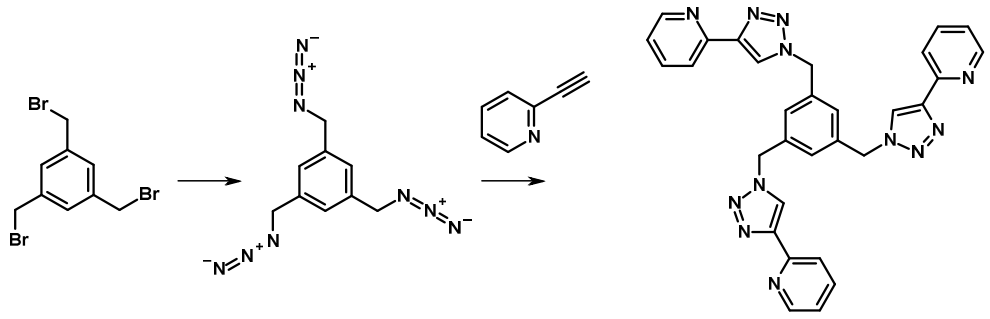

1,3,5-tribromomethylbenzene (0.1 g, 0.28 mmol) and sodium azide (0.055 g, 1.92 mmol) were combined in dimethyl sulfoxide (10 mL). The mixture was stirred at room temperature for two hours. The following reagents were then added to the reaction mixture in the following order: water (4.7 mL), pyridyl acetylene (0.095 g, 0.92 mmol), $CuSO_4$ (1M aqueous solution 2.50 mL), sodium ascorbate solution (1M aqueous solution 3.98 mL), and 2,6-lutidine (0.3 mL). The mixture was stirred at room temperature for 12 hours. The reaction mixture was then diluted with water (25 mL) and the solid filtered and washed with water (25 mL) and dilute ammonia (25 mL) and the product was recrystallised from dichloromethane and hexane to yield a white coloured solid. (0.098 g, 63.4 %)

^{1}H NMR (Me_2SO-d_6) δ (ppm): 8.67 (s, 3H, Tz); 8.57 (d, 4.5 Hz, 3H, py H-6); 8.00 (d, J = 7.5 Hz, 3H, py H-3); 7.88 (td, J = 7.8 & 1.7 Hz, 3H, py H-4); 7.37 (s, 3H, benzyl); 7.34 (dd, J = 4.7 & 1.1 Hz, 3H, py H-5); 5.69 (s, 6H, CH_2-Benzyl); ^{13}C NMR (Me_2SO-d_6) δ (ppm): 149.7; 149.4; 147.3; 137.0; 136.9; 127.2; 123.3; 122.8; 119.2; 52.3 MS (ESI) *m/z* 575.2 (M + Na) HRMS (ESI) calcd: 575.213910, found: 575.214384.

2.3 Synthesis of Rhenium Complexes

2.3.1 Synthesis of [Re(bpy)(CO)$_3$(1a)] (2a)

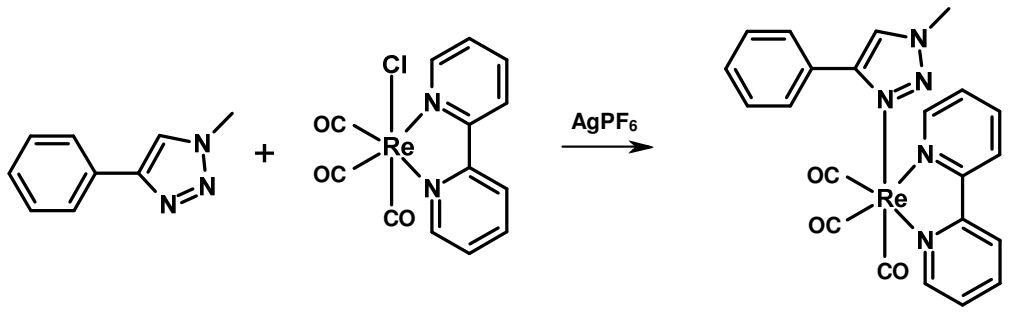

[Re(bpy)(CO)$_3$Cl] (0.1 g, 0.217 mmol) and silver hexafluorophosphate (0.06 g, 0.237 mmol) was dissolved in dichloromethane (15 mL) and stirred at room temperature for 12 hour in the dark. 4-phenyl-1-methyl-1,2,3-triazole (0.0380 g, 0.239 mmol) was added to the solution and the mixture was stirred at room temperature for 48 hours in the dark. The solution was then filtered over celite and the filtrate was then evaporated to dryness under reduced pressure. The resulting residue was recrystallised from dichloromethane/diethyl ether to yield a yellow solid. (87 mg, 69%)

^{1}H NMR (CD_3CN) δ (ppm) 8.70 (d, J = 5.5 Hz, 2H, bpy); 8.31 (d, J = 8.2 Hz, 2H, bpy); 8.14 (t, J = 7.8 Hz, 2H); 7.66 (s, 1H, Tz); 7.55 (tt, J = 7.6, 1.7 Hz, 1H, p-Ph); 7.45 (ddd, J = 7.0, 5.5, 1.2 Hz, 2H, bpy); 7.43 (t, J = 7.6 Hz, 2H, m-Ph); 7.16 (d, J = 7.7 Hz, 2H, o-Ph); 3.77 (s, 3H, Me); ^{13}C NMR (CD_3CN) δ (ppm) 153.3; 152.7; 140.1; 138.9; 129.9; 128.9; 127.2; 126.8; 126.7; 124.8; 123.0; 38.1; MS (ESI) m/z 586.1 (M^+) HRMS (ESI) calcd: 586.088342, found: 586.088352.

2.3.2 Synthesis of [Re(bpy)(CO)$_3$(1b)] (2b)

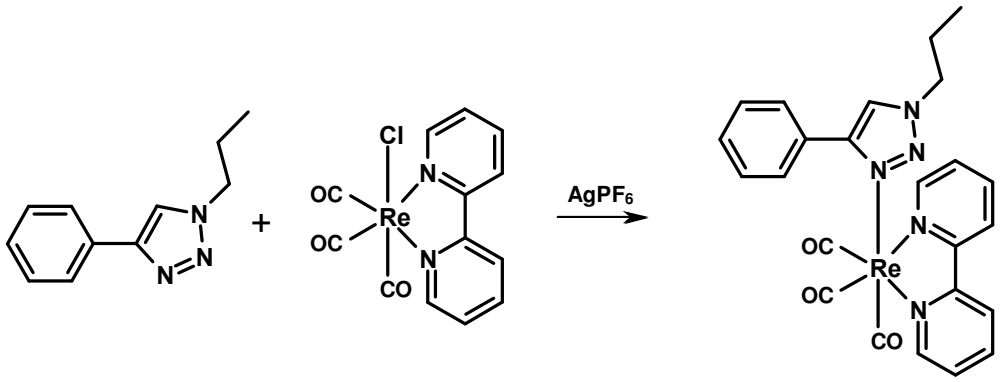

[Re(bpy)(CO)$_3$Cl] (0.1 g, 0.217 mmol) and silver hexafluorophosphate (0.06 g, 0.237 mmol) was dissolved in dichloromethane (15 mL) and stirred at room temperature for 12 hour in the dark. 4-phenyl-1-propyl-1,2,3-triazole (0.045 g, 0.239 mmol) was added to the solution and the mixture was stirred at room temperature for 48 hours in the dark. The solution was then filtered over celite and the filtrate was then evaporated to dryness under reduced pressure. The resulting residue was recrystallised from dichloromethane/diethyl ether to yield a yellow solid. (101 mg, 76%)

^{1}H NMR (CD_3CN) δ (ppm): 8.72 (d, J = 6.1 Hz, 2H); 8.32 (d, J = 8.1 Hz, 2H); 8.14 (t, J = 8.1 Hz, 2H) 7.69 (s, 1H); 7.56 (t, J = 7.4 Hz, 1H); 7.49–7.40 (m, 4H); 7.22 (d, J = 8.1 Hz, 2H); 4.05 (t, J = 6.1 Hz, 2H); 1.57 (sextet, J = 7.1 Hz, 2H); 0.48 (t, J = 7.4 Hz, 3H); ^{13}C NMR (CD_3CN) δ (ppm): 155.7; 152.7; 150.0; 140.2; 129.9; 129.8; 128.9; 127.9; 126.9; 125.4; 124.8; 53.4; 31.0; 10.9. MS (ESI) m/z 614.1 (M^+). HRMS (ESI) calcd: 614.119642, found: 614.118959.

2.3.3 Synthesis of [Re(bpy)(CO)$_3$(1c)] (2c)

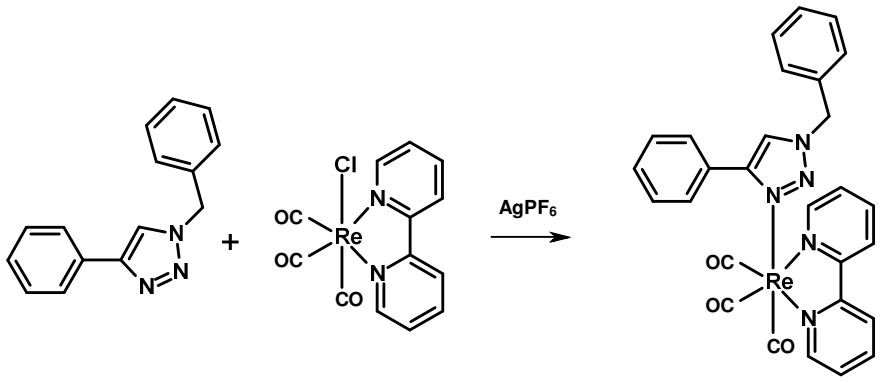

[Re(bpy)(CO)$_3$Cl] (0.1 g, 0.217 mmol) and silver hexafluorophosphate (0.06 g, 0.237 mmol) was dissolved in dichloromethane (15 mL) and stirred at room temperature for 12 hour in the dark. 4-phenyl-1-benzyl-1,2,3-triazole (0.056 g, 0.239 mmol) was added to the solution and the mixture was stirred at room temperature for 48 hours in the dark. The solution was then filtered over celite and the filtrate was then evaporated to dryness under reduced pressure. The resulting residue was recrystallised from dichloromethane/diethyl ether to yield a yellow solid. (109 mg, 76%)

^{1}H NMR (CD_3CN) δ (ppm) 8.69 (d, J = 5.5 Hz, 2H, bpy); 8.24 (d, J = 8.2 Hz, 2H, bpy); 8.11 (td, J = 7.8, 1.5 Hz, 2H, bpy); 7.80 (s, 1H, Tz); 7.56 (t, J = 7.6 Hz, 1H, p-Ph); 7.45 (t, J = 7.8, 2H, m-Ph); 7.42 (ddd, J = 7.6, 5.5, 1.2 Hz, 2H, bpy); 7.37 (t, J = 7.4 Hz, 1H, p-Bz); 7.31 (t, J = 7.5 Hz, 2H m-Bz); 7.25 (d, J = 7.5 Hz, 2H o-Ph); 6.94 (d, J = 7.7 Hz, 2H, o-Bz); 5.23 (s, 2H, CH_2); ^{13}C NMR (CD_3CN) δ (ppm) 156.9; 154.7; 151.8; 141.4; 134.2; 131.2; 131.1; 130.0; 129.9; 129.9; 129.3; 129.2; 128.7; 126.6; 124.9; 55.9; MS (ESI) m/z 662.1 (M^+). HRMS (ESI) calcd: 662.119642, found: 662.118805.

2.3.4 Synthesis of [Re(bpy)(CO)$_3$(1d)] (2d)

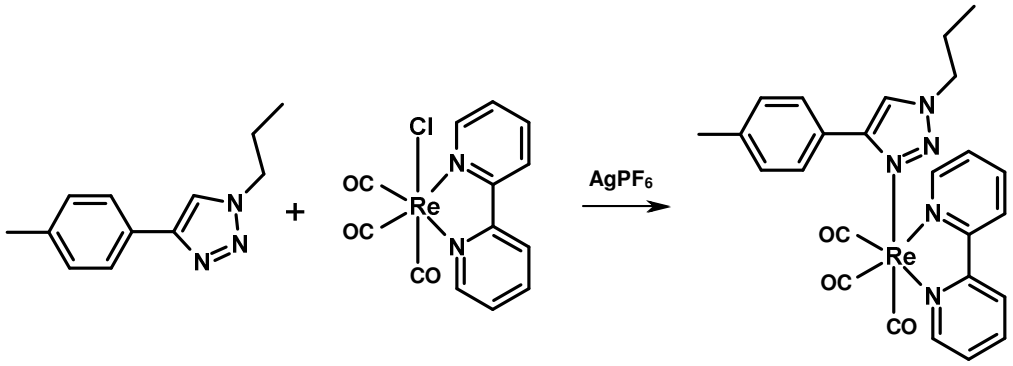

[Re(bpy)(CO)$_3$Cl] (0.1 g, 0.217 mmol) and silver hexafluorophosphate (0.06 g, 0.237 mmol) was dissolved in dichloromethane (15 mL) and stirred at room temperature for 12 hour in the dark. 4-(*p*-tolyl)-1-propyl-1,2,3-triazole (0.048 g, 0.239 mmol) was added to the solution and the mixture was stirred at room temperature for 48 hours in the dark. The solution was then filtered over celite and the filtrate was then evaporated to dryness under reduced pressure. The resulting residue was recrystallised from dichloromethane/diethyl ether to yield a yellow solid. (98 mg, 72%).

^{1}H NMR (CD_3CN) δ (ppm): 8.71 (d, J = 5.5 Hz, 2H, bpy); 8.30 (d, J = 8.3 Hz, 2H, bpy); 8.13 (t, J = 8.0 Hz, 2H, bpy); 7.66 (s, 1H); 7.44 (t, J = 6.6 Hz, 2H, bpy); 7.23 (d, J = 7.9 Hz, 2H, Ar); 7.06 (d, J = 7.9 Hz, 2H, Ar); 4.05 (t, J = 6.7 Hz, 2H); 2.44 (s, 3H); 1.58 (sextet, J = 7.1 Hz, 2H); 0.49 (t, J = 7.4 Hz, 3H); ^{13}C NMR (CD_3CN) δ (ppm) 156.8; 154.7; 151.4; 141.4; 130.7; 130.4; 129.2; 128.6; 126.4; 126.3; 124.8; 54.0; 23.4; 21.4; 10.8; MS (ESI) m/z 628.1 (M^+). HRMS (ESI) calcd: 628.135292, found: 628.135919.

2.3.5 Synthesis of (4-phenyl-1-(2,2'-bipyrid-4-yl)-1,2,3-triazole)$ReCl(CO)_3$ (18)

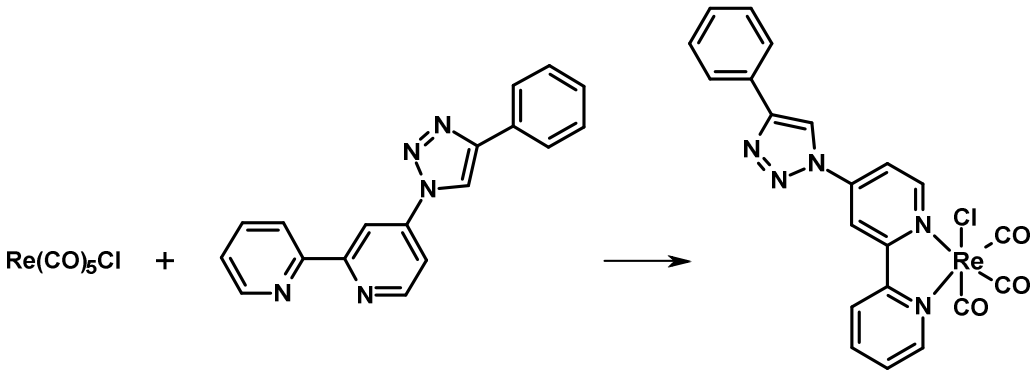

$[Re(CO)_5Cl]$ (0.1 g, 0.28 mmol) and ligand (0.092 g, 0.308 mmol) was refluxed in toluene (25 mL) for 4 hours. The reaction mixture was allowed to cool to room temperature, at which point a yellow solid precipitated. The solid was collected by filtration and washed with ether. (0.12 g, 75 %)

^{1}H NMR (CD_3CN) δ (ppm): 9.72 (s, 1H, Tz); 9.24-9.20 (m, 2H, bpy H-3 & bpy H-6); 9.09 (d, J = 5.6 Hz, 1H, bpy H-3'); 8.95 (d, J = 8.2 Hz, 1H, bpy H6'); 8.46 (t, J = 7.9 Hz, 1H, bpy H-5'); 8.36 (dd, J = 2.2 & 6.2 Hz, 1H, bpy H-5); 7.98 (d, J = 7.7 Hz, 2H, o-Ph); 7.85 (t, J = 6.6 Hz, 1H, bpy H-4'); 7.58 (t, J = 7.6 Hz, 2H, m-Ph); 7.46 (t, J = 7.4 Hz, 1H, p-Ph)

2.3.6 Synthesis of (4-ferrocenyl-1-(2,2'-bipyrid-4-yl)-1,2,3-triazole)$ReCl(CO)_3$ (15)

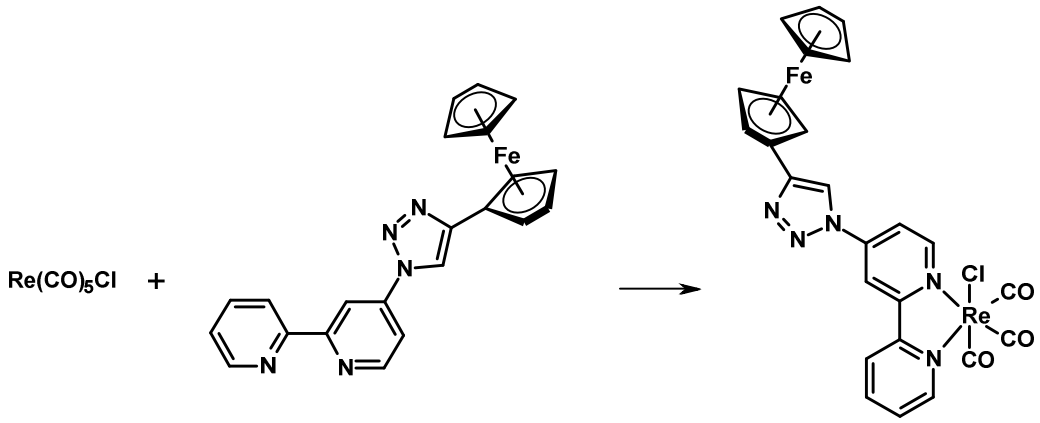

$[Re(CO)_5Cl]$ (0.1 g, 0.28 mmol) and ligand (0.125 g, 0.308 mmol) was refluxed in toluene (25 mL) for 4 hours. The reaction mixture was allowed to cool to room temperature, at which point a orange solid precipitated. The solid was collected by filtration and washed with ether. (0.15 g, 73 %)

^1H NMR (CD_3CN) δ (ppm): 9.30 (s, 1H, Tz); 9.19-9.16 (m, 2H, bpy H-3 & bpy H-6); 9.09 (d, J = 5.5 Hz, 1H, bpy H-3'); 8.98 (d, J = 8.4 Hz, 1H, bpy H6'); 8.47 (td, J = 1.2 & 7.8 Hz, 1H, bpy H-5'); 8.34 (dd, J = 2.2 & 6.4 Hz, 1H, bpy H-5); 7.84 (t, J = 6.5 Hz, 1H, bpy H-4'); 4.84 (t, J = 2.6, 2H, C_5H_4Fe); 4.45 (t, J = 1.7, 2H, C_5H_4Fe); 4.14 (s, 5H, Cp);

2.4 Synthesis of Ruthenium Complexes

2.4.1 Synthesis of [(4-azido-2,2'-bipyridyl)RuCl(*p*-cymene)]PF_6 (6a)

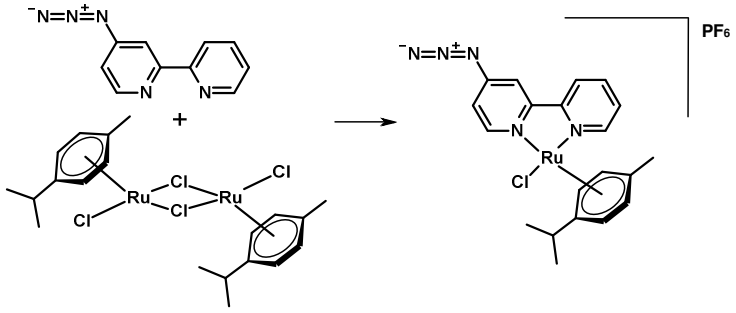

$[RuCl_2(p\text{-cymene})]_2$ (0.1 g, 0.16 mmol) and 4-azido-2,2'-bipyridyl (0.098 g, 0.5 mmol) was reacted in methanol (30 mL) for 12 hours at room temperature. The orange solution was concentrated to half its volume and treated with excess $NaPF_6$ to yield an yellow-orange precipitate, which was collected by filtration and washed with diethyl ether. (0.15 g, 76 %)

^{1}H NMR (CD_3CN) δ (ppm): 9.34 (ddd, J = 5.7, 1.3 & 0.7 Hz, 1H, bpy H-6'); 9.15 (d, J = 6.3 Hz, 1H bpy H-6); 8.35 (d, J = 8.1 Hz, 1H, bpy H-3'); 8.19 (td, J = 8.0 & 1.4 Hz, 1H, bpy H-4'); 7.92 (d, J = 2.5 Hz, 1H, bpy H-3); 7.72 (ddd, J = 7.6, 5.7 & 1.4 Hz, 1H, bpy H-5'); 7.37 (dd, J = 6.3 & 2.5 Hz, bpy H-5); 5.91 (t, J = 5.7 Hz, 2H, Cym C*H*-CiPr); 5.71 (m, 2H, Cym C*H*-CMe); 2.65 (sept, J = 7.0 Hz, iPr C*H*); 2.21 (s, 3H, Cym Me); 1.04 (d, J = 7.0 Hz, 3H, iPr CH_3); 1.03 (d, J = 7.0 Hz, 3H, iPr CH_3). ^{13}C NMR (CD_3CN) δ (ppm): 159.9; 159.8; 156.6; 155.3; 154.1; 140.9; 129.0; 125.0; 118.8; 115.4; 106.1; 104.6; 87.4; 85.2; 31.9; 22.2; 19.0 MS (ESI) m/z 468.1 (M^+) HRMS: calcd: 468.052349, found: 468.054448. IR (ATR) 2124 cm^{-1}.

2.4.2 Synthesis of [(4,4'-azido-2,2'-bipyridyl)RuCl(*p*-cymene)]PF_6 (6b)

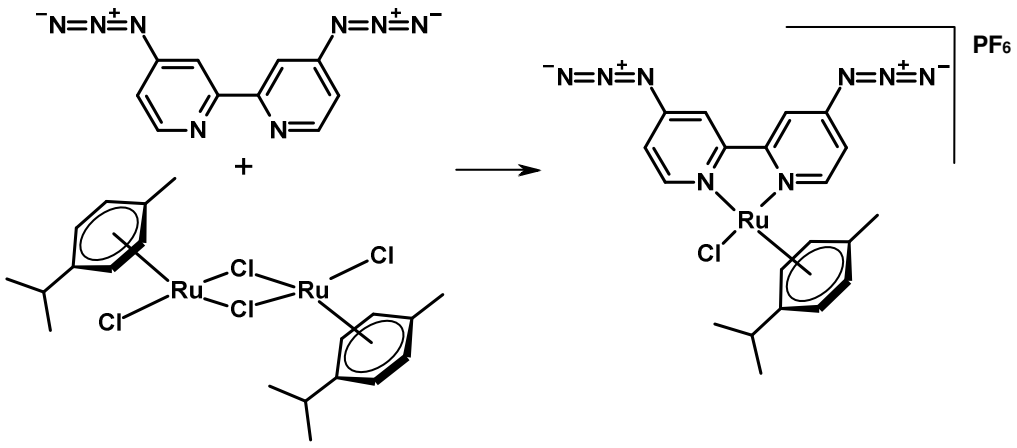

$[RuCl_2(p\text{-cymene})]_2$ (0.1 g, 0.16 mmol) and 4,4'-azido-2,2'-bipyridyl (0.120 g, 0.5 mmol) was reacted in methanol (30 mL) for 12 hours at room temperature. The orange solution was concentrated to half its volume and treated with excess $NaPF_6$ to yield an yellow-orange precipitate, which was collected by filtration and washed with diethyl ether. (0.14 g, 66 %)

^{1}H NMR (CD_3CN) δ (ppm): 9.15 (d, J = 6.4 Hz, 2H, bpy H-6); 7.94 (d, J = 2.4 Hz, 2H, bpy H-3); 7.37 (dd, J = 6.4 & 2.4 Hz, 2H, bpy H-5) 5.90 (d, J = 6.2 Hz, 2H, Cym C*H*-CiPr); 5.69 (d, J = 6.2 Hz, 2H, Cym C*H*-CMe); 2.65 (sept, J = 7.0 Hz, iPr C*H*); 2.21 (s, 3H, Cym Me); 1.05 (d, J = 7.0 Hz, 3H, iPr CH_3); ^{13}C NMR (CD_3CN) δ (ppm): 157.0; 156.5; 154.3; 119.1; 115.7; 105.9; 104.6; 87.3; 85.0; 31.9; 22.3; 19.0 MS (ESI) m/z 509.1 (M^+) HRMS: calcd: 509.0537, found: 509.0559. IR (ATR) 2125 cm^{-1}.

2.4.3 Synthesis of [(4-phenyl-1-(2,2'-bipyrid-4-yl)-1,2,3-triazole)RuCl(*p*-cymene)]PF_6 (8a)

Route A

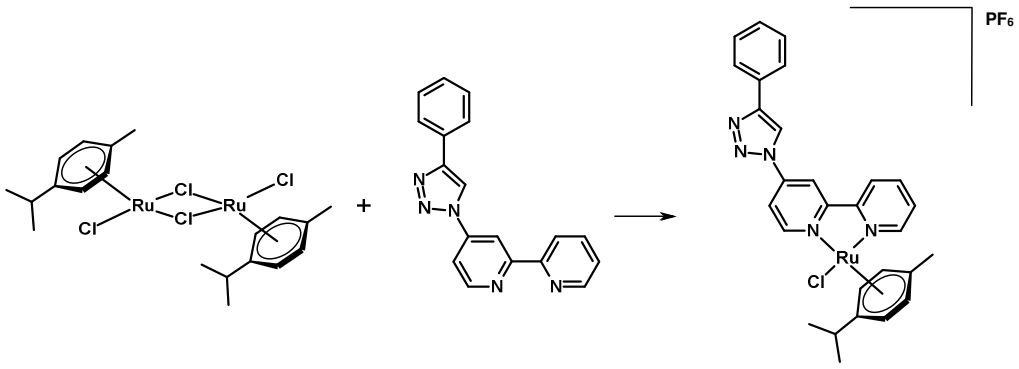

Route B

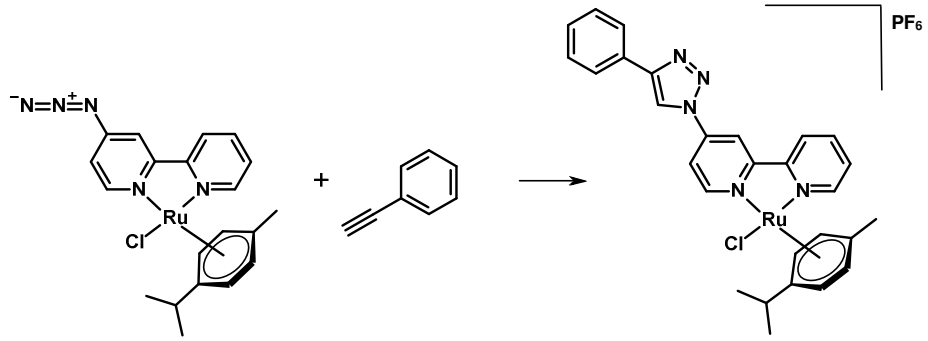

Route A

$[RuCl_2(p\text{-cymene})]_2$ (0.1 g, 0.16 mmol) and 4-phenyl-1-(2,2'-bipyrid-2-yl)-1,2,3-triazole (0.150 g, 0.5 mmol) was reacted in methanol (30 mL) for 12 hours at room temperature. The yellow solution was concentrated to half its volume and treated with excess $NaPF_6$ to yield an orange precipitate, which was collected by filtration and washed with diethyl ether. (0.15 g, 66%)

Route B

[(4-azido-2,2'-bipyridyl)RuCl(*p*-cymene)] (0.1 g, 0.214 mmol) and phenylacetylene (0.033 g, 0.321 mmol) was dissolved in THF (30 mL) and water was added (30 mL). At 20 °C was added $CuSO_4$ (1M aqueous solution 0.214 mL) was added followed by freshly prepared sodium ascorbate solution (1M aqueous solution 0.428 mL) dropwise. The solution was allowed to stir at room temperature for 12 hours. After removing the THF under vacuum, dichloromethane (30 mL) and concentrated ammonia solution (15 mL) was added to the solution. The solution was allowed to stir for a further 30 mins. at room temperature to remove remaining Cu(I). The organic phase was washed twice with water (30 mL) and once with brine (30 mL) and dried over $MgSO_4$. The solvent was removed under vacuum and the product was recrystallised from acetonitrile and ether to yield an orange coloured solid. (0.097 g, 80 %)

^{1}H NMR (CD_3CN) δ (ppm): 9.47 (d, J = 6.5 Hz, 1H, bpy H-6); 9.39 (d, J = 5.8 Hz, 1H, bpy H-6'); 8.99 (s, 1H, Tz); 8.78 (d, J = 2.4 Hz, 1H, bpy H-3); 8.52 (d, J = 8.1 Hz, 1H, bpy H-3'); 8.27 (td, J = 7.9 & 1.3 Hz, 1H, bpy H-4'); 8.21 (dd, J = 6.3 & 2.4 Hz, 1H, bpy H-5); 8.00 (m, 2H, o-Ph); 7.78 (ddd, 7.6, 5.7 & 1.3 Hz, 1H, bpy H-5'); 7.57 (t, J = 7.8 Hz, 2H, m-Ph); 7.48 (tt, J = 7.4 & 1.2 Hz, 1H, p-Ph); 5.98 (m, 2H, Cym C*H*-CiPr); 5.78 (d, J = 6.3 Hz, 2H, Cym C*H*-CMe); 2.71 (sept, J = 7.0 Hz, 1H, iPr CH); 2.25 (s, 3H, Cym CH_3); 1.08 (d, J = 7 Hz, iPr CH_3); 1.07 (d, J = 7 Hz, iPr CH_3). ^{13}C NMR (CD_3CN) δ (ppm): 157.9; 157.5; 156.7; 155.0; 149.9; 146.3; 141.0; 130.5; 130.2; 130.0; 129.2; 126.7; 125.3; 120.1; 117.7; 114.4; 106.5; 104.7; 87.5; 87.4; 85.5; 85.4; 31.8; 22.1; 18.9. MS (ESI) m/z 570.1 (M^+) HRMS: calcd: 570.099300, found: 570.099993

2.4.4 Synthesis of [(4-ferrocenyl-1-(2,2'-bipyrid-4-yl)-1,2,3-triazole)RuCl(*p*-cymene)]PF_6 (8b)

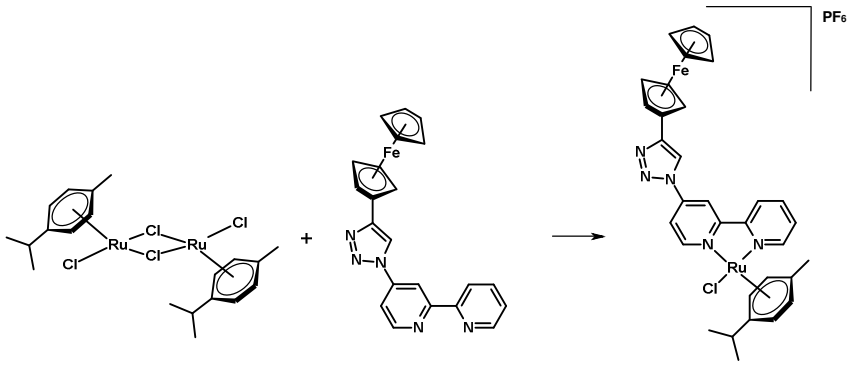

Route A

Route B

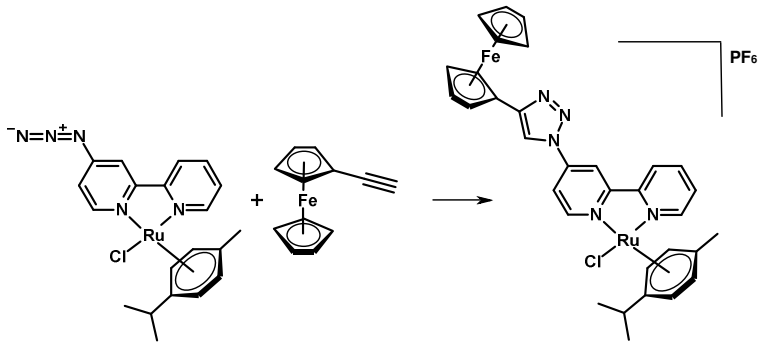

Route A

$[RuCl_2(p\text{-cymene})]_2$ (0.1 g, 0.16 mmol) and 4-ferrocenyl-1-(2,2'-bipyrid-4-yl)-1,2,3-triazole (0.204 g, 0.5 mmol) was reacted in methanol (30 mL) for 12 hours at room temperature. The red solution was concentrated to half its volume and treated with excess $NaPF_6$ to yield an orange-red precipitate, which was collected by filtration and washed with diethyl ether. (0.21g, 79%)

Route B

[(4-azido-2,2'-bipyridyl)RuCl(*p*-cymene)] (0.1 g, 0.214 mmol) and ethynylferrocene (0.067 g, 0.321 mmol) was dissolved in THF (30 mL) and water was added (30 mL). At 20 °C was added $CuSO_4$ (1M aqueous solution 0.214 mL) was added followed by freshly prepared sodium ascorbate solution (1M aqueous solution 0.428 mL) dropwise. The solution was allowed to stir at room temperature for 12 hours. After removing the THF under vacuum, dichloromethane (30 mL) and concentrated ammonia solution (15 mL) was added to the solution. The solution was allowed to stir for a further 30 mins. at room temperature to remove remaining Cu(I). The organic phase was washed twice with water (30 mL) and once with brine (30 mL) and dried over $MgSO_4$. The solvent was removed under vacuum and the product was recrystallised from acetonitrile and ether to yield a red coloured solid. (0.10 g, 69 %)

^{1}H NMR (CD_3CN) δ (ppm): 9.44 (d, 6.2 Hz, 1H, bpy H-6'); 9.38 (d, H = 5.5 Hz, 1H, bpy H-6); 8.73 (bs, 1H, bpy H-3); 8.64 (s, 1H, Tz); 8.53 (d, J = 7.9 Hz, 1H, bpy H-3'); 8.27 (t, J = 7.9 Hz, 1H, bpy H-4'); 8.17 (d, J = 5.6 Hz, 1H, bpy H-5); 7.77 (t, J = 6.5 Hz, 1H, bpy H-5'); 5.98 (t, J = 5.6 Hz, 2H, Cym C*H*-CiPr); 5.78 (d, J = 6.5 Hz, 2H, Cym C*H*-CMe); 4.85 (s, 2H, Fc -C_5H_4); 4.42 (s, 2H, Fc -C_5H_4); 4.13 (s, 5H, Cp); 2.70 (sept, J = 6.9 Hz, iPr CH); 2.24 (s, 3H, Cym Me); 1.07 (d, J = 6.9 Hz, iPr CH_3); 1.07 (d, J = 6.9 Hz, iPr CH_3). ^{13}C NMR (CD_3CN) δ (ppm): 157.9; 157.5; 156.8; 155.2; 149.9; 146.4; 141.1; 129.3; 125.4; 118.8; 117.6; 114.2; 106.5; 104.9; 87.6; 87.5; 85.5; 85.4; 70.8; 70.4; 68.0; 31.9; 22.3; 19.0 MS (ESI) m/z . 678.1 (M^+) HRMS: calcd: 678.065542 , found: 678.068143

2.4.5 Synthesis of [(4-pyrid-2-yl-1-(2,2'-bipyrid-4-yl)-1,2,3-triazole)RuCl(*p*-cymene)]PF6 (8c)

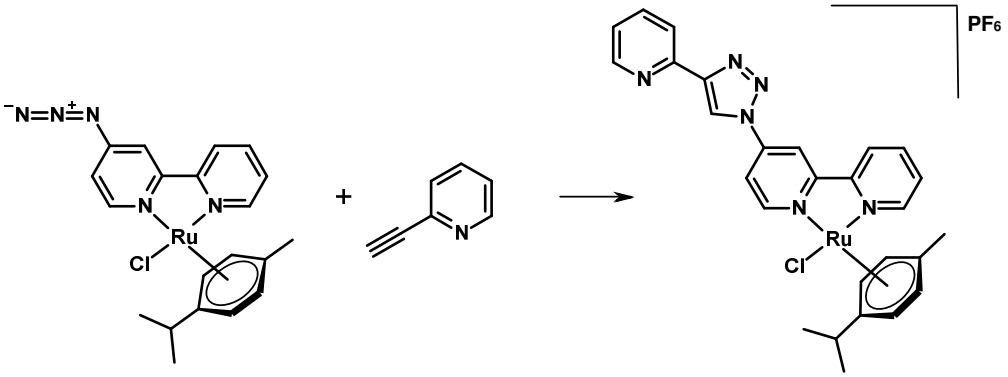

[(4-azido-2,2'-bipyridyl)RuCl(*p*-cymene)] (0.1 g, 0.214 mmol) and 2-ethynylpyridine (0.033 g, 0.321 mmol) was dissolved in THF (30 mL) and water was added (30 mL). At 20 °C was added $CuSO_4$ (1M aqueous solution 0.214 mL) was added followed by freshly prepared sodium ascorbate solution (1M aqueous solution 0.428 mL) dropwise. The solution was allowed to stir at room temperature for 12 hours. After removing the THF under vacuum, dichloromethane (30mL) and concentrated ammonia solution (15 mL) was added to the solution. The solution was allowed to stir for a further 12 hours. at room temperature to remove any remaining Cu(I). The organic phase was washed twice with water (30 mL) and once with brine (30 mL) and dried over $MgSO_4$. The solvent was removed under vacuum and the product was recrystallised from acetonitrile and ether to yield an orange coloured solid. (0.057 g, 47 %)

^{1}H NMR (CD_3CN) δ (ppm): 9.45 (d, J= 6.4 Hz, 1H, bpy H-6); 9.36 (dd, J = 5.7 & 1.0 Hz, 1H, bpy-H6'); 9.14 (s, 1H, Tz); 8.74 (d, J = 1.9 Hz, 1H; bpy-H3); 8.66 (s, 1H, Py-H3); 8.50 (d, J = 7.6 Hz, 1H, bpy-H3'); 8.28-8.16 (m, 3H, bpy-H4', bpy-H5 & Py-H4); 7.91 (t, J = 7.7 Hz, 1H, Py-H5); 7.73 (td, J = 6.4 & 1.0 Hz, 1H, bpy-H5'); 7.39 (s, 1H, Py-H6); 5.9 (t, J = 6.3 Hz, 2H, Cym C*H*-CiPr); 5.76 (d, J = 6.3 Hz, 2H, Cym C*H*-CMe); 2.68 (sept, J = 6.8 Hz, 1H, iPr CH); 2.16 (s, 3H, Cym CH_3); 1.06 (d, J = 1.8 Hz, iPr CH_3); 1.04 (d, J = 1.8 Hz, iPr CH_3). ^{13}C NMR (CD_3CN) δ (ppm): 157.9; 157.6; 156.8; 155.0; 151.1; 150.9; 150.0; 146.3; 141.1; 138.3; 129.3; 125.5; 124.9; 122.1; 121.3; 118.1; 114.6; 106.5; 104.8; 87.6; 87.5; 85.5; 85.4; 31.9; 22.2; 19.0 MS (ESI) m/z . 571.1 (M^+) HRMS: calcd: 571.094548, found: 571.095033

2.4.6 Synthesis of [(4-pyridyl-1-(2,2'-bipyrid-4-yl)-1,2,3-triazole)(RuCl(*p*-cymene))$_2$]2PF$_6$ (9)

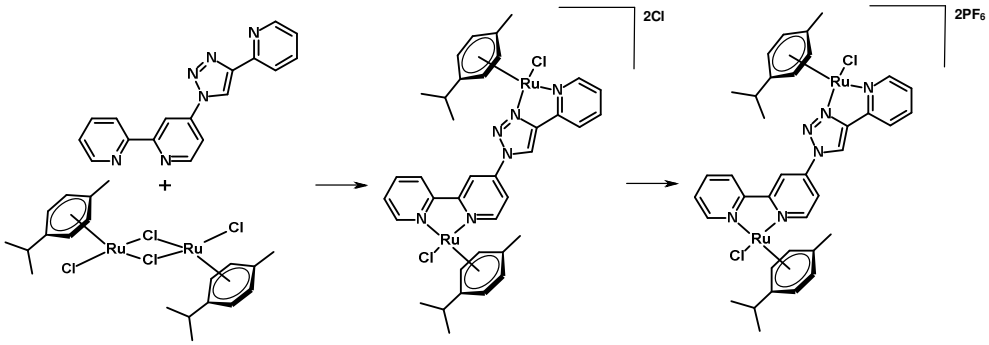

$[RuCl_2(p\text{-cymene})]_2$ (0.313 g, 0.5 mmol) and 4-pyridyl-1-(2,2'-bipyrid-4-yl)-1,2,3-triazole (0.150 g, 0.5 mmol) was reacted in ethanol (50 mL) for 48 hours. Hexane was added under stirring to the orange-yellow solution until slight turbidity was achieved. The mixture was allowed to stand at 4 °C for 2 hours and then filtered. Evaporating the solution to dryness afford the product as an orange-brown solid which was dissolved in acetonitrile (3 mL) and a solution of $AgPF_6$ (0.06 g, 0.22 mmol) in acetonitrile (2 mL) was added dropwise whilst stirring. The reaction mixture was stirred for a further 10 minutes and filtered through celite, and evaporated to dryness to yield an orange-brown solid. (0.22 g, 88 %)

^{1}H NMR (CD_3CN) δ (ppm): 9.58 (dd, J = 5.2 & 1.6 Hz, 1H, bpy H-6); 9.44 (d, J = 9.6 Hz, 1H, Tz); 9.39 (dt, J = 5.6 & 1.3 Hz, 1H, bpy H-6'); 9.33 (d, J = 5.4 Hz, 1H, Py H6); 8.34 (dd, J = 13.2 & 2.3 Hz, 1H, bpy H-3); 8.56 (t, J = 7.7 Hz, bpy H-3'); 8.25 (m, 3H, bpy H-4', bpy H-5 & Py H-4); 8.08 (d, J = 7.9 Hz, 1H, Py H-3); 7.80 (m, 1H, bpy H-5'); 7.69 (t, J = 6.6 Hz, 1H, Py H-5); 6.09 (d, 6.0 Hz, 1H, cymene pytz); 6.00 (m, 3H, cymene bpy); 5.89 (dd, J = 6.0 & 2.5 Hz, 1H, cymene bpy); 5.81 (m, 3H, cymene pytz); 2.78 (sept, J = 6.4 Hz, 1H, iPr CH pytz); 2.69 (m, 1H, iPr CH bpy); 2.23 (d, J = 3.6 Hz, 3H, Cym Me bpy); 2.21 (s, 3H, Cym Me pytz); 1.16 (dd, 6.4 & 1.6 Hz, 3H, iPr CH_3 pytz); 1.11 (d, 6.8 Hz, 3H, iPr CH_3 pytz); 1.07 (d, J = 7.0 Hz, 6H, iPr CH_3 bpy) ^{13}C NMR (CD_3CN) δ (ppm): 158.4; 158.0; 156.9; 156.8; 154.7; 149.0; 148.0; 148.3; 145.3; 145.2; 141.7; 141.3; 141.2; 129.7; 128.0; 125.7; 124.4; 124.3; 124.0; 118.6; 118.5; 118.3; 115.3;115.2; 107.2; 107.2; 107.0; 106.9; 105.1; 105.1; 104.0; 103.9; 87.9; 87.8; 87.6; 87.2; 87.2; 86.2; 85.8; 85.7; 85.7; 85.6; 85.6; 84.8; 32.0; 31.9; 22.5; 22.3; 22.3; 22.0; 22.0; 19.0; 18.9 MS (ESI) m/z . 421.0 (M^{2+}) HRMS: calcd: 421.038376, found: 421.040178

2.4.7 Synthesis of [(4-pyrid-2-yl-1-benzyl-1,2,3-triazole)RuCl(*p*-cymene)]PF_6 (11)

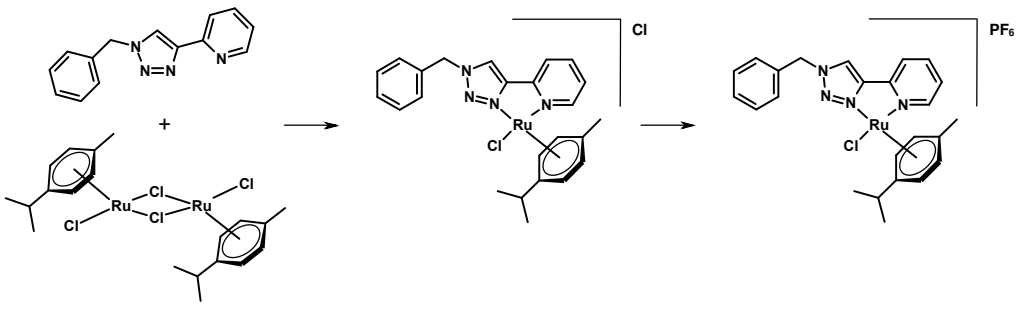

$[RuCl_2(p\text{-cymene})]_2$ (0.313 g, 0.5 mmol) and 4-pyridyl-1-benzyl-1,2,3-triazole (0.223 g, 1.0 mmol) was reacted in ethanol (50 mL) for 48 hours. Hexane was added under stirring to the orange-yellow solution until slight turbidity was achieved. The mixture was allowed to stand at 4 °C for 2 hours and then filtered. Evaporating the solution to dryness afford an orange-brown solid which was dissolved in acetonitrile (3 mL) and a solution of $AgPF_6$ (0.143 g, 0.564 mmol) in acetonitrile (2 mL) was added dropwise whilst stirring. The reaction mixture was stirred for a further 10 minutes and filtered through celite, and evaporated to dryness to yield an orange-brown solid. (0.34 g, 93%)

^{1}H NMR (CD_3CN) δ (ppm): 9.23 (d, J = 5.4 Hz, 1H, Py H-6); 8.56 (s, 1H, Tz); 8.09 (td, J = 7.9 & 1.3 Hz, 1H, Py H-4); 7.92 (d, J = 7.9 Hz, 1H, Py H-3); 7.57 (td, J = 6.9 & 1.3, 1H, Py H-5) 7.46 (m, 5H, benzyl) 6.00-5.60 (m, 6H, Cym C*H*-CiPr, Cym C*H*-Me & CH_2-Benzyl); 2.63 (sept, J = 6.9 Hz, iPr CH); 2.16 (s, 3H, Cym Me); 1.09 (d, J = 6.9 Hz, iPr CH_3); 0.94 (d, J = 6.9 Hz, iPr CH_3) ^{13}C NMR (CD_3CN) δ (ppm):156.3; 149.1; 147.4; 141.1; 134.8; 130.2; 129.6; 127.0; 125.8; 123.5; 106.1; 103.1; 86.5; 85.2; 85.1; 84.5; 56.9; 31.7; 22.4; 21.6; 18.7; MS (ESI) m/z . 507.1 (M^+) HRMS: calcd: 507.088400 , found: 507.090438

2.4.8 Synthesis of [(di-([1-{2,2'-bipyrid-4-yl}-1,2,3-triazol-4-yl]methyl)ether)(RuCl(*p*-cymene))$_2$]2PF$_6$ (12)

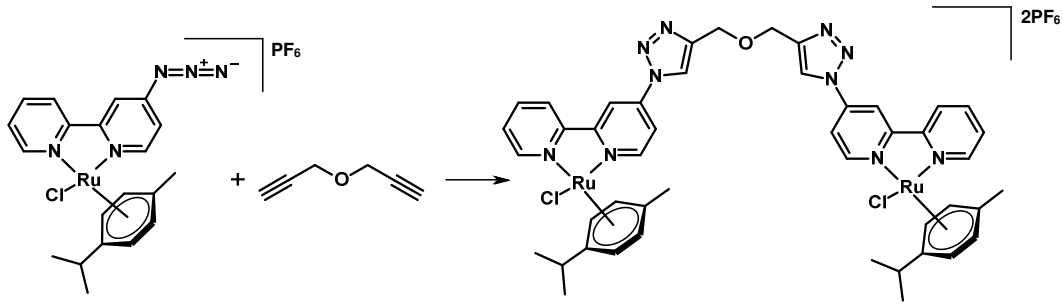

[(4-azido-2,2'-bipyridyl)RuCl(*p*-cymene)] (0.1 g, 0.214 mmol) and propargyl ether (0.012 g, 0.130 mmol) was dissolved in THF (30 mL) and water was added (30 mL). At 20 °C was added $CuSO_4$ (1M aqueous solution 0.214 mL) was added followed by freshly prepared sodium ascorbate solution (1M aqueous solution 0.428 mL) dropwise. The solution was allowed to stir at room temperature for 24 hours. After removing the THF under vacuum, dichloromethane (30 mL) and concentrated ammonia solution (15 mL) was added to the solution. The solution was allowed to stir for a further 2 hours at room temperature to remove any remaining Cu(I). The organic phase was washed twice with water (30 mL) and once with brine (30 mL) and dried over $MgSO_4$. The solvent was removed under vacuum and the product was recrystallised from acetonitrile and ether to yield a red coloured solid. (0.084 g, 60 %)

^{1}H NMR (CD_3CN) δ (ppm): 9.47 (dd, 6.3 & 1.3 Hz, 2H, bpy H-6); 9.39 (d, J = 5.7 Hz, 2H, bpy H-6'); 9.30 (2 x s, 2H, Tz); 9.14 (dd, J = 2.2 & 7.2 Hz, 2H, bpy H-3); 8.90 (t, J = 8.3 Hz, 2H, bpy H-3'); 8.37 (dt, J = 6.3 & 2.2 Hz, 2H, bpy H-5); 8.21 (tt, J = 7.7 & 1.3 Hz, 2H, bpy H-4'); 7.76 (tt, J = 6.6 & 1.3 Hz, 2H, bpy H-4'); 5.99 (t, J = 7.4 Hz, 4H, Cym C*H*-CiPr); 5.79 (d, J = 6.5 Hz, 4H, Cym C*H*-CMe); 4.86 (s, 4H, Tz-*CH2*-O); 2.70 (sept, J = 6.8 Hz, 2H, iPr CH); 2.23 (s, 6H, Cym Me); 1.07 (d, J = 6.8 Hz, iPr CH_3); 1.06 (d, J = 6.8 Hz, iPr CH_3) ^{13}C NMR (CD_3CN) δ (ppm): 157.9; 157.8; 156.7; 155.4; 147.7; 147.7; 146.7; 141.1; 129.2; 126.0; 123.9; 114.9; 106.5; 104.8; 87.6; 87.5; 85.6; 85.5; 64.1; 31.9; 22.3; 19.0 MS (ESI) m/z . 515.1 (M^{2+}) HRMS: calcd: 515.0733 , found: 515.0781

2.4.10 Synthesis of [Ru(bpy)$_2$(4-phenyl-1-(2,2'-bipyrid-4-yl)-1,2,3-triazole)](PF$_6$)$_2$ (16)

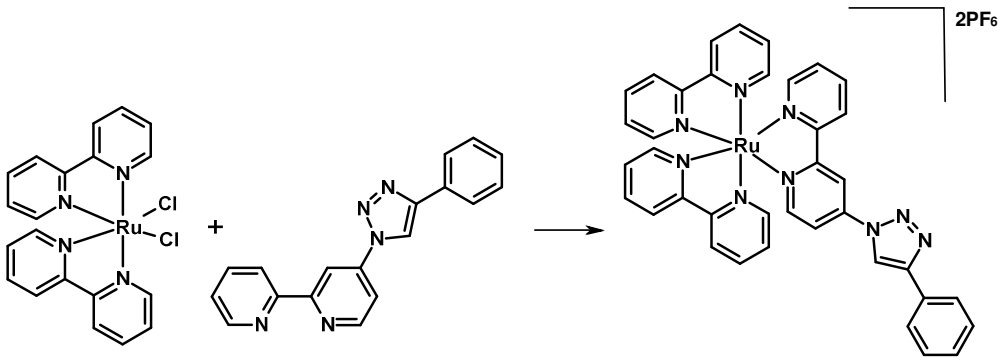

[Ru(bpy)$_2$Cl$_2$] (0.1 g, 0.21 mmol) and ligand **5a** (0.068 g, 0.231 mmol) were dissolved in ethanol (25 mL). The resulting solution was refluxed for 4 hours. The solution was allowed to cool to room temperature and was purified by column chromatography (silica gel, MeCN/H$_2$O/sat. KNO$_{3\ (aq.)}$ (7:1:0.5)). The desired fraction was evaporated to dryness and then redissolved in ethanol, the product was precipitated as red crystals by addition of excess NaPF$_6$. (0.13 g, 61 %)

^{1}H NMR (CD_3CN) δ (ppm): 8.98 (s, 1H, Tz); 8.94 (d, J = 1.1 Hz, 1H, Tz sub-bpy H-3) 8.72 (d, J = 8.0 Hz, 1H, Tz sub-bpy H-3'); 8.52 (t, J = 8.5 Hz, 4H unsub-bpy); 8.12 (t, J = 7.9 Hz, 1H, Tz sub-bpy H-4') 8.10-8.04 (m, 4H, unsub-bpy); 7.95 (d, J = 7.2, 2H, o-Ph); 7.89 (d, J = 1.3 Hz, 1H, Tz sub-bpy H-5 & Tz sub-bpy H-6); 7.85 (d, J = 5.2 Hz, 1H, unsub-bpy); 7.79 (t, J = 5.8 Hz, 2H, Tz sub-bpy H-6' & unsub-bpy); 7.75 (t, J = 6.4 Hz, unsub-bpy); 7.51-7.45 (m, 2H, m-Ph & unsub-bpy) 7.45-7.37 (m, 5H, Tz sub-bpy H-5' & p-Ph & unsub-bpy); (CD_3CN) δ (ppm): 160.0; 158.0; 157.9; 157.9; 157.4; 154.3; 152.9; 152.8; 152.7; 152.6; 149.8; 144.8; 138.9; 130.6; 130.1; 129.9; 129.2; 128.7; 128.6; 128.6; 126.7; 125.9; 125.3; 125.3; 119.9; 117.9; 115.0 (ESI) m/z 858.1 (M^+ PF_6^-). HRMS (ESI) calcd:, 858.122574 found: 858.1208

2.4.11 Synthesis of [Ru(bpy)$_2$(4-ferrocenyl-1-(2,2'-bipyrid-4-yl)-1,2,3-triazole)](PF$_6$)$_2$ (13)

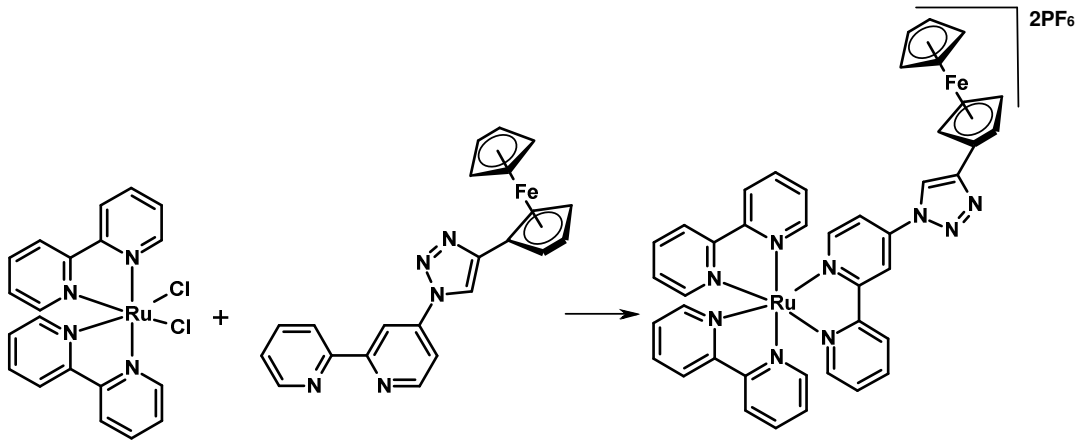

[Ru(bpy)$_2$Cl$_2$] (0.1 g, 0.21 mmol) and ligand **5b** (0.094 g, 0.231 mmol) were dissolved in ethanol (25 mL). The resulting solution was refluxed for 4 hours. The solution was allowed to cool to room temperature and was purified by column chromatography (silica gel, MeCN/H$_2$O/sat. KNO$_3$ $_{(aq.)}$ (7:1:0.5)). The desired fraction was evaporated to dryness and then redissolved in ethanol, the product was precipitated as red crystals by addition of excess NaPF$_6$. (0.17 g, 72 %)

^{1}H NMR (CD_3CN) δ (ppm): 8.89 (d, J = 2.0 Hz, 1H, Tz sub-bpy H-3); 8.69 (d, J = 8.1 Hz, 1H, Tz sub-bpy H-3') 8.60 (s, 1H, Tz); 8.51 (t, J = 8.0 Hz, 4H unsub-bpy); 8.12 (t, J = 8.0, 1H, Tz sub-bpy H-4'); 8.09-8.04 (m, 4H, unsub-bpy); 7.88-7.81 (m, 3H, Tz sub-bpy H-5 & unsub-bpy); 7.79-7.71 (m, 4H, Tz sub-bpy H-6' & unsub-bpy); 7.45 (t, J = 6.5 Hz, sub-bpy H-5'); 7.43-7.38 (m, 4H, Tz sub-bpy H-6 & unsub-bpy); 4.82 (t, J = 1.8 Hz, 2H, C_5H_4Fe); 4.39 (t, J = 1.6 Hz, 2H, C_5H_4Fe); 4.14 (s, 5H, Cp); ^{13}C NMR (CD_3CN) δ (ppm): 159.9; 158.0; 157.5; 154.3; 153.0; 152.8; 152.7; 149.9; 144.9; 139.0; 129.2; 128.7; 128.6; 125.9; 125.4; 117.7; 114.9; 75.1; 70.6; 70.2; 67.9 (ESI) m/z 966.1 (M^+ PF_6^-). HRMS (ESI) calcd: 966.088816 found: 966.0797.

2.4.12 Synthesis of [{Ru(bpy)$_2$}$_2$(4-pyrid-2-yl-1-(2,2'-bipyrid-4-yl)-1,2,3-triazole)](PF$_6$)$_4$ (24)

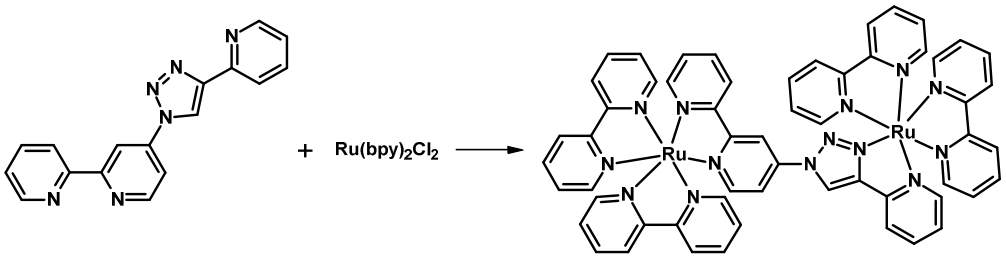

$Ru(bpy)_2Cl_2$ (0.323 g, 0.666 mmol), ligand **5c** (0.1 g, 0.333 mmol) and $AgPF_6$ (0.168 g, 0.666 mmol) were dissolved in ethanol (100 mL). The resulting solution was refluxed for 48 hours with exclusion of light. The solution was allowed to cool to room temperature and was filtered through celite to remove AgCl as a white solid and washed with acetonitrile (25 mL). The product was purified by column chromatography (silica gel, MeCN/H_2O/sat. $KNO_{3\ (aq.)}$ (7:1:0.5)). The desired fraction was evaporated to dryness and then redissolved in ethanol, the product was precipitated as red crystals by addition of excess $NaPF_6$. (0.22 g, 39%)

^{1}H NMR (CD_3CN) δ (ppm): 9.84 & 9.82 (2 x s, 1H, Tz); 8.84 (dd, J = 13.4 & 2.4 Hz, 1H); 8.68 (t, J = 7.8 Hz, 1H); 8.55-8.39 (m, 8H); 8.30 (dd, J = 7.7 & 4.4 Hz, 1H; 8.14-7.95 (m, 11H); 7.89 (t, J = 6.1 Hz, 1H); 7.85-7.80 (m, 2H); 7.79-7.73 (m, 3H); 7.73-7.67 (m, 3H); 7.66 (d, J = 5.9 Hz, 1H); 7.61 (dt, J = 5.9 & 2.1 Hz); 7.48-7.30 (m, 10H) ^{13}C NMR (CD_3CN) (ppm): 160.5; 160.4; 158.6; 158.6; 158.3; 158.2; 158.0; 157.9; 157.1; 154.6; 153.3; 153.2; 153.2; 153.1; 153.0; 153.0; 153.0; 152.8; 152.7; 151.0; 150.6; 150.5; 143.5; 139.7; 139.2; 139.2; 139.1; 138.9; 129.5; 128.8; 128.7; 128.6; 127.9; 127.8; 126.2; 126.1; 125.4; 125.3; 125.0; 125.0; 125.0; 124.6; 124.3; 124.3; 115.3 (ESI) m/z 282.1 (M^{4+}) HRMS (ESI) calcd: 282.0485, found: 282.0503

2.4.13 Synthesis of $[Ru(bpy)_2(4\text{-pyrid-2-yl-1-benzyl-1,2,3-triazole})](PF_6)_2$ (26)

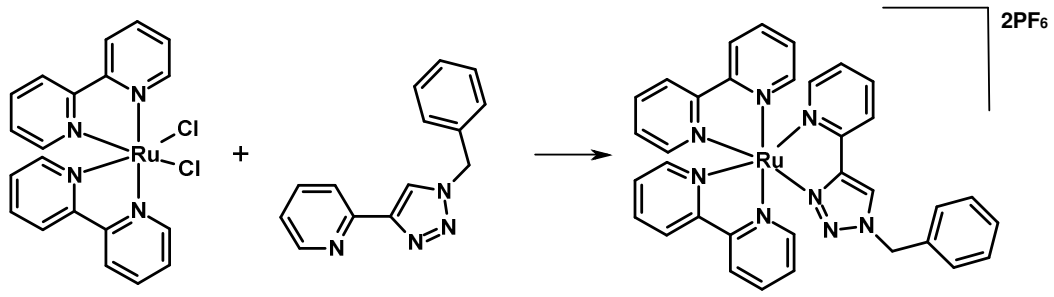

$[Ru(bpy)_2Cl_2]$ (0.1 g, 0.21 mmol) and ligand **10** (0.055 g, 0.231 mmol) were dissolved in ethanol (25 mL). The resulting solution was refluxed for 4 hours. The solution was allowed to cool to room temperature and was purified by column chromatography (silica gel, $MeCN/H_2O$/sat. $KNO_{3\ (aq.)}$ (7:1:0.5)). The desired fraction was evaporated to dryness and then redissolved in ethanol, the product was precipitated as red crystals by addition of excess $NaPF_6$. (0.12 g, 61%)

^1H NMR (CD_3CN) δ (ppm): 8.64 (s, 1H, Tz); 8.54 (dd, J = 8.1 & 3.0 Hz, 2H); 8.46 (dd, J = 13.0 & 8.8 Hz, 2H); 8.12-8.06 (m, 4H); 8.03 (td, J = 7.8 & 1.3 Hz, 1H); 7.98 (td, J = 7.8 & 1.3 Hz, 1H); 7.89 (d, J = 5.8 Hz, 2H); 7.83 (d, J = 5.2 Hz, 1H); 7.76 (d, J = 5.6 Hz, 1H); 7.61 (d, J = 5.6 Hz, 1H); 7.48-7.34 (m, 6H); 7.30 (td, J = 6.3 & 1.4 Hz, 1H); 7.18 (dd, J = 7.4 & 1.4 Hz, 2H); 5.54 (d, J = 2.5 Hz, 2H, benzyl H) ^{13}C NMR (CD_3CN) (ppm): 158.7; 158.4; 158.3; 158.1; 153.2; 153.1; 152.8; 152.7; 151.9; 148.9; 139.3; 138.8; 138.8; 138.8; 138.7; 134.7; 130.1; 130.1; 129.2; 128.6; 128.5; 128.5; 127.8; 127.0; 126.7; 125.3; 125.2; 124.8; 124.5; 123.8; 56.6 (ESI) m/z 325.1 (M^{2+}) HRMS (ESI) calcd: 325.0735, found: 325.0738

2.5 Synthesis of Iridium Complexes

2.5.1 Synthesis of $[Ir(ppy)_2(4,4'\text{-azido-}2,2'\text{-bipyridyl})]PF_6$ (7).

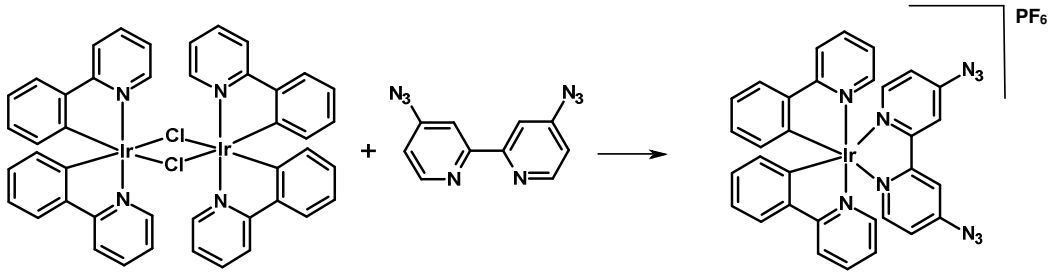

$[Ir(ppy)_2Cl]_2$ (262 mg, 0.24 mmol) and $AgPF_6$ (140 mg, 0.55 mmol) were dissolved in acetonitrile (20 cm^3) and stirred in the dark for 2 hours. The mixture was then filtered through celite, the celite pad was washed with dichloromethane (40 cm^3) and the combined filtrate and washing were reduced to dryness. The residue was dissolved in dichloromethane (20 cm^3) and **4b** was added (117 mg, 0.48 mmol) and the mixture stirred for 1 hour. During this time, the reaction mixture turned dark brown. The volume of solution was reduced by half and diethylether (50 cm^3) was added with stirring to precipitate the complex as a brownish yellow powder which was filtered and washed with diethylether. (376 mg, 89 %)

^{1}H NMR ($CDCl_3$) δ 8.00 (d, J = X Hz, 2H, bpy(N_3)$_2$ H-3); 7.91 (d, J = X Hz, 2H, ppy H-X); 7.81 (d, J = X Hz, 2H, bpy(N_3)$_2$ H-6); 7.78 (t, J = X Hz, 2H, ppy H-X); 7.67 (m, 4H, ppy H-X & H-X); 7.13 (d, J = X Hz, 2H, ppy H-X); 7.03 (m, 4H, ppy H-X & bpy(N_3)$_2$ H-5); 6.92 (t, J = X Hz, 2H, ppy H-X); 6.31 (d, J = X Hz, 2H, ppy H-X).MS (ESI) m/z 739.2 (M^+) HRMS: calcd: 739.165266, found: 739.165101. IR (ATR) 2119 cm^{-1}.

2.5.2 Synthesis of [Ir(ppy)$_2$(4-phenyl-1-(2,2'-bipyrid-4-yl)-1,2,3-triazole)](PF$_6$) (17)

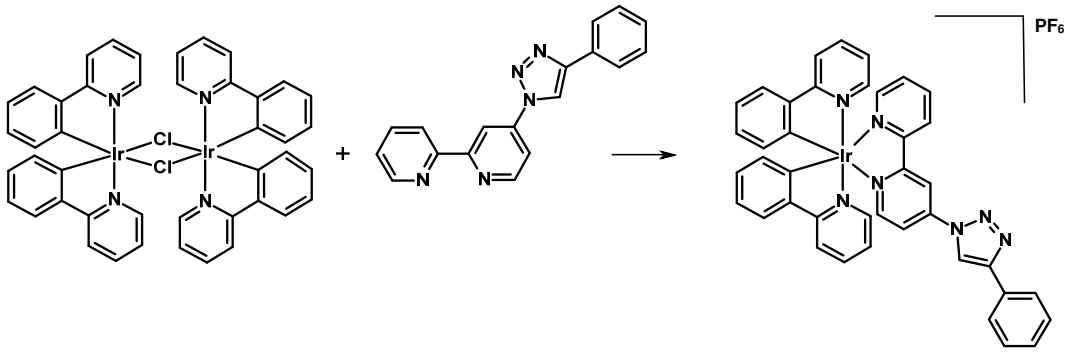

[Ir(ppy)$_2$Cl]$_2$ (0.107 g, 0.10 mmol) and AgPF$_6$ (0.053 g, 0.21 mmol) were dissolved in MeCN (25 mL) and stirred for 2 hours at room temperature in the dark. The yellow solution was filtered through celite to remove AgCl as a white solid and washed with acetonitrile (10 mL). To the resulting yellow solution, was added ligand **5a** (0.063 g, 0.21 mmol) and the solution was stirred for a further 24 hours at room temperature in the dark. The solvent was removed and the resulting orange solid was recrystallised to with dichloromethane/ether to yield yellow crystals. (0.11 g, 58 %)

^{1}H NMR (CD_3CN) δ (ppm): 8.99 (s, 1H, Tz); 8.97 (d, J = 2.7 Hz, 1H, Tz sub-bpy H-3) 8.73 (d, J = 8.2 Hz, 1H, Tz sub-bpy H-3'); 8.19 (t, J = 7.0 Hz, 1H, Tz sub-bpy H-4'); 8.11 (d, J = 6.0 Hz, 1H, Tz sub-bpy H-6); 8.07 (t, J = 7.4 Hz, 2H, ppy); 8.03 (d, J = 5.7 Hz, 1H, Tz sub-bpy H-6'); 7.99 (dd, J = 6.4 & 2.3 Hz, 1H, Tz sub-bpy H-5); 7.96 (d, J = 7.0 Hz, 2H, o-Ph); 7.88-7.79 (m, 4H, ppy); 7.71 (d, J = 5.7 Hz, 1H, ppy); 7.65 (d, J = 5.3 Hz, 1H, ppy); 7.56 (t, J = 6.4 Hz, 1H, Tz sub-bpy H-5'); 7.52 (t, J = 7.4 Hz, 2H, m-Ph); 7.43 (t, J = 8.0 Hz, 1H, p-Ph); 7.09-7.01 (m, 4H, ppy); 6.96-6.90 (m, 2H, ppy); 6.29 (t, J = 7.4 Hz, 2H, ppy) ^{13}C NMR (CD_3CN) δ (ppm): 168.3; 159.1; 156.1; 153.3; 151.9; 150.9; 150.8; 150.3; 150.3; 149.9; 145.9; 145.1; 145.0; 140.5; 139.6; 132.6; 132.5; 131.4; 131.4; 130.6; 130.2; 130.0; 130.0; 126.7; 126.2; 125.9; 125.9; 124.6; 124.4; 123.7; 123.6; 120.9; 120.0; 118.7; 115.4 (ESI) m/z 800.2 (M^+) HRMS (ESI) calcd: 800.200819, found: 800.195416

2.5.3 Synthesis of [Ir(ppy)$_2$(4-ferrocenyl-1-(2,2'-bipyrid-4-yl)-1,2,3-triazole)](PF$_6$) (14)

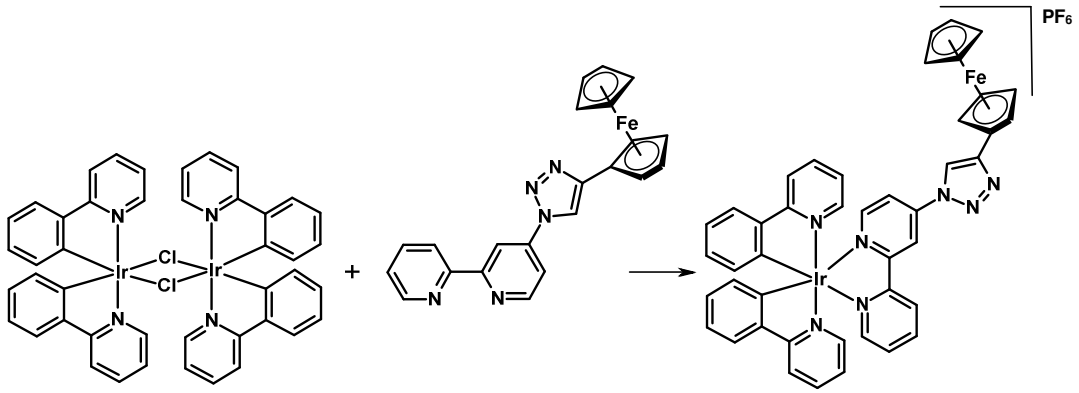

$[Ir(ppy)_2Cl]_2$ (0.107 g, 0.10 mmol) and $AgPF_6$ (0.053 g, 0.21 mmol) were dissolved in acetonitrile (25 mL) and stirred for 2 hours at room temperature in the dark. The yellow solution was filtered through celite to remove AgCl as a white solid and washed with acetonitrile (10 mL). To the resulting yellow solution, was added ligand **5b** (0.063 g, 0.21 mmol) and the solution was stirred for a further 24 hours at room temperature in the dark. The solvent was removed and the resulting orange solid was recrystallised to with dichloromethane/ether to yield yellow crystals. The product was purified by column chromatography (silica gel, MeCN/H_2O/sat. $KNO_{3\ (aq.)}$ (7:1:0.5)) and the desired fraction was evaporated to dryness and redissolved in dichloromethane and stirred with excess $NaPF_6$ for 2 hours. Water was added to the solution and the dichloromethane layer was kept, the aqueous layer was washed with dichloromethane (3 x 25 mL) and the combined dichloromethane fractions were evaporated to dryness to yield an orange solid. (0.13 g, 62 %)

^{1}H NMR (CD_3CN) δ (ppm): 8.90 (d, J = 2.0 Hz, 1H, Tz sub-bpy H-3); 8.71 (d, J = 8.0 Hz, 1H, Tz sub-bpy H-3') 8.59 (s, 1H, Tz); 8.20 (t, J = 8.4, 1H, Tz sub-bpy H-4'); 8.11-8.05 (m, 4H, Tz sub-bpy H-3' & ppy); 8.03 (d, J = 4.7 Hz1H, Tz sub-bpy H-6'); 7.94 (dd, J = 6.4 & 2.0 Hz, 1H, Tz sub-bpy H-5); 7.88-7.79 (m, 4H, ppy); 7.70 (d, J = 6.4 Hz, 1H, ppy); 7.65 (d, J = 5.7 Hz, 1H, ppy); 7.56 (t, J = 6.4 Hz, 1H, Tz sub-bpy H-5') 7.10-7.01 (m, 4H, ppy); 6.96-6.90 (m, 2H, ppy); 6.29 (t, J = 7.0 Hz, 2H, ppy); 4.82 (t, J = 1.7 Hz, 2H, C_5H_4Fe); 4.39 (t, J = 1.7 Hz, 2H, C_5H_4Fe); 4.14 (s, 5H, Cp); ^{13}C NMR (CD_3CN) (ppm): 168.5; 159.1; 156.2; 153.3; 151.9; 150.8; 150.4; 150.3; 149.9; 145.9; 145.1; 145.1; 140.5; 139.7; 132.6; 132.6; 131.5; 131.5; 130.1; 126.2; 126.0; 126.0; 124.6; 124.5; 123.7; 123.7; 121.0; 118.7; 118.6; 115.3; 75.1; 70.6; 70.2; 67.9 (ESI) m/z 908.2 (M^+) HRMS (ESI) calcd: 908.177062, found: 908.1532

2.5.4 Synthesis of [{Ir(ppy)$_2$}$_2$(4-pyrid-2-yl-1-(2,2'-bipyrid-4-yl)-1,2,3-triazole)](PF$_6$)$_2$ (25)

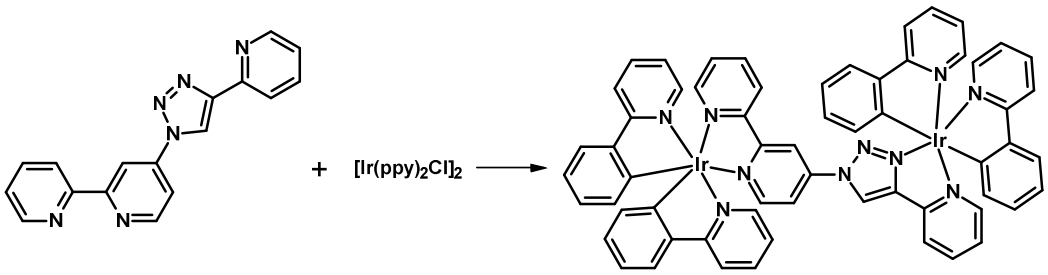

[Ir(ppy)$_2$Cl]$_2$ (0.356 g, 0.333 mmol) and $AgPF_6$ (0.168 g, 0.666 mmol) were dissolved in MeCN (100 mL) and stirred for 2 hours at room temperature in the dark. The yellow solution was filtered through celite to remove AgCl as a white solid and washed with acetonitrile (25 mL). To the resulting yellow solution, was added ligand **5c** (0.10 g, 0.333 mmol) and the solution was stirred for a further 48 hours at reflux in the dark. The solvent was removed and the resulting orange solid was recrystallised to with dichloromethane/ether to yield yellow crystals. The product was purified by column chromatography (silica gel, MeCN/H_2O/sat. $KNO_{3\ (aq.)}$ (7:1:0.5)) and the desired fraction was evaporated to dryness and redissolved in dichloromethane and stirred with excess $NaPF_6$ for 2 hours. Water was added to the solution and the dichloromethane layer was kept, the aqueous layer was washed with dichloromethane (3 x 25 mL) and the combined dichloromethane fractions were evaporated to dryness to yield an orange solid. (0.24 g, 45 %)

^{1}H NMR (CD_3CN) δ (ppm): 9.84 & 9.72 (2 x s, 1H, Tz); 9.51 & 9.42 (2 x d, 1H); 9.47 (t, J = 8.9 Hz, 1H); 8.23-7.90 (m, 9H); 7.90-7.75 (m, 10H); 7.75-7.64 (m, 3H); 7.62 & 7.58 (2 x d, 1H); 7.53 (t, J = 6.4 Hz, 1H); 7.42 (t, J = 6.8 Hz, 1H); 7.11-6.87 (m, 11H); 6.85-6.80 (m, 1H); 6.28-6.23 (m, 4H) ^{13}C NMR (CD_3CN) (ppm): 167.3; 167.3; 167.1; 167.0; 167.0; 166.9; 166.7; 166.7; 158.7; 158.6; 154.8; 152.3; 152.3; 150.4; 150.2; 150.1; 150.1; 149.6; 149.6; 149.4; 149.2; 149.1; 149.0; 148.9; 148.5; 148.5; 145.4; 145.3; 144.1; 144.1; 144.0; 143.8; 143.7; 143.7; 143.7; 139.8; 139.3; 138.4; 138.4; 138.3; 138.3; 138.2; 131.5; 131.2; 131.1; 131.0; 130.9; 130.1 ;130.0; 129.3; 129.3; 128.8; 128.8; 127.0; 126.5; 126.4; 126.2; 126.1; 124.6; 124.5; 124.0; 124.0; 123.3; 123.2; 123.2; 123.2; 123.1; 123.1; 123.0; 122.5; 122.3; 122.0; 119.6; 119.6; 119.5; 119.4; 119.3; 117.8; 117.7; 115.4; 115.3 (ESI) m/z 651.2 (M^{2+}) HRMS (ESI) calcd: 651.149896, found: 651.1499

2.5.5 Synthesis of [Ir(ppy)$_2$(4-pyrid-2-yl-1-benzyl-1,2,3-triazole)](PF$_6$) (27)

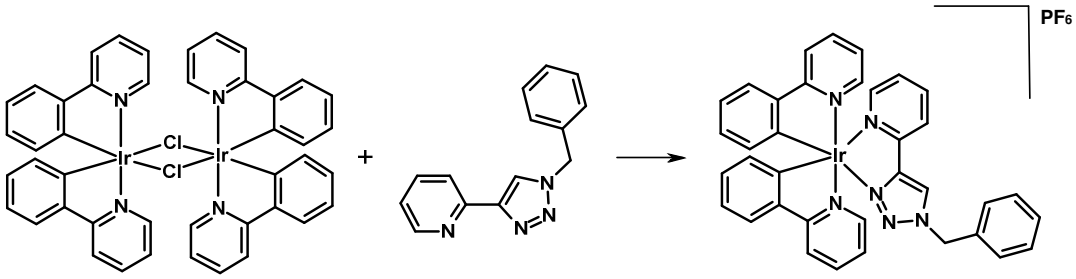

$[Ir(ppy)_2Cl]_2$ (0.107 g, 0.10 mmol) and $AgPF_6$ (0.053 g, 0.21 mmol) were dissolved in acetonitrile (25 mL) and stirred for 2 hours at room temperature in the dark. The yellow solution was filtered through celite to remove AgCl as a white solid and washed with acetonitrile (10 mL). To the resulting yellow solution, was added ligand **10** (0.055 g, 0.21 mmol) and the solution was stirred for a further 24 hours at room temperature in the dark. The solvent was removed and the resulting yellow solid was recrystallised to with dichloromethane/ether to yield yellow crystals. The product was purified by column chromatography (alumina, 2% methanol in dichloromethane) and the desired fraction was evaporated to dryness and redissolved in dichloromethane and recrystallised with ether. (0.13 g, 74 %)

^{1}H NMR (CD_3CN) δ (ppm): 8.60 (s, 1H, Tz); 8.07 (t, J = 7.5 Hz, 2H); 8.01 (td, J = 8.3 & 1.3 Hz, 2H); 7.85 (t, J = 7.5 Hz, 2H); 7.81 (d. J = 5.5 Hz, 1H); 7.77 (d, J = 7.7 Hz, 1H); 7.73 (d, J = 6.8 Hz, 2H); 7.60 (d, J = 5.5 Hz, 1H); 7.41-7.36 (m, 3H); 7.34 (dt, J = 7.0 & 1.7 Hz, 1H); 7.23 (dd, J = 7.6 & 1.7 Hz, 2H); 7.07 (t, J = 6.2 Hz, 1H); 7.05-7.00 (m, 2H); 6.95 (t, J = 7.6 Hz, 1H); 6.90 (td, J = 7.4 & 1.1 Hz, 1H); 6.82 (t, J = 7.4 Hz, 1H); 6.25 (t, J = 8.1 Hz, 2H); 5.58 (d, J = 2.27 Hz, 2H, benzyl H) ^{13}C NMR (CD_3CN) (ppm): 168.7; 168.3; 151.4; 150.7; 150.5; 150.4; 150.3; 149.9; 147.5; 145.4; 145.3; 140.7; 139.6; 139.5; 134.6; 132.9; 132.5; 131.4; 130.7; 130.2; 130.1; 129.3; 127.8; 127.2; 125.9; 125.4; 124.5; 124.3; 123.9; 123.7; 123.3; 120.9; 120.7; 56.5 (ESI) m/z 737.2 (M^+) HRMS (ESI) calcd: 737.1999, found: 737.2000

3 ELECTRONIC AND PHOTOPHYSICAL EFFECTS OF 1,2,3-TRIAZOLE BASED LIGANDS

3.1 Introduction

In the last few decades rhenium(I) bipyridyl tricarbonyl complexes have attracted a great deal of interest for their luminescent and photophysical properties. These complexes have been used as photocatalysts for CO_2 reduction, [169-173] emitters for electroluminescent devices, [174-176] biological imaging agents [177-180] and as supramolecular building blocks. [181, 182] Indeed, *fac*-[Re(bpy)$(CO)_3$Cl] and its derivatives represent one of the most widely studied transition metal complex synthons. Luminescent emission, energy transfer, and electron transfer occur mainly through triplet metal-to-ligand-charge transfer (^{3}MLCT) or triplet ligand-centred (^{3}IL) excited states. The chloride ion can readily be replaced with other ions or neutral ligands such as pyridine, acetonitrile and phosphines. Similarly the bipyridyl ligand can be replaced with other bidentate nitrogen donor ligands such as 1,10-phenanthroline, 2,2'-bipyrazine and 2,2'-bipyrimidine etc. The 1,2,3-triazole moiety therefore has the potential to act as either an axial donor ligand in place of Cl^- or form part of a bidentate donor ligand when coupled with another nitrogen donor moiety.

In this chapter we explore the use of the 1,2,3-triazole ligand as a monodentate axial coordinating ligand and investigate the electronic and photophysical properties of the corresponding rhenium complexes. Similarly we explore the use of 4-(pyridyl)-1,2,3-triazole ligands and investigate the electronic and photophysical properties of the resultant rhenium complexes.

3.2 Synthesis and characterisation

3.2.1 Ligand Synthesis for monodentate coordinating triazole ligands

Ligands **1a-1d** where prepared in a one-pot CuAAC synthetic procedure (Scheme 3.1) starting from the corresponding alkyl halide and alkyne. All four of the starting azides were prepared *in situ* from corresponding alkyl halides by nucleophilic substitution with a slight excess of sodium azide in dimethylsulfoxide at room temperature for 2 hours. **Warning:** low molecular weight azides are often thermally and shock sensitive and may detonate, therefore they should not be isolated and should only be generated and used *in situ*. Upon completion of the substitution reaction, the remainder of the starting material required for the CuAAC was added to the reaction; a slight excess of the alkyne was added in the presence of a catalytic quantity of $CuSO_4$, sodium ascorbate and 2,6-lutidine. The products were isolated by simple filtration of the reaction mixture and were further purified by recrystallisation from dichloromethane and hexane. All ligands were isolated in moderate to good yields.

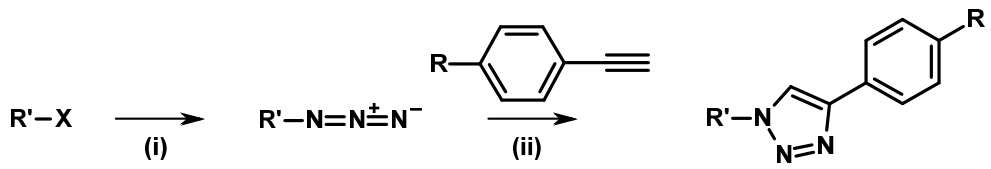

	X =	R' =	R =
1a	I	Me	H
1b	Br	*n*-Pr	H
1c	Br	Bn	H
1d	Br	*n*-Pr	Me

Scheme 3.1 One-pot synthesis of 1,2,3-triazole ligands starting from corresponding halide. (i) dimethyl sulfoxide and NaN_3 at room temperature; (ii) dimethyl sulfoxide/H_2O, $CuSO_4$ (aq.), sodium ascorbate (aq.) and 2,6-lutidene at room temperature.

Ligand **1c** was also prepared from isolated benzyl azide. Benzyl azide was prepared by reaction of benzyl bromide with an excess of sodium azide in dimethylsulfoxide. Upon completion, the reaction was quenched with water, and the azide extracted into diethyl ether. Benzyl azide was stored at -4°C and used in subsequent reactions. The benzyl triazole was formed by reaction of the azide with an excess of phenyl acetylene in the presence of one equivalent of $CuSO_4$ and two equivalents of sodium ascorbate in THF and water. After stirring at room temperature for 30 minutes, isolation of the product was achieved by partitioning between dichloromethane and aqueous ammonia to remove copper. Purification of the ligand was achieved by recrystallisation from dichloromethane and hexane.

Ligands **1a-1d** have been fully characterised using ^{1}H and ^{13}C NMR spectroscopy and mass spectrometry. The ^{1}H NMR spectra for the free ligands show a distinct diagnostic signal for the C-H proton of the triazole ring (Figure 3.1). These appear as singlet resonances over the range of δ 7.5-8.6. These signals show nOe interactions in their two dimensional NOESY spectra with the *ortho*-protons of the 4-aryl substituent and the α-protons of the 1-alkyl group therefore confirming the 1,4-regiochemistry of the 1,2,3-triazole. Successful synthesis of **1a-1d** was also confirmed using FT-IR spectroscopy where the lack of the azide and acetylene stretching modes at around 2100 to 2150cm^{-1} indicated that no starting materials were present and that the reactions had gone to completion.

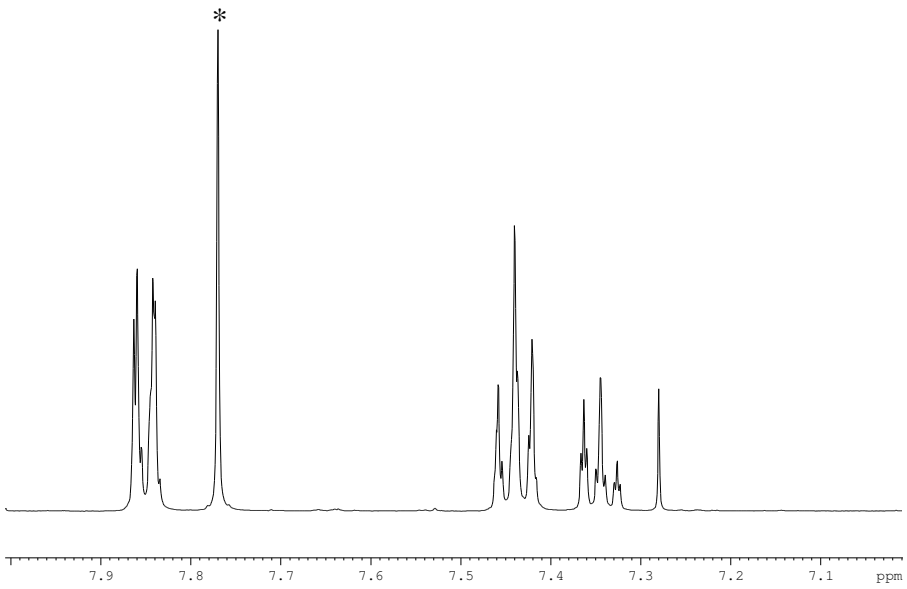

*Figure 3.1 Aromatic region of the ^{1}H NMR spectrumof ligand **1b** ($CDCl_3$). *CH proton of the triazole ring.*

3.2.2 Synthesis of cationic rhenium(I) triazole complexes

The rhenium(I) complexes, were prepared by firstly isolating the starting material *fac*-[Re(bpy)$(CO)_3$Cl] using a similar procedure to that of Meyer *et al.*[163] by heating rhenium pentacarbonylchloride with a slight excess of 2,2'-bipyridyl at reflux in toluene. The yellow precipitate was collected and used without further purification. Stirring *fac*-[Re(bpy)$(CO)_3$Cl] with an excess of silver hexafluorophosphate overnight in the dark and in the presence of slight excess of the appropriate triazole ligand in dichloromethane resulted in a green solution. The products were recrystallised from dichloromethane and ether to yield yellow solids in good yields. The complexes [Re(bpy)$(CO)_3$(**1a-1d**)]PF_6 (**2a-2d**) have been fully characterised using ^{1}H and ^{13}C NMR spectroscopy, mass spectrometry, high resolution mass spectrometry and FT-IR spectroscopy. The known pyridine complex [Re(bpy)$(CO)_3$(Py)]PF_6 (**2e**) was also prepared for comparison [163].

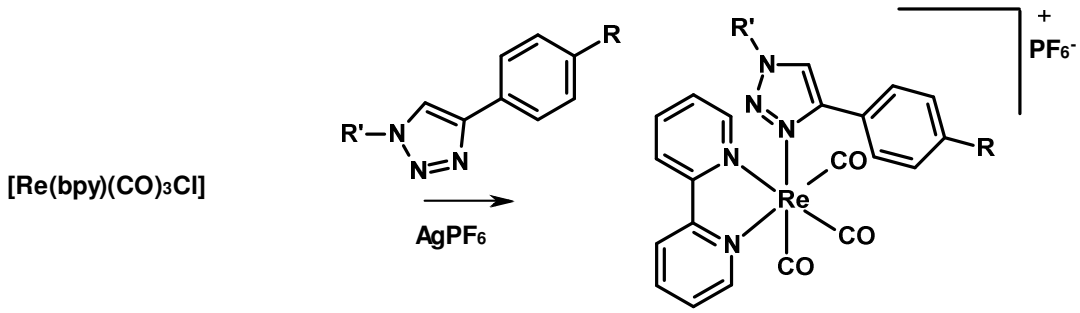

*Scheme 3.2 Preparation of [Re(bpy)$(CO)_3$(**1a-1d**)]PF_6. (2a-2d)*

^{1}H and ^{13}C NMR spectroscopy was used to confirm that all four triazole complexes had been successfully prepared. The ^{1}H NMR spectra of **2a-2d** each show four signals for the bipyridyl ligand along with the resonance for the proton of the triazole ring. These resonances for the triazole proton appear between δ 7.66-7.80, and are shielded with respect to those of the free ligands.

The infrared spectra of the complexes show two bands corresponding to the ν_{CO} stretching modes with the symmetric stretches appearing at ~2035 cm^{-1} with the approximately coincident asymmetric stretches centred at ~1926 cm^{-1}, slightly lower in energy than those observed for the pyridine complex. These data therefore suggest that the monodentate triazole ligands are perhaps marginally better but comparable donors to pyridine in agreement with binding competition experiments for their Pd and Pt [70] complexes and spectroscopic data from known Re pytz and btz complexes. [56, 96] FT-IR data for all complexes are shown in Table 2.1

*Table 3.1 Carbonyl stretching frequencies for complexes [Re(bpy)(CO)$_3$(**L**)]$^{+/0}$: [Re(bpy)(CO)$_3$(**1a-1d**)]PF$_6$ (**2a-2d**) and reference complexes [Re(bpy)(CO)$_3$(Py)]PF$_6$ and [Re(bpy)(CO)$_3$Cl]*

Complex	L	ν_{CO} (cm^{-1})
2a	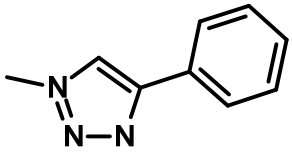	2035, 1929
2b	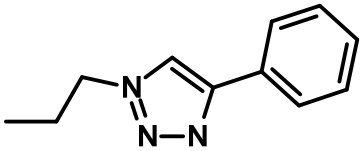	2035, 1923
2c	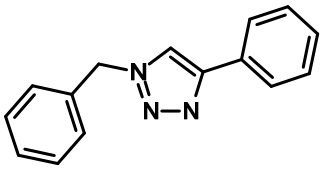	2035, 1923
2d	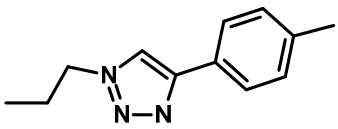	2033, 1928
2e	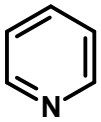	2037, 1932
2f	**Cl$^-$**	2024, 1928 & 1888

3.2.2.1 Crystallographic analysis

Single crystals of X-ray diffraction quality of three of the complexes were obtained through slow diffusion of hexane into dichloromethane solutions of the complexes. The data obtained for complexes $[Re(bpy)(CO)_3(\mathbf{1a})]PF_6$ and $[Re(bpy)(CO)_3(\mathbf{1b})]PF_6$ were of good quality, however the X-ray crystal structure which was obtained for complex **2c** $[Re(bpy)(CO)_3(\mathbf{1c})]PF_6$ showed disorder in the phenyl substituent of the triazole ligand which could not be successfully modelled. This structure is included here only for completeness. We were unable to grow any further crystals of diffraction quality for this complex and no suitable crystals of diffraction quality could be obtained for complex **2d**. Figure 3.2, Figure 3.3 and Figure 3.4 depict the molecular structures of each of the cationic complexes, $[Re(bpy)(CO)_3(\mathbf{1a\text{-}1c})]^+$ whilst selected bond lengths and angles are provided in Table 3.2.

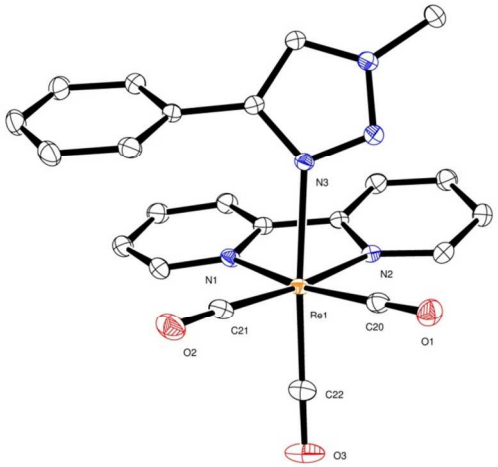

Figure 3.2 ORTEP plot of the structure of the cation $[Re(bpy)(CO)_3(\mathbf{1a})]^+(\mathbf{2a})$ (hydrogen atoms and PF_6^- counterion omitted for clarity, ellipsoids at 50% probability).

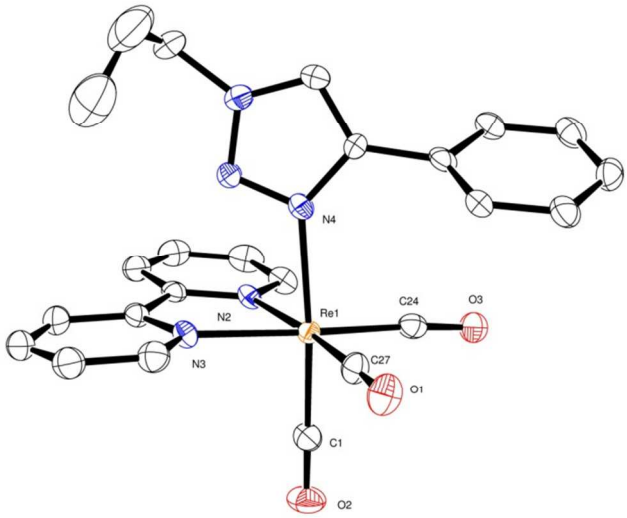

*Figure 3.3 ORTEP plot of the structure of the cation $[Re(bpy)(CO)_3(\mathbf{1b})]^+$ (**2b**) (hydrogen atoms and PF_6^- counterion omitted for clarity, ellipsoids at 50% probability).*

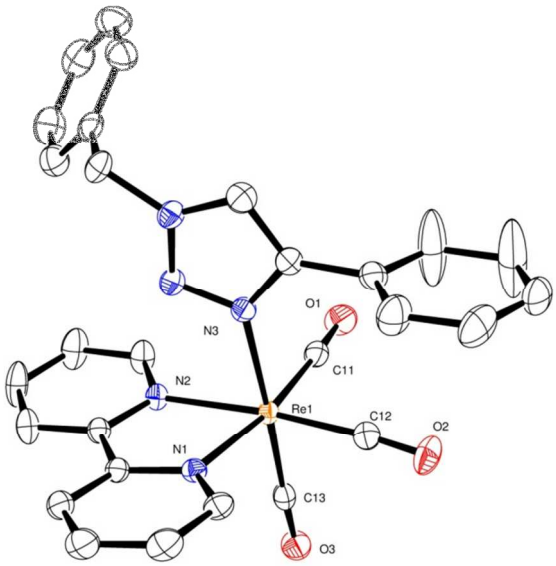

*Figure 3.4 ORTEP plot of the structure of the cation $[Re(bpy)(CO)_3(\mathbf{1c})]^+$ (**2c**) (hydrogen atoms and PF_6^- counterion omitted for clarity, ellipsoids at 50% probability).*

*Table 3.2 Selected bond lengths (Å) and angles (°) for single-crystal X-ray structures of [Re(bpy)(CO)$_3$(**1a**)]PF$_6$ (**2a**), [Re(bpy)(CO)$_3$(**1b**)]PF$_6$ (**2b**) and [Re(bpy)(CO)$_3$(**1c**)]PF$_6$ (**2c**)*

[Re(bpy)(CO)$_3$(1a)]$^+$ (2a)			
Re-N1	2.1733(13)	Re-C22	1.9176(18)
Re-N2	2.1711(14)	C20-O1	1.150(2)
Re-N3	2.2186(14)	C21-O2	1.154(2)
Re-C20	1.9319(17)	C22-O3	1.152(2)
Re-C21	1.9221(18)		
N1-Re-N2	74.80(5)	C22-Re-C21	87.69(8)
N1-Re-N3	83.92(5)	C20-Re-C21	88.56(7)
N2-Re-N3	78.82(5)	C20-Re-C22	89.16(7)
C22-Re-N3	172.82(7)		
[Re(bpy)(CO)$_3$(1b)]$^+$ (2b)			
Re-N2	2.164(4)	Re-C27	1.922(5)
Re-N3	2.170(4)	C1-O2	1.150(6)
Re-N4	2.198(4)	C24-O3	1.155(6)
Re-C1	1.915(5)	C27-O1	1.145(6)
Re-C24	1.930(5)		
N2-Re-N3	75.07(14)	C1-Re-C24	88.2(2)
N2-Re-N4	82.70(14)	C1-Re-C27	88.1(2)
N3-Re-N4	83.90(14)	C24-Re-C27	86.9(2)
C1-Re-N4	174.50(18)		

$[Re(bpy)(CO)_3(1c)]^+$ (2c)			
Re-N1	2.1703(18)	Re-C13	1.917(2)
Re-N2	2.1707(18)	C11-O1	1.149(3)
Re-N3	2.2034(19)	C12-O2	1.155(3)
Re-C11	1.924(2)	C13-O3	1.151(3)
Re-C12	1.921(2)		
N1-Re-N2	74.87(6)	C24-Re-C26	89.00(9)
N1-Re-N3	84.43(6)	C25-Re-C26	85.62(8)
N2-Re-N3	83.43(6)	C24-Re-C25	89.36(9)
C26-Re-N3	177.36(7)		

$[Re(bpy)(CO)_3(\mathbf{1a})]PF_6$ crystallises in the space group C2/c whilst $[Re(bpy)(CO)_3(\mathbf{1b})]PF_6$ and $[Re(bpy)(CO)_3(\mathbf{1c})]PF_6$ crystallised in the space groups Pbca and P-1 respectively. As can be seen in Figure 3.2, Figure 3.3 and Figure 3.4 all the complexes adopt distorted octahedral geometries with facial arrangements of the carbonyl ligands. It can also be seen that the triazole ligand coordinates to the rhenium metal centre through the N3 atom of the 1,2,3-triazole ring which would be expected as this is the more basic nitrogen of the two potential nitrogen donor atoms. The Re-N bonds to the 2,2'-bipyridyl ligands are all approximately the same length at ~2.17 Å. The Re-N bond lengths to the axial triazole ligands are 2.2186, 2.198 and 2.2034 Å for ligands **1a-1c** respectively. These bond lengths are within the range observed for related tricarbonylrhenium

diimine complexes. For example the corresponding axial Re-N bond length in [Re(bpy)$(CO)_3$(Py)]OTf [183] is 2.194(6) Å and in [Re(1,10-phenanthroline)$(CO)_3$(imidazole)]$_2SO_4$ [184] the corresponding Re-N bond length is 2.185(5) Å.

The C-O bond lengths for the carbonyl ligands in all three of the complexes are unremarkable and vary between 1.145-1.155 Å. The Re-C bond lengths to the carbonyl which are *trans* to the triazole ligands are slightly shorter when compared to those *trans* to bpy and are 1.9176, 1.916 and 1.917 Å for complexes **2a**, **2b** and **2c** respectively. This shortening of the Re-C bond length is complementary to the results obtained from the infra-red experiments, and could be indicative of the slightly greater donor strength of the triazole ligands when compared to the pyridyl donors of the bipyridyl ligand. However this shortening isn't significant with respect to experimental error and there is no accompanying elongation of the C-O bond length for the carbonyl *trans* to the triazole compared to those *trans* to the bipyridyl.

Although there is only a slight difference in the chemical structures of complexes **2a** and **2b** (in terms of the substituent at the 1-position of the triazole ligand changing from methyl to propyl respectively), the orientation of the triazole ligands in the solid state is quite different. For the 1-propyl-4-phenyl-1,2,3-trialzole complex **2b** , and indeed the 1-benzyl-4-phenyl-1,2,3-triazole complex **2c**, the Re-triazole bond lengths are ~2.20 Å and the triazole ligands are orientated in such a way that their respective phenyl groups lie over the carbonyl ligands. However, for the 1-methyl-4-phenyl-1,2,3-triazole complex **2a** the Re-N(triazole)

bond length is elongated with respect to those in **2b** and **2c**, and is 2.2192 Å. Here, the triazole is orientated such that the phenyl group lies over one of the pyridyl rings of the bipyridyl ligand. The phenyl and pyridyl rings are almost coplanar and are separated by a distance of approximately 3.3 Å indicative of a π-stacking interaction. The formation of this π-stacking interaction leads to a significant twist in the bipyridyl ligand and a tilt in the triazole ligand. The plane of the triazole ring is tilted by 13 ° with respect to the Re-N(triazole) bond which compares to a much smaller tilt of only 5.2 ° for the propyl-substituted ligand. As a result of the π-stacking interaction with the phenyl ring of the ligand **1a** the participating pyridyl ring is twisted such that it is inclined by 3.4° with respect to the N1-Re bond and is twisted by 8.5° with respect to the plane defined by the Re atom and the carbonyl carbon atoms *trans* to bpy. This twisting also results in an angle of 8.5° between the planes of the two pyridyl rings and a more severe deviation in coplanarity of the second pyridyl ring with respect to the square plane about the Re centre. Here, the ring has an inclination of the 15° with respect to the N2-Re bond and a twist of 21.2° relative to the same plane defined by the Re atom and carbonyl ligands. Similar distortions of the bpy ligand have also been observed in related complexes with axial phosphine ligands due to π-π interactions between the bpy ligand and the aryl substituents of the phosphine. [185] In comparison, the propyl triazole complex (**2b**) experiences much less distortion. The twist between rings of the bpy ligand of is only 5.3°, the rings have inclinations with respect to their Re-N bonds of only 1.9 and 3.2° and are twisted relative to the plane of the Re atom and the *trans* carbonyl carbon atoms by 2.7 and 2.6°.

The increase in steric bulk of the propyl and benzyl groups compared to that of the methyl substituent could explain the distortion observed in the geometry for the complex **2a**. In the solid state, the methyl carbon of one $[Re(bpy)(CO)_3(\mathbf{1a})]^+$ cation comes within 3.0 Å of the carbonyl oxygen of one of the neighbouring cations. It maybe that the extra steric bulk of the propyl and benzyl groups of ligands **1b** and **1c** therefore hinder the adoption of the crystal packing arrangement that promotes the formation of this π-stacking interaction which is observed for complex **2a**.

3.2.2.2 Photophysical studies

UV-vis absorption spectra of complexes **2a-2d** along with those of $[Re(bpy)(CO)_3Cl]$ and $[Re(bpy)(CO)_3(Py)]PF_6$ where recorded in acetonitrile. The UV-vis spectra that were obtained for complexes **2a-2d** are almost identical to each other as can be seen in Figure 3.5. Photophysical data are summarised in Table 3.3

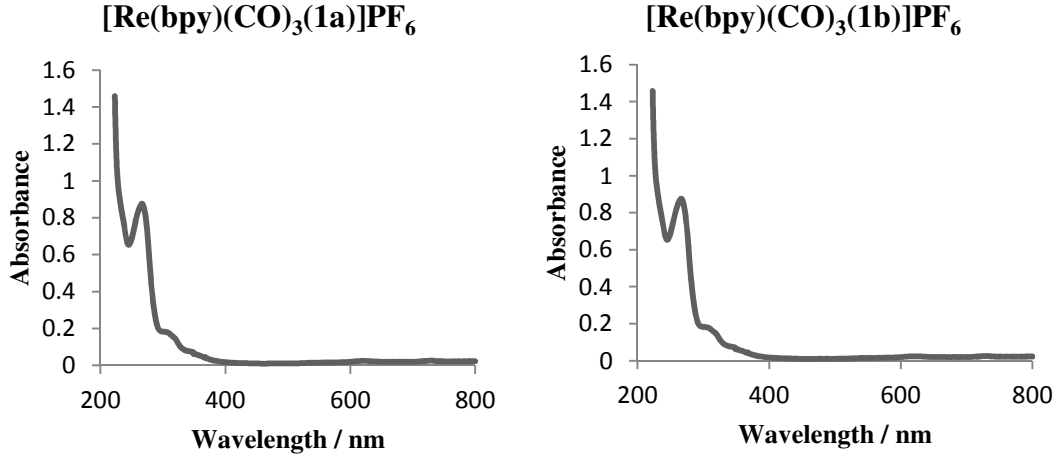

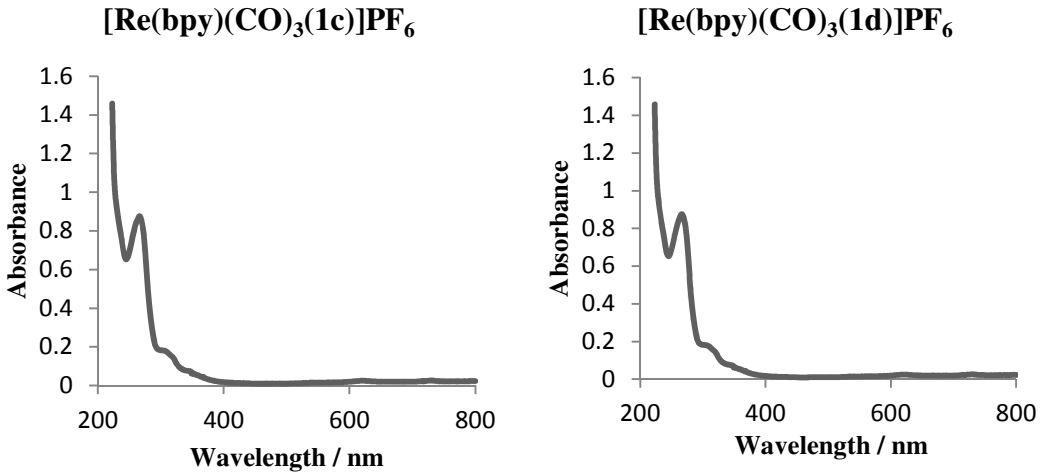

*Figure 3.5 UV-vis absorption spectra for [Re(bpy)(CO)$_3$(**1a-1d**)]PF$_6$ in acetonitrile*

For these complexes the dominant absorption bands in the shorter wavelength region at 250-270 nm were assigned to the intraligand $\pi \rightarrow \pi^*$ transitions. These assignments were made on assessment of closely related metal complexes in the literature. The low energy broad bands at approximately 325 nm are attributed to the metal to ligand charge-transfer (^{1}MLCT) dπ(Re) $\rightarrow \pi^*$ (bpy) transitions. All the MLCT absorption bands of complexes **2a-2d** are similar to those observed in related Re(I) carbonyl complexes [96, 184, 185] and exhibit a blue shift in absorption in comparison to the parent halide complex [Re(bpy)(CO)$_3$Cl]. This is explained by replacement of the π-donor chloride ligand with the π-accepting triazole ligand which would therefore lead to a decrease in the energy of the dπ(Re) HOMO with respect to the LUMO, resulting in higher energy MLCT transitions.

Luminescence measurements were recorded at room temperature in aerated dichloromethane and acetonitrile with an excitation wavelength of 400 nm. Figure 3.6 shows the normalised emission spectra for the four triazole complexes **2a-2d**

as well as the pyridine complex $[Re(bpy)(CO)_3(Py)]^+$ and the parent chloride complex $[Re(bpy)(CO)_3(Cl)]$.

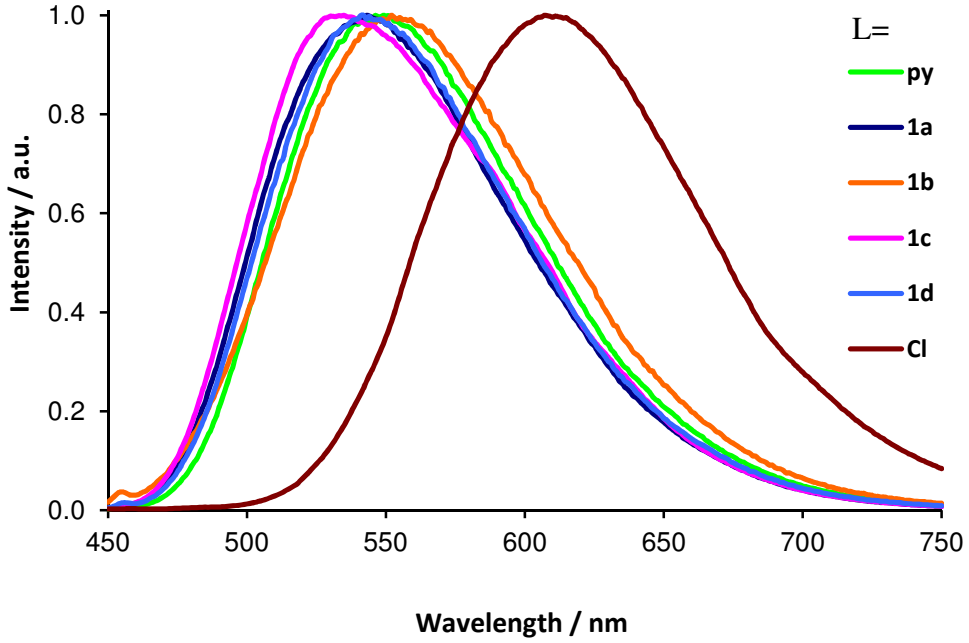

Figure 3.6 Normalised luminescence spectra for the complexes $[Re(bpy)(CO)_3(L)]^{+/0}$ *(L= 1a-d, Py, Cl⁻)*

Broad emission bands are observed with λ_{max} appearing over a 10 nm range for the triazole complexes between 542 to 552 nm in dichloromethane solutions. These bands are assigned to phosphorescent emission from triplet metal-to-ligand charge-transfer (^{3}MLCT) excited states. These emission bands are significantly blue-shifted relative to that of the parent chloride complex $[Re(bpy)(CO)_3Cl]$ (612 nm) consistent with the replacement of a π-donor with a moderately π-accepting ligand leading to stabilisation of the HOMO relative to the LUMO. The analogous pyridine complex $[Re(bpy)(CO)_3(Py)]^+$ exhibits

an emission band at 549 nm under the same conditions. This is consistent with observations of other cationic rhenium tricarbonyl complexes diimine complexes where changing the nature of the axial N-donor ligand has very little effect on the emission properties of the complexes. [96] Very little difference in the position of emission maximum is observed when changing solvent from dichloromethane to acetonitrile.

Luminescence lifetime measurements were recorded for all complexes in aerated dichloromethane solutions at room temperature by time-correlated single photon counting spectroscopy. The decay traces for the emission from complexes **2a-2d** are shown in Figure 3.7. Long luminescent lifetimes of between 475 and 513 ns were observed for the triazole containing complexes consistent with phosphorescent emission from the ^{3}MLCT state. These lifetimes are significantly longer than that of the chloride complex (42 ns) and slightly longer than that measured for the pyridine complex $[Re(bpy)(CO)_3(Py)]^+$ measured under identical conditions (466 ns). When the lifetimes were measured in acetonitrile, much shorter lifetimes were determined of 130–140 ns.

*Table 3.3 Photophysical properties for [Re(bpy)(CO)$_3$(**1a-1d**)]PF$_6$, [Re(bpy)(CO)$_3$(Py)]PF$_6$ and [Re(bpy)(CO)$_3$(Cl)] in dichloromethane*

Complex	λ^{abs} / nm	λ_{max}^{em} / nm	τ / ns
[Re(bpy)(CO)$_3$(1a)]PF$_6$	266, 298, 337	543	482
[Re(bpy)(CO)$_3$(1b)]PF$_6$	266, 298, 338	552	475
[Re(bpy)(CO)$_3$(1c)]PF$_6$	266, 301, 339	535	513
[Re(bpy)(CO)$_3$(1d)]PF$_6$	265, 300, 340	542	477
[Re(bpy)(CO)$_3$(Cl)]	264, 300, 346	612	42
[Re(bpy)(CO)$_3$(Py)]PF$_6$	266, 299, 345	549	466

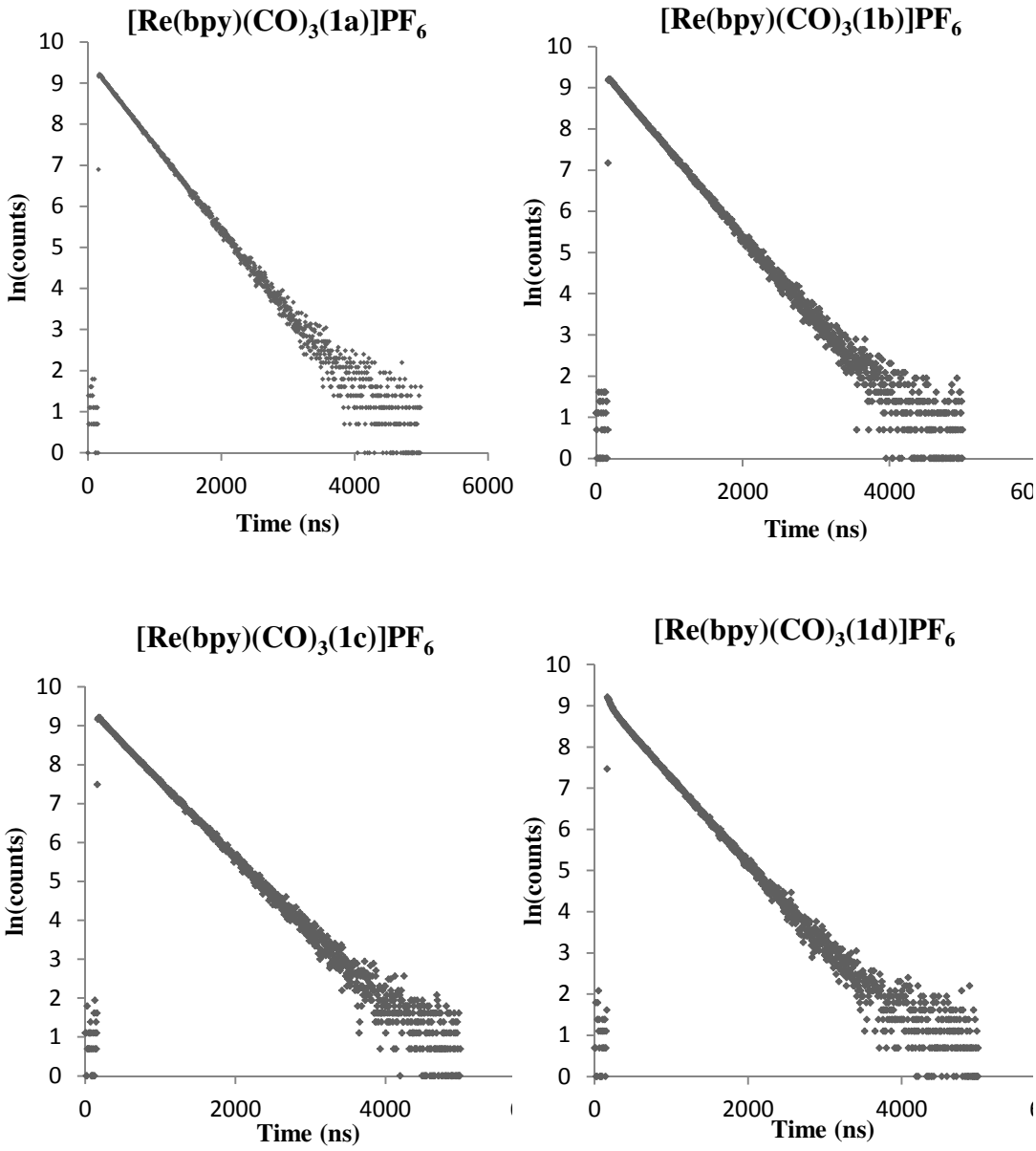

*Figure 3.7 Luminescent lifetime measurements for [Re(bpy)(CO)$_3$(**1a-1d**)]PF$_6$ in dichloromethane.*

A series of cationic bipyridyltricarbonylrhenium(I) complexes (**2a-2d)** with axial monodentate 1,2,3-triazole ligands have been prepared and fully characterised. It has been shown that subtle changes in the ligand scaffold can have an impact on the solid state structural properties of these types of molecules. This is evident in the single-crystal X-ray structure of **2a,** the cation adopts a highly distorted structure due to the π-stacking interaction between the triazole phenyl substituent and one ring of the bpy ligand. Infrared data suggest that the triazole ligands (**1a-1d)** are slightly better donors than pyridine also the rhenium complexes of these ligands have long luminescent lifetimes in aerated dichloromethane at room temperature with λ_{max}^{em} comparable to that of $[Re(bpy)(CO)_3(Py)]^+$.

3.3 Rhenium tricarbonyl complexes with bidentate pyridyl-1,2,3-triazole ligands

Whereas replacing the Cl^- ligand by the triazole modulates the energy of the HOMO with respect to the LUMO, changing the bidentate ligand by replacing the bipyridyl ligand by pyridine-triazole ligand would be expected to elevate the LUMO with respect to the HOMO.

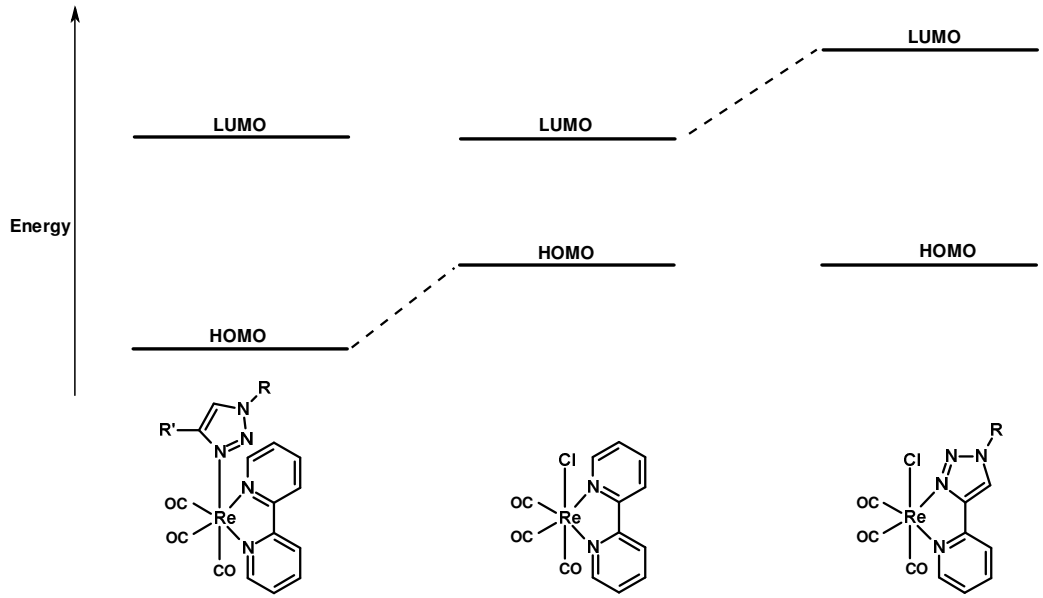

Figure 3.8 Energy level diagram of rhenium tricarbonyl complexes showing modulation of the HOMO and LUMO on replacement of Cl^- and bpy ligands respectively.

Described in this section of the chapter is the synthesis and characterisation of 1-cyclohexyl-4-(pyrid-2-yl)-1,2,3-triazole and its corresponding rhenium complex. We had tried to probe the effects on the photophysical properties of the complex isomers of the ligand as the alternative isomer 4-cyclohexyl-1-(pyrid-2-yl)-1,2,3-triazole should be accessible from ethynyl cyclohexane and 2-azidopyridine. Unfortunately the alternative isomer of this ligand could not be successfully isolated. Therefore we have studied these systems computationally and calculated the electronic and photophysical properties of these complexes.

3.3.1 Synthesis and characterisation of [Re(1-cyclohexyl-4-(pyrid-2-yl)-1,2,3-triazole)$(CO)_3$Cl

The ligand 1-cyclohexyl-4-(pyrid-2-yl)-1,2,3-triazole (**3a**) was prepared by a two step synthesis. (Scheme 3.3) Firstly cyclohexyl bromide was converted into cyclohexyl azide through a nucleophilic substitution reaction in the presence of excess of sodium azide in dimethylsulfoxide. Water was then added to quench the reaction after 12 hours and the cyclohexyl azide was isolated as a colourless oil in good yield after extraction with diethyl ether. 2-Ethynylpyridine was added to the azide with a catalytic quantity of $CuSO_4$ with sodium ascorbate as a reducing agent in a 1:1 water/THF mixture. Ligand **3a** was obtained as a white solid after purification by column chromatography in good yield (73%).

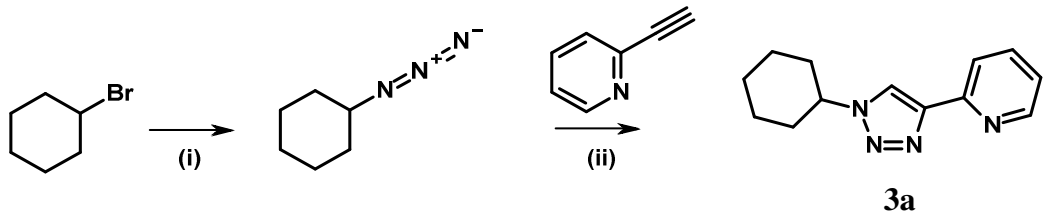

3a

*Scheme 3.3 Two step synthesis of 1-cyclohexyl-4-pyridyl-1,2,3-triazole (**1e**) (i) DMSO and NaN_3 at room temperature; (ii) THF/H_2O, $CuSO_4$ (aq.) and sodium ascorbate (aq.) at room temperature.*

Ligand **3a** has been fully characterised using ^{1}H and ^{13}C NMR spectroscopy and mass spectrometry. The ^{1}H NMR spectrum shows signals for the cyclohexyl group with the α-proton at δ 4.53 and the remaining cyclohexyl protons as a series of multiplets in the region δ 2.40-1.20. The pyridyl protons appear at δ 8.57, 8.18, 7.78 and 7.22 typical of a 2-substituted pyridyl ring. A distinct diagnostic signal for the triazole C-H proton appears as a singlet at δ 8.18. Successful synthesis of the ligands was also confirmed using infrared spectroscopy which shows a lack of the azide and alkyne stretching modes at ~2100cm^{-1} and ~2150cm^{-1} respectively indicating that no starting material was present and that the reaction had gone to completion.

The ligand **3a** was combined with rhenium pentacarbonyl chloride in toluene for 12 hours at reflux resulting in the formation of a yellow solution which on cooling resulted in precipitation of the complex *fac*-[Re(**3a**)$(CO)_3$Cl] (**4a**) as a pale yellow crystalline solid. A further crop of product was obtained by removing some toluene under reduced pressure and leaving the solution at 2 °C overnight.

The ^{1}H NMR spectrum of **4a** shows the pyridyl-triazole signals which are shifted downfield compared to the free ligand and appear at δ 9.05, 7.99, 7.79 and 7.44 with the resonance for triazole C-H proton at δ 8.17. The complex exhibits three distinct bands in the carbonyl region of the infra red spectrum with the symmetric stretch at 2021 cm^{-1} and the asymmetric stretches at 1949 and 1874 cm^{-1}. These are shifted with respect to the bpy analogue, which appear at 2024, 1928 and 1888 cm^{-1} respectively. This is indicative of the triazole ligand is a marginally better donor than bpy. Luminescence measurements of complex **4a** and [Re(bpy)$(CO)_3$Cl] were recorded at room temperature in aerated acetonitrile with an excitation wavelength of 400 nm and are shown in Figure 3.9. A broad band is observed at 542 nm for complex **4a** which is significantly blue-shifted with respect to the bpy analogue (612 nm). This blue shift in emission maximum is explained due to the fact that the HOMO for both of these complexes is localised on the Re(I) and the Cl atoms where as the LUMO is localised on the pytz and bpy ligands respectively. Therefore approximately the same energy level would be observed for the HOMO for both complexes whereas the LUMO for complex **4a** would be at higher energy due to the smaller π-system of the triazole ligand. Whilst this work was being undertaken Obata *et al.* [96] reported a similar rhenium complex with the ligand 1-benzyl-4-(pyrid-2-yl)-1,2,3-triazole, which exhibited similarly blue-shifted emission maximum which appeared at 538 nm. This is discussed further in the chapter.

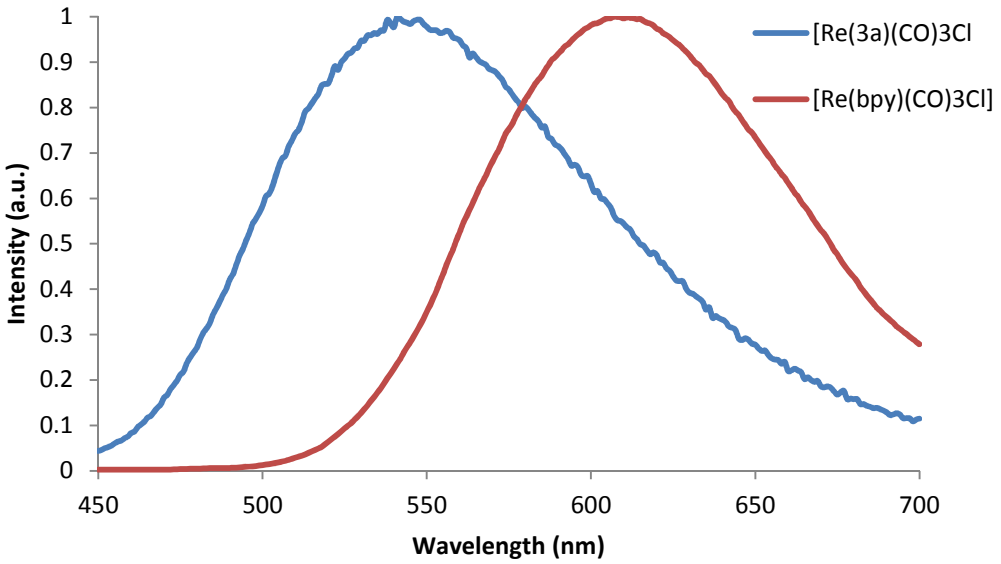

*Figure 3.9 Normalised luminescence spectra for [Re(**3a**)(CO)$_3$Cl] (**4a**) and [Re(bpy)(CO)$_3$Cl]*

3.3.2 Attempted synthesis of [Re(4-cyclohexyl-1-(pyrid-2-yl)-1,2,3 triazole)(CO)$_3$Cl]

In order to fully investigate the electronic effects of the pyridyl triazole ligand on the properties of the metal we decided to prepare the alternative isomer of the ligand, 1-(pyrid-2-yl)-4-cyclohexyl-1,2,3-triazole (**3b**), which would coordinate to the metal by N2 of the triazole ring rather than N3. Three different synthese were explored: reacting the pyridyl halide with sodium azide, conversion of 2-amino pyridine to 2-azido pyridine using sodium nitrite and sodium azide in an acidic solution and finally reacting -amino pyridine with n-BuLi followed by an azidophosphonium salt, however no products could be isolated.

After further examination of the literature it was noted that 2-azidopyridine exists in an equilibrium with its fused tetrazole form and that at temperatures between -

10 °C and 150 °C the equilibrium lies greatly in favour of the tetrazole (Figure 3.10 Equilibrium of 2-pyridyl azide with its fused tetrazole.). When subsequently used in an attempt to form the target ligand no product was formed. It is therefore possible that this isomerism inhibits the desired "click" reaction.

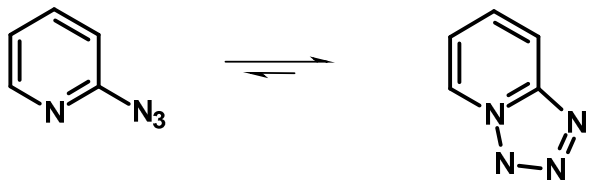

Figure 3.10 Equilibrium of 2-pyridyl azide with its fused tetrazole.

Others have since synthesised this ligand however this work was carried out at the beginning of the project and we had subsequently moved on to other areas and so we have not pursued it further.

Due to these problems encountered in the synthesis of the second ligand, density functional theory (DFT) studies were undertaken in collaboration with an MSc student, Somaia Kamouka, and Paul Elliott in order to investigate the donor properties of these isomeric ligands and the electronic and photophysical properties of the complexes.

3.3.3 DFT Calculations

We have carried out DFT calculations on the 4-(pyrid-2-yl)-1,2,3-triazole complex [Re(**3a'**)$(CO)_3$Cl] (**4a'**) as well as the complex of the isomeric 1-(pyrid-2-yl)-1,2,3-triazole complex, [Re(**3b**)$(CO)_3$Cl] (**4b**). Additionally we have also carried out calculations on the complex of the further possible ligand isomer 2-(pyrid-2-yl)-1,2,3-triazole, [Re(**3c**)$(CO)_3$Cl] (**4c**). Structures of ligands **3a'**, **3b** and **3c** are shown in Figure 3.11. Rhenium tricarbonyl chloride complexes are a good system for chelate ligand comparison, as the donor character can be assigned from the infrared data with electronic effects determined from the absorbance and emission data. Further, this particular ligand set allows us to look at ligand tuning and isolate electronic effects in ligands that are isosteric. For the computational calculations the cyclohexyl substituent was replaced by a methyl group because it is computationally less time consuming whilst being electronically almost identical. Firstly the geometries of the complexes were optimised using the B3LYP level of theory. [186] The Stuttgart relativistic small core potential [187] was used for rhenium and 6-311G* basis sets [188] were used for all the other atoms. Ground state geometry optimisations and molecular orbital analyses were carried out using the GAMESS-UK software package. [189] Excited state geometry optimisations, TDDFT and Δ-SCF calculations were carried out using the NWChem 5.1 software package. [190]

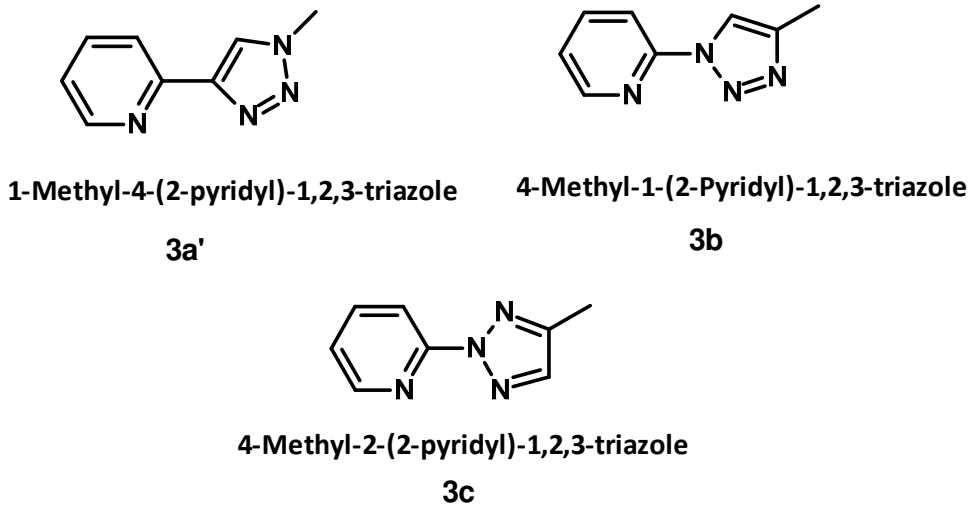

Figure 3.11 Isomers of methyl and pyridylsubstituted-1,2,3-triazoles.

3.3.3.1 Optimised ground state and triplet excited state geometries

Table 3.4 shows the selected calculated bond lengths for both the singlet ground state (S_0) and the lowest triplet excited states (T_1) for all three pyridyl triazole complexes and for the [Re(bpy)$(CO)_3$Cl] parent complex. Molecular structures for the ground states are shown in Figure 3.12, with XYZ coordinates included in the appendix. All complexes exhibit a distorted octahedral geometry with the calculated Re-Cl bond lengths for all of the complexes within the range 2.520-2.528 Å. The calculated Re-carbonyl bond lengths for the pyridyl triazole complexes are similar to those of the [Re(bpy)$(CO)_3$Cl] parent complex with those *trans* to the chelating ligand ranging between 1.147 and 1.152 Å. The C-O bond length for the ligand *trans* to the chloride are comparatively elongated at 1.155 to 1.157 Å consistent with the presence of the *trans* π-donor. For the pytz complexes, the Re-C bonds are shorter and the C-O bonds longer for the carbonyl

ligands *trans* to the triazole ring compared to the ligands *trans* to pyridine expect for that of **3c** suggesting that the triazole is a slightly better overall donor. The calculated Re-N_{tz} bond length for [Re(**3b**)$(CO)_3$Cl] is slightly shorter at 2.184 Å than those for the other two pyridyl triazole complexes despite the N2 donor atom being expected to be less basic than the N3 atom. This may be due to the C-N bond length which connects the triazole to the pyridine within the ligand being shorter when compared to the corresponding bonds in the other two pyridyl triazole complexes.

The geometries of the lowest triplet excited states for all complexes were calculated using the constraint of a triplet spin multiplicity. Differences are observed in the geometries when moving from the singlet ground state (S_0) to the lowest triplet excited state (T_1). The HOMO of all complexes is dπRe-pπCl antibonding in character whilst the LUMO is centred on the chelating ligand. The excitation of an electron from the largely metal-based HOMO with π*-antibonding character to the chloride thereby results in a shortening of the Re-Cl bond by approximate 0.07 to 0.1 Å for all complexes (Table 3.4). Consistent with the loss of electron density from the rhenium tricarbonyl fragment in this ^{3}MLCT state, Re-C bond lengths are elongated and C-O bonds shortened due to diminished back-bonding.

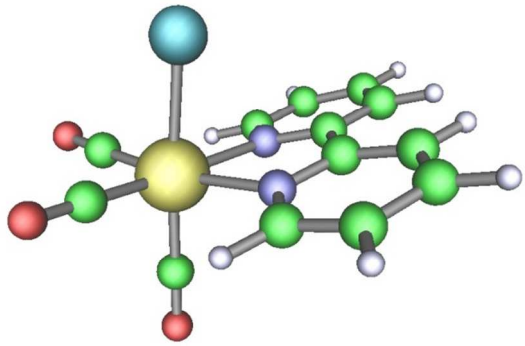

[Re(bpy)(CO)$_3$Cl]

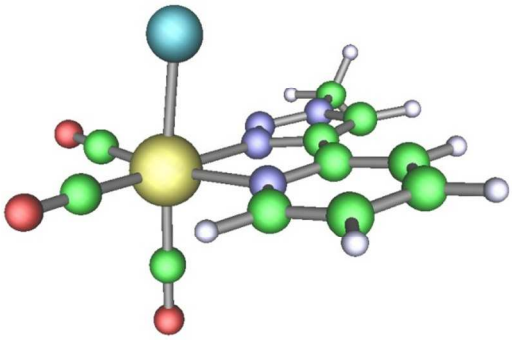

[Re(3a')(CO)$_3$Cl]

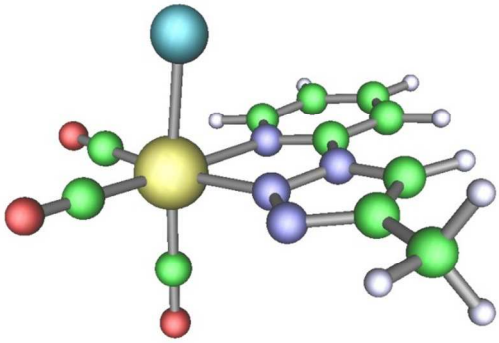

[Re(3b)(CO)$_3$Cl]

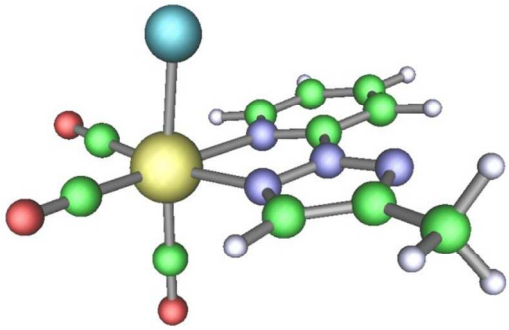

[Re(3c)(CO)$_3$Cl]

*Figure 3.12 Optimised ground state geometries for the complexes [Re(L)(CO)$_3$Cl], (L=**3a'-c**, bpy).*

*Table 3.4 Selected bond lengths for optimised singlet ground states and lowest lying triplet excited states for complexes [Re(L)(CO)$_3$Cl], (L=**3a'-c**, bpy).*

	Re(bpy)(CO)$_3$Cl		**Re(3a')(CO)$_3$Cl**		**Re(3b)(CO)$_3$Cl**		**Re(3c)(CO)$_3$Cl**	
	S_0	T_1	S_0	T_1	S_0	T_1	S_0	T_1
Re-Cl	2.525	2.424	2.528	2.439	2.524	2.456	2.520	2.447
Re-C(*trans* to Cl)	1.931	1.997	1.931	1.985	1.932	1.979	1.934	1.983
Re-C(*trans* to Py)	1.944	1.987	1.945	2.016	1.949	1.963	1.938	1.959
Re-C(*trans* to Tz)	na	na	1.940	1.958	1.941	2.010	1.943	2.014
C-O(*trans* to Cl)	1.156	1.141	1.157	1.144	1.155	1.145	1.155	1.144
C-O(*trans* to Py)	1.151	1.144	1.148	1.141	1.147	1.143	1.150	1.145
C-O(*trans* to Tz)	na	na	1.152	1.147	1.151	1.142	1.150	1.142
Re-N_{Py}	2.218	2.157	2.254	2.138	2.240	2.216	2.254	2.213
Re-N_{Tz}	na	na	2.193	2.170	2.184	2.073	2.197	2.091

3.3.3.2 IR Data

Vibrational frequency calculations were carried out in order to determine relative carbonyl stretching frequencies. Table 3.5 shows the calculated carbonyl stretching frequencies for both the singlet ground state as well those for the lowest lying triplet excited state for all of the complexes studied. The calculated infrared data predicts that complexes [Re(**3a'**)(CO)$_3$Cl] and [Re(**3c**)(CO)$_3$Cl] have very similar electron donating properties due to the triazole being bonded to the metal centre through the outer N1 and N3 nitrogen atoms of the triazole respectively.

Complex [Re(**3b**)$(CO)_3$Cl] has highest CO stretching frequencies suggesting that **3b** is the weakest donor. This would be expected due to the ligand being bonded to the metal centre through the less basic N2 atom of the triazole ring.

As expected for generation of a MLCT state, decrease in electron density at the metal decreases back bonding leading to the carbonyl stretching frequencies being significantly shifted up in energy, when moving from a singlet ground state, to the T_1 excited state. This increase in calculated frequency is of similar magnitude to those reported by George *et al.* [191] for [Re(bpy)$(CO)_3$Cl]. Time-resolved infrared spectroscopy on the bpy complex showed that the carbonyl stretching frequencies shifted from 2024, 1921 and 1899 cm^{-1} to 2064, 1987 and 1957 cm^{-1} when moving from the ground state to the excited triplet state.

*Table 3.5 Calculated ν_{CO} stretching frequencies for the singlet ground states and lowest triplet states for complexes [Re(L)$(CO)_3$Cl], (L=**3a'-c**, bpy).*

	Re(bpy)$(CO)_3$Cl		**Re(3a')$(CO)_3$Cl**		**Re(3b)$(CO)_3$Cl**		**Re(3c)$(CO)_3$Cl**	
	S_0	T_1	S_0	T_1	S_0	T_1	S_0	T_1
	1991	2051	1988	2040	1997	2047	1997	2046
ν_{CO}	2016	2060	2020	2060	2028	2065	2024	2060
	2090	2119	2095	2119	2101	2125	2097	2121

3.3.3.3 MO Energies

Table 3.6 and Figure 3.13 Energy level diagram for the frontier molecular orbitals of the complexes [Re(L)$(CO)_3$Cl], (L=**3a'-c**, bpy). shows the HOMO and LUMO energies along with the magnitude of the HOMO-LUMO gap for the four complexes investigated. The bipyridyl complex has the smallest HOMO-LUMO gap at 2.87 eV. [Re(**3a'**)$(CO)_3$Cl] and [Re(**3c**)$(CO)_3$Cl] have very similar HOMO-LUMO gaps of 3.13 and 3.12 eV respectively. This is due to the raising in energy of the ligand centred LUMO relative to the HOMO by replacing one of the pyridine rings with the smaller π-system of the triazole ring. Of the pyridyltriazole complexes, [Re(**3b**)$(CO)_3$Cl] has the smallest HOMO-LUMO gap at 2.95 eV, some 0.08 eV larger than that of the bpy complex. The LUMO for complex [Re(**3a'**)$(CO)_3$Cl] is destabilised with respect to the bpy analogue whereas the LUMO for complexes [Re(**3b**)$(CO)_3$Cl] and [Re(**3c**)$(CO)_3$Cl] are both stabilised with respect to the bpy complex. HOMO of **4c** is stabilised to greater extent than the LUMO compared to the bpy complex leading to a larger HOMO-LUMO gap.

*Table 3.6 Calculated energies (eV) of the HOMO and LUMO and the HOMO-LUMO gap for the complexes [Re(L)$(CO)_3$Cl], (L=**3a'-c**, bpy).*

	Re(bpy)$(CO)_3$Cl	**Re(3a')$(CO)_3$Cl**	**Re(3b)$(CO)_3$Cl**	**Re(3c)$(CO)_3$Cl**
	Energy / eV	**Energy / eV**	**Energy / eV**	**Energy / eV**
LUMO	-2.95	-2.50	-2.90	-2.83
HOMO	-5.81	-5.64	-5.85	-5.95
HOMO-LUMO	2.87	3.13	2.95	3.12

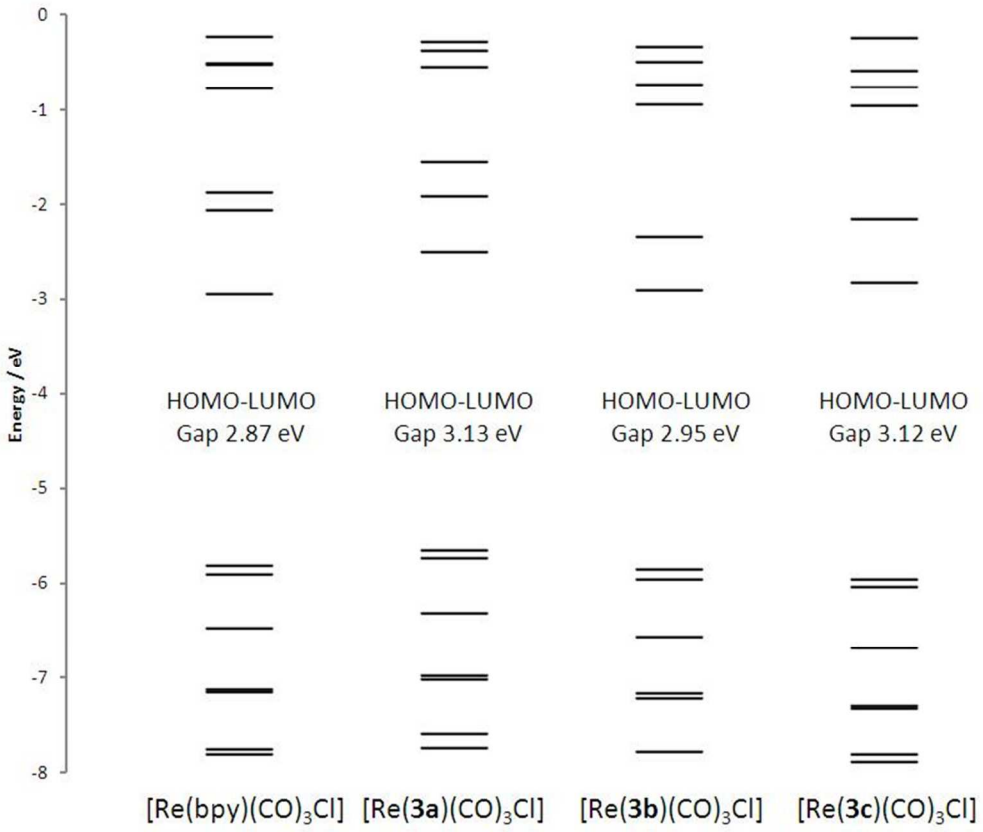

*Figure 3.13 Energy level diagram for the frontier molecular orbitals of the complexes [Re(L)(CO)$_3$Cl], (L=**3a'-c**, bpy).*

The singly occupied molecular orbitals (SOMOs) of the T_1 states for these complexes are similarly situated to the HOMOs and LUMOs of their singlet ground states confirming MLCT character

3.3.3.4 Time dependent DFT (TDDFT) Calculations

Vertical excitation energies for the singlet ground state were calculated for each complex by TDDFT calculations and used to derive simulated optical absorption spectra. Calculated spectra are shown in Figure 3.14 and the wavelengths, energies, oscillator strengths and compositions of selected transitions are given in Table 3.7. The lowest energy singlet excitations (S_1) for [Re(**3a'**)$(CO)_3$Cl] and [Re(**3c**)$(CO)_3$Cl], are almost entirely HOMO→LUMO ^{1}MLCT in character and appear at 520 and 526 nm respectively, blue-shifted by some 68 and 62 nm respectively to that of the parent bpy complex. These are of low oscillator strength and therefore will contribute little to the observed spectrum. The more intense HOMO-1→LUMO ^{1}MLCT transitions for these complexes appear at 484 and 487 nm and are blue-shifted by 49 and 46 nm respectively relative to that of the bpy complex. Transitions between 250 and 350 nm are dominated by intraligand $\pi\rightarrow\pi^*$ excitations.

By comparison, for [Re(**3b**)$(CO)_3$Cl] the corresponding S_1 and S_2 ^{1}MLCT transitions at 570 and 517 nm respectively are blue-shifted by only 18 and 16 nm respectively to those of [Re(bpy)$(CO)_3$Cl]. These data suggest that despite the smaller π-system for the **3b** ligand compared to bpy there is only a modest shift in the energies of the optical transitions for this complexes and that the complex will have comparable spectroscopic absorption properties to the bpy analogue.

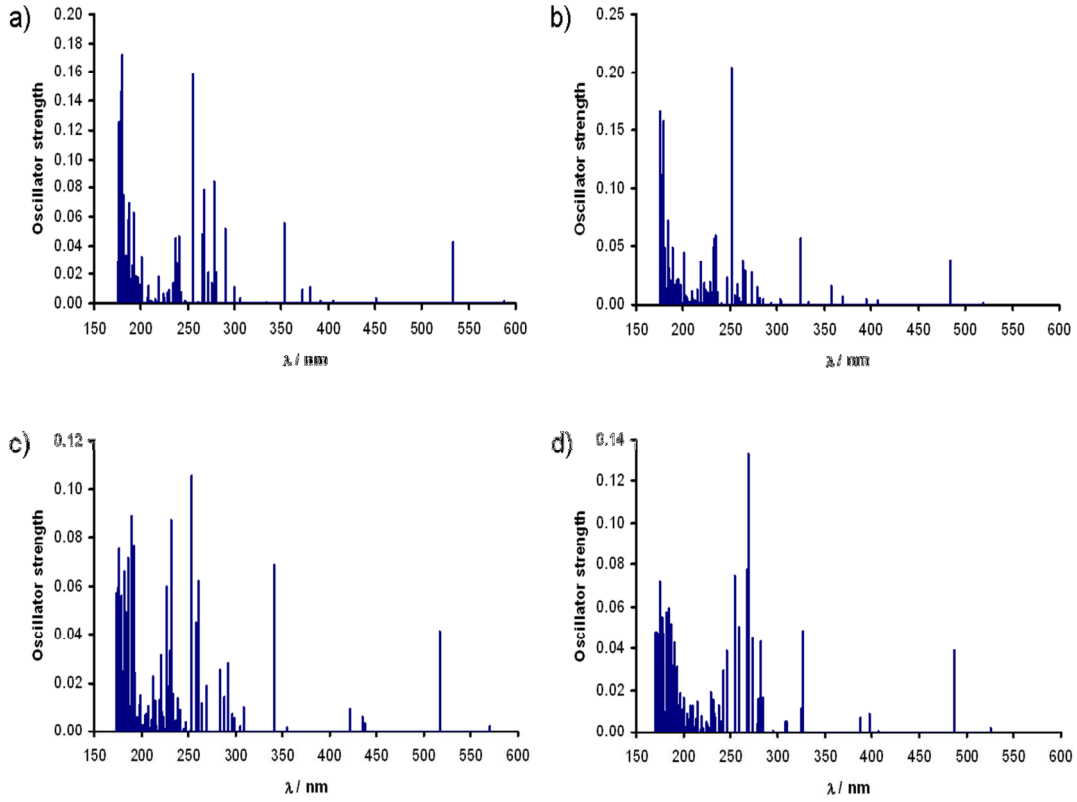

*Figure 3.14 Calculated UV-Vis absorption spectra from TDDFT derived vertical excitation energies for complexes [Re(L)(CO)$_3$Cl], a) [Re(bpy)(CO)$_3$Cl], b) [Re(**3a'**)(CO)$_3$Cl], c) [Re(**3b**)(CO)$_3$Cl] and d) [Re(**3c**)(CO)$_3$Cl].*

Table 3.7 Selected energies (eV) (oscillator strength, f, in parentheses), wavelength (nm) and compositions of vertical excitations from TDDFT calculations

Complex	Transition	Energy / eV	λ/ nm	Composition/character	
Re(bpy)(CO)$_3$Cl	S_1	2.11 (0.002)	588	HOMO → LUMO	MLCT
	S_2	2.32 (0.042)	533	HOMO-1 → LUMO	MLCT
	S_9	3.51 (0.055)	353	HOMO-4 → LUMO	π-π*
	S_{16}	4.28 (0.052)	290	HOMO-3 → LUMO	π-π*
	S_{18}	4.45 (0.084)	278	HOMO-3 → LUMO+1	π-π*
	S_{21}	4.63(0.078)	268	HOMO-1 → LUMO+5	π-π*
	S_{25}	4.85 (0.159)	256	HOMO-2 → LUMO+3	π-π*
Re(3a')(CO)$_3$Cl	S_1	2.39 (0.002)	520	HOMO → LUMO	MLCT
	S_2	2.56 (0.038)	484	HOMO-1 → LUMO	MLCT
	S_{10}	3.81 (0.058)	325	HOMO-4 → LUMO	π-π*
	S_{25}	4.93 (0.204)	252	HOMO-6→ LUMO & HOMO-4 → LUMO+2	π-π*
Re(3b)(CO)$_3$Cl	S_1	2.17 (0.002)	570	HOMO → LUMO	MLCT
	S_2	2.40 (0.041)	517	HOMO-1 → LUMO	MLCT
	S_8	3.63 (0.069)	342	HOMO-4 → LUMO	π-π*
	S_{19}	4.75 (0.062)	261	HOMO-5 → LUMO+1 & HOMO-6 → LUMO	π-π*
	S_{20}	4.79 (0.045)	259	HOMO-5 → LUMO	π-π*
	S_{21}	4.88 (0.105)	254	HOMO-2 → LUMO+3	π-π*

Re(3c)(CO)$_3$Cl	S_1	2.36 (0.002)	526	HOMO → LUMO	MLCT
	S_2	2.55 (0.039)	487	HOMO-1 → LUMO	MLCT
	S_7	3.80 (0.048)	326	HOMO-4 → LUMO	π-π*
	S_{13}	4.39 (0.043)	282	HOMO-5 → LUMO	π-π*
	S_{16}	4.53 (0.045)	274	HOMO → LUMO+3	π-π*
	S_{17}	4.61 (0.133)	269	HOMO-1 → LUMO+4 & HOMO-5 → LUMO	π-π*
	S_{18}	4.64 (0.078)	267	HOMO-1 → LUMO+4	π-π*
	S_{20}	4.88 (0.074)	254	HOMO-2 → LUMO+3	π-π*

3.3.3.5 Calculated emission energies

The theoretical emission energies cannot be directly derived from the calculations of the triplet excited state but are derived through Δ-SCF calculations. Since emission under Frank-Condon emission conditions occurs without movement of the nuclei, the energies of the singlet ground states at the optimised T_1 geometries calculated in single point calculations can be used to derive the emission energy. The corresponding difference in energy between the T_1 states and these S_0 states at the T_1 geometries are therefore the calculated emission energies. These are presented in Table 3.8 along with the corrected values derived from the ratio of the theoretical and experimental values for the bpy complex. This ratio is then applied to all other complexes. The emission energies for the complexes [Re(**3a'**)(CO)$_3$Cl] and [Re(**3c**)(CO)$_3$Cl] are blue shifted by 84 nm and 69 nm respectively compared to [Re(bpy)(CO)$_3$Cl], which would be expected on the basis of the blue shift in their absorption transitions. The blue shift in calculated emission observed in [Re(**3a'**)(CO)$_3$Cl] when compared to that of

[Re(bpy)$(CO)_3$Cl] is slightly greater than the experimentally observed blue-shift of [Re(**3a**)$(CO)_3$Cl] (542 nm) when compared to [Re(bpy)$(CO)_3$Cl] (612 nm). The emission wavelength for complex [Re(**3b**)$(CO)_3$Cl] on the other hand is slightly red shifted with respect to the bpy analogue. Again, this shows **4b** should have similar spectroscopic properties to its bpy analogue.

The calculations show significant tuning of the spectroscopic properties through modulation of the frontier orbitals energies despite the ligands having the same size π-system.

*Table 3.8 Calculated emission wavelengths for complexes [Re(L)$(CO)_3$Cl], (L=**3a-c**, bpy).*

	Re(bpy)$(CO)_3$Cl	**Re(3a')$(CO)_3$Cl**	**Re(3b)$(CO)_3$Cl**	**Re(3c)$(CO)_3$Cl**
T_1 - S_0 / eV	1.68	1.95	1.67	1.89
λ^{em} / nm	737	636	744	655
Corrected λ^{em} / nm	612	528	617	543

3.4 Conclusions

A series of cationic bipyridyltricarbonylrhenium(I) complexes **2a–d** with axial monodentate 1,2,3-triazole ligands have been prepared and fully characterised. Single-crystal X-ray structures were determined for complexes **2a** and **2b** with 1-methyl-4-phenyl-1,2,3 triazole and 4-phenyl-1-propyl-1,2,3-triazole ligands, respectively. Despite the small difference in the alkyl substituents between the

two complexes, significant differences in structure are observed in the solid state. The cation **2a** is highly distorted due to the adoption of a π-stacking interaction between the triazole phenyl substituent and one ring of the bpy ligand. This interaction results in a distortion in the complex, where the triazole ring is significantly tilted with respect to the metal ligand bond, and the bpy ligand is severely twisted with respect to the plane of the equatorial donor atoms around the metal centre. Infrared data suggest that the ligands are slightly better net donors than pyridine, through being worse π-acceptors, confirming findings of others comparing the complexes $[Re(bpy)(CO)_3Cl]$ and $[Re(pytz)(CO)_3Cl]$ where a pyridine ring of the chelating diimine ligand is replaced by triazole. The complexes are luminescent with λ_{max}^{em} comparable to that of $[Re(bpy)(CO)_3(Py)]^+$ with long luminescent lifetimes in aerated dichloromethane solutions at room temperature. Phosphorescent d^6 metal complexes have attracted a large amount of interest as luminescent tags in biological imaging agents. The long luminescent lifetimes for complexes **2a–c**, their cationic character which would increase solubility and the facile CuAAC derivatisation of many biologically relevant molecules might therefore allow complexes of this type to be utilised as time-gated luminescent imaging agents as has been demonstrated with other cationic rhenium -based analogues (Figure 3.15). [178, 179]

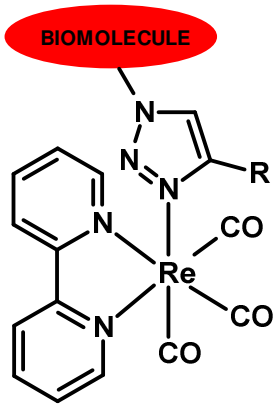

Figure 3.15 Rhenium polypyridine biological imaging agents

Chelating pyridyl triazole ligand **3a** and its rhenium complex **4a** were prepared and characterised. A blue shift in emission maximum was experimentally observed for complex **4a**, at (λ_{max}^{em} 542 nm) and the emission maximum of [Re(bpy)$(CO)_3$Cl] at 612 nm. Unfortunately we were unable to isolate the isomer of this bidentate ligand in which the ligand coordinates through the N2 atom of the triazole ring. However, through our computational calculations we have shown that replacing the chelating bipyridyl ligand with a pyridine triazole ligand, generally results in a blue shift of absorbance and emission energy. This blue shift is more evident for ligands **3a'** and **3c** but not for **3b**. Indicating that ligand **3b** is more similar in character to bpy. The Re-C bonds are slightly shorter and the C-O bonds longer for the carbonyl ligands *trans* to the triazole ring compared to the ligands *trans* to pyridine suggesting that the triazole overall is a slightly better net donor. The data show that the small changes in these complexes due to these ligand isomers allows effective tuning of electronic and photophysical properties of their complexes.

4 SYNTHESIS AND CHARACTERIZATION OF AZIDOBIPYRIDYL RUTHENIUM COMPLEXES AND THEIR "CLICK" CHEMISTRY DERIVATIVES

4.1 Introduction

The synthesis and preparation of supramolecular architectures containing photo- and redox- active transition metal complexes has become an area of intense interest. The traditional method for the preparation of such metallosupramolecular materials has relied on the formation of bridging ligands with multiple coordination sites into which metal centres can be subsequently incorporated.[150] However this approach has disadvantages in terms of controlling the selectivity of metal binding, when for example heterometallic structures are required and where the bridging ligand is non-symmetric. A more advantageous route would be to couple preformed complexes into supramolecular architectures using suitable, highly efficient coupling reactions.

Described in this chapter are the syntheses and characterisation of mono- and bis(azido)bipyridyl and the click modification of these ligands. Also described are the results on the coordination of mono- and bis(azido)bipyridyl in their [Ru(η^6-cymene)Cl]$^+$ complexes and the CuAAC modification thereof.

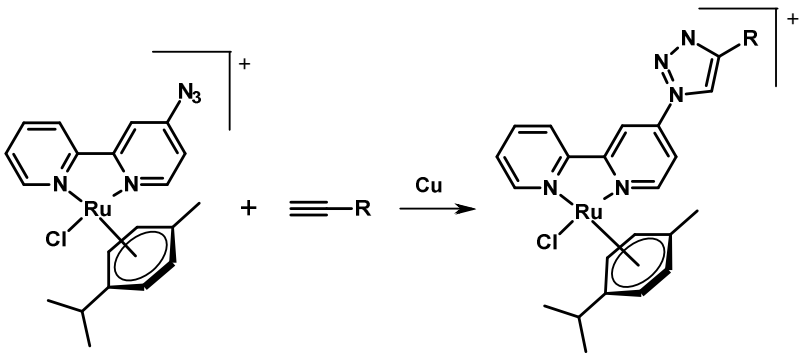

Figure 4.1 'Click' modification of [Ru(p-cymene)(4-azido-2,2'-bipyridyl)Cl]$^+$complex

4.2 Synthesis and CuAAC reactions of azido bpy ligands

The synthesis of two azido-bipyridyl ligands was carried out in a multi-step procedure starting from commercially available 2,2'-bipyridyl. Scheme 4.1 shows the multistep synthesis for the monoazido-substituted ligand 4-azido-2,2'-bipyridyl (**4a**). Ligand **4a** was prepared by slowly reacting 2,2'-bipyridyl with 1 equivalent of *meta*-chloroperoxybenzoic acid (*m*CPBA) for 12 hours to form 2,2'-bipyridyl-N-oxide. The C4 position of the oxidised pyridyl ring then underwent nitration in the presence of concentrated nitric acid and concentrated sulfuric acid to form 4-nitro-2,2'-bipyridyl-*N*-oxide which was isolated by adjusting the pH of the reaction mixture to 13. 4-nitro-2,2'-bipyridyl-*N*-oxide was then refluxed in phosphorus trichloride to remove the oxygen atom from the nitrogen to yield 4-nitro-2,2'-bipyridyl. The monoazido-substituted ligand 4-azido-2,2'-bipyridyl (**4a**) was then prepared from this nitro-substituted analogue by reaction with sodium azide in dimethylformamide at 100 °C in a procedure modified from that reported previously by Al-Fallapour.[167] After purification by flash chromatography **4a** was isolated as a pale yellow solid in excellent yield (96 %). Ligand **4a** was fully characterised by ^{1}H and ^{13}C NMR spectroscopy and mass spectrometry. The ^{1}H NMR spectrum exhibits a total of seven resonances typical of a 4-substituted 2,2'-bipyridyl ligand. The resonances of the azido substituted pyridine ring appear at δ 8.58, 8.15, and 6.94 and are shifted relative to those of the precursor 4-nitro-2,2'-bipyridyl which appear at δ 9.06, 8.84, and 7.91. The presence of the azide group was confirmed by the observation of a peak for the azide N-N stretch at 2115 cm^{-1} in the infrared spectrum.

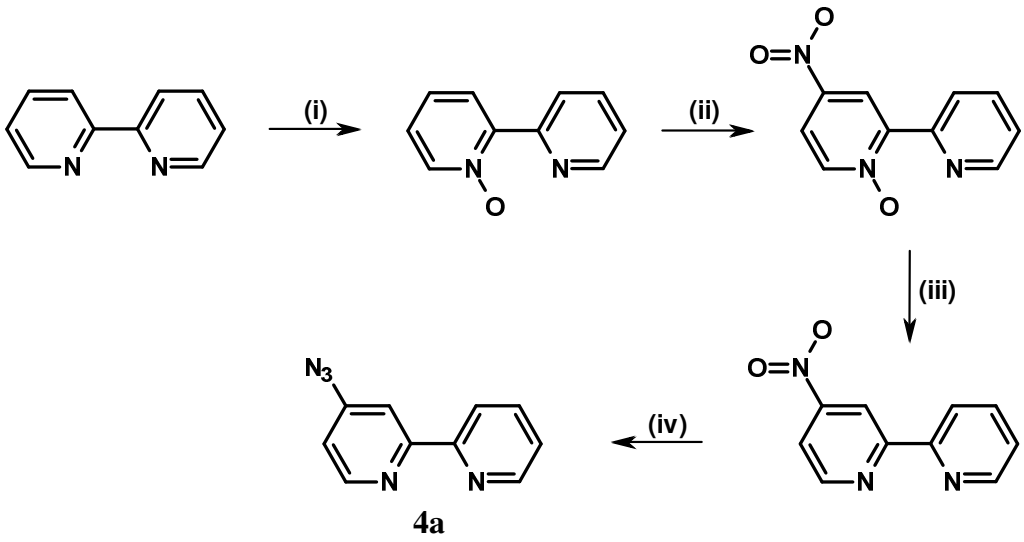

Scheme 4.1 The synthesis of 4-azido-2,2'-bipyridyl starting from 2,2'-bipyridyl. (i) mCPBA in DCM at room temperature, (ii) HNO_3 and H_2SO_4 at 100 °C, (iii) PCl_3 at reflux, (iv) NaN_3 in DMF at 100 °C

Scheme 4.2 outlines the multistep synthesis required for 4,4'-diazido-2,2'-bipyridyl (**4b**). Ligand **4b** was synthesised in a similar manner to **4a** but with a differing initial N-oxidation step in which hydrogen peroxide and glacial acetic acid were used as oxidising agents. The remainder of the synthesis was very similar with only changes to the necessary equivalences of reactants. The product was isolated after purification as a yellow solid, again in excellent yield. 4,4'-diazido-2,2'-bipyridyl was similarly fully characterised by ^{1}H and ^{13}C NMR spectroscopy and mass spectrometry. The ^{1}H NMR spectrum exhibits three resonances at δ 8.58, 8.14 and 6.96. These peaks are characteristic of a 4,4'-disubsituted-2,2'-bipyridyl which are again shifted relative to those of the dinitro precursor (δ 9.22, 9.05 and 8.14). As with ligand **4a** the presence of the azide

groups was confirmed by the diagnostic azide stretch at 2117 cm^{-1} in the infrared spectrum.

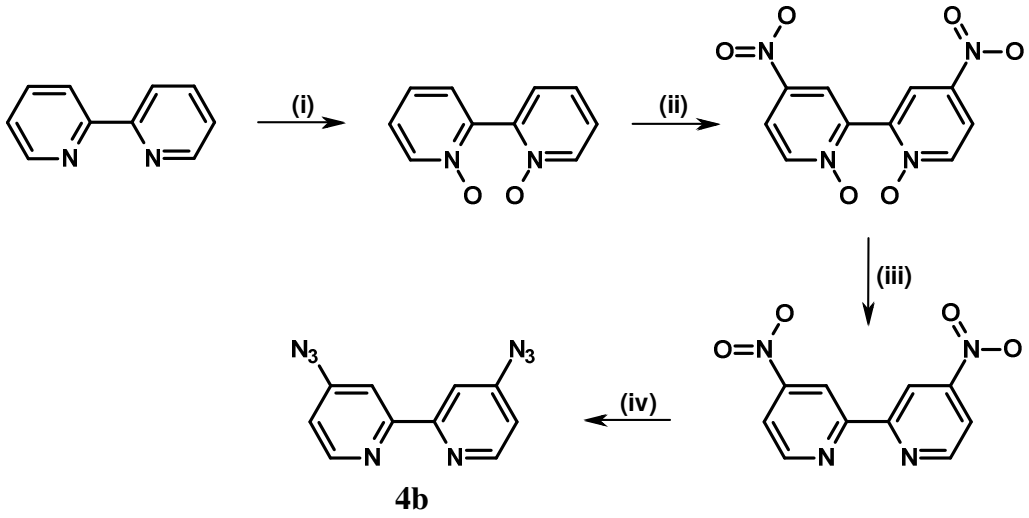

Scheme 4.2 The synthesis of 4,4'-diazido-2,2'-bipyridyl starting from 2,2'-bipyridyl. (i) H_2O_2 and glacial CH_3COOH at 80 °C, (ii) HNO_3 and H_2SO_4 at 100°C, (iii) PCl_3 at reflux, (iv) NaN_3 in DMF at 100 °C

Having isolated and fully characterised these two ligands, **4a** and **4b**, we decided to investigate the uses of these azido bipyridyl ligands in CuAAC reactions. We therefore reacted the azido ligands with a range of commercially available acetylenes, including phenylacetylene, ethynyl ferrocene and pyridylacetylene.

Scheme 4.3 outlines the synthesis of 4-phenyl-1-(2,2'-bipyrid-4-yl)-1,2,3-triazole (**5a**) and was carried out in a one pot CuAAC synthesis, starting from 4-azido-2,2'-bipyridyl and excess phenylacetylene in the presence of copper sulfate and sodium ascorbate in a 1:1 mixture of tetrahydrofuran and water. Upon completion of the reaction the product was extracted from the reaction mixture by partitioning

it between dichloromethane and aqueous ammonia. The desired triazole ligand was then isolated in good yield (74%) after purification by recrystallisation from dichloromethane and hexane.

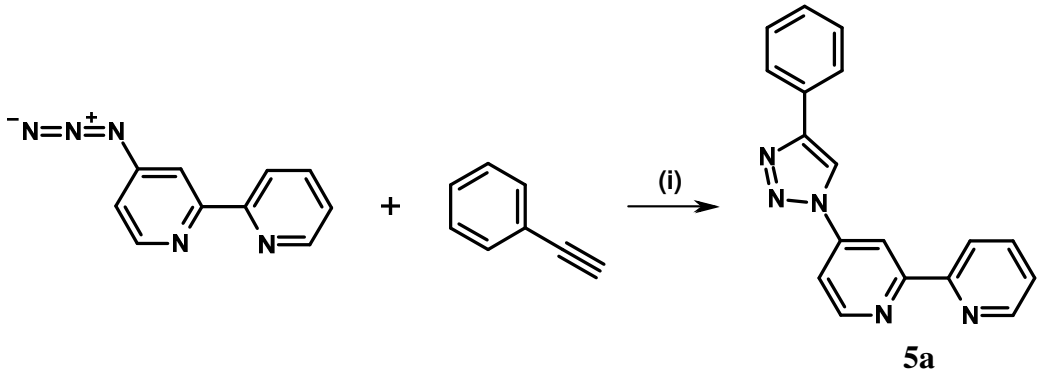

5a

Scheme 4.3 One-pot synthesis of 4-phenyl-1-(2,2'-bipyrid-4-yl)-1,2,3-triazole ligand. (i) THF/H_2O, $CuSO_4$ and sodium ascorbate at room temperature.

Ligand **5a** was fully characterised by ^{1}H and ^{13}C NMR spectroscopy, and mass spectrometry. In the ^{1}H NMR spectrum the diagnostic singlet signal corresponding to the triazolyl proton is clearly observed and appears as a singlet at δ 8.48. This is accompanied by an upfield shift observed in resonances for the bpy protons of the triazole substituted pyridyl ring of the bpy compared to the azide analogue which now appear at δ 8.84, 8.75, and 7.99. This shift is indicative of the change from the electron donating azide substituent to a relatively electron withdrawing triazolyl substituent. The phenyl resonances are well resolved with the *ortho*- and *meta*-proton signals appearing at δ 7.94 and 7.48 respectively with the resonance for the *para*-position overlapping with one of the signals arising from the pyridyl protons at δ 7.39. Infra-red spectroscopy confirmed the lack of an

azide stretch at 2115 cm^{-1} indicating that no remaining 4-azido-2,2-bipyridyl was present.

4-Ferrocenyl-1-(2,2'-bipyrid-4-yl)-1,2,3-triazole (**5b**) was prepared in a one-pot CuAAC synthesis in a similar fashion to that for the phenyl triazole substituted ligand. 4-Azido-2,2'-bipyridyl was reacted with ethynyl ferrocene in the presence of $CuSO_4$ and sodium ascorbate (Scheme 4.4). Purification and work up of the reaction was exactly the same as that for ligand **5a** and an orange solid was isolated as the product in moderate yield (43 %).

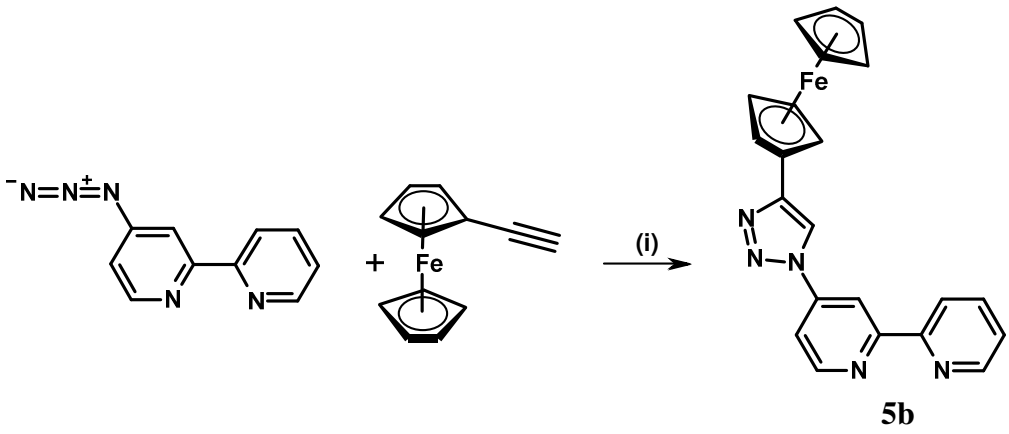

5b

Scheme 4.4 One-pot synthesis of 4-ferrocenyl-1-(2,2'-bipyrid-4-yl)-1,2,3-triazole ligand. (i) THF/H_2O, $CuSO_4$ and sodium ascorbate at room temperature.

As for ligand **5a**, ligand **5b** was fully characterised using ^1H and ^{13}C NMR spectroscopy and mass spectrometry. The ^1H NMR spectrum of the ligand shows a characteristic singlet resonance for the proton of the triazole ring at δ 8.18. Figure 4.2 shows selected regions of the ^1H NMR spectrum for ligand **5b**. The resonances of the bpy protons of the substituted pyridyl ring are again shifted upfield and appear at δ 8.83, 8.69, and 8.01 when compared to those of 4-azido-

2,2'-bipyridyl. The resonances of the substituted cyclopentadienyl (Cp) ring of the ferrocene moiety appear at δ 4.82 and 4.37 whilst the protons of the unsubstituted Cp ring gives rise to a singlet at δ 4.12. Formation of the cycloaddition product was also confirmed by the absence of the azide stretch in the infrared spectrum.

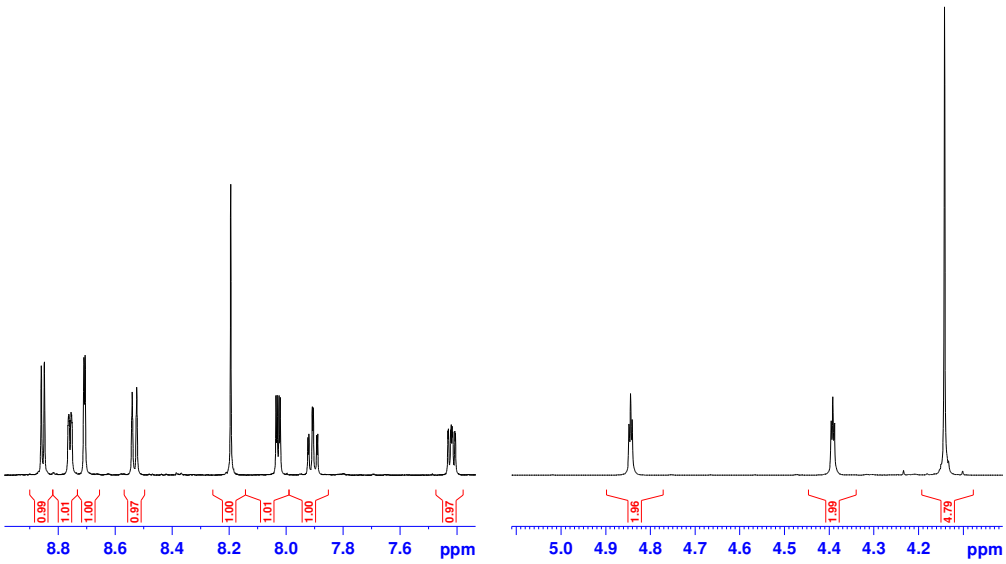

Figure 4.2 Selected regions of the ^{1}H NMR spectrum for 4-ferrocenyl-1-(2,2'-bipyrid-4-yl)-1,2,3-triazole.

Scheme 4.5 shows the synthesis of 4-(pyrid-2-yl)-1-(2,2'-bipyrid-4-yl)-1,2,3-triazole ligand (**5c**). Reaction of 4-azido-2,2'-bipyridyl with 2-ethynylpyridine resulted in the formation of the heteroditopic ligand with two potential metal binding sites; a bipyridyl domain, and a second pyridyl-triazole domain. 4-(Pyrid-2-yl)-1-(2,2'-bipyrid-4-yl)-1,2,3-triazole (**5c**) was fully characterised by ^{1}H and ^{13}C NMR spectroscopy and mass spectrometry. Twelve clearly identifiable signals are visible in the ^{1}H NMR spectrum within the region of δ 7-9 with the diagnostic triazole singlet resonance appearing at δ 8.92. The resonances for the triazole substituted pyridine ring of the bpy moiety appear at δ 7.97, 8.85 and 8.88. Two

sets of four signals for the other two pyridine rings are also observed. Infra-red spectroscopy confirmed no azide stretch at 2115cm^{-1} indicating that no 4-azido-2,2-bipyridyl was present.

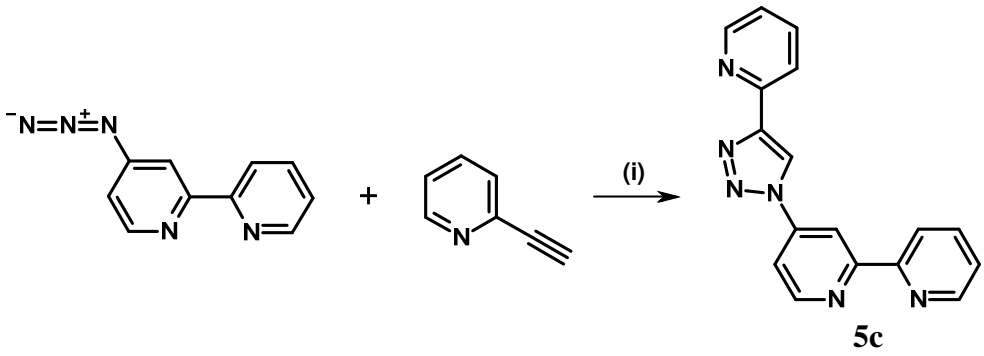

5c

Scheme 4.5 One-pot synthesis of 4-(pyrid-2-yl)-1-(2,2'-bipyrid-4-yl)-1,2,3-triazole ligand. (i) THF/H_2O, $CuSO_4$ and sodium ascorbate at room temperature.

After having investigated the CuAAC coupling reactions of the mono-azido bpy **4a** it was decided to investigate the CuAAC chemistry of the diazido analogue **4b**.

The CuAAC coupling of **4b** were attempted with phenylacetylene and 2-ethynylpyridine and it appeared to result in their triazole products. However, these products proved to be rather insoluble and therefore very difficult to characterise and therefore the results are not discussed further. The reaction of ethynylferrocene with 4,4'-azido-2,2'-bipyridyl to produce the desired bis(ferrocenyltriazolyl)bpy ligand was also attempted however this proved unsuccessful with no product being isolable despite several attempts under various conditions. It is possible that the failure of this reaction is due to the decomposition of the diazido starting material.

4.3 Synthesis of complexes

The coordination chemistry of these new azide substituted bpy ligands and their CuAAC derivatives were explored. Scheme 4.6 shows the formation of [Ru(*p*-cymene)(**4a**)Cl]$^+$ (**6a**) and [Ru(*p*-cymene)(**4b**)Cl]$^+$ (**6b**). The starting material [Ru(*p*-cymene)$(Cl)_2]_2$ was stirred with ligand **4a** or **4b** in methanol at room temperature for 12 hours leading to a bright yellow solution with subsequent isolation of the complexes **6a** and **6b** respectively as their PF_6^- salts after treatment with $NaPF_6$.

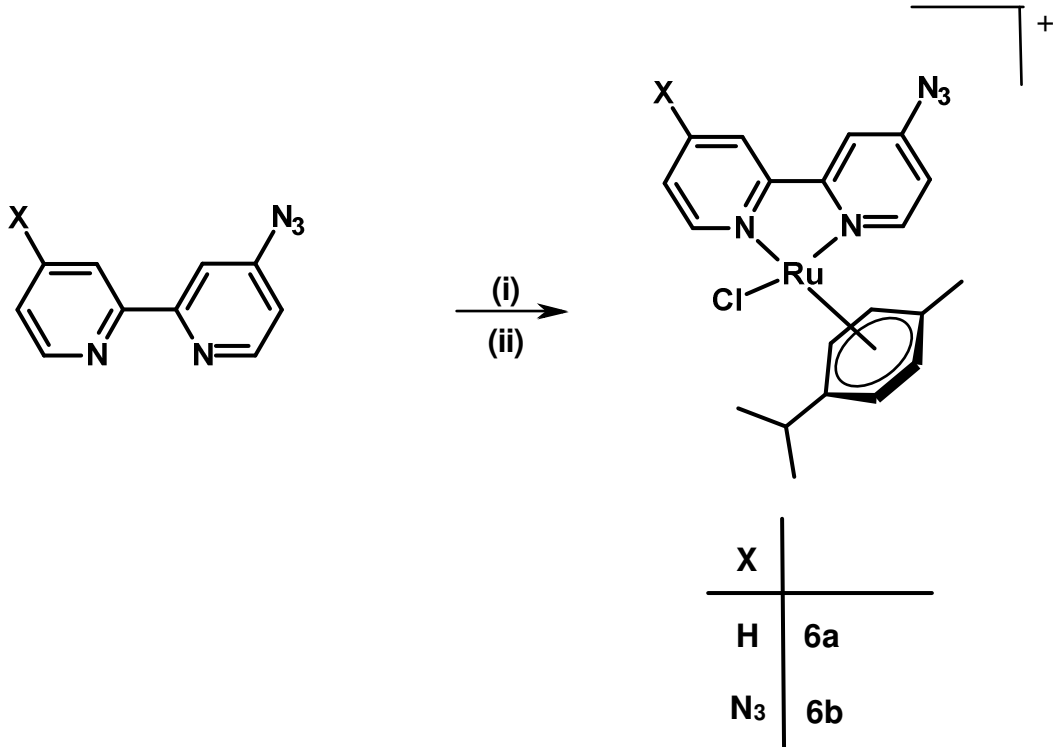

*Scheme 4.6 Synthesis of [Ru(p-cymene)(**4a-4b**)Cl]$^+$ (i) [Ru(p-cymene)$(Cl)_2]_2$, MeOH at room temp. (ii) $NaPF_6$*

Both new complexes **6a** and **6b** were fully characterised by ^{1}H and ^{13}C NMR, mass spectrometry and high resolution mass spectrometry as well as infrared spectroscopy. The infrared spectrum of **6a** shows a characteristic azide stretch at 2124 cm^{-1} which is shifted to higher energy by 9 cm^{-1} relative to the non-coordinated ligand. Similarly, complex **6b** exhibits a similar stretching frequency for the azido substituents with a slightly broader band than that for complex **6a** at 2122 cm^{-1} and is shifted to higher energy by 5 cm^{-1} compared with the non-coordinated ligand.

For complex **6a** the ^{1}H NMR spectrum of the complex contains seven resonances in the aromatic region due to the aromatic protons of the bipyridyl ligand. The signals for the non-substituted pyridyl ring are all deshielded upon coordination as is the H-6 proton of the azide-substituted ring which appears at δ 9.15. The resonances for the arene protons of the cymene ligand appear at δ 5.91 and 5.71. These appear as apparent triplets rather than a pair of doublets as in the ^{1}H NMR spectrum of the precursor $[Ru(p\text{-cymene})(Cl)_2]_2$ showing that the symmetry of the cymene has been broken by the asymmetry of the coordinated ligand **4a**. In addition, the ^{1}H NMR spectrum exhibits two closely overlapping doublets corresponding to the methyl groups of the isopropyl substituent of the cymene ligand at δ 1.04 and 1.03. This is presumably due to the chirality of the ruthenium centre. These characteristics can be clearly observed in Figure 4.3.

Complex **6b** exhibits three resonances in the aromatic region which are attributed to the symmetrical bipyridyl ligand. The resonances for the two protons *ortho*- to the azide group are both deshielded due to the change in environment. The resonances from the arene protons of the cymene ligand in complex **6b** appear as two doublets at δ 5.88 and 5.67. The methyl groups of the isopropyl of the cymene ligand are magnetically equivalent and give rise to a doublet at δ 1.02 (Figure 4.4).

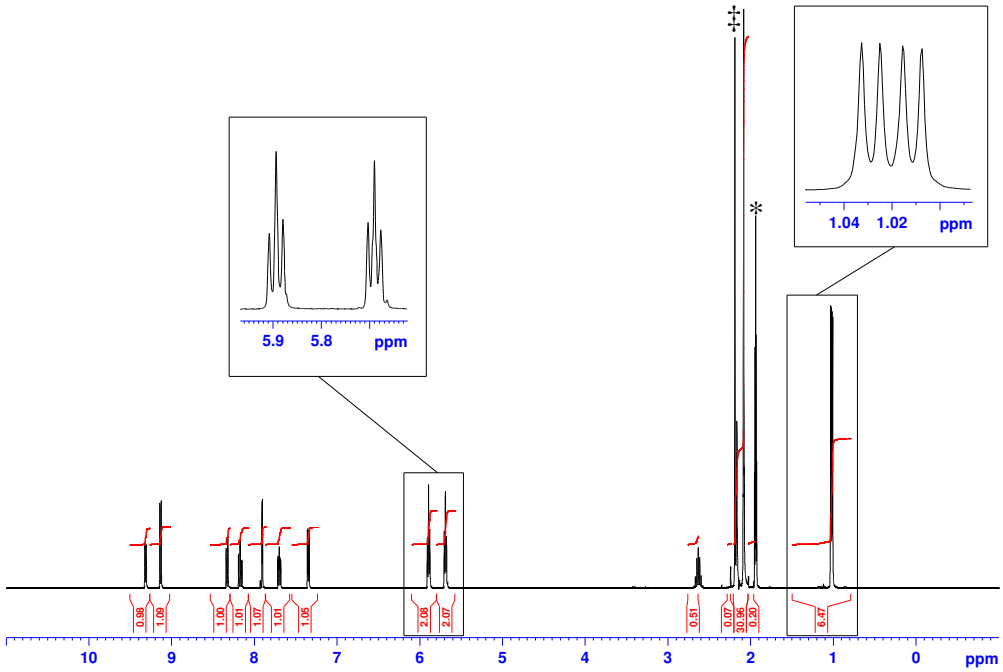

Figure 4.3 ^{1}H *NMR of [Ru(p-cymene)(**4a**)Cl]PF_6 (**6a**) with expanded regions in CD_3CN * residual solvent signal ‡ solvent impurities.*

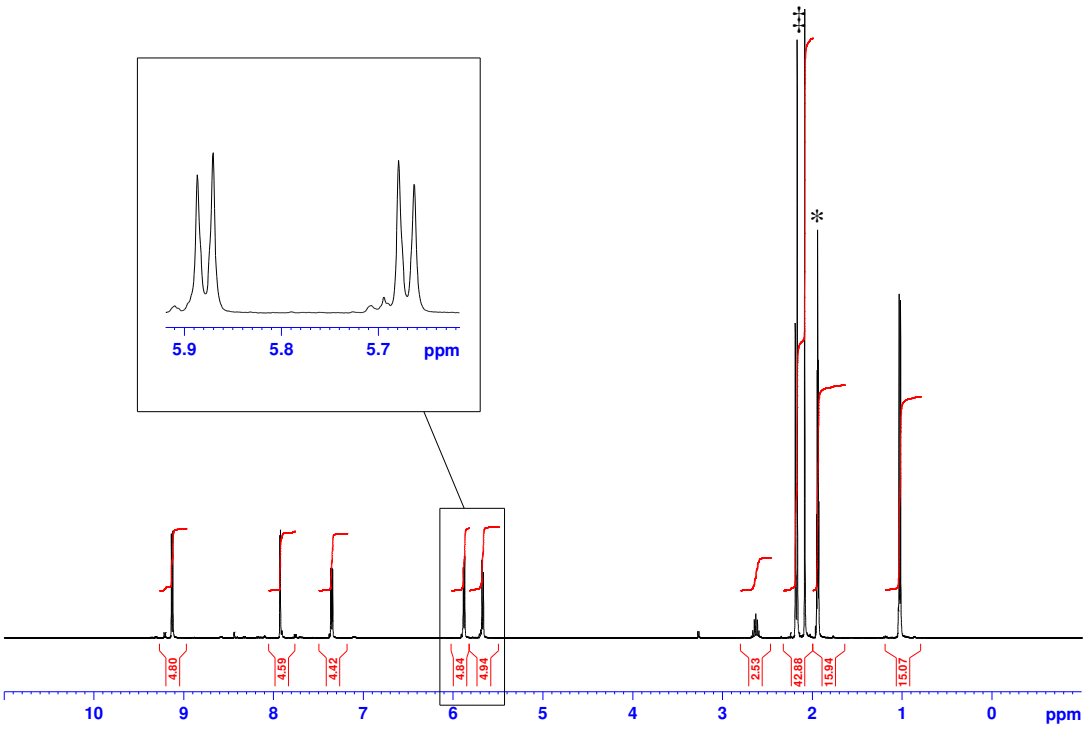

Figure 4.4 *^{1}H NMR of [Ru(p-cymene)(**4b**)Cl]PF_6 (**6b**) with expanded regions in CD_3CN * residual solvent signal ‡ solvent impurities.*

Single crystals were obtained for complex **6b** by slow diffusion of diethyl ether into an acetonitrile solution of the complex. Unfortunately the data was not of publishable quality and the structure is presented here only for information. Figure 4.5 depicts the molecular structure of the cation [Ru(*p*-cymene)(**4b**)Cl)]$^{+}$ whilst selected bond lengths and angles are provided in Table 4.1. [Ru(*p*-cymene)(**4b**)Cl))]PF_6 (**6b**) crystallises in the space group P-1. The C-N bonds between the bpy and the azide groups are 1.449 and 1.429 Å and the N-N bonds within the azide are between 1.143-1.128Å. These are similar to those reported by Constable *et al.* [150] in an iron azidoterpyridine complex where the corresponding C-N bonds are 1.419 and 1.423 Å and the azide N-N bond lengths are between 1.135-1.239Å. The C-N-N bond angles between the carbon of the bpy and the

central nitrogen of the azide are 115.9 and 116.2°, and the N-N-N angles of the azide nitrogens are 172.1 and 172.9°, again very similar to those reported by Constable (171.4 and 170.3°).

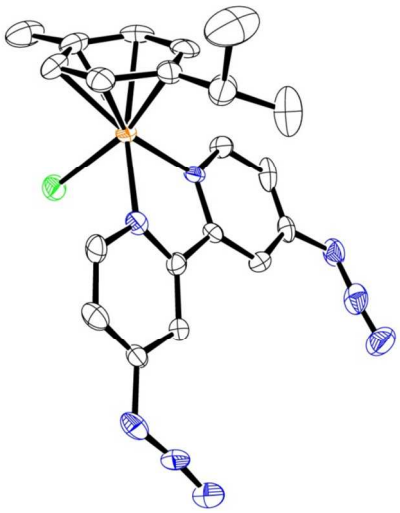

*Figure 4.5 ORTEP plot of the structure of the cation [Ru(p-cymene)(**4b**)Cl]$^+$ (hydrogen atoms and PF_6^- counterion omitted for clarity, ellipsoids at 50% probability)*

*Table 4.1 Selected bond lengths (Å) and angles (°) for single-crystal X-ray structures of [Ru(p-cymene)(**4b**)Cl]$^+$*

[Ru(*p*-cymene)(4b)Cl]$^+$ (6a)			
C22-N14	1.449(16)	C27-N11	1.429(14)
N14-N15	1.236(16)	N11-N12	1.219(15)
N15-N16	1.128(17)	N12-N13	1.143(15)
Ru-Cl	2.392(3)	Ru-N9	2.099(9)
		Ru-N10	2.086(9)
C22-N14-N15	116.2(11)	C27-N11-N12	115.9(10)
N14-N15-N16	172.1(13)	N11-N12-N13	172.9(12)

As a further example, the iridium complex $[Ir(ppy)_2(\mathbf{4b})]PF_6$ (**7**), was prepared (where ppy is 2-phenylpyridine). The dimer $[Ir(ppy)_2Cl]_2$ in acetonitrile was first treated with $AgPF_6$ for the *in situ* generation of the cationic solvento complex followed by the addition of ligand **4b** to yield the complex **7** (Scheme 4.7). The ^{1}H NMR spectrum of the complex shows the expected eight resonances for the cyclometallated ppy ligands along with a further three resonances for the bis(azido) bipyridyl ligand which appear at δ 7.98, 7.79 and 7.00. The proton resonances for the H-6 and H-6' positions of ligand **4b** are significantly shifted downfield to δ 7.79 due to the ring current effect of the adjacent phenyl ring of the cyclometallated ppy ligands over which they are situated. Confirmation of the

presence of the azide substitutued ligand was confirmed by observation of the azide stretch at 2119 cm^{-1} in the infrared spectrum.

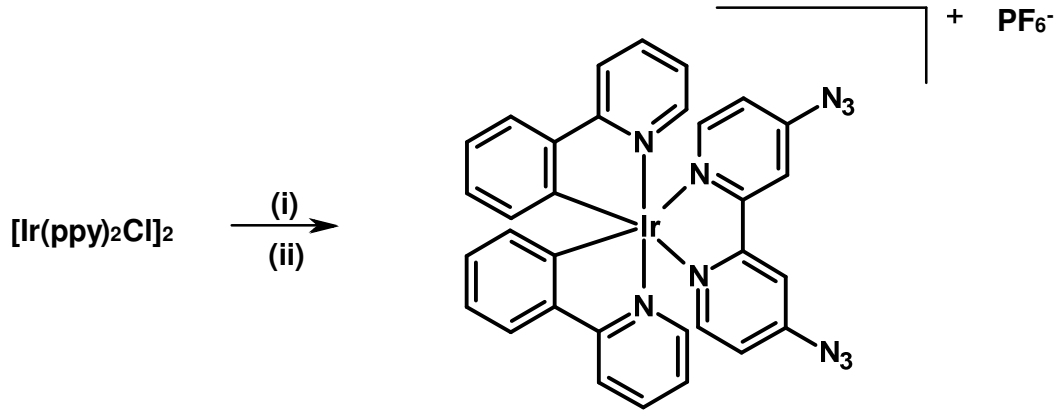

7

*Scheme 4.7 Synthesis of [Ir(ppy)$_2$(**4b**)]$^+$. (i) [$AgPF_6$], MeCN at room temp. (ii)* ***4b***

Having explored the coordination chemistry of the azide substituted bpy ligands we moved on to investigate the coordination chemistry of their triazole derivatives.

Two further ruthenium cymene complexes were prepared by the same route as for those of **6a** and **6b**. The addition of ligands **5a** and **5b** to [Ru(*p*-cymene)$(Cl)_2]_2$ led to the isolation of complexes [Ru(*p*-cymene)(**5a**)Cl]PF_6 (**8a**) and [Ru(*p*-cymene)(**5b**)Cl]PF_6 (**8b**) respectively (Scheme 4.8). The ^{1}H NMR spectrum of **8a** displays a distinct triazole proton resonance at δ 8.99 and seven bpy resonances appearing at δ 9.47, 8.78 and 8.21 for the triazole substituted pyridyl ring and δ 9.39, 8.52, 8.27 and 7.78 for the unsubstituted pyridyl ring. A further three resonances are observed for the phenyl ring at δ 8.00, 7.57 and 7.48 for the *ortho-*,

meta-and *para*- protons respectively. The resonances for the arene protons of the cymene ligand appear at δ 5.98 and 5.78. In addition, the ^{1}H NMR spectrum exhibits two closely overlapping doublets corresponding to the methyl groups of the isopropyl substituent of the cymene ligand at δ 1.08 and 1.07.

The ^{1}H NMR spectrum of **8b** exhibits a resonance at δ 8.64 for the proton of the triazole ring, and a further seven protons for the bpy appearing at δ 9.38, 8.73 and 8.17 for the triazole substituted pyridyl ring and δ 9.44, 8.53, 8.27 and 7.77 for the unsubstituted ring. The resonances of the substituted cyclopentadienyl (Cp) ring of the ferrocene moiety appear at δ 4.85 and 4.42 whilst the protons of the unsubstituted Cp ring gives rise to a singlet at δ 4.13. The resonances for the arene protons of the cymene ligand appear at δ 5.98 and 5.78 and those of the methyl groups of the isopropyl substituent are observed as two closely overlapping doublets centred at δ 1.07.

The resonances for the arene protons adjacent to the *i*-propyl group appear as apparent triplets, whereas the resonance for the arene protons adjacent to the methyl substituent appear as doublets for both complexes **8a** and **8b**.

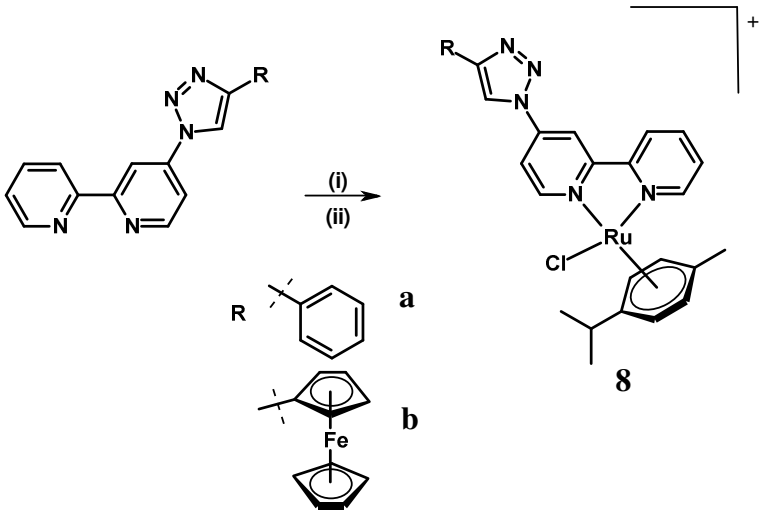

*Scheme 4.8 Synthesis of [Ru(p-cymene)(5**a-b**)Cl]$^+$. (i) [Ru(p-cymene)(Cl)$_2$]$_2$, MeOH at room temp. (ii) NaPF$_6$*

When [Ru(*p*-cymene)(Cl)$_2$]$_2$ was allowed to react with an equivalent of the ditopic ligand **5c**, in ethanol for 48 hours the dinuclear complex **9** was formed and isolated as its PF_6^- salt (Scheme 4.9).

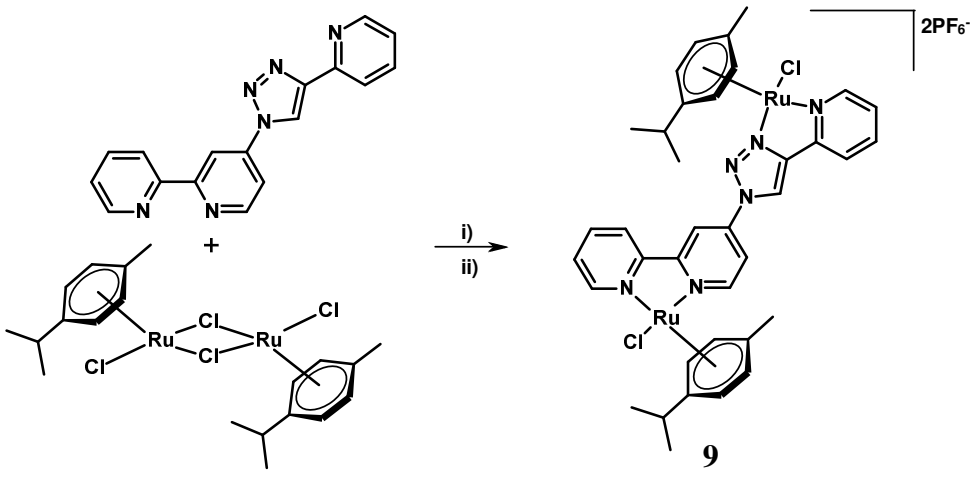

*Scheme 4.9 Synthesis of [{Ru(p-cymene)Cl}$_2$(**5c**)](PF$_6$)$_2$.(**9**) (i) [Ru(p-cymene)(Cl)$_2$]$_2$, MeOH at room temp. (ii) AgPF$_6$ and MeCN*

The resultant complex [{Ru(*p*-cymene)Cl}$_2$(**5c**)](PF$_6$)$_2$ (**9**) was characterised by ^{1}H and ^{13}C NMR spectrometry and mass spectrometry. The aromatic region of the ^{1}H NMR spectrum appears to show more signals than the twelve resonances required for the bridging ligand (Figure 4.6). Examination of the ^{1}H NMR spectrum of the complex reveals two singlet resonances for the triazole ring proton at δ 9.45 and 9.43 indicating the formation of magnetically inequivalent "meso" and "rac" diastereoisomers. These are assigned due to their lack of coupling in the COSY spectrum (Figure 4.8). This would be expected in a dinuclear complex of this type due to the chirality of the ruthenium centres upon coordination in the asymmetric chelating domains of the bridging ligand (structures shown in Figure 4.7). Similar duplicate resonances centered at δ 8.83 and 9.58 are also observed for the 3- and 6-position protons respectively of the pyridyl ring of the bpy domain to which the triazole ring is attached (Figure 4.6). The remaining resonances for the bridging ligand were assigned based on the two-dimensional COSY and NOESY spectra (Figure 4.8 and Figure 4.9). Further overlapping signals from this mixture of isomers are observed for the aryl cymene proton at δ 6.15 and 5.75, the cymene methine proton at δ 2.78 and 2.69 and for the isopropyl methyl groups between δ 1.2 and 1.0.

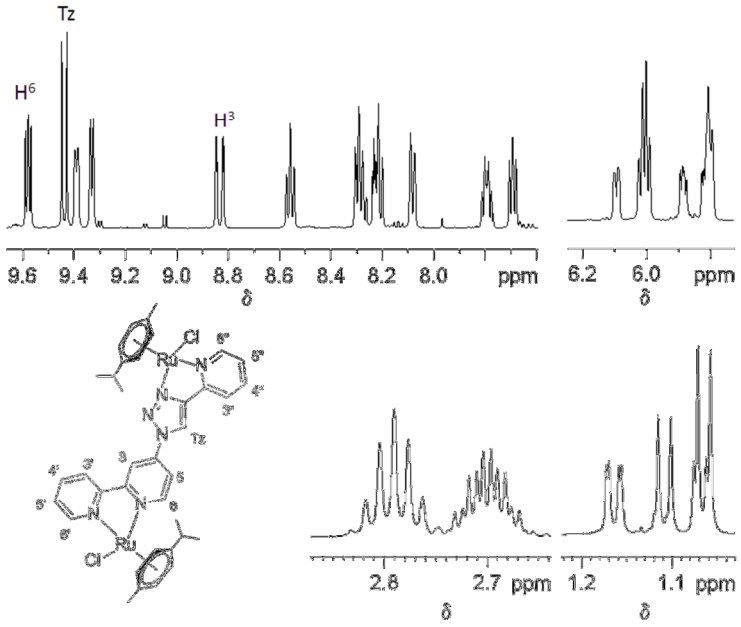

*Figure 4.6 Selected regions of the ^{1}H NMR spectrum for [{Ru(p-Cymene)Cl}$_2$(**5c**)](PF$_6$)$_2$ (**9**) in CD$_3$CN*

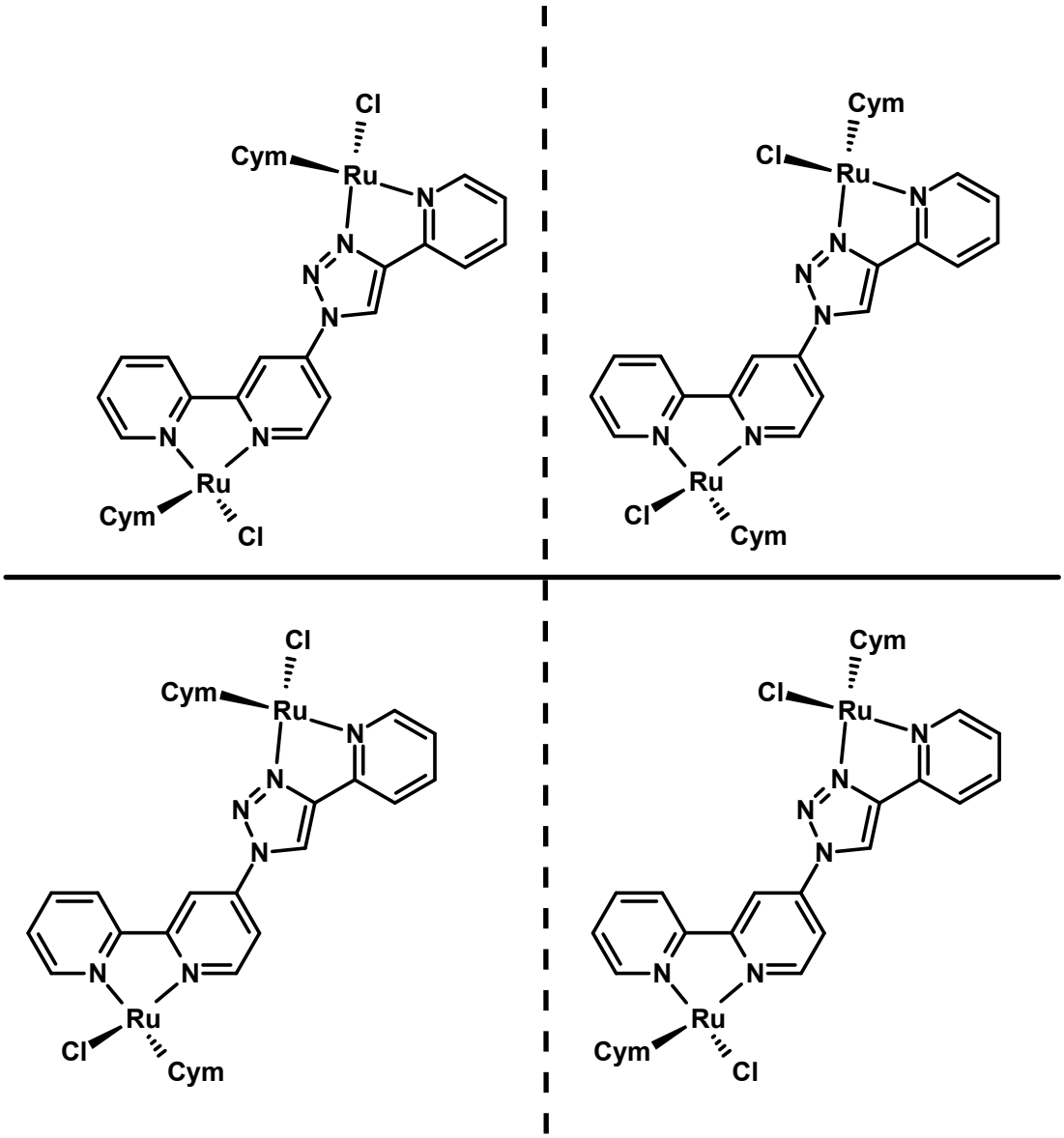

*Figure 4.7 Diastereoisomers of [{Ru(p-cymene)Cl}$_2$(**5c**)](PF$_6$)$_2$ (**9**) (Cym= p-cymene)*

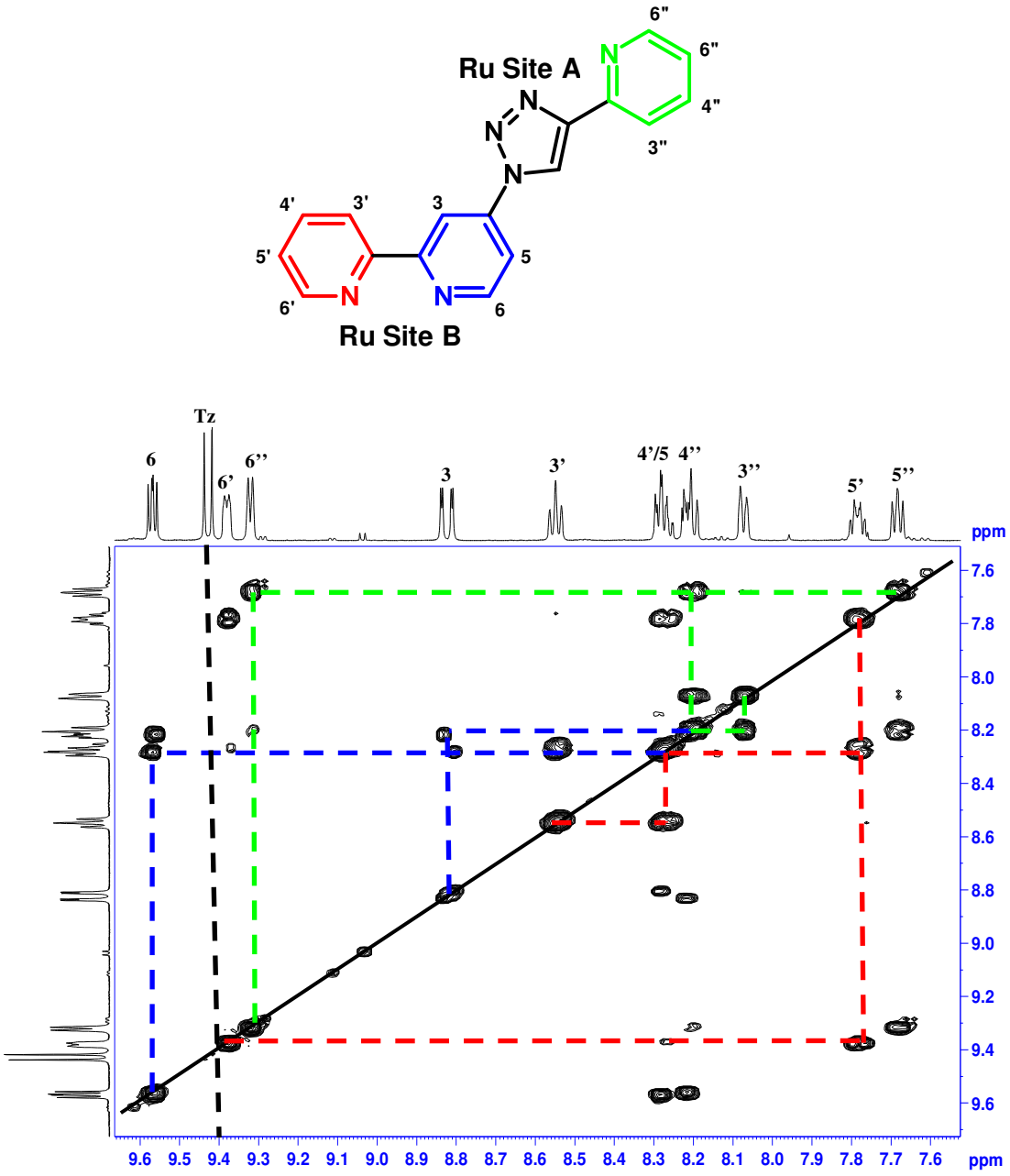

*Figure 4.8 2D H-H COSY NMR spectrum of [{Ru(p-cymene)Cl}$_2$(**5c**)](PF$_6$)$_2$*

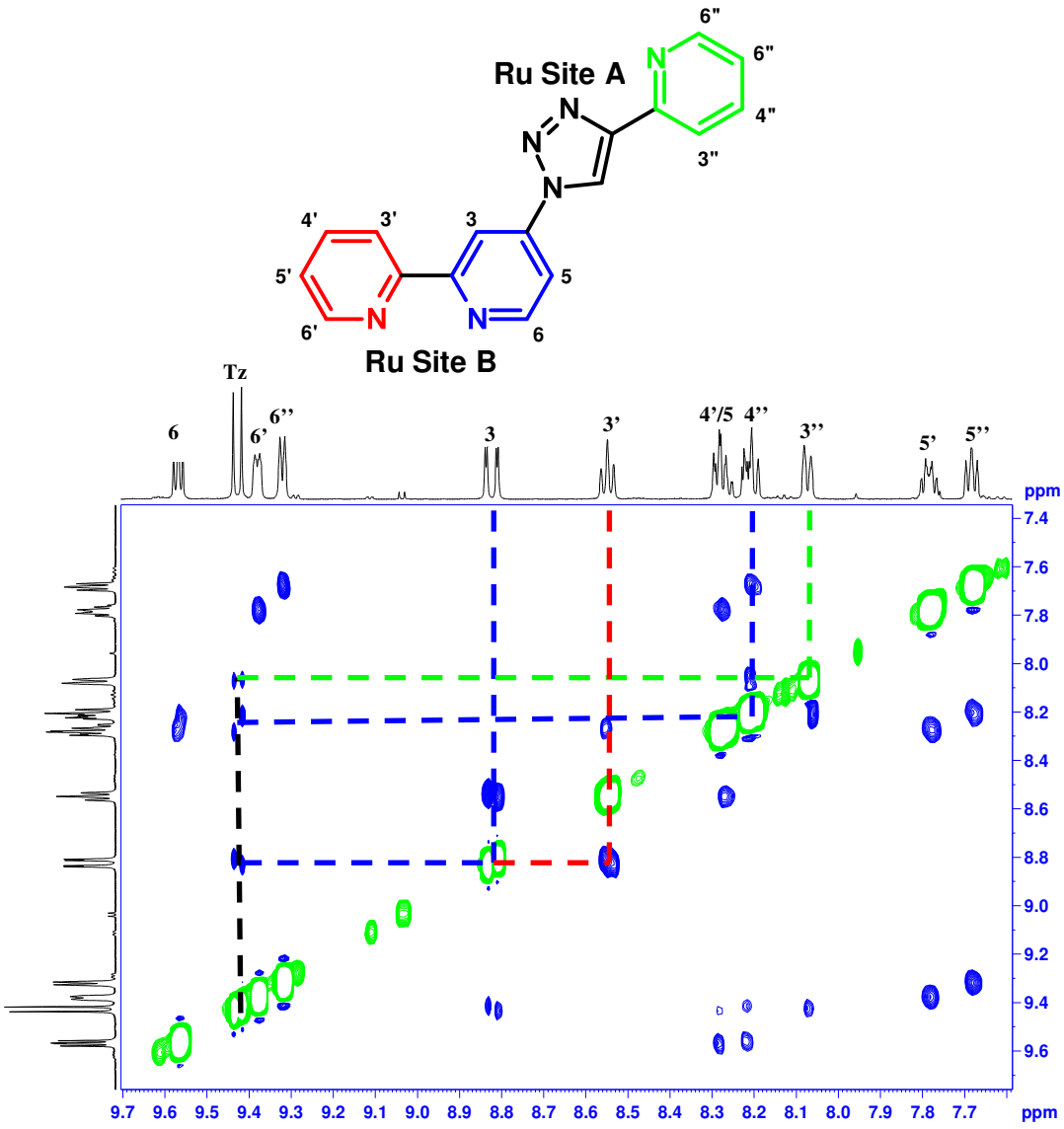

*Figure 4.9 2D H-H NOESY NMR spectrum of [{Ru(p-cymene)Cl}$_2$(**5c**)](PF$_6$)$_2$*

NOESY data was then used to assign the signals for the cymene methyl substituents in terms of which domain of the bridging ligand they are associated with. This was achieved through nOe cross peaks between resonances for the cymene substituent proton signals and those of the bridging ligand.

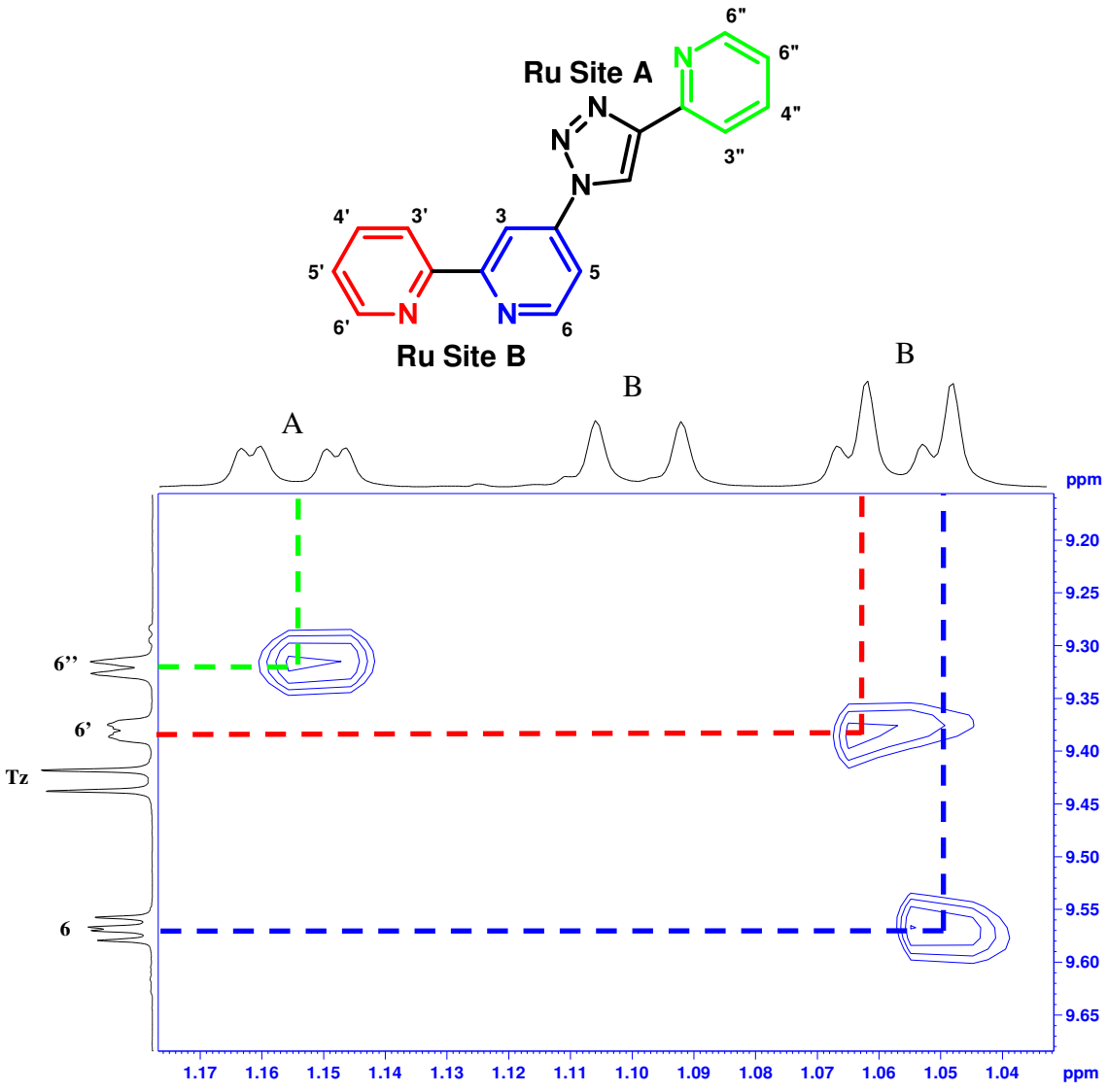

*Figure 4.10 2D H-H NOESY NMR spectrum of [{Ru(p-cymene)Cl}$_2$(**5c**)](PF$_6$)$_2$*

Using the ligand 1-benzyl-4-(pyrid-2-yl)-1,2,3-triazole (**10**), we also prepared the complex [Ru(*p*-cymene)Cl(**10**)]PF$_6$ (**11**) as a spectroscopic model for the pytz domain of **9**. Firstly **10** was prepared through a standard click procedure in which benzyl azide was prepared *in situ* and reacted with phenyl acetylene. [96] The ligand was characterised by ^{1}H NMR spectroscopy, and the diagnostic signal for the

triazole proton is observed at δ 8.06. Four signals due to protons of the pyridyl ring appear at δ 8.56, 8.20, 7.79, and 7.23, whilst signals corresponding to the aromatic benzyl protons appear as a multiplet between δ 7.44-7.32. A further singlet corresponding to the methylene protons is observed at δ 5.61.

Ligand **10** was stirred with [Ru(*p*-cymene)Cl_2]$_2$ in ethanol for 48 hours, after which the solvent was removed and the product was isolated as a chloride salt. The complex was converted into its PF_6, by dissolving the complex in a small amount of acetonitrile and stirring with an equivalent of $AgPF_6$. The solution was filtered to remove silver chloride and the solvent was removed. The complex [Ru(*p*-cymene)Cl(**10**)]PF_6 was characterised by ^{1}H NMR spectroscopy and exhibits a diagnostic triazole signal at δ 8.56, which is shielded by 0.87 ppm relative to that of the dinuclear complex (**9**). The shift in the triazole proton resonance is ascribed to the presence of the more electron donating benzyl substituent of the pytz ligand compared to the bpy moiety that is attached to the triazole in **9**. Four signals arising from the pyridyl ring at δ 9.22, 8.08, 7.91 and 7.57 are at positions close to those observed for the comparable protons in **9**. Signals from the aromatic benzyl protons appear as a large multiplet between δ 7.52-7.40 with an integration for five protons whilst the methylene protons for the benzyl group appear as a singlet δ 5.76 and overlaps with those of the arene protons of the cymene ligand. The ^{1}H NMR spectrum exhibits two doublets corresponding to the methyl groups of the isopropyl group of the cymene ligand at δ 1.09 and 0.94, which are again shielded by 0.03 and 0.13 ppm respectively, with respect to **9**, showing loss of magnetic equivalence.

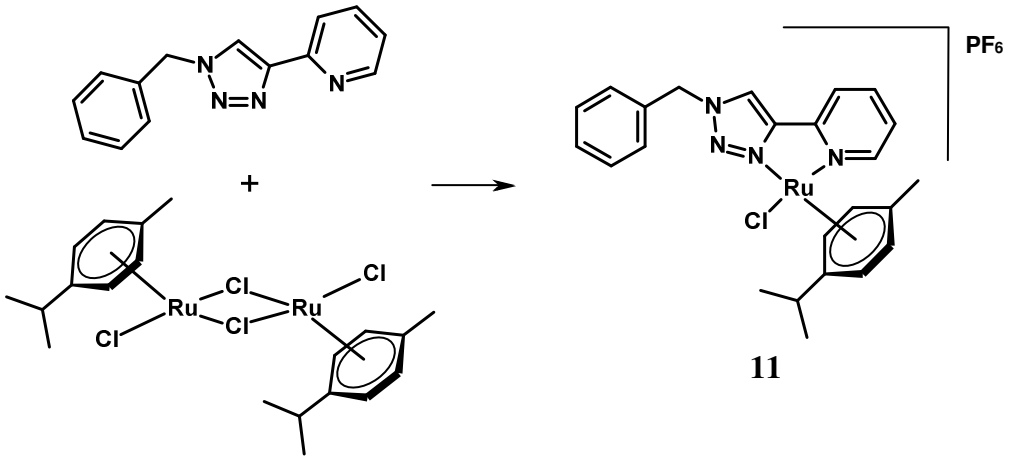

*Scheme 4.10 Synthesis of [Ru(p-cymene)Cl(**10**)]PF_6 (**11**). (i) [Ru(p-cymene)$(Cl)_2]_2$, MeOH at room temp. (ii) $AgPF_6$ and MeCN*

After preparing the ruthenium cymene complexes with pre-clicked ligands **5a-c** our attention turned to the ruthenium cymene complexes with azido substituted ligands and their reactivity with respect to CuAAC reactions. The complex (**6a**) was shown to undergo CuAAC modification of the outer coordination sphere with phenylacetylene and ethynylferrocene as an alternative route to the complexes [Ru(*p*-cymene)(**5a-b**)Cl]PF_6 (**8a-b**). A THF/water mixture was decided upon as the most effective conditions and allowed for easy extraction of product resulting in the highest yields. [Ru(*p*-cymene)(**4a**)Cl]PF_6 (**6a**)was dissolved in a 1:1 mixture of THF and water and an excess of the appropriate alkyne was added along with copper sulfate and sodium ascorbate. The tetrahydrofuran was removed under reduced pressure and the complexes were extracted into dichloromethane and purified by recrystallisation with acetonitrile and ether (Scheme 4.11). Figure 4.11 and Figure 4.12 show that the ^{1}H NMR spectra of complexes [Ru(*p*-cymene)(**5a**)Cl]PF_6 (**8a**) and [Ru(*p*-cymene)(**5b**)Cl]PF_6 (**8b**)

prepared through the alternative route are identical to those of the same complexes prepared with the pre-clicked ligands. This therefore demonstrates the potential application of azide substituted metal complexes as supramolecular synthons through peripheral CuAAC modification.

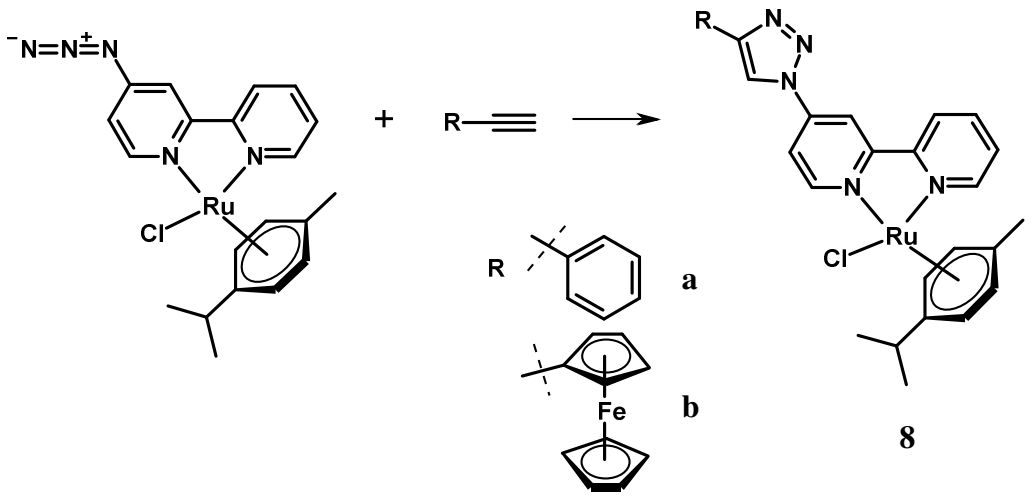

*Scheme 4.11 Alternative synthesis of the complexes [Ru(p-cymene)(**5a-b**)Cl]$^+$ (**8a-b**). (THF/water 1:1, $CuSO_4$ and sodium ascorbate at room temp.)*

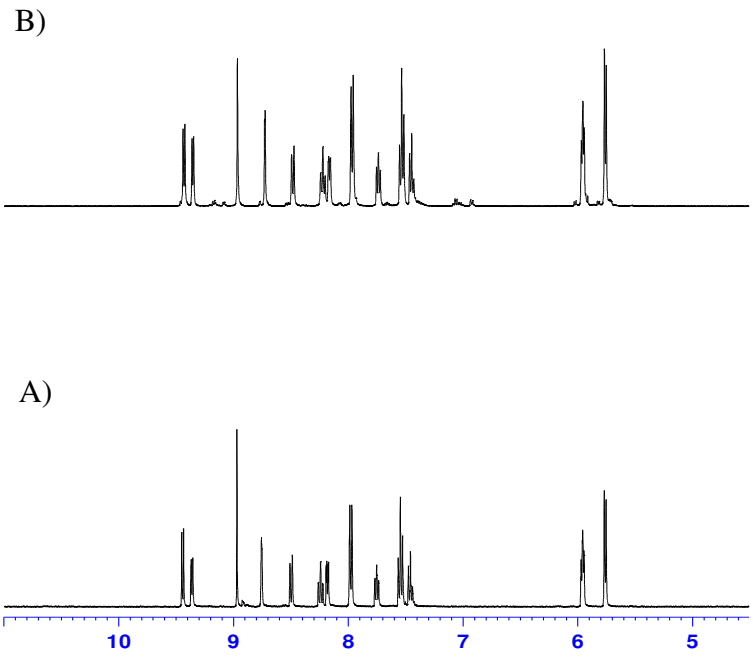

Figure 4.11 ^{1}H *NMR spectra of [Ru(p-cymene)(**5a**)Cl]*PF_6 *A) pre-clicked ligand complex and B) clicked at the metal*

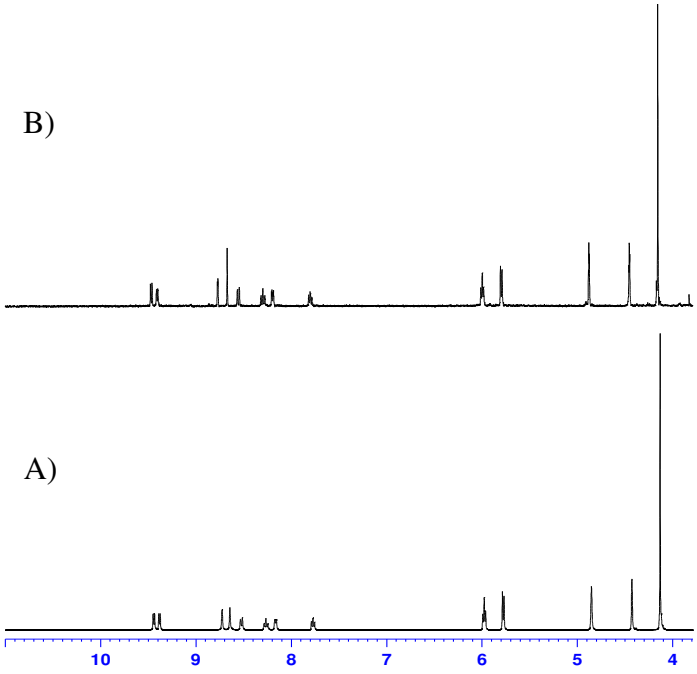

Figure 4.12 ^{1}H *NMR spectra of [Ru(p-cymene)(**5b**)Cl]*PF_6 *A) pre-clicked ligand complex and B) clicked at the metal complex*

When [Ru(*p*-cymene)(**4a**)Cl]PF_6 was "click" coupled with 2-ethynylpyridine the complex [Ru(*p*-cymene)(**5c**)Cl]PF_6 (**8c**) was formed (Scheme 4.12). The ^{1}H NMR spectrum of the product shows signals characteristic of the 4-substitutued bpy ligand along with broad signals for the triazole ring proton and the protons of the third pendant pyridyl ring. The broad nature of these resonances is most likely due to the coordination and exchange of paramagnetic copper(II) remaining from the CuAAC reaction mixture in the pyridyl-triazole domain. After washing a dichloromethane solution of the product with aqueous ammonia solution in order to remove the remaining copper ions, the protons of the coordinatively vacant pyridyltriazole moiety sharpen in the ^{1}H NMR spectrum (Figure 4.13). Resonances at δ 7.39 and 8.66 are still slightly broad in appearance and so we cannot rule out the presence of a small quantity of remaining Cu(II).

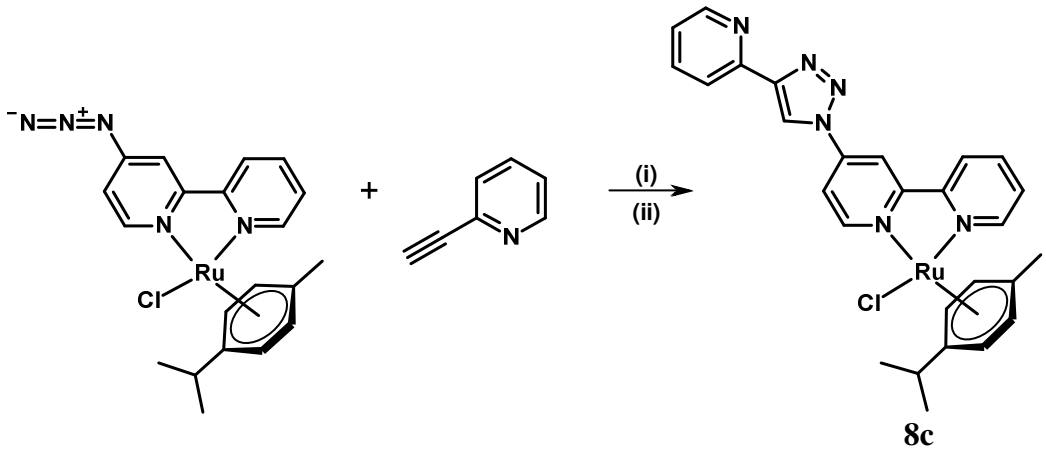

*Scheme 4.12 Synthesis of [Ru(p-cymene)(**5c**)Cl]$^+$. (i) THF/water 1:1, $CuSO_4$ and sodium ascorbate at room temp. (ii) NH_4OH*

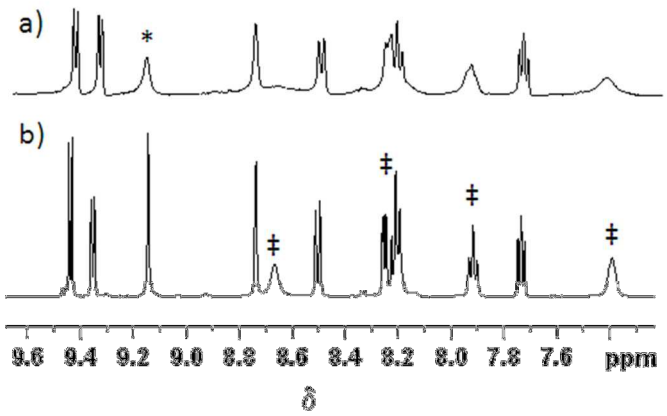

Figure 4.13 *^{1}H NMR spectra of [Ru(p-cymene)(**5c**)Cl]$^+$ a) prior to washing with conc. NH_3, b) after washing (* triazole ring proton, ‡ pendant pyridyl ring protons).*

We then investigated the use of **6a** as a potential building block for metallo-supramolecular assemblies. Since we have successfully demonstrated that **6a** can act as the azido component in a range of click reactions, this was therefore extended to investigate the reaction of this complex with a linker with multiple reaction sites. Therefore **6a** was dissolved in a 1:1 mixture of THF and water with half an equivalent of dipropargyl ether in the presence of 2 equivalents of copper sulfate and excess sodium ascorbate (Scheme 4.13). The product, [{Ru(*p*-cymene)Cl}$_2${di([1-{2,2'-bipyrid-4-yl}-1,2,3-triazol-4-yl]methyl)ether}]2PF_6 (**12**) was purified by extracting with dichloromethane solution and purified by column chromatography, using silica gel and MeCN/H_2O/$KNO_{3(aq.)}$ 7:1:0.5 (v/v) and isolated as its PF_6^- salt after treatment with $NaPF_6$.

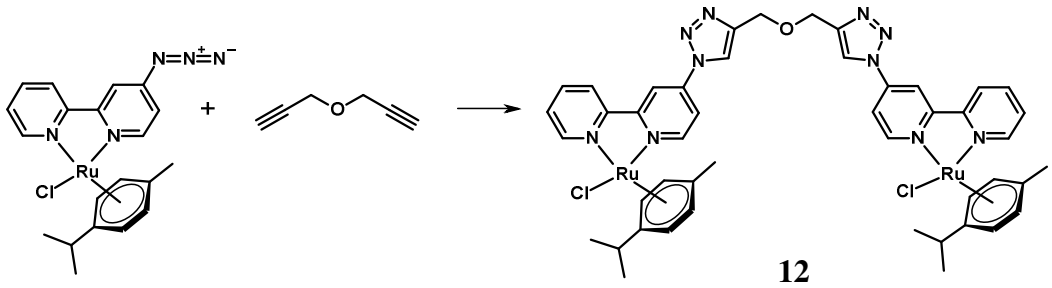

*Scheme 4.13 Synthesis of [{Ru(p-cymene)Cl}$_2${di([1-{2,2'-bipyrid-4-yl}triazol-4-yl]methyl)ether}].2PF$_6$ (**12**).(THF/water 1:1, CuSO$_4$ and sodium ascorbate at room temp.)*

The new clicked complex **12** was fully characterised by ^{1}H and ^{13}C NMR along with mass spectrometry and high resolution mass spectrometry. The ^{1}H NMR spectrum of the complex shows two signals for the triazole ring proton centered at δ 9.29 as does the resonance at δ 9.14 for the H-3 proton of the triazole functionalised pyridine ring. Again, we assign this as being due to the formation of meso- and rac- isomeric mixtures of complexes due to the chirality at each ruthenium site as observed in complex **9**. There are 7 clearly defined signals in the aromatic region of the spectrum which arise from the two 4-substituted bipyridyl units. The resonances associated to the arene protons from the *p*-cymene ligand appear as an apparent triplet at δ 5.97 and a doublet at δ 5.77. A single resonance at δ 4.84 as a singlet is also observed which is due to the methylene protons from the ether bridge (Figure 4.14). Mass spectrometry data shows the detection the dication [{Ru(*p*-cymene)Cl}$_2$(**21**)]$^{2+}$ at m\z 515.1 with an isotope pattern consistent with the presence of two ruthenium centres.

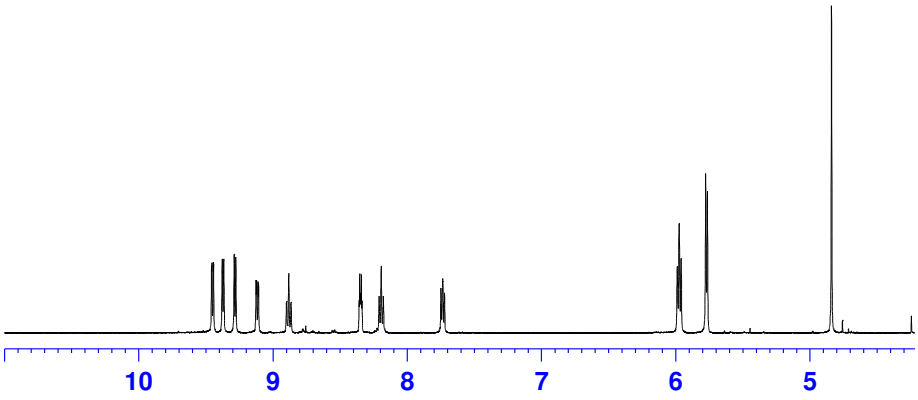

*Figure 4.14 ^{1}H NMR of [{Ru(p-cymene)Cl}$_2$\{di([1-{2,2'-bipyrid-4-yl}-1,2,3-triazol-4-yl]methyl)ether}].2PF$_6$ (**12**).*

4.4 Conclusion

In conclusion, we have successfully developed new 'clicked' ligands from 4-azido-2,2'-bipyridyl, with either single or multiple binding sites. We have shown successfully that these ligands can be successfully coordinated to $[Ru(\eta^6\text{-cymene})Cl]^+$ and a have fully characterised these complexes. In similar reactions we have shown that we can coordinate 4-azido-2,2'-bipyridyl and 4,4'-diazido-2,2'-bipyridyl to $[Ru(\eta^6\text{-cymene})Cl]^+$ and we have demonstrated that the azido unit remains intact upon coordination. Indeed this azido unit can undergo'click' reactions and provide an alternative method to synthesising the same complexes as those made with prepared ligands. Further we were able to introduce a second domain through this approach. Finally we have demonstrated that **6a** and "click" chemistry can be used as a potential tool in building metallo-supramolecular species. We have therefore made some of the first steps towards the goal of the development of a general "click" chemistry-based methodology for the construction of functional supramolecular architectures *via* azide-functionalised transition metal complexes.

Future work in this area could include preparation of hetereobimetallic complexes of the bridging ligand **5c** through this "clicked at the complex" route.

5 1,2,3-Triazole Bridged Luminescent Redox Switches

5.1 Introduction

Molecular switches refer to molecules which can be reversibly shifted between two or more stable states in response to various external triggers. [192] These molecules can respond to a range of different stimuli, for example pH, light, temperature, electrical current or the presence of a ligand. [192-195] One of the most attractive fields of research within molecular switches is the redox switching of fluorescence due to the interest in designing reversible luminescent sensors for the determination of local environmental redox properties and as bio-sensor elements to study electron and energy transfer mechanisms. [195] Aukauloo [196] and Galoppini [197] have used the mono azido bpy and bis azido ligand precursors respectively and showed that both of these ligands can be 'click' modified and can be used for the preparation of ruthenium complexes. Both groups note efficient electron transfer across the triazole ring. The group of Molina and Tárraga have shown that luminescent properties of ruthenium and iridium complexes with tethered ferrocene can be manipulated by a reversible process between the oxidized and reduced states of the ferrocene unit. [195, 198, 199] These results encouraged us to pursue complexes of 4-ferrocenyl-1-(2,2'-bipyrid-4-yl)-1,2,3-triazole (**5c**) as potential luminescent switches.

Described in this chapter is the synthesis and characterisation of metal complexes of ferrocenyl-bipyridyl ligand in which the ferrocene unit is tethered to the bipyridyl through a 1,2,3-triazole linkage. The photophysical properties of these complexes are reported along with efforts to use these as reversible luminescent switches.

5.2 Ligand Synthesis

The synthesis of ligand **5b** was carried out in a one-pot CuAAC synthesis as described previously. Briefly, 4-azido-2,2'-bipyridine was mixed with a slight excess of ethynylferrocene in the presence of copper sulfate and sodium ascorbate in a 1:1 mixture of THF and water at room temperature (Scheme 5.1). Upon completion of the reaction the product was isolated from the reaction mixture by portioning it between dichloromethane and aqueous ammonia and the desired triazole substituted ligand was purified by recrystallisation from dichloromethane and hexane and isolated in excellent yields. Ligand **5b** was fully characterised using ^{1}H and ^{13}C NMR spectroscopy and mass spectrometry.

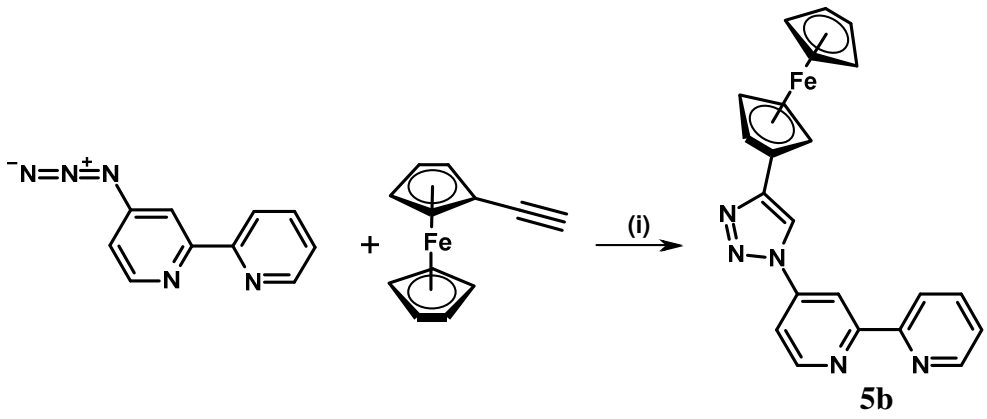

Scheme 5.1 Synthesis of 4-ferrocenyl-1-(2,2'-bipyrid-4-yl)-1,2,3-triazole ligand. (i) THF/H_2O, $CuSO_4$ and sodium ascorbate at room temperature.

5.3 Synthesis of ferrocenyltriazolyl-bipyridyl complexes

5.3.1 Synthesis of $[Ru(bpy)_2(5b)][PF_6]_2$ (13)

Ligand **5b** was reacted with one equivalent of $[Ru(bpy)_2Cl_2]$ in EtOH and the mixture stirred at reflux for 4 hours under an inert atmosphere (Scheme 5.2). Upon cooling the resulting purple solution was passed through a silica column and MeCN/H_2O/sat. $KNO_{3\ (aq.)}$ (7:1:0.5) was used to elute the desired fraction. The product was then isolated as its PF_6^- salt after treatment with $NaPF_6$. The ESI-MS and high resolution ESI-MS spectra confirmed the resulting solid as $[Ru(bpy)_2(\mathbf{5b})](PF_6)_2$ (**13**) with a signal at *m/z* 966.1 corresponding to the ion-pair $[Ru(bpy)_2(\mathbf{5b})](PF_6)^+$ showing the expected isotope pattern for a Ru complex. The identity of the complex was also confirmed by ^1H and ^{13}C NMR studies in deuterated acetonitrile. The diagnostic singlet resonance corresponding to the triazole ring proton is clearly observed at δ 8.63 (Figure 5.1). Peaks which relate to both the substituted and unsubstituted Cp rings are clearly defined as a set of two triplet signals for the substituted Cp ring at δ 4.85 and 4.42, each with an integration of two protons and a large singlet at δ 4.12 for the unsubstituted ring with an integration of five protons. A number of multiplets are observed in the aromatic region of the spectrum, some of which overlap, and are associated with substituted and un-substituted bpy ligands. The signals for the ferrocenyl triazole substituted ligand are easily identifiable through two dimensional NOESY and COSY NMR spectroscopy. The protons for the 4-substituted pyridyl ring of ligand **5b** in the complex are observed at δ 8.89, 7.84 and 7.41 whilst the protons for the unsubstituted pyridyl appear at δ 8.70, 8.12, 7.34 and 7.45. The remaining

resonances, some of which overlap, are assigned to the two remaining bpy ligands of the complex.

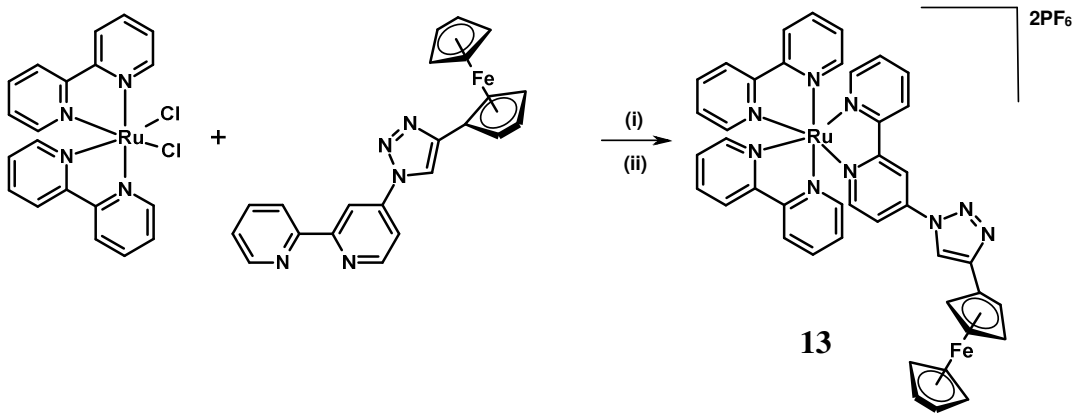

*Scheme 5.2 Synthesis of [Ru(bpy)$_2$(**5b**)](PF$_6$)$_2$ (i) EtOH at reflux (ii) NaPF$_6$.*

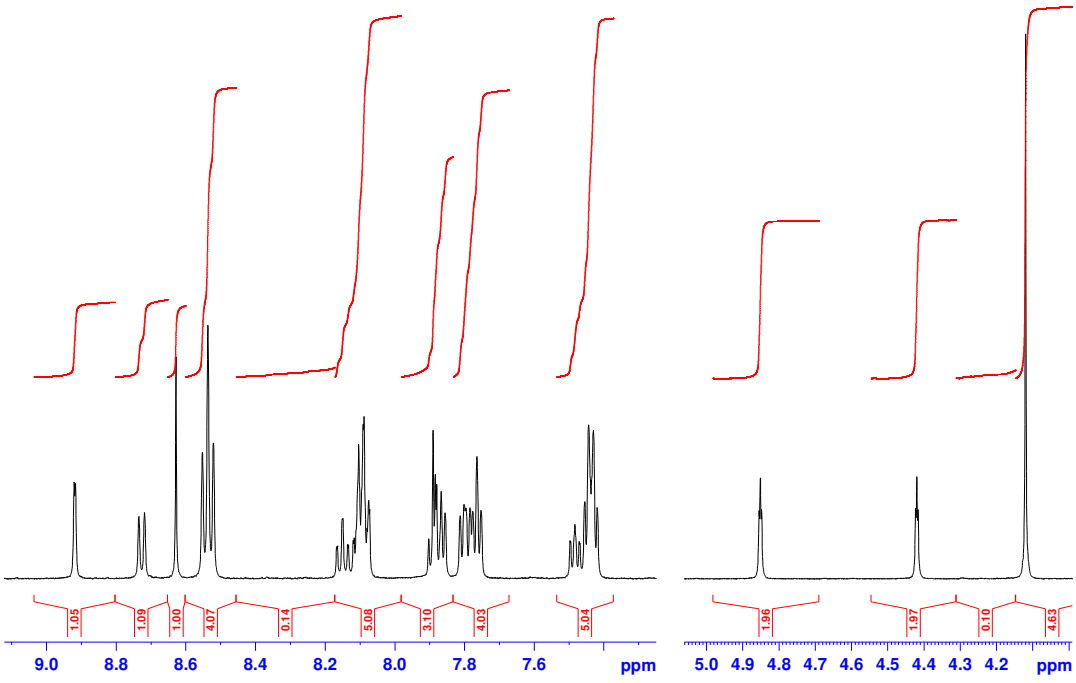

*Figure 5.1 Selected regions of the ^{1}H NMR spectrum for [Ru(bpy)$_2$(**5b**)]PF$_6$ showing the aromatic region and the Cp ring region for the ferrocene sub unit.*

5.3.2 Synthesis of $[Ir(ppy)_2(5b)][PF_6]$ (14)

Ligand **5b** was reacted with half an equivalent of the iridium dimer $[Ir(ppy)_2Cl]_2$ in the presence of silver hexafluorophosphate in acetonitrile with the exclusion of light. The resulting orange solution was passed through a silica column and $MeCN/H_2O$/sat. $KNO_{3\ (aq.)}$ (7:1:0.5) was used to elute the desired fraction. Fractions containing the product were evaporated to dryness and redissolved in dichloromethane and stirred with excess $NaPF_6$ for 2 hours (Scheme 5.3). Water was added to the solution and the product was extracted as the PF_6^- salt into dichloromethane. Further purification was carried out by recrystallisation from dichloromethane and ether resulting in $[Ir(ppy)_2(\mathbf{5b})]PF_6$ (**14**). ESI-MS was used to confirm identity of the product and a molecular ion was observed with m/z 908.2 corresponding to $[Ir(ppy)_2(\mathbf{5b})]^+$ with the expected isotope pattern for an iridium complex. NMR studies were also carried out in deuterated acetonitrile and a few similarities were observed between iridium complex and the corresponding ruthenium bipyridyl complex. The distinct signal for the triazolyl proton was clearly defined at δ 8.60 and the ferrocenyl signals were also clearly observed with two triplet resonances at δ 4.82 and 4.40 for the substituted Cp ring and a singlet at δ 4.10 for the unsubstituted Cp ring. As with the ruthenium complex there are also another 15 signals in the aromatic region which correspond, with some overlap, to the 23 protons of the bpy and ppy ligands. The protons of the substituted pyridyl ring of ligand **5b** in the complex appear at δ 8.90, 8.09 and 7.94 and those of the unsubstituted ring appear at δ 8.71, 8.19, 8.03 and 7.56.

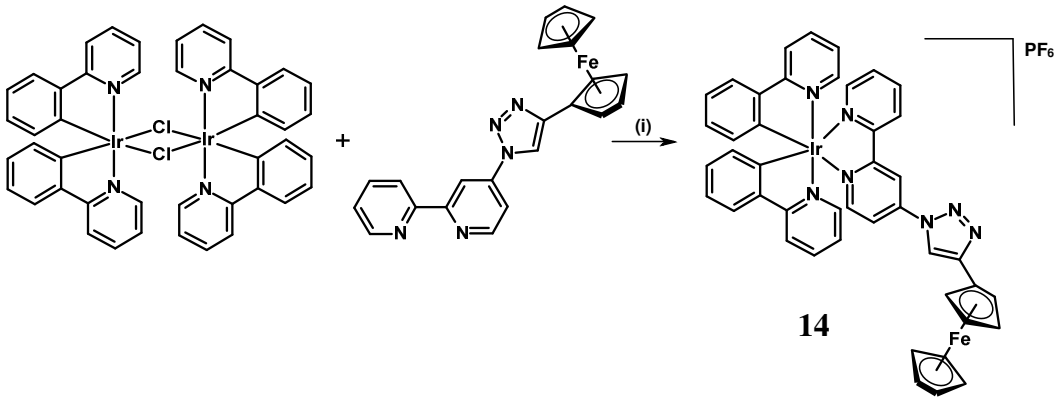

*Scheme 5.3 Synthesis of [Ir(ppy)$_2$(**5b**)](PF$_6$) (AgPF$_6$, MeCN in the dark at room temperature)*

5.3.3 Synthesis of [Re(5b)(CO)$_3$Cl] (15)

Ligand **5b** was refluxed with an equivalent of [Re(CO)$_5$Cl] in toluene and upon cooling [Re(**5b**)(CO)$_3$Cl] (**15**) was collected as an orange-brown solid (Scheme 5.4). Mass spectrometry indicated that this synthesis had been successful with an ion with m/z 678.0 being observed corresponding to [Re(**5b**)(CO)$_3$]$^+$ through loss of the Cl$^-$ ligand. The ^{1}H NMR spectrum in deuterated acetonitrile of the complex contains all of the expected signals arising from the ferrocenyl triazolyl bpy ligand which are shifted relative to those of the free ligand in the same solvent. The triazole proton gives rise to a singlet resonance at δ 9.31 which is deshielded by 1.1 ppm on coordination. The signals for the substituted ring of the bpy appear at δ 9.18, 9.17 and 8.34 and those of the unsubstituted ring appear at δ 9.09, 8.98, 8.47 and 7.85. Again, ferrocenyl signals were also clearly observed with two triplet resonances at δ 4.84 and 4.44 for the substituted ring and a singlet at δ 4.14 for the unsubstituted ring. The infrared spectrum of complex 15 was recorded

using ATR. The complex exhibits three distinct bands in the carbonyl region of the infrared spectrum with the symmetric stretch at 2019 cm-1 and the asymmetric stretches at 1934 and 1909 cm^{-1}. The carbonyl stretching frequencies shift to higher wavenumbers with respect to the bpy analogue, which appear at 2010, 1890 and 1870 cm^{-1} respectively using the same technique, which is indicative of a greater π-accepting character for the ligand **5b** compared to bpy.

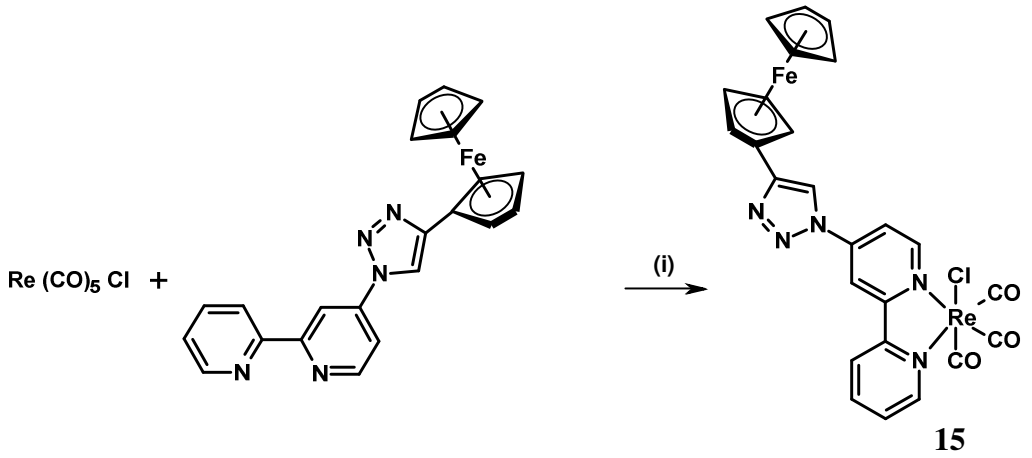

15

*Scheme 5.4 Synthesis of [Re(**5b**)(CO)$_3$Cl] (i) Toluene at reflux.*

5.4 Synthesis of phenyltriazolyl-bipyridyl complexes

In order to probe the effect of the ferrocene moiety on the photophysical properties of the ruthenium and iridium complexes of ligand **5b** we have prepared the analogous series of complexes bearing the ligand **5a**, 4-phenyl-1-(2,2'-bipyrid-4-yl)-1,2,3-triazole. Further, comparison of these complexes to the analogous unsubstituted bpy parent complexes will allow us to gauge the effects of the triazole linker on the photophysical properties.

The synthesis of ligand **5a** has been reported in a previous chapter. Briefly, 4-azido-2,2'-bipyridyl was reacted with phenylacetylene in the presence of $CuSO_4$ and sodium ascorbate (see chapter 4).

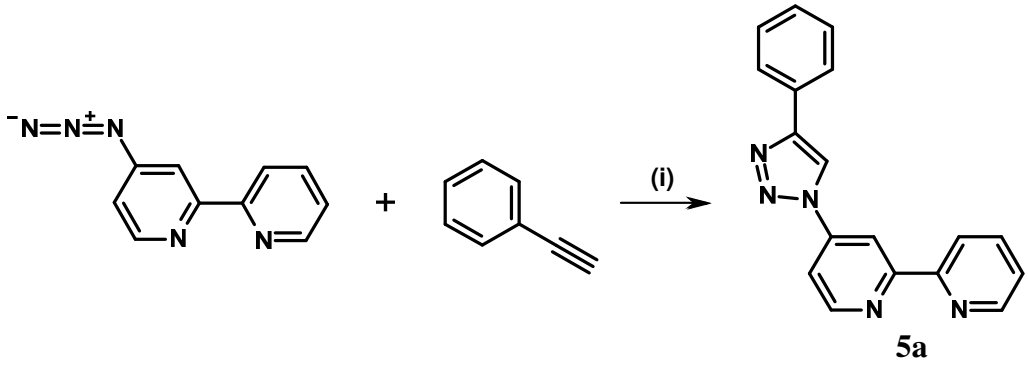

Scheme 5.5 Synthesis of 4-phenyl-1-(2,2'-bipyridyl)-1,2,3-triazole ligand. (i) THF/H_2O, CuSO4 and sodium ascorbate at room temperature.

5.4.1 Synthesis of $[Ru(bpy)_2(5a)][PF_6]_2$ (16)

Ligand **5a** was reacted with an equivalent of $[Ru(bpy)_2Cl_2]$ in ethanol and the mixture was stirred at reflux for 4 hours under an inert atmosphere (Scheme 5.6). Upon cooling the resulting purple solution was passed through a silica column and MeCN/H2O/sat. KNO3 (aq.) (7:1:0.5) was used to elute the desired fraction. The complex $[Ru(bpy)_2(\mathbf{5a})](PF_6)_2$ (**16**) was isolated as its PF_6^- salt as a red solid. ESI-MS was used to identify the product and a peak was observed at m\z 858.1108 corresponding to the ion-pair $[Ru(bpy)_2(\mathbf{5a})]PF_6^+$. The complex was also characterised by NMR spectroscopy and as with the other complexes of this sort a singlet signal is observed at δ 8.98 for the triazole ring proton all other resonances associated with the bipyridyl protons are observed in the region δ 7.36-8.96. The

resonances which correspond to the ligand **5a** were distinguished by two-dimensional NMR spectroscopy. The phenyl resonances are well resolved with the *ortho*- and *meta*-proton signals appearing at δ 7.94 and 7.48 respectively with the resonance for the *para*-position overlapping with one of the signals arising from the unsubstituted bpy ligands at δ 7.42. The resonances for the protons of the triazole substituted pyridyl ring are observed at δ 8.94 for the proton at 3-position and the signals for the 5- and 6- positions appear coincident at δ 7.89. The resonances for the unsubstituted pyridyl ring protons of ligand **5a** appear at δ 8.72, 8.12, 7.79 and 7.42.

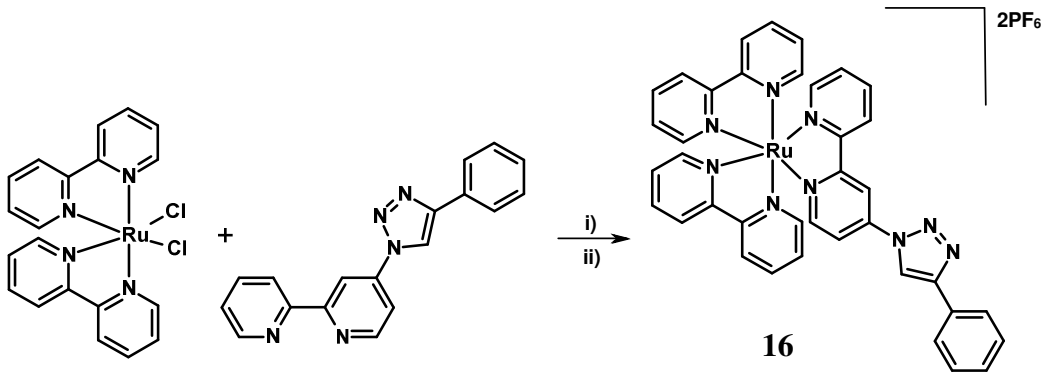

*Scheme 5.6 Synthesis of [Ru(bpy)$_2$(**5a**)](PF$_6$)$_2$ (i) EtOH at reflux (ii) NaPF$_6$.*

5.4.2 Synthesis of [Ir(ppy)$_2$(5a)][PF$_6$] (17)

In a similar procedure to that for the iridium ferrocene substituted complex **14**, ligand **5a** was reacted with half an equivalent of the iridium dimer [Ir(ppy)$_2$Cl]$_2$ in the presence of silver hexafluorophosphate in MeCN with the exclusion of light. The resulting orange solution was passed through a silica column and MeCN/H$_2$O/sat. KNO$_3$ (aq.) (7:1:0.5) was used to elute the desired fraction.

Further purification was carried out by recrystallisation from dichloromethane and diethyl ether and metathesis to the PF_6 to yield $[Ir(ppy)_2(\mathbf{5a})]PF_6$ (**17**). The complex was characterised by NMR spectroscopy and as with the other complexes in this series a singlet signal is observed at δ 8.99 assigned to the triazolyl ring proton. All other resonances associated with the cyclometallated bipyridyl protons are observed in the region δ 6.20-9.00 with the *ortho*, *meta* and *para* protons of the phenyl ring appearing at δ 7.96, 7.52 and 7.43 respectively. The resonances for the bpy protons of the triazole substituted pyridyl ring of ligand **5a** are observed at δ 8.97, 8.11 and 7.99, and those of the unsubstituted pyridyl ring of **5a** are observed at δ 8.74, 8.19, 8.03 and 7.56.

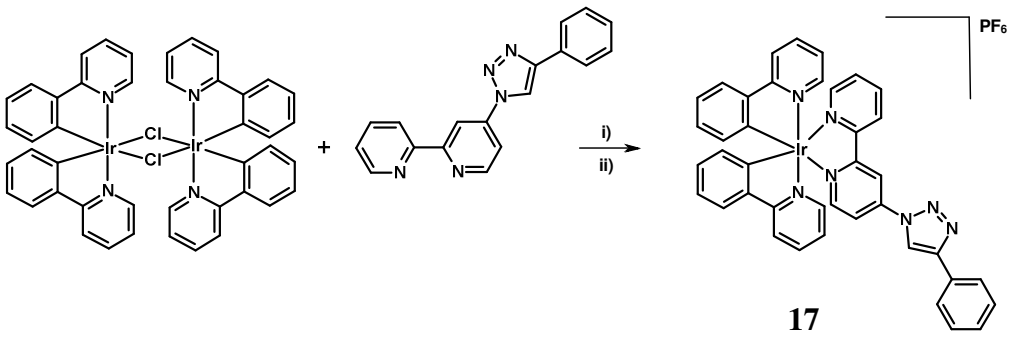

17

Scheme 5.7 *Synthesis of $[Ir(ppy)_2(\mathbf{5a})](PF_6)$ (i) MeCN and $AgPF_6$ (ii) $NaPF_6$.*

5.4.3 Synthesis of [Re(5a)(CO)$_3$Cl] (18)

Ligand **5a** was also coordinated to rhenium by reaction with $[Re(CO)_5Cl]$ in refluxing toluene. The complex $[Re(\mathbf{5a})(CO)_3Cl]$ (**18**) was characterised by ^1H NMR spectroscopy and the spectrum shows the same number of signals as for the uncomplexed ligand but which appear shifted relative to those of the free ligand. The triazole ring proton is observed as a characteristic singlet resonance at δ 9.72,

which is deshielded by 1.5 ppm compared to that of the free ligand. The resonances for the substituted pyridyl ring of the bpy have characteristic resonances at δ 9.23, 9.21 and 8.36 and those of the unsubstituted ring appear at δ 9.09, 8.95, 8.46 and 7.85. This complex proved rather insoluble and so obtaining mass spectrometry data for this complex was not possible. The infrared spectrum of complex **18** shows three distinct carbonyl stretching frequencies at 2019 cm^{-1} and the asymmetric stretches at 1926 and 1890 cm^{-1} again at higher wavenumbers compared to the bpy analogue.

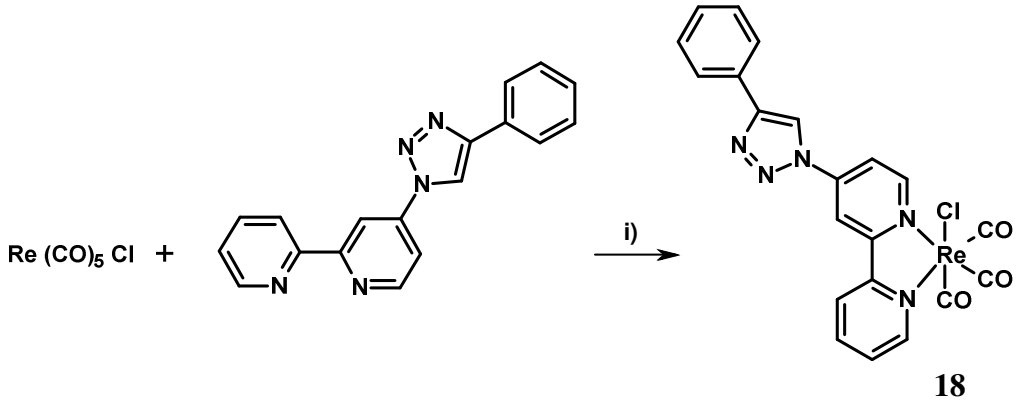

18

*Scheme 5.8 Synthesis of [Re(**5a**)(CO)$_3$Cl](i) Toluene at reflux.*

5.5 Photophysical Studies

UV-vis absorption and luminescence data for $[Ru(bpy)_2(\mathbf{5a})](PF_6)_2$, $[Ru(bpy)_2(\mathbf{5b})](PF_6)_2$, $[Ru(bpy)_3](PF_6)_2$ $[Ir(ppy)_2(\mathbf{5a})](PF_6)$, $[Ir(ppy)_2(\mathbf{5b})](PF_6)$ and $[Ir(ppy)_2(bpy)](PF_6)$ are summarised in Table 5.1 UV-vis absorption spectra of ruthenium complexes **13** and **16** along with that of $[Ru(bpy)_3](PF_6)_2$ (**19**) were recorded in acetonitrile and are shown in Figure 5.2. The spectra for complexes **13**, **16** and **19** all show an intense absorption band at approximately 290 nm, assigned to bpy-centred $\pi \rightarrow \pi^*$ excitations. The complexes also exhibit a broad band between 400–500 nm, assigned to ^{1}MLCT-based transitions. On replacing one of the bpy ligands in $[Ru(bpy)_3]^{2+}$ with a triazole substituted bpy ligand these MLCT bands are observed to redshift appearing at 460 nm for **13** and 461 nm for **16**, compared to 452 nm for **19**. This is explained by the extended π-system in the derivatised bpy ligand which will result in a lowering of the energy of the LUMO and hence the ^{1}MLCT state relative to the ground state.

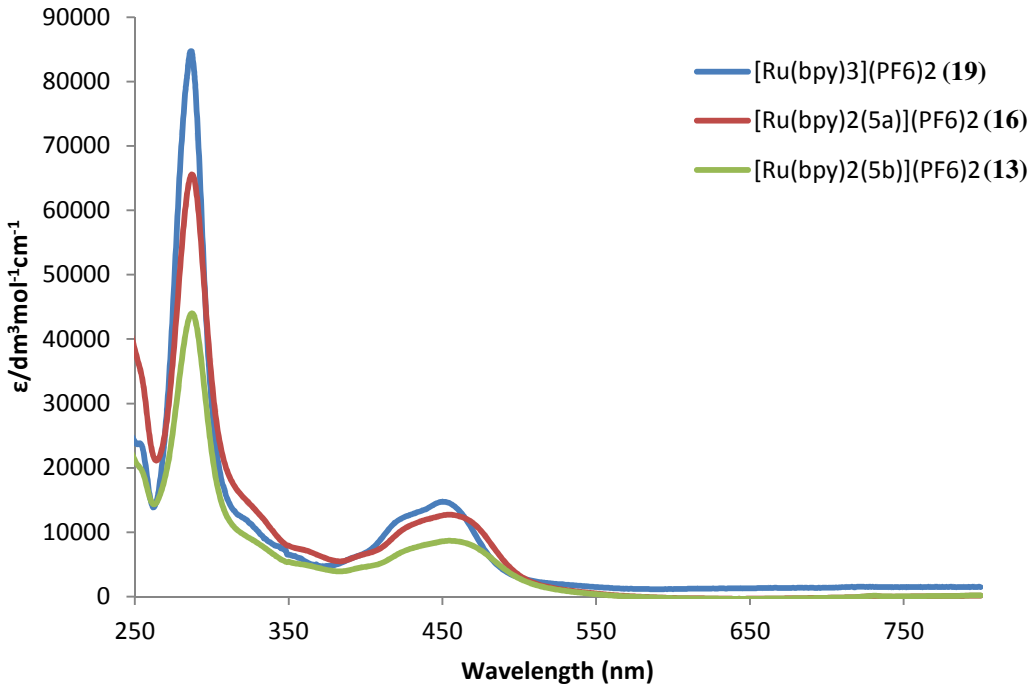

*Figure 5.2 UV-vis absorption spectra for [Ru(bpy)$_2$(**5a**)](PF$_6$)$_2$, [Ru(bpy)$_2$(**5b**)](PF$_6$)$_2$ and [Ru(bpy)$_3$](PF$_6$)$_2$*

UV-vis absorption spectra of the iridium complexes **14** and **17** were also recorded in acetonitrile, along with that of the bpy analogue [Ir(ppy)$_2$(bpy)](PF$_6$) (**20**), and are presented in Figure 5.3. The compounds show absorption features similar to those reported for other [Ir(ppy)$_2$] complexes with typical strong $\pi \rightarrow \pi^*$ transitions in the UV region below 300 nm localized on the ppy and the bpy ligands. Weaker ^{1}MLCT bands are observed at lower energies between 370 and 470 nm. On replacing one of the bpy ligand in **20** with a triazole substituted bpy ligand these weak ^{1}MLCT bands are observed to very slightly blueshift appearing at 468 nm for **14** and 466 nm for **17**, compared to 470 nm for **20**.

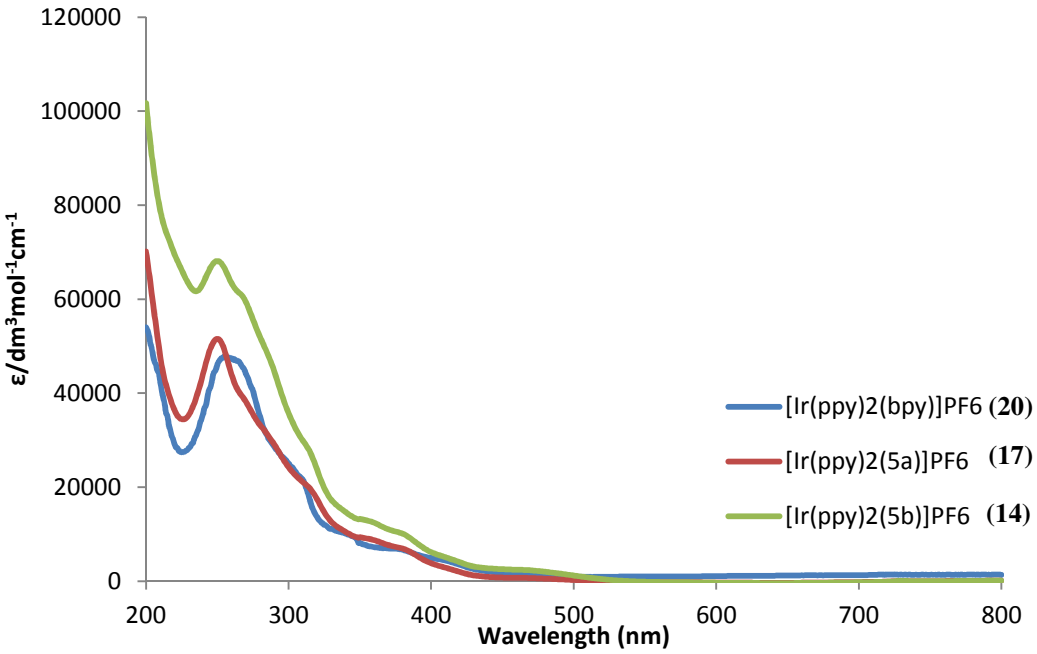

*Figure 5.3 UV-vis absorption spectra for [Ir(ppy)$_2$(**5a**)](PF$_6$), [Ir(ppy)$_2$(**5b**)](PF$_6$) and [Ir(ppy)$_2$(bpy)](PF$_6$)*

Luminescence measurements were recorded at room temperature in aerated acetonitrile with an excitation wavelength of 400 nm. Figure 5.4 and Figure 5.5 shows the emission spectra for truthenium complexes **13, 16** and **19** and the iridium complexes **14**, **17** and **20** respectively.. Figure 5.4 shows broad emission bands with λ_{max} of 639 and 611 nm for complexes **16** and **19** respectively, which are assigned to phosphorescent emission from triplet metal-to-ligand charge-transfer (^{3}MLCT) excited states. The ferrocene containing complex **13** shows largely quenched room temperature emission compared to emission from **14** and **16**. The emission profile of both the triazole containing complexes is red-shifted relative to that of the homoleptic bpy complex **19** (611 nm) and is observed at 639 nm for **16** and very weak emission at 642 nm for **13**. The red-shift in the emission

band reflects the shift observed in the absorption spectra showing a stabilisation of the ^{3}MLCT state due to the extended π-system of the triazole substituted ligands.

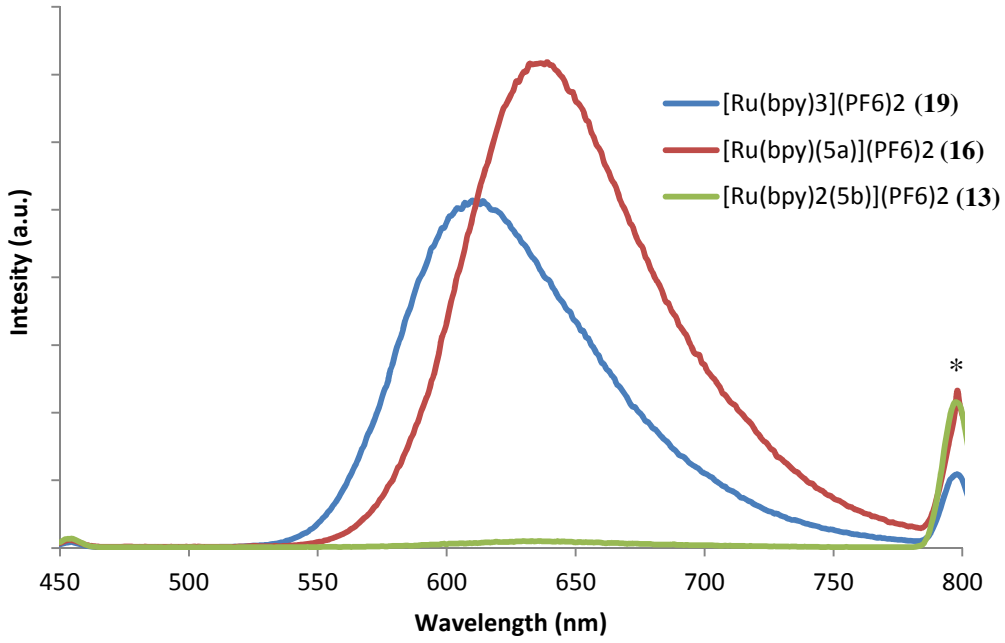

*Figure 5.4 Equimolar luminescence spectra for[Ru(bpy)$_2$(**5a**)](PF$_6$)$_2$, [Ru(bpy)$_2$(**5b**)](PF$_6$)$_2$ and [Ru(bpy)$_3$](PF$_6$)$_2$ (* 2nd harmonic scattering)*

Figure 5.5 shows the emission profiles for the iridium complexes **15**, **17** and **20**. As with the ruthenium complexes, broad emission bands are observed for the unsubstituted bpy complex (**20**) and the phenyl-triazole substituted bpy complex (**17**). Similarly to the ruthenium analogue, the ferrocene containing iridium complex (**15**) shows largely quenched room temperature emission. The emission profiles of both the triazole containing complexes are again red-shifted relative to that of the bpy complex (590 nm) and are observed at 624 nm for **17** and 640 nm for **14**. This is indicative of a lowering of the bpy-centered LUMO and hence stabilisation of the ^{3}MLCT state.

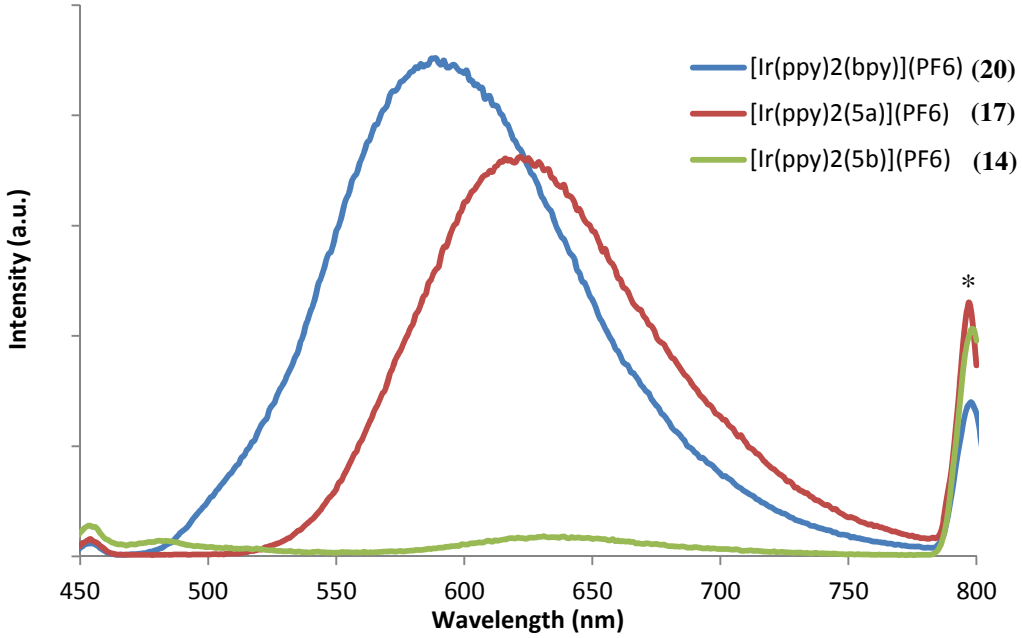

*Figure 5.5 Equimolar luminescence spectra for[Ir(ppy)$_2$(**5a**)](PF$_6$), [Ir(ppy)$_2$(**5b**)](PF$_6$) and [Ir(ppy)$_2$(bpy)](PF$_6$) (* 2nd harmonic scattering)*

*Table 5.1 UV-vis absorption and luminescence data for [Ru(bpy)$_2$(**5a**)](PF$_6$)$_2$, [Ru(bpy)$_2$(**5b**)](PF$_6$)$_2$, [Ru(bpy)$_3$](PF$_6$)$_2$ [Ir(ppy)$_2$(**5a**)](PF$_6$), [Ir(ppy)$_2$(**5b**)](PF$_6$) and [Ir(ppy)$_2$(bpy)](PF$_6$)*

Complex	λ^{abs} / nm	λ_{max}^{em} / nm
[Ru(bpy)$_2$(**5a**)](PF$_6$)$_2$ (**16**)	288, 461	639
[Ru(bpy)$_2$(**5b**)](PF$_6$)$_2$ (**13**)	287, 460	642
[Ru(bpy)$_3$](PF$_6$)$_2$ (**19**)	286, 452	611
[Ir(ppy)$_2$(**5a**)](PF$_6$) (**17**)	250, 315, 373, 466	624
[Ir(ppy)$_2$(**5b**)](PF$_6$) (**14**)	250, 314, 378, 468	640
[Ir(ppy)$_2$(bpy)](PF$_6$) (**20**)	258, 310, 379, 470	590

5.6 Complex Stability

After a period of six months the complex [Ru(bpy)$_2$(**5b**)](PF$_6$)$_2$ appears to undergo oxidation of the ferrocene moiety to ferrocenium. This is characterised by a broadening of the resonances for the substituted bpy ligand and absence of the signals for the Cp rings of the ferrocene due to the paramagnetic effects. The signals for the unsubstituted bpy ligand can still be seen however.

Sodium ascorbate and N-ethylmorpholine were used to effect reduction of the ferrocene back to Fe(II). Treatment with sodium ascorbate was not successful, however, treatment with N-ethylmorpholine in acetonitrile results in restoration of the ferrocene and the substituted bpy ligand signals (Figure 5.6).

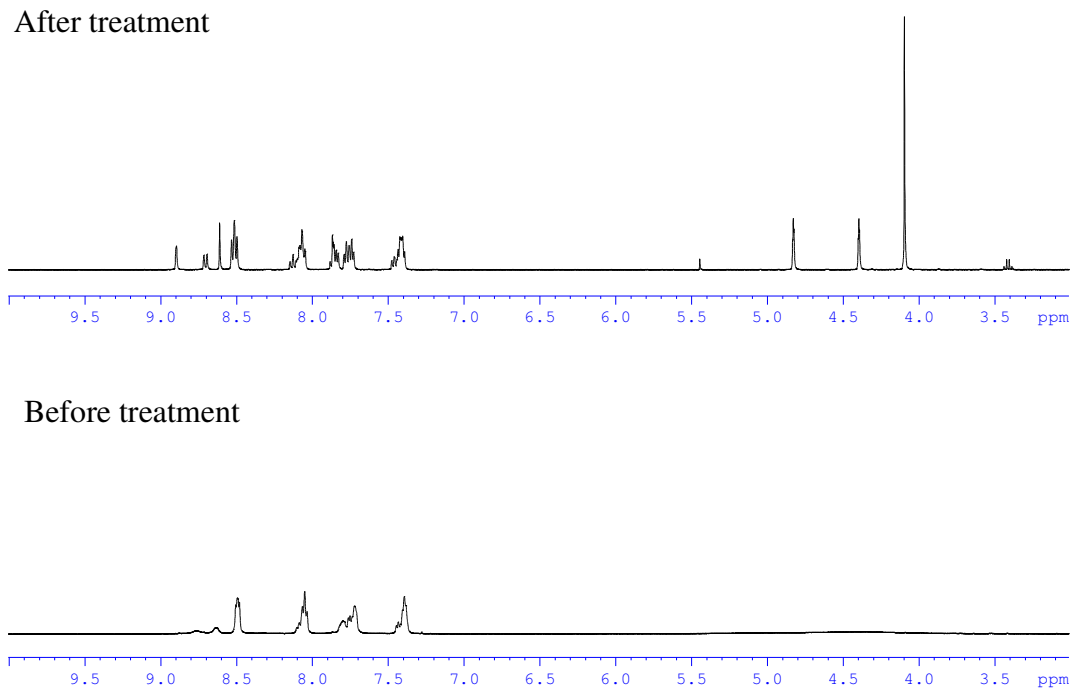

Figure 5.6 *^1H NMR spectra for $[Ru(bpy)_2(\mathbf{5b})]PF_6$ showing the aromatic region and the Cp ring region before and after treatment with N-ethylmorpholine.*

The same oxidation was observed for the iridium complex however the broadening of the peaks were less pronounced and the iridium complex was reduced and purified in the same way and all complexes were subsequently kept at -18 °C under nitrogen.

5.7 Cyclic Voltammetry Studies

Cyclic voltammetry was carried on 0.9-1.0 mM solutions of the complexes in acetonitrile using tetrabutylammonium tetrafluoroborate as the electrolyte and a silver/silver chloride reference electrode referenced to ferrocene/ferrocenium (0 V). Cyclic voltammetry experiments were carried out on the ligand and its complexes to probe their electrochemical properties. The redox data for all ligands and complexes are summarised in Table 5.2. Firstly the cyclic voltammogram of

commercially available ferrocene was obtained to optimise the equipment and provide a reference potential, after which 4-ferrocenyl-1-(2,2'-bipyrid-4-yl)-1,2,3-triazole (**5b**) was scanned using the same procedure. Figure 5.7 shows a comparative trace of ferrocene and ligand **5b**. Ligand **5b** exhibits a reversible oxidation curve at a potential of 0.074 V relative to Fc/Fc^+ E=0.0 V. The data suggests that the Fe d_{z^2} centred HOMO of ligand **5b** is slightly stabilised compared to that of ferrocene.

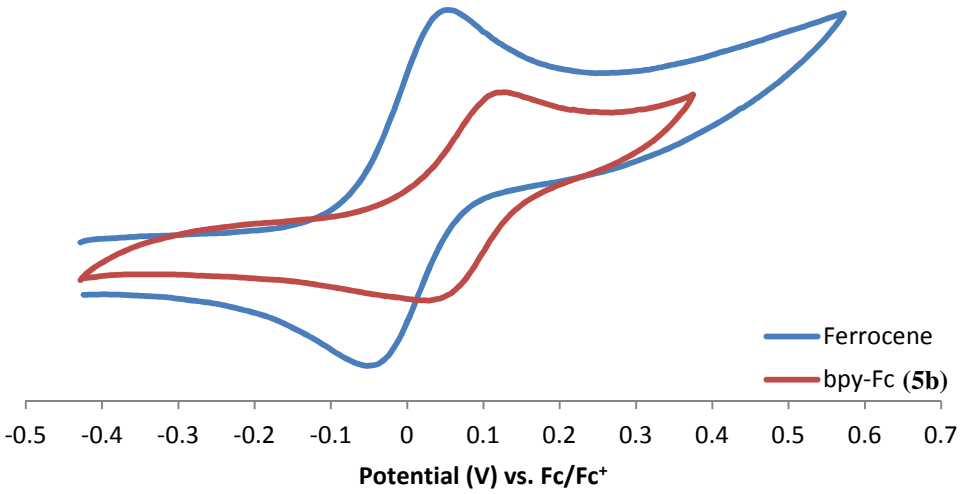

*Figure 5.7 Cyclic voltammogram traces of ferrocene and ligand **5b***

Upon determining the redox potential for the ferrocene substituted ligand **5b** in isolation the oxidation potential for the ruthenium complex $[Ru(bpy)_2(\mathbf{5a})](PF_6)_2$ (**16**) was determined. The cyclic voltammogram of complex **16** is shown in Figure 5.8 in which clearly defined reversible oxidation is observed at 0.9 V. Upon comparing the redox potentials of the ferrocene and ruthenium of the complexes it can be seen that the ferrocene moiety redox potential of $[Ru(bpy)_2(\mathbf{5b})](PF_6)_2$ appears at 0.14 V which is shifted by +0.066 V compared to that of the free

ligand. The redox potential for the ruthenium centre of complex $[Ru(bpy)_2(\mathbf{5b})](PF_6)_2$ (**13**) is shifted by +0.035 eV compared to those of $[Ru(bpy)_2(\mathbf{5a})](PF_6)_2$ (**16**). The redox wave for the ruthenium metal centre in complex **13** is not as well resolved as it is in complex **16**, and appears only partially reversible.

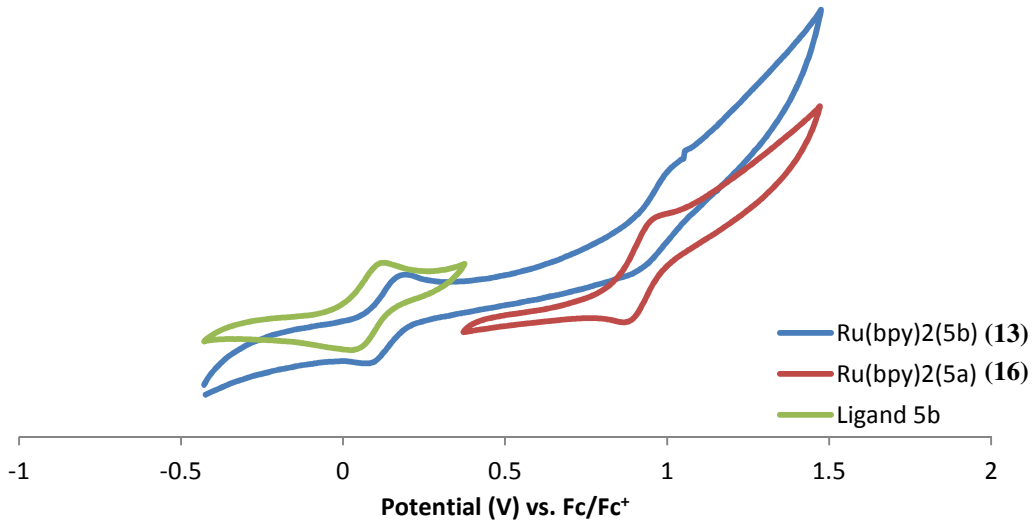

*Figure 5.8 Overlay of cyclic voltammogram traces of $[Ru(bpy)_2(\mathbf{5b})]PF_6$, $[Ru(bpy)_2(\mathbf{5a})]PF_6$ and ligand **5b**.*

Similar experiments were also carried out for the iridium and rhenium complexes. Figure 5.9 shows the overlay of the traces obtained for the iridium complexes **14** and **17**. $[Ir(ppy)_2(\mathbf{5a})]^+$ exhibits a partially reversible oxidation centred at 0.90 V. The ferrocenyl appended complex $[Ir(ppy)_2(\mathbf{5b})]^+$ shows a reversible Fc/Fc^+ oxidation potential at 0.095 V which is shifted to more positive potential when

compared to that of the free ligand as well as largely irreversible oxidation at 0.91 V.

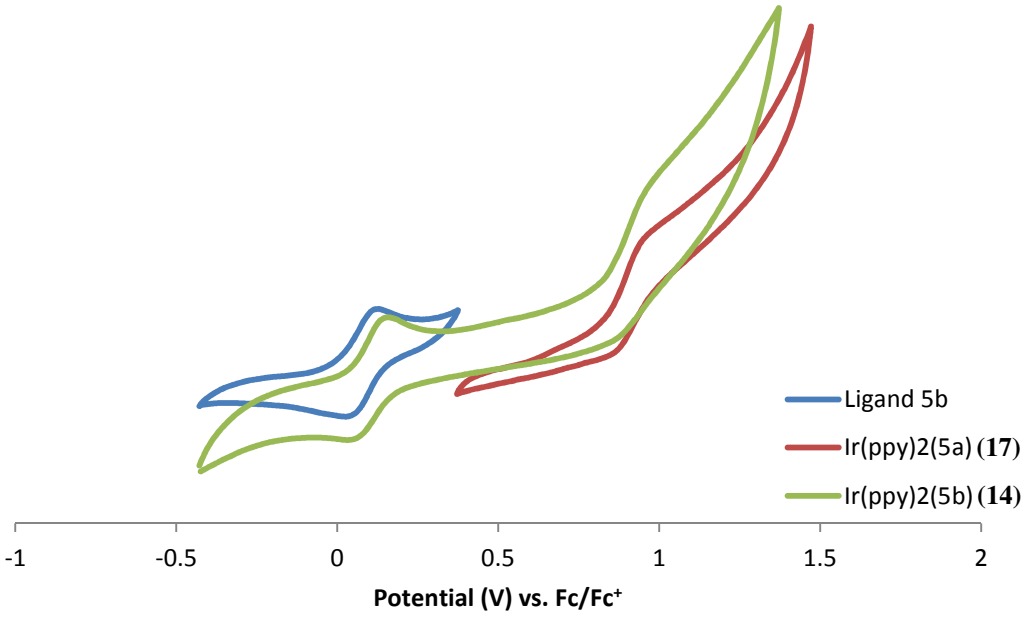

*Figure 5.9 Overlay of cyclic voltammogram traces of [Ir(ppy)$_2$(**5b**)]PF$_6$, [Ir(ppy)$_2$(**5a**)]PF$_6$ and ligand **5b**.*

The rhenium complex [Re(CO)$_3$(**5b**)Cl] exhibits a partially reversible Fc/Fc$^+$ oxidation potential at 0.18 V (Figure 5.10) which is again at a more positive potential when compared to that of the free ligand, however there is a greater separation of the oxidation and reduction potentials. The redox wave for the rhenium is not well defined for either of the complexes with possible irreversible oxidations appearing at 0.95 V and 1.06 V for the complexes [Re(CO)$_3$(**5b**)Cl] and [Re(CO)$_3$(**5a**)Cl] respectively. Studies on these complexes were hampered due to low solubility of the complexes which may have adversely affected the cyclic voltammetry measurements.

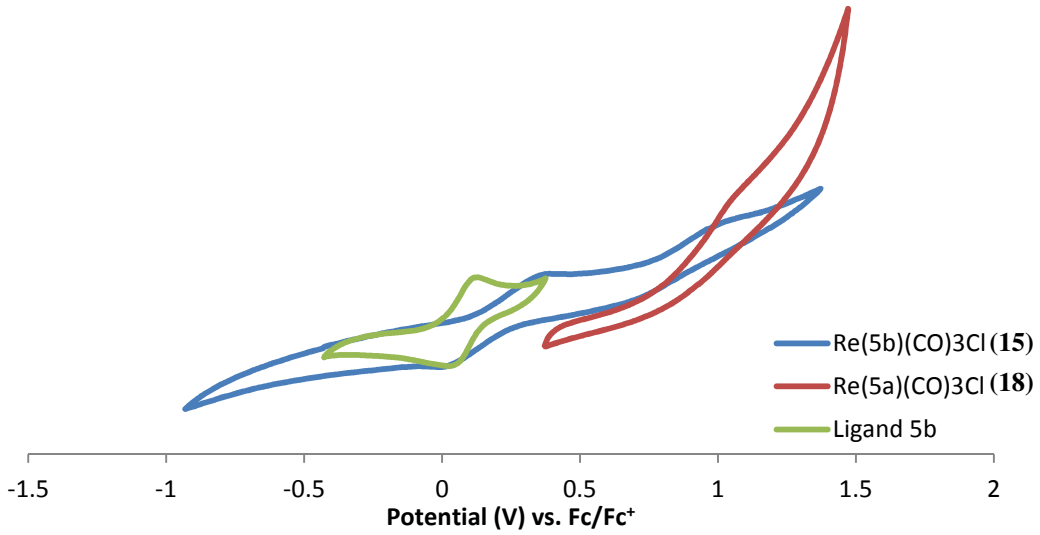

*Figure 5.10 Overlay of Cyclic voltammogram of [Re(CO)$_3$(**5b**)Cl], [Re(CO)$_3$(**5a**)Cl] and Ligand **5b**.*

*Table 5.2 Redox data for [Ru(bpy)$_2$(**5a**)](PF$_6$)$_2$, [Ru(bpy)$_2$(**5b**)](PF$_6$)$_2$, [Ru(bpy)$_3$](PF$_6$)$_2$ [Ir(ppy)$_2$(**5a**)](PF$_6$), [Ir(ppy)$_2$(**5b**)](PF$_6$), [Ir(ppy)$_2$(bpy)](PF$_6$), [Re(CO)$_3$(**5b**)Cl], [Re(CO)$_3$(**5a**)Cl] and Ligand **5b** ([a] Ferrocenyl redox potential, [b] ruthenium redox potential, [c] iridium redox potential and [d] rhenium redox potential)*

Complex	Redox Potential / eV vs. Fc/Fc^+
Ligand **5b**	0.074
[Ru(bpy)$_2$(**5b**)](PF$_6$)$_2$ (**13**)	0.14[a], 0.96[b]
[Ru(bpy)$_2$(**5a**)](PF$_6$)$_2$ (**16**)	0.93[b]
[Ir(ppy)$_2$(**5b**)](PF$_6$) (**14**)	0.095[a], 0.91[c]
[Ir(ppy)$_2$(**5a**)](PF$_6$) (**17**)	0.90[c]
[Re(CO)$_3$(**5b**)Cl] (**15**)	0.18[a], 0.95[d]
[Re(CO)$_3$(**5a**)Cl] (**18**)	1.06[d]

5.8 Luminescent Switching Studies

Electrochemical luminescence switching studies were carried out on the ferrocene appended metal complexes, in an attempt to turn on the emission through oxidation of the ferrocene moiety. Molina [199] had previously reported that such oxidative turning on of luminescent emission could be achieved in [Ru(bpy)$_2$] complexes of a ferrocene appended imidazophenanthroline ligand.

Initial work was carried out, using voltammetric methods for switching the oxidation state of the ferrocene. From the cyclic voltammetry experiments

discussed earlier, the oxidation potentials of the ferrocene and metal moieties had been determined. A potential was applied to a solution containing the Ru complex, more positive than that required for the oxidation of the ferrocene, but lower than that of the ruthenium redox couple. It was hoped that this would selectively oxidise the ferrocene moiety thereby switching on luminescent emission. Therefore a potential of 0.57 V with respect to Fc/Fc^+ was applied to a 1 mM solution of $[Ru(bpy)_2(\mathbf{5b})](PF_6)_2$ for 120 minutes and aliquots were taken out at regular intervals at which point the luminescent emission of the aliquot was recorded. The luminescent intensities of the samples did not differ from that of the original solution and could be due to the limitations of our cyclic voltammetry instrumentation.

Through our stability work we successfully showed that the use of a mild reducing agent could regenerate the ferrocene from ferrocenium. Therefore, if the complex could be reduced chemically, then the use of a mild chemical oxidising agent should oxidise the ferrocene and increase the luminescent intensity of the complex. Molina *et al.* [198] had shown that Cu(II) triflate could be used to increase the luminescent intensity of ferrocene containing ruthenium complexes and we therefore carried out a similar experiment. Figure 5.11 shows spectra before and after reaction with 1 equivalent of copper(II) trifluoromethanesulfonate for a solution of the $[Ru(bpy)_2(\mathbf{5b})](PF_6)_2$ in acetonitrile. As can be seen luminescence intensity increases by greater than 20 fold demonstrating electrochemical switch on of emission through chemical oxidation.

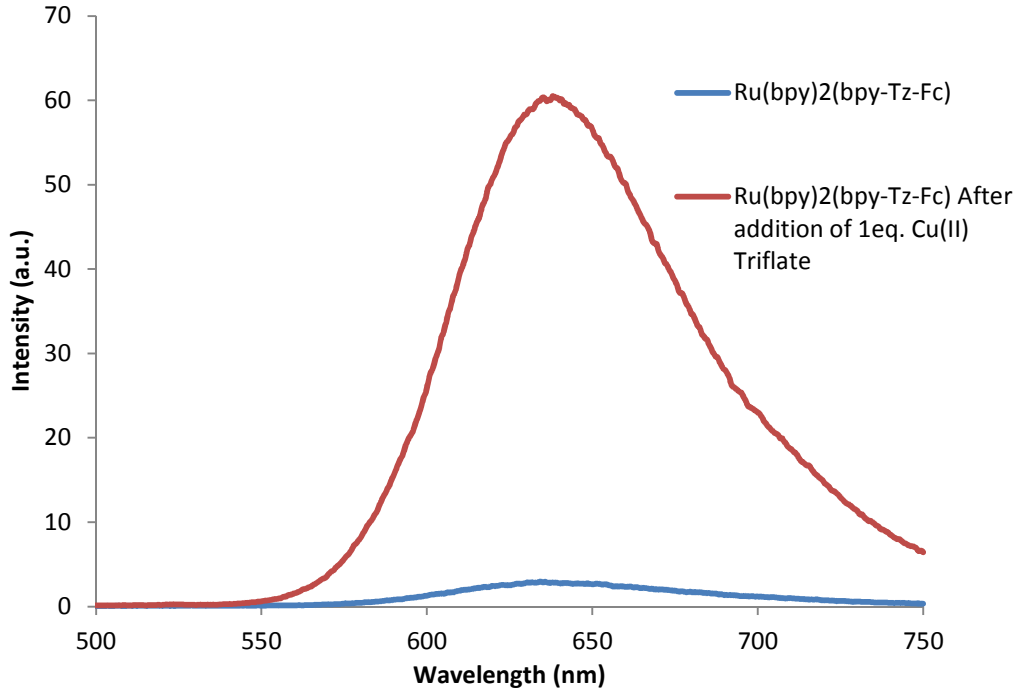

*Figure 5.11 Fluorescence intensity of [Ru(bpy)$_2$(**5b**)]PF$_6$ before and after the addition of 1 equivalent of copper(II)triflate.*

After this encouraging initial result the effect on luminescent intensity with respect to the amount of copper triflate was also investigated. Figure 5.12 shows the change in luminescence intensity with increasing copper triflate concentration. The data shows a general correlation with luminescence intensity to copper triflate added, however the results obtained did not show a linear relationship.

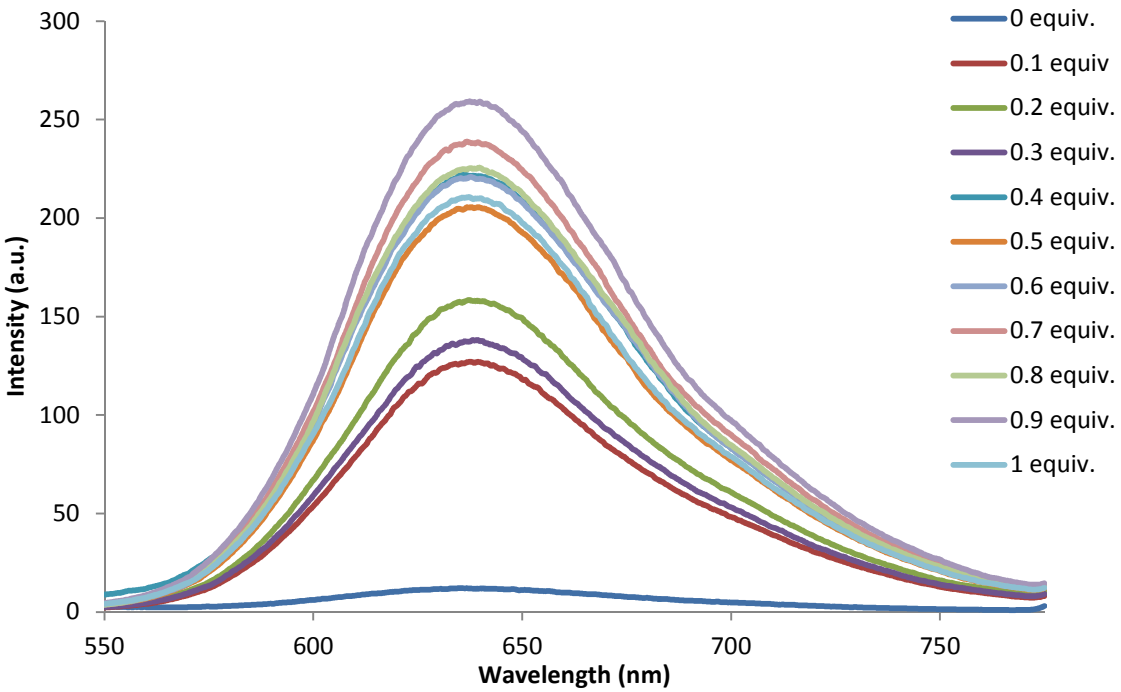

*Figure 5.12 Fluorescence intensity of [Ru(bpy)$_2$(**5b**)]PF$_6$ with respect to the amount of copper(II)triflate added.*

A solution of one equivalent of copper triflate and ruthenium complex was kept for a period of one week. The fluorescence intensity was recorded immediately upon addition of [Cu(OTf)$_2$], then after 24 hours and then again after 1 week. Figure 5.13 shows that the luminescent intensity of the ruthenium complex increases with time. We are uncertain why the oxidation appears slow but could be due to solubility, though no precipitation of [Cu(OTf)$_2$] was noticed.

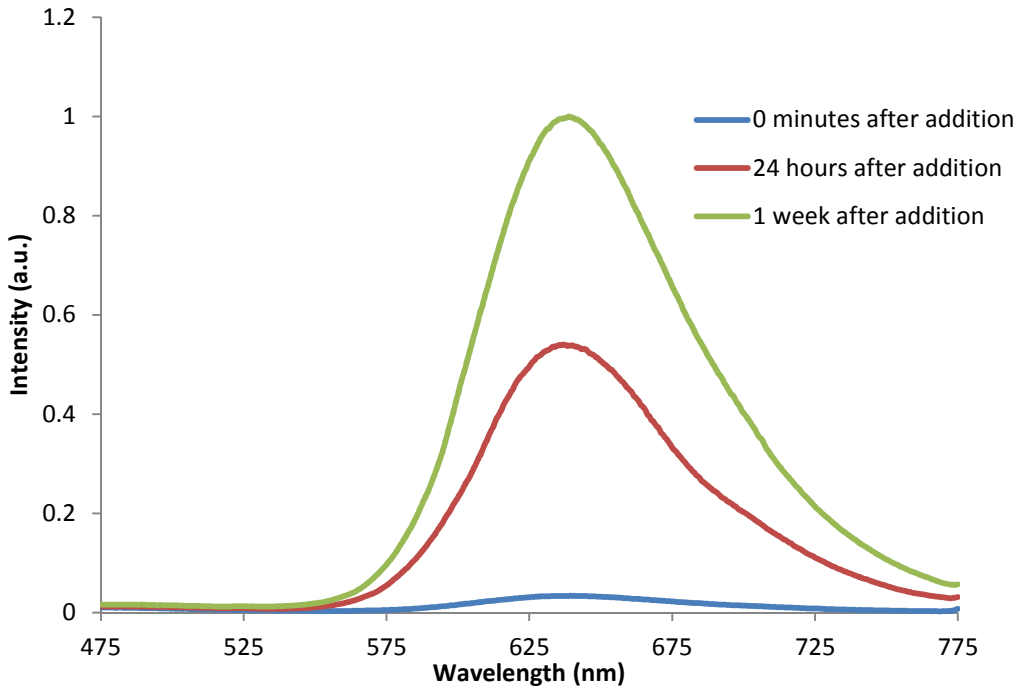

*Figure 5.13 Fluorescence intensity of [Ru(bpy)$_2$(**5b**)]PF$_6$ with 1 equivalent of copper(II)triflate added over time.*

Our investigation was extended and bromine was used as chemical oxidising agent in the hope that the reaction would be faster. Bromine was added to an acetonitrile solution of the complex [Ru(bpy)$_2$(**5b**)](PF$_6$)$_2$ in 0.1 equivalent aliquots. Figure 5.14 shows the luminescent intensity of the ruthenium complex with respect to the amount of bromine added. The data show that increase in Br$_2$ concentration yields increased luminescent intensity.

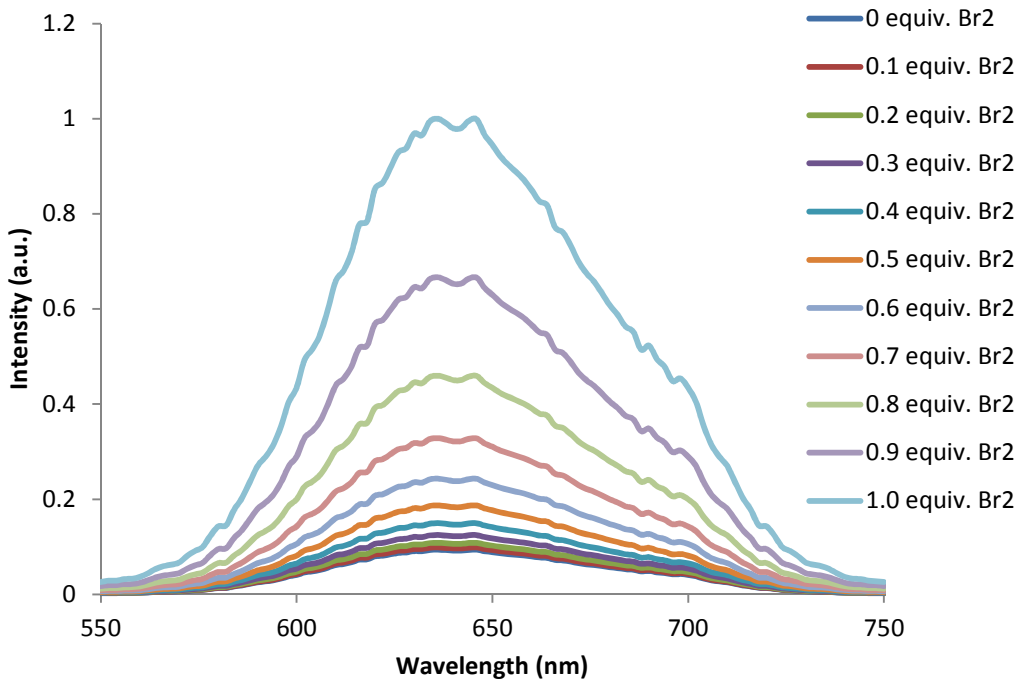

*Figure 5.14 Luminescence spectra of [Ru(bpy)$_2$(**5b**)]PF$_6$ with increasing bromine concentration.*

The bromine switching experiment was also carried out on the iridium complex **14** with similar results (Figure 5.15). Again the luminescence intensities of the complex increase with the amount of bromine added. Unfortunately due to the solubility of the rhenium complex **15** this switching experiment could not be carried out.

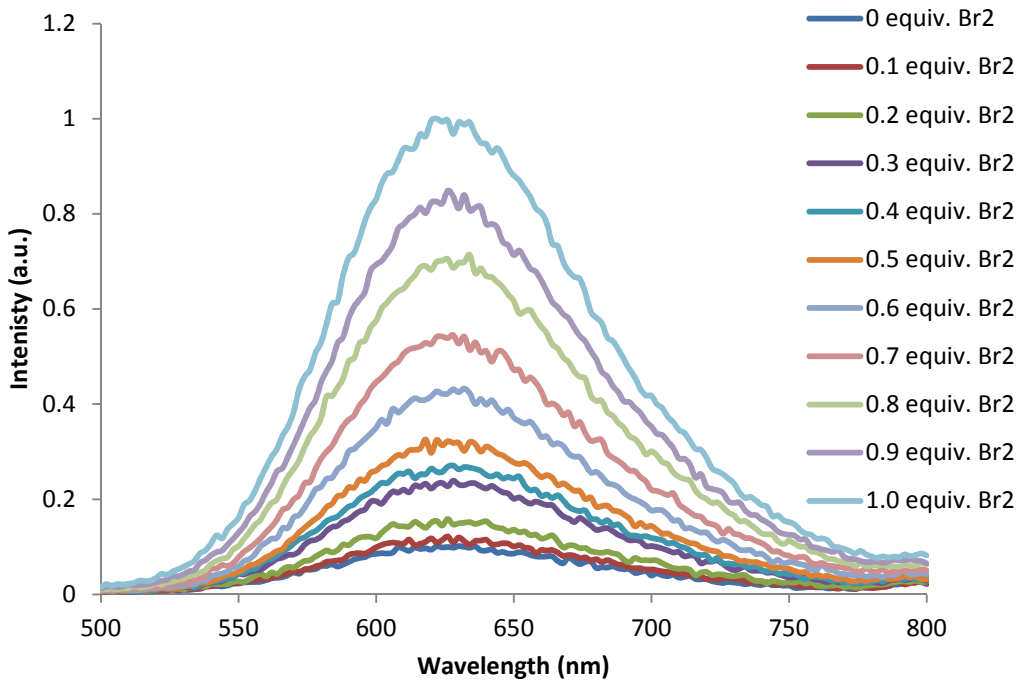

*Figure 5.15 Fluorescence intensity of [Ir(ppy)$_2$(**5b**)]PF$_6$ with respect to the amount of bromine added.*

5.9 Conclusion

In conclusion we have developed two potential luminescent switches with ferrocene tagged bipyridyl ligands containing a CuAAC derived triazole linker. The ferrocene moiety quenches the Ru/Ir based luminescent emission, presumably by electron transfer across the triazole bridge. The complexes undergo slow oxidation on standing in air therefore the complexes must be stored under nitrogen at -18 °C, however the complexes can be regenerated through N-ethylmorpholine. We have demonstrated that the luminescent emission can be switched on by oxidation of the Fc moiety to Fc^+.

The quenching of emission shows that there is good electronic communication across the triazole bridge in agreement with recently reported systems. Ruthenium and iridium conjugates with ferrocene linked by a triazole moiety have been shown to yield luminescent emission intensity that can be modulated by oxidation of the ferrocene. Unfortunately this oxidation and the switching on of luminescence is not terribly well controlled and this will be a focus of further work in this area.

6 TRIAZOLE BASED BRIDGING LIGANDS: PHOTOPHYSICS OF DINUCLEAR RU AND IR COMPLEXES

6.1 Introduction

Oligonuclear complexes involving polypyridyl ligand moieties have attracted a great deal of recent attention, largely due to their potential as the basis of novel functional materials.[200-202] In particular polymetallic assemblies based on ruthenium, iridium and rhenium have been widely studied due to their electrochemical, photochemical and photophysical properties.[203-206] For the majority of the complexes studied, the metal centres are linked by a ligand bridge, with the nature of the bridge having a fundamental influence on the electronic interaction between the metal centres and therefore on the characteristics of the material.[150, 207] A wide range of bridging ligands have been used in recent years. In most cases the bridging ligands contain pyridine-type coordinating units (particularly chelating sites like bpy) either directly connected or separated by a variety of spacers. Non-rigid bridging ligands have limitations, in terms of energy and electron transfer, as the geometry (metal-to-metal distance) of the system is not defined, therefore rigid spacers are much preferred.[204]

Jean-Pierre Sauvage has studied the electrochemical and photophysical properties of ruthenium(II) and osmium(II) bis(terpyridine) linked by a rigid spacer attached at their 4'-postion (Figure 6.1a). [208-210] Both homo- and heteronuclear complexes were prepared and it was found that the strong electronic interaction observed when the two metal ions are separated by the tpy-tpy bridge decreases upon introduction of one or two phenylene spacers but remains large enough to allow fast energy transfer. The same group have also prepared ruthenium and osmium complexes with biscyclometalating bridging ligands (Figure 6.1b). [210, 211]

In comparison with analogous complexes containing non-cyclometallating bridging ligands, where the MLCT excited states involved in the energy transfer step are localized in the bridge and very fast energy transfer takes place, energy transfer in the cyclometalated complexes is slower because the involved MLCT excited states are directed toward the terminal ligands.

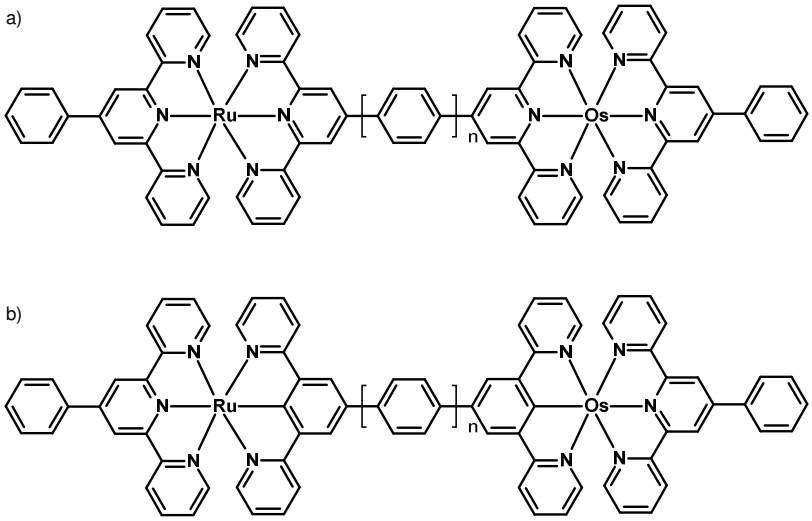

Figure 6.1 Ruthenium-osmium terpyridine bridged complexes.

Bipyridyl-based bridging ligands have also been prepared. The simplest of which are 2,3-bis(dipyridyl)pyrazine or 2,5-bis(dipyridyl)pyrazine (dpp). Very high nuclearity structures have been developed based on ruthenium(II) and osmium(II) centres connected by these ligands (Figure 6.2). [204, 212]

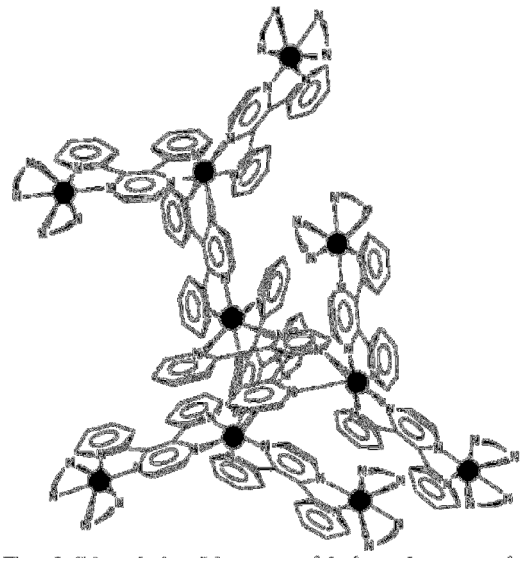

Figure 6.2 Decanuclear species bridged by 2,3-bis(dipyridyl)pyrazine .[212]

Ward and co-workers have also used the asymmetric bis(bipyridyl) bridging ligand 2,2':3',2'':6'',2'''-quaterpyridine ligand [213] and prepared mononuclear ruthenium complexes and heterodinuclear ruthenium-rhenium complexes (Figure 6.3). [214, 215] They found that that the pendant $[Re(CO)_3Cl]$ fragments exert an electron-withdrawing effect on the $[Ru(bpy)3]^{2+}$ core such that the Ru(II)/Ru(III) redox couple moves to more positive potentials as the number of pendant $[Re(CO)_3Cl]$ fragments increases. They also showed that Re-Ru energy transfer takes place with 100% efficiency in all cases. Ishitani and co-workers have shown that ruthenium–rhenium bridged complexes act as efficient photocatalysts for the reduction of CO_2. [169, 171, 216, 217]

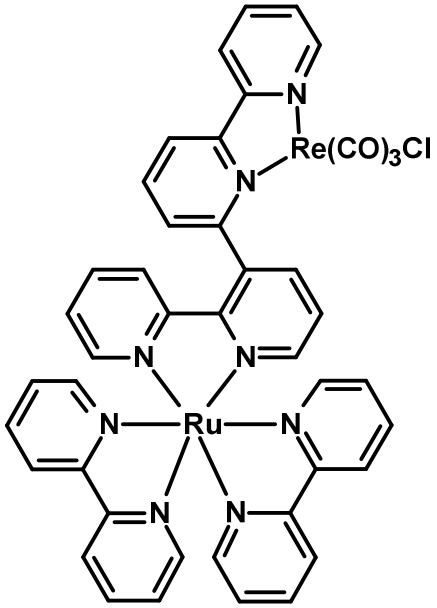

Figure 6.3 Ruthenium-rhenium complex bridged by 2,2':3',2'':6'',2'''-quaterpyridine ligand

Described in this chapter is the synthesis and characterisation of a range of ligands, incorporating the 1,2,3-triazole moiety, which have designed to act as bridging ligands for the construction of supramolecular assemblies. Also described in this chapter is synthesis, characterisation and photophysical study of ruthenium and iridium complexes utilising some of these ligands.

6.2 Ligand Synthesis

In order to explore the versatility of the CuAAC reaction for the preparation of novel bridging ligands for supramolecular architectures a number of new triazole containing oligotopic ligands were prepared and characterised and are described below.

The synthesis and characterisation of ligand **5c** has been discussed in a previous chapter, and was prepared from 4-azido-2,2-bipyridyl and 2-ethynlypyridine in the presence of copper(I) under standard click reaction conditions (Scheme 6.1). This resulted in the formation of a heteroditopic ligand with two potential metal binding domains; a bipyridyl moiety, and a second pyridyl-triazole domain.

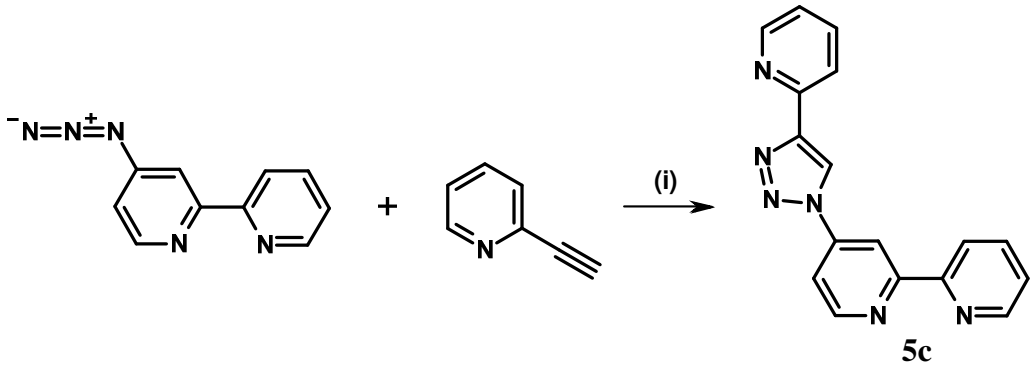

Scheme 6.1 Synthesis of 4-pyrid-2-yl-1-(2,2'-bipyrid-4-yl)-1,2,3-triazole ligand. (i) THF/H_2O, $CuSO_4$ and sodium ascorbate at room temperature.

The ether-bridged ditopic bidentate ligand, **21** (Scheme 6.2) was prepared through a similar procedure, starting from 4-azido-2,2-bipyridyl and half an equivalent of dipropargyl ether in the presence of copper sulfate and sodium ascorbate in a 1:1 mixture of THF and water. The bridging ligand has been reported in a previous

chapter however this was constructed from the ligated azido bpy ligands using the complex [Ru(*p*-cymene)(**4a**)Cl]$^+$.

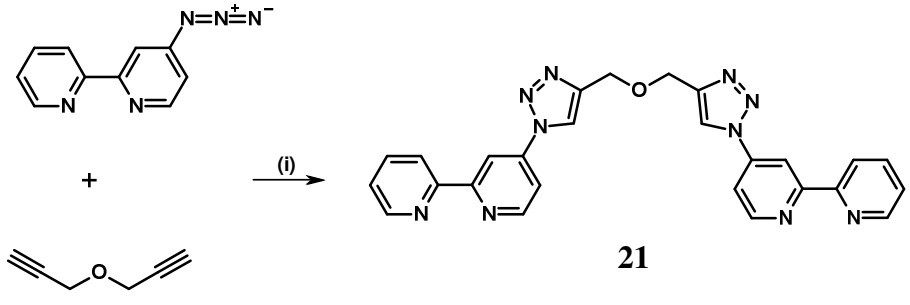

Scheme 6.2 Synthesis of di-([1-{2,2'-bipyrid-4-yl}-1,2,3-triazol-4-yl]methyl)ether ligand. (i) THF/H_2O, $CuSO_4$ and sodium ascorbate at room temperature.

Ligand **21** was fully characterised by ^{1}H and ^{13}C NMR spectroscopy, along with mass spectrometry. Due to the symmetry of this ligand, across the ether linkage, the ^{1}H NMR spectrum exhibits a total of nine resonances for the bpy, triazole and methylene protons. A diagnostic singlet signal for the triazole ring protons appears at δ 8.36. There are seven clearly defined signals within the aromatic region of the spectrum arising from the bipyridyl moieties, with the protons of the substituted pyridyl ring appearing at δ 8.83, 8.76 and 7.92 and resonances at δ 8.70, 8.48, 7.87 and 7.37 arising from the unsubstituted pyridyl rings. A single resonance at δ 4.92 which appears as a singlet is also observed and corresponds to the methylene protons from the ether bridge. Formation of the product was also confirmed by the absence of the azide stretch in the infrared spectrum, ESI-MS was also used to confirm the successful synthesis of the ligand and a sodium adduct is observed with m/z 511.2.

The synthesis of the ligands 1,4-bis-{4-(pyridi-2-yl)-1,2,3-triazol-1-yl}methylbenzene and 1,3,5-tris-{4-(pyridi-2-yl)-1,2,3-triazol-1-yl}methylbenzene (**22** and **23** respectively) were both prepared in a simple two-step/one-pot synthesis. Scheme 6.3 and Scheme 6.4 shows the CuAAC procedure starting from the corresponding halide and acetylene starting materials. The azides were prepared *in situ* from their corresponding bromomethyl-substituted benzene analogues by nucleophilic substitution with a slight excess of NaN_3 in dimethylsulfoxide at room temperature for 2 hours. Upon completion of the substitution reaction, 2-ethynylpyridine was added to the reaction vessel along with catalytic quantity of $CuSO_4$ and excess sodium ascorbate along with an equivalent of 2,6-lutidine per acetylene. The compounds **22** and **23** were purified by recrystallisation from dichloromethane and hexane and isolated in good yields.

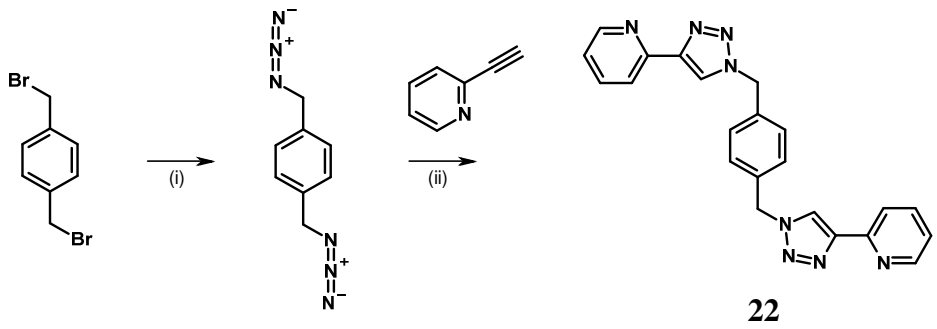

22

*Scheme 6.3 One-pot synthesis of 1,4-bis-({4-(pyrid-2-yl)-1,2,3-triazol-1-yl}methyl)benzene ligands (**22**) starting from corresponding halide. (i) dimethylsulfoxide and NaN_3 at room temperature; (ii) dimethylsulfoxide/H_2O, $CuSO_4$, sodium ascorbate and 2,6-lutidine at room temperature.*

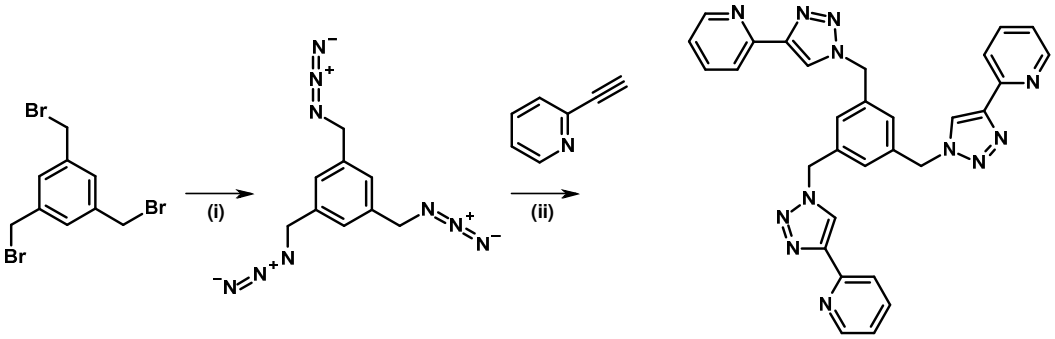

23

*Scheme 6.4 One-pot synthesis of 1,3,5-tris-({4-(pyrid-2-yl)-1,2,3-triazol-1-yl}methyl)benzene (**23**) ligands starting from corresponding halide. (i) dimethylsulfoxide and NaN_3 at room temperature; (ii) dimethylsulfoxide/H_2O, $CuSO_4$, sodium ascorbate and 2,6-lutidine at room temperature.*

Both polytypic ligands **22** and **23** where fully characterised ^{1}H and ^{13}C NMR spectroscopy. The symmetrical nature of the bis-triazole ligand **22** results in a simple set of resonances in the ^{1}H NMR spectrum. A characteristic singlet resonance arising from the triazole protons is observed at δ 8.07, and is clearly distinguishable as with other triazole signals as there is no coupling to any other protons evident in the COSY spectrum. Four signals for the pyridyl rings are also observed at δ 8.46, 8.10, 7.70 and 7.15 and a singlet at δ 7.37 arises from the four aromatic protons of the benzyl ring. A singlet at δ 5.60 is assigned to the methylene protons. These singlet resonances are assigned on the basis of NOESY data.

Similarly the tris triazole derivative **23** was also characterised by ^{1}H NMR spectroscopy and the diagnostic signal for the triazole protons is observed at δ 8.65. Four signals for the tethered pyridine units were also observed in the

aromatic region of the spectrum at δ 8.57, 8.00, 7.88 and 7.34. Finally a singlet at δ 7.36 was also observed corresponding to the three protons of the benzene ring whilst the resonances for the methylene protons appear at δ 5.68 and were assigned through the NOESY interaction with the benzene ring and triazole ring protons.

Both ligands were also characterised by ESI-MS, with the ditopic ligand (**22**) having a m/z peak at 417.2 and the tritopic ligand (**23**) having a m/z peak at 575.2 corresponding to their sodium adducts. Elemental composition was confirmed using high resolution mass spectrometry.

The intention was to use these ligands for metal complexation. However the pytz appended benzene ligands **22** and **23** appeared in the literature whilst we were carrying out this work [11] and we therefore decided to concentrate our efforts on the coordination chemistry and photophysical properties of ligand **5c** as we anticipated further publications appearing on these already published ligands.

We also felt that complexes of ligand **5c** would be more interesting, due to the fact that there is direct π-conjugation between the two coordinating domains and thus the potential for good metal to metal communication.

6.3 Synthesis and Characterisation of Dinuclear Ruthenium and Iridium Complexes

Bis-ruthenium and bis-iridium complexes utilising the heteroditopic ligand **5c** were prepared. The bis-ruthenium complex $[\{Ru(bpy)_2\}_2(\mathbf{5c})](PF_6)_4$ (**24**) was prepared by refluxing two equivalents of $[Ru(bpy)_2Cl_2]$ with ligand **5c** in ethanol under nitrogen atmosphere for 48 hours, after which time the mixture was passed through a column containing silica gel using MeCN/H_2O/sat. $KNO_{3\ (aq.)}$ (7:1:0.5) as a eluent (Scheme 6.5). A deep-red luminescent fraction was eluted and the product was crystallised as the hexafluorophosphate salt by adding excess $NaPF_6$.

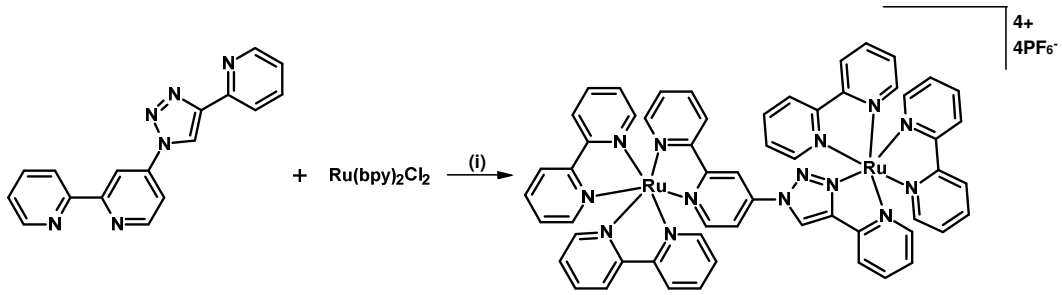

24

Scheme 6.5 Synthesis of $[\{Ru(bpy)_2\}_2(\mathbf{5c})](PF_6)_4$ (i) Ethanol at reflux under N_2 for 48 hours.

The bis-iridium complex $[\{Ir(ppy)_2\}_2(\mathbf{5c})](PF_6)_2$ (**25**) was prepared by reacting ligand **5c** with an equivalent of the dimer $[Ir(ppy)_2Cl]_2$ in the presence of $AgPF_6$ in dichloromethane under an inert atmosphere of nitrogen and exclusion of light (Scheme 6.6). Purification of the product was carried out in a similar manner to that for the bis-ruthenium complex and a yellow/orange luminescent fraction was eluted from the column. Isolation of the product was carried out by removing the

solvent by rotary evaporation, adding water and extracting the product into dichloromethane, and adding $NaPF_6$ in methanol. Further purification of both the homoleptic complexes was carried out through recrystallisation from acetonitrile and diethylether.

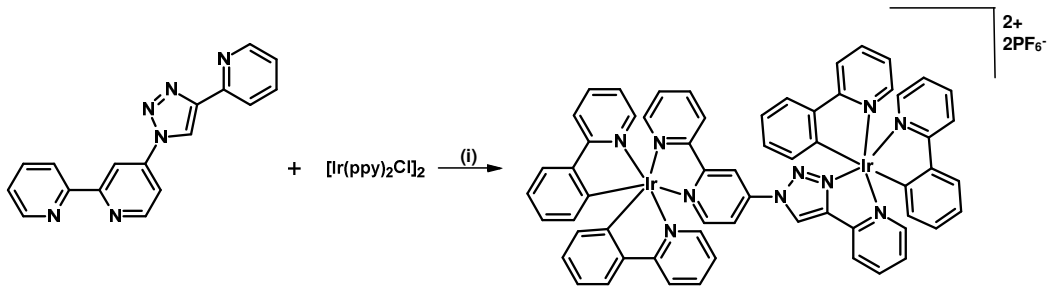

25

*Scheme 6.6 Synthesis of [{Ir(ppy)$_2$}$_2$(**5c**)](PF$_6$)$_2$ (i) AgPF$_6$ in DCM at reflux under N$_2$ with light exclusion.*

^{1}H NMR characterisation of the ditopic complexes is problematic due to the large number of aromatic resonances that are present which result in significant overlapping of signals. The asymmetery of the bridging ligand renders every proton magnetically unique. This is further complicated by the presence of two sets of signals corresponding to the two sets of meso- and rac- diastereoisomers due to the Δ and Λ stereochemistry at the coordinated metal centres (Figure 6.4). This is highlighted by the observation of two triazole signals in each of the complexes. The ruthenium complex **24** exhibits two triazole signals at δ 9.90 and 9.85 and similarly the iridium complex **25** exhibits two triazole signals at δ 9.84 and 9.72. Each complex has 13 signals arising from ligand **5c** as well as 32 bpy/ppy protons, each of which are magnetically unique, hence (13 + 32) × 2= 90 resonances, therefore making it difficult to fully characterise. However mass

spectrometry and high resolution mass spectrometry were used to confirm the identity of the complexes as well as their elemental composition, with complex **24** giving a molecular ion at m/z 282.1 for the 4+ species, $[\{Ru(bpy)_2\}_2(\mathbf{5c})]^{4+}$, and complex **25** giving a molecular ion at m/z 651.2 for the 2+ species, $[\{Ir(ppy)_2\}_2(\mathbf{5c})]^{2+}$.

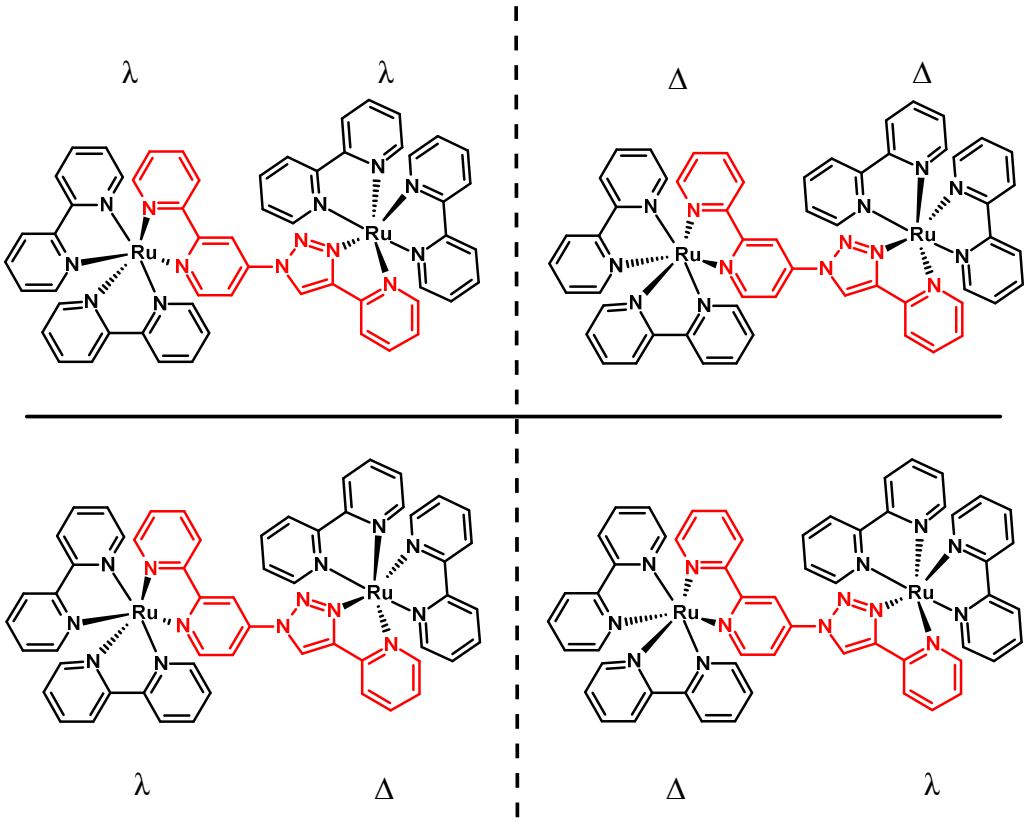

Figure 6.4 Diastereoisomers of $[\{Ru(bpy)_2\}_2(\mathbf{5c})].4\,PF_6$ *(**24**)*

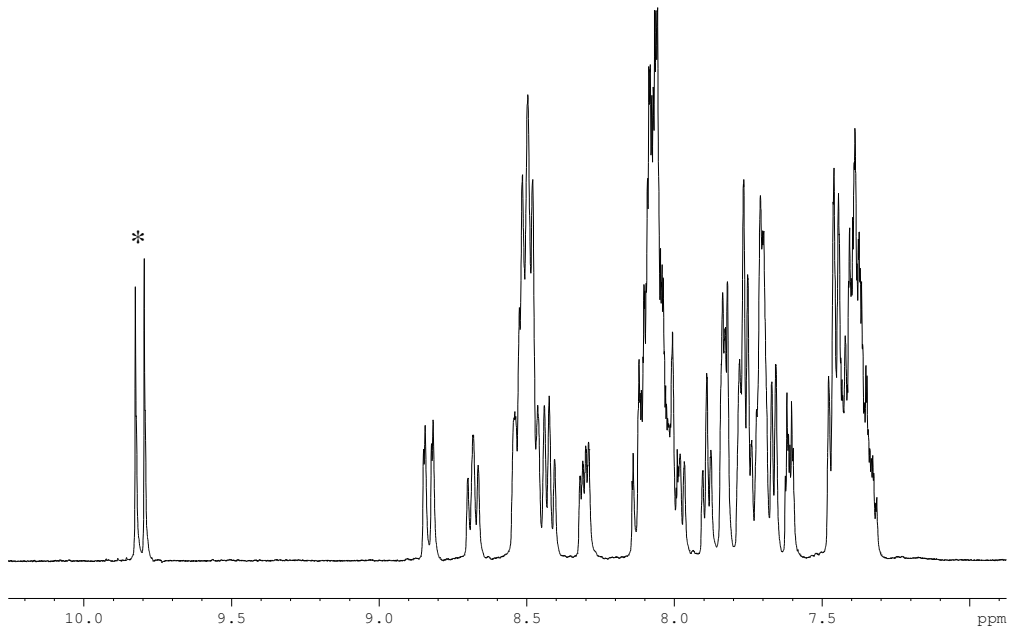

Figure 6.5 ^{1}H *NMR spectrum for* $[\{Ru(bpy)_2\}_2(\mathbf{5c})](PF_6)_4$ *(* triazole resonance)*

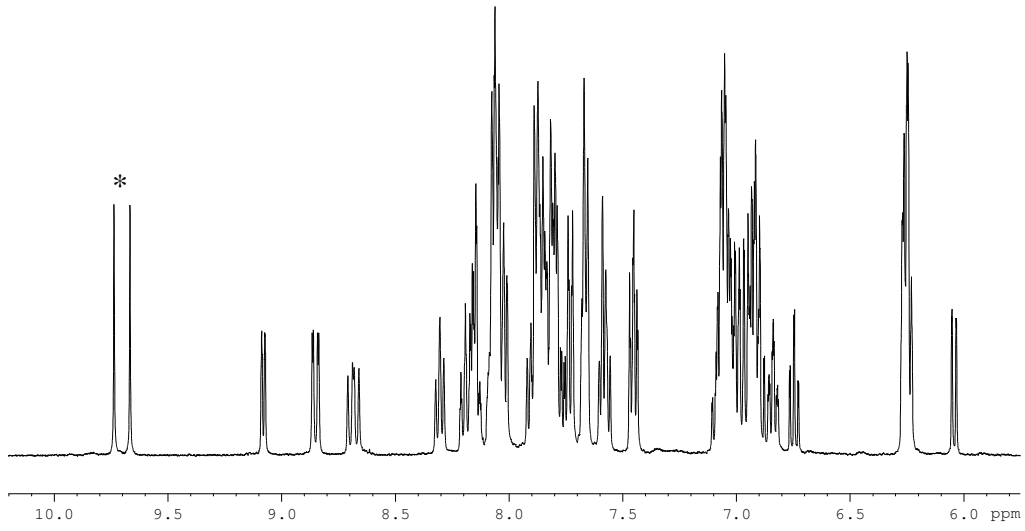

Figure 6.6 ^{1}H *NMR spectrum for* $[\{Ir(ppy)_2\}_2(\mathbf{5c})](PF_6)_2$ *(* triazole resonance)*

To aid with the photophysical studies of these dinuclear species, mono nuclear model analogues of the bipyridyl and the pyridyl-triazole domains of the dinuclear complexes were prepared. To model the bipyridyl domain the $Ru(bpy)_2$ and $Ir(ppy)_2$ complexes of ligand **5a** were used (Figure 6.7). The synthesis and characterisation of the these complexes have been discussed in the previous chapter. To model the pyridyl-triazole domain the $Ru(bpy)_2$ and $Ir(ppy)_2$ complexes of the 1-benzyl-4-pyrid-2-yl triazole ligand (**10**) were prepared.

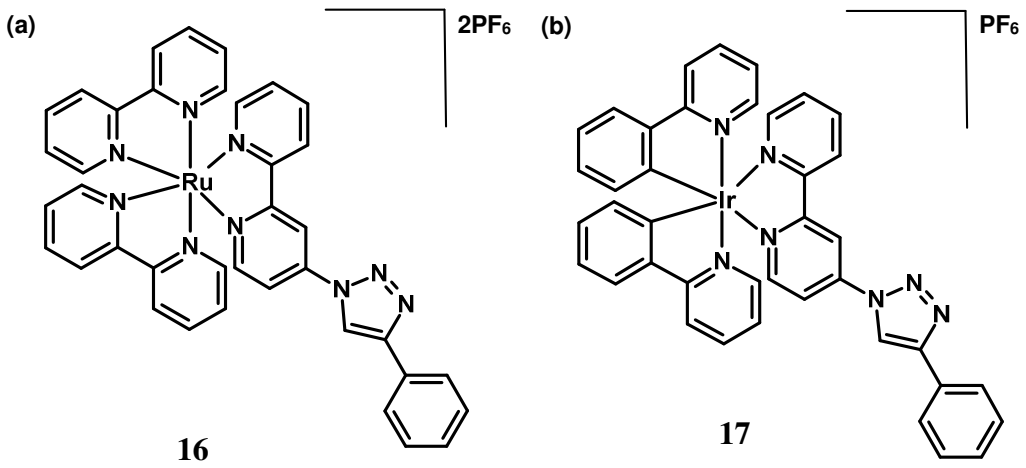

*Figure 6.7 Mononuclear species to model the bipyridyl domain of the bimetallic species (a) [Ru(bpy)$_2$(**5a**)](PF$_6$)$_2$ and (b) [Ir(ppy)$_2$(**5a**)](PF$_6$).*

During the course of this work the $Ru(bpy)_2$ and $Ir(ppy)_2$ complexes of ligand **10** have also been independently prepared and characterised by the groups of Schubert [10, 99] and De Cola. [98, 101, 102, 124] The synthesis of [Ru(bpy)$_2$(**10**)](PF$_6$)$_2$ (**26**) was carried out by refluxing [Ru(bpy)$_2$Cl$_2$] with **10** in ethanol under an atmosphere of nitrogen for 4 hours. The resultant solution of the complex was

passed through a column containing silica gel using MeCN/H_2O/sat. $KNO_{3\ (aq.)}$ (7:1:0.5) as the eluent. A deep-red fraction was eluted and the product was crystallised by addition of excess $NaPF_6$ in methanol (Scheme 6.7).

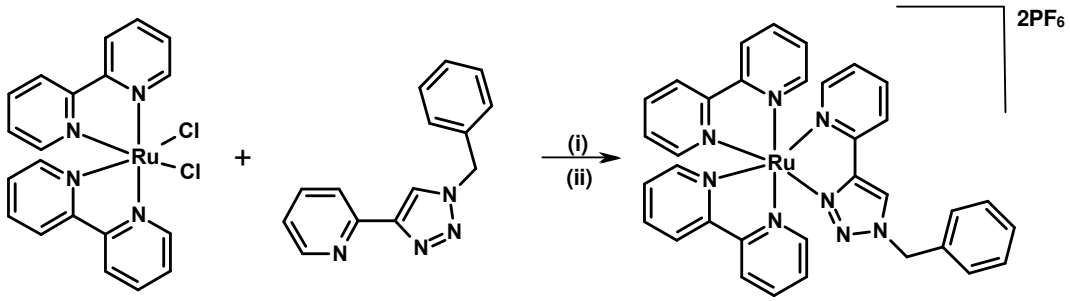

26

*Scheme 6.7 Synthesis of [Ru(bpy)$_2$(**10**)](PF$_6$)$_2$ (i) Ethanol at reflux under N_2 for 4 hours.(ii) $NaPF_6$, MeOH*

Complex **26** was characterised by ^{1}H NMR spectroscopy. The complex exhibits a diagnostic signal for a triazole proton which appears as a singlet at δ 8.63. The remaining protons of the pytz ligand can be assigned through nOe interactions with the triazole proton and resultant COSY connections. Due to the asymmetry of the pytz ligand, this renders the remaining 16 protons of the bpy ligands as unique this making the full NMR assignment difficult due to the significant overlap. The resonance at δ 5.54, with integration equivalent to two protons, arises from the methyl protons adjacent to the benzyl ring and appears as a geminal AB doublet of doublets with roofing. This is due to the chirallity of the ruthenium centre therefore producing two diasetereoisomers, could also be due to the hindered rotation of the benzyl substituent and the C_2 symmetry of the

$[Ru(bpy)_2]$ fragment which thus renders these protons diastereotopic. Confirmation of the identity of the ruthenium complex was carried out using MS and HRMS which showed a peak at 325.1 m/z and 795.1 m/z for the ion $[Ru(bpy)_2(\mathbf{10})]^{2+}$ and the ion pair $\{[Ru(bpy)_2(\mathbf{10})]PF_6\}^+$ respectively. In addition the correct ruthenium isotope pattern was observed for each of these signals.

$[Ir(ppy)_2(\mathbf{10})](PF_6)$ (**27**) was prepared from the corresponding $[Ir(ppy)_2Cl]_2$ dimer, by stirring it with $AgPF_6$ in MeCN for 2 hours at room temperature with the exclusion of light after which the solution was passed through celite to remove AgCl. This was then stirred with an equivalent of ligand **10** per iridium in MeCN for a further 24 hours. Purification of the complex was carried out by column chromatography and recrystallisation (Scheme 6.8).

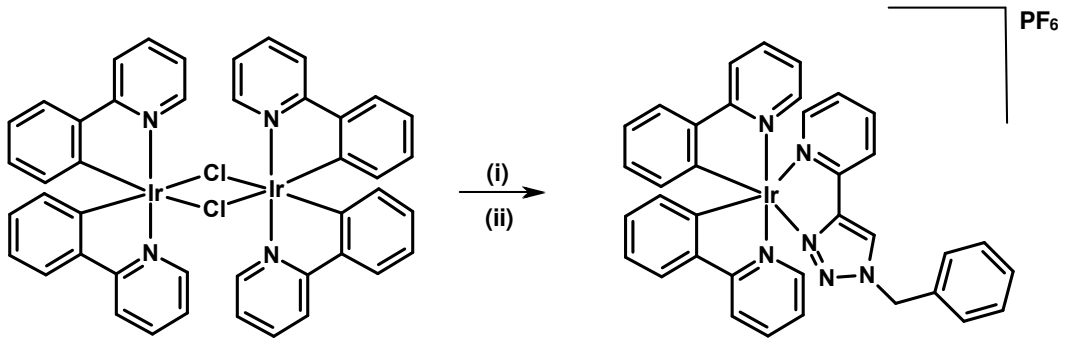

27

Scheme 6.8 Synthesis of $[Ir(ppy)_2(\mathbf{10})](PF_6)$ (i) $AgPF_6$ in MeCN for 24 hours (ii) ligand 10 in MeCN

As with complex **26**, the iridium complex **27** exhibits a signal in the ^1H NMR spectrum at δ 8.63 for the triazole proton. The methylene signal is observed at δ 5.61 and exhibits the same geminal AB doublet of doublets with roofing. Mass

spectrometry was used to confirm the preparation of the product and a peak was observed at m/z 737.2 for the cation $[Ir(ppy)_2(\mathbf{10})]^+$.

6.3.1 Cyclic Voltammetry Studies

Cyclic voltammetry experiments were carried out on the ruthenium family of complexes in order to characterise their electrochemical properties. Figure 6.8 shows an overlay of the cyclic voltammograms for the three ruthenium complexes in this series (**16**, **24** and **26**) and Table 6.1 contains the observed oxidation potentials for comparison.

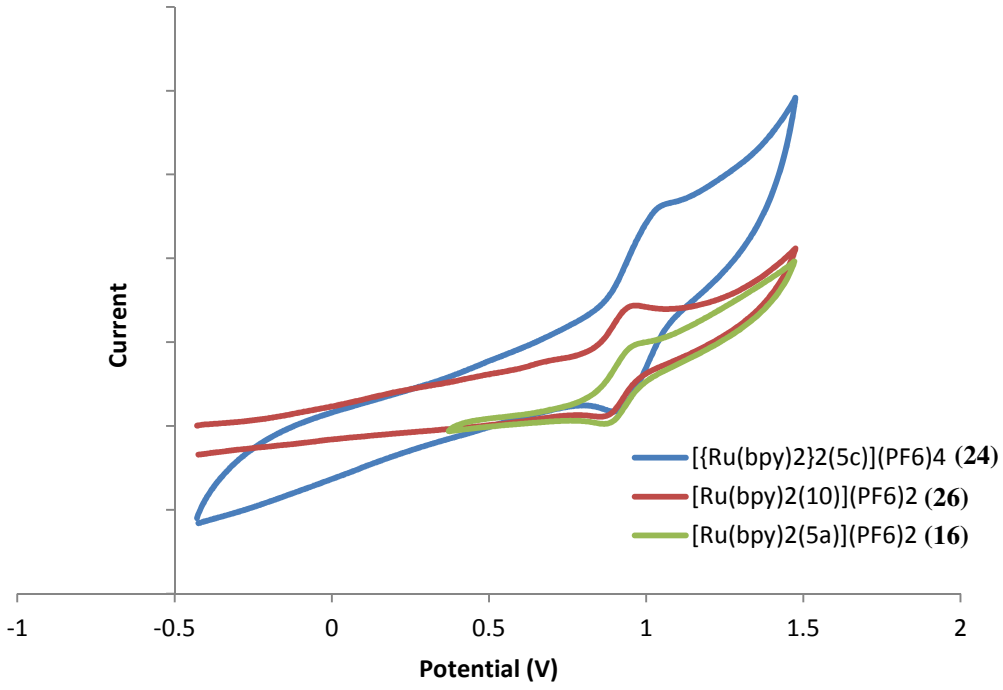

Figure 6.8 Overlay of cyclic voltammograms for $[\{Ru(bpy)_2\}_2(\mathbf{5c})][PF_6]_4$, $[Ru(bpy)_2(\mathbf{5a})][PF_6]_2$ *and* $[Ru(bpy)_2(\mathbf{10})][PF_6]_2$

The data show that the oxidation and reduction potentials of the two mononuclear ruthenium complexes are approximately coincident. This is not unexpected as the HOMO in these complexes is expected to be Ru d_{z^2} in character with little involvement of ligand centred orbitals. The oxidation peak potential for the mononuclear species **16** and **26** occurs at 0.94 V and the reduction peak potential of the oxidised complex is 0.84 V. The cyclic voltammogram for the dinuclear ruthenium complex **24** where the ruthenium is coordinated in both domains again shows a similar shape, with only 1 oxidation peak potential and 1 reduction peak potential of the oxidised complex, with the oxidation peak potential at 1.03 V and the reduction peak potential of this oxidised complex at 0.93 V. This indicates that both the ruthenium centres present are oxidised and reduced simultaneously and do not form an intermediate mixed valence Ru(II)/Ru(III) species. We had hoped to observe two redox waves indicative of the formation of a mixed valence Ru(II)/Ru(III) complex as an intermediate for which we might have expected to see near infrared (NIR) intervalence charge transfer transition.

*Table 6.1 Redox data for [{Ru(bpy)$_2$}$_2$(**5c**)](PF$_6$)$_4$, [Ru(bpy)$_2$(**5a**)] (PF$_6$)$_2$ and [Ru(bpy)$_2$(**10**)] (PF$_6$)$_2$*

Complex	Redox Potential / eV
[{Ru(bpy)$_2$}$_2$(**5c**)](PF$_6$)$_4$(**24**)	0.95
[Ru(bpy)$_2$(**5a**)](PF$_6$)$_2$ (**16**)	0.89
[Ru(bpy)$_2$(**10**)] (PF$_6$)$_2$ (**26**)	0.89

6.3.2 Photophysical Studies

UV-visible absorption spectra of all three ruthenium complexes **16**, **24** and **26** were recorded in acetonitrile (Figure 6.9). For these complexes the dominant absorption bands in the lower region at 250-270nm we assigned as intraligand π → π* transitions. These assignments were made on comparison to closely related metal complexes in the literature. [10, 99, 218] The low energy broad bands in the near UV region approximately 400-500 nm are attributed to the metal to ligand charge-transfer (MLCT) dπ(Ru) → π* (N-N) transitions. The MLCT band of complex **26** is blue-shifted with respect to that of the substituted tris bpy complex **16**. This is expected as replacing the bpy ligand with a ligand with a smaller π system will destabilise the LUMO of the complex relative to the HOMO and thus increase the energy of the ^{1}MLCT state relative to the ground state. The MLCT band of dinuclear complex **24** also appears slightly broadened relative to **26** as there is contribution from both metal centres in bpy and pytz domains. **.**

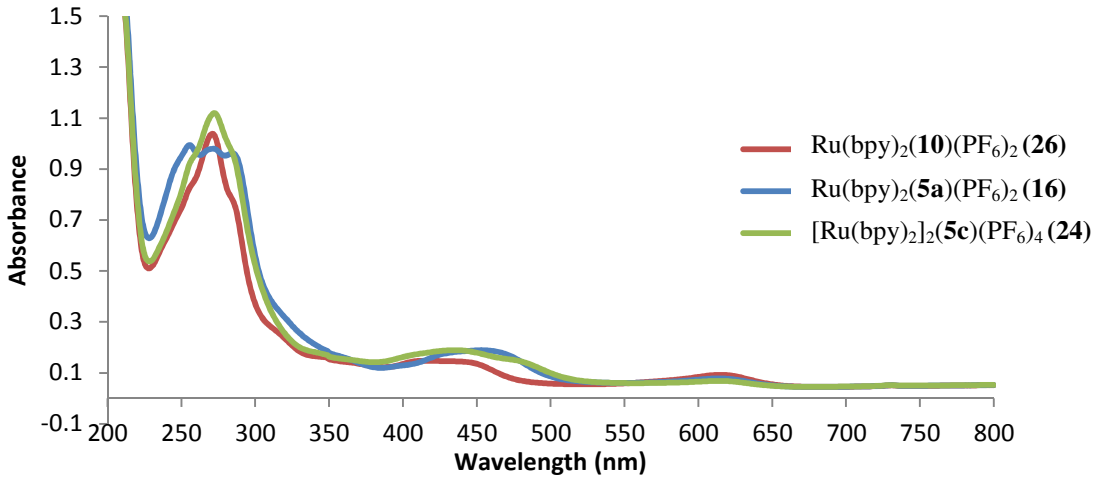

*Figure 6.9 UV-vis absorption spectra for [{Ru(bpy)$_2$}$_2$(**5c**)](PF$_6$)$_4$ (**24**), [Ru(bpy)$_2$(**5a**)] (PF$_6$)$_2$ (**16**) and [Ru(bpy)$_2$(**10**)] (PF$_6$)$_2$ (**26**)*

UV-visible absorption spectra of the iridium complexes were also recorded in acetonitrile. The absorption spectra of complexes, **17, 25** and **27** are presented in Figure 6.10. The compounds show absorption features similar to those reported for other $Ir(ppy)_2$ complexes with typical strong $\pi \rightarrow \pi^*$ transitions in the UV region localized on the ppy and the bpy ligands at approximately 250-300 nm and weaker metal-to-ligand charge transfer bands at lower energies between 350 and 430 nm.

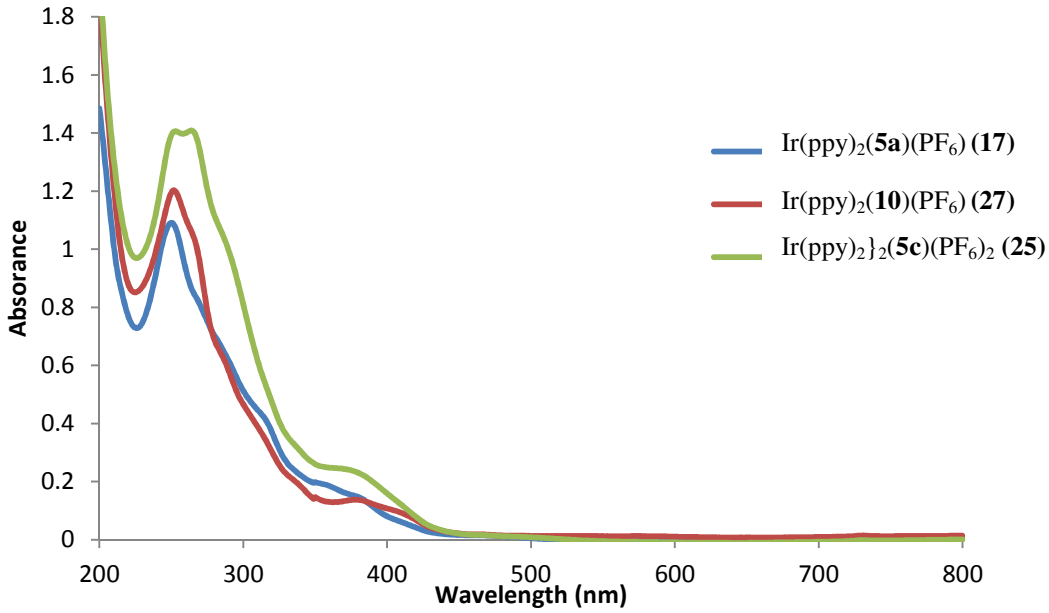

*Figure 6.10 UV-vis absorption spectra for [{Ir(ppy)$_2$}$_2$(**5c**)](PF$_6$)$_2$ (**25**), [Ir(ppy)$_2$(**5a**)] (PF$_6$) (**17**) and [Ir(ppy)$_2$(**10**)] (PF$_6$) (**27**)*

Luminescence measurements were recorded at room temperature in aerated acetonitrile and recorded with an excitation wavelength of 400 nm. Figure 6.11 shows the emission spectra for the three ruthenium complexes **16**, **24** and **26**. The emission for complex **16,** displays an intense broad and unstructured emission band at 639 nm that is assigned as arising from a ^{3}MLCT state. This is red-shifted

when compared to that of $[Ru(bpy)_3]^{2+}$ (611 nm) due to the extended π-system of the phenyl triazole substituted bpy ligand. That lowers the LUMO and hence stabalises the ^{3}MLCT state. The emission band for complex **26** is blue shifted compared to $[Ru(bpy)_3]^{2+}$ in a similar manner to the shift observed for the MLCT absorption and appears at 612 nm. The emission for complex **26** is highly quenched which is an agreement with observations of Schubert, and is likely due to the raised ^{3}MLCT state becoming closer to ^{3}MC therefore enabling more efficient thermal population of the latter and non radiative deactivation to the ground state. [10, 99] The dinuclear complex **24** displays an intense emission band at 653 nm which is red-shifted relative to the phenyl-triazole substituted bpy complex **16**. This could be due to the fact that coordination of the ruthenium to the pytz domain makes the pyridine and triazole rings coplanar which may not be the case for the phenyl-triazole substituted complex **16**. Coordination to the pytz domain make it more electron withdrawing hence lowering the LUMO of the bpy fragment. Also, the steric demands of the $[Ru(bpy)_2]$ moieties are likely to force planarity of the bridging ligand also extending the π-system thus lowering the LUMO. The dinuclear complex **24**, showed greater than 100% enhancement in luminescent intensity when compared to emission for **26**, We assign this as being due to photoinduced energy transfer (PEnT) from the pytz coordinated ruthenium centre with emission from the bpy domain coordinated ruthenium centre.. Hence, whilst the $[Ru(bpy)_2(pytz)]$ fragment is not particularly emissive it acts as a sensitising chromophore for the emission from the $[Ru(bpy)_3]$ domain. However, quenching due to singlet O_2 can not be entirely ruled out as the samples were recored in aerated solvents.

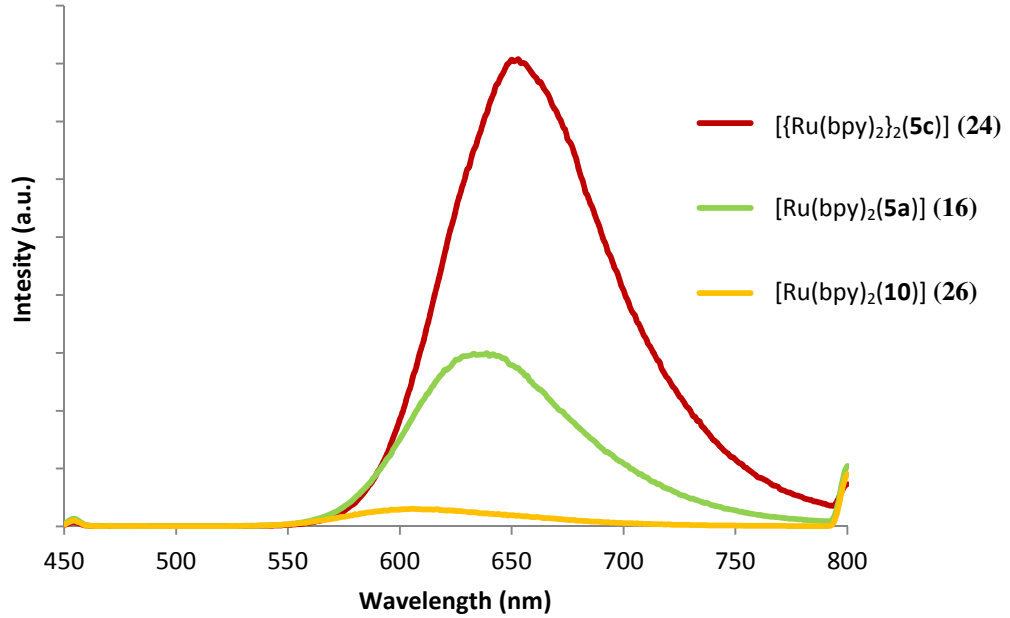

*Figure 6.11 Luminescence spectra for [{Ru(bpy)$_2$}$_2$(**5c**)](PF$_6$)$_4$, [Ru(bpy)$_2$(**5a**)] (PF$_6$)$_2$ and [Ru(bpy)$_2$(**10**)] (PF$_6$)$_2$*

Figure 6.12 shows the emission spectra for the three iridium complexes **17**, **25** and **27**. The emission band for complex **17** is red-shifted relative to that of the complex [Ir(ppy)$_2$(bpy)]$^+$ (590 nm) and appears at 624 nm which is similar to the observation observed for the related ruthenium complex **16** and assigned as emission from a ^{3}MLCT/^{3}LLCT state centred on the bpy ligand. For the pytz iridium complex **27** an intense structured emission band with vibronic progressions at 472 and 510 nm is observed, as observed by De Cola *et al* [98, 100, 124]. This is indicative of a significant amount of ^{3}LC character in the emission state which is ppy ligand centred. The emission is intense in comparison to the ruthenium complex **26** as 5d metals have larger ligand field splitting and therefore higher lying ^{3}MC states that minimise thermal deactivation of emission. Also, the

cyclometalled ligand is a strong anionic C-donor ligand which similarly destabilises the ^{3}MC state making it less thermally accessible. Overall, this results in minimal quenching of emission when compared to that of the ruthenium complex **26**. In a similar fashion to the emission of the dinuclear ruthenium complex **24**, the dinuclear iridium complex **25** shows enhanced and red-shifted emission due to the same reasons as stated for **24**. Emission from the iridium in the pytz domain is actively quenched and emission occurs from an excited state localised on the bridging ligand possibly indicating PEnT-based sensitisation. Photophysical data for all complexes is summarised in Table 6.2.

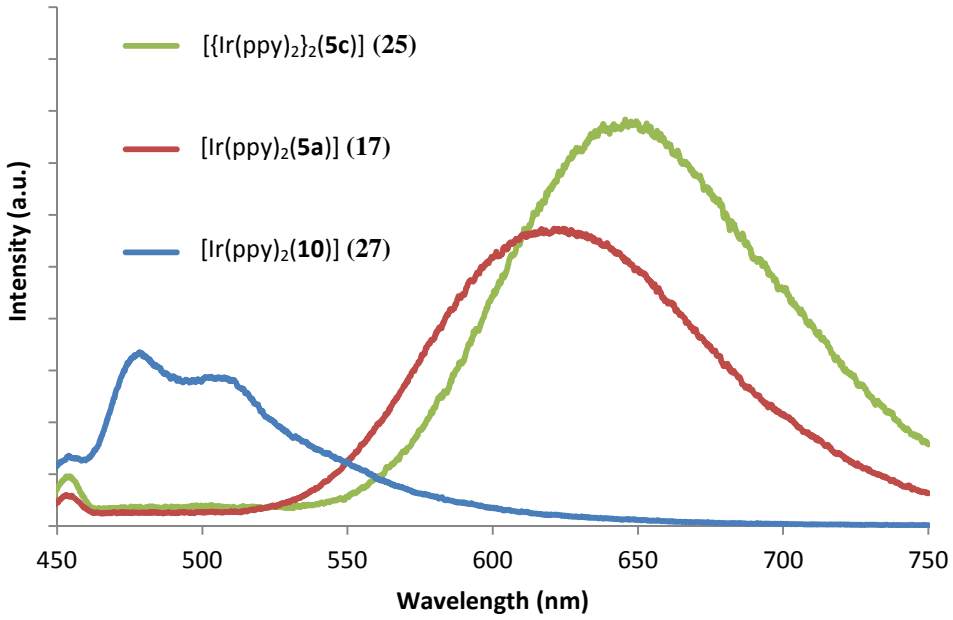

*Figure 6.12 Luminescence spectra for [{Ir(ppy)$_2$}$_2$(**5c**)](PF$_6$), [Ir(ppy)$_2$(**5a**)](PF$_6$) and [Ir(ppy)$_2$(**10**)](PF$_6$)*

*Table 6.2 UV-vis absorption and luminescence data for [{Ru(bpy)$_2$}$_2$(**5c**)](PF$_6$)$_4$, [Ru(bpy)$_2$(**5a**)](PF$_6$)$_2$, [Ru(bpy)$_2$(**10**)](PF$_6$)$_2$, [{Ir(ppy)$_2$}$_2$(**5c**)](PF$_6$)$_2$, [Ir(ppy)$_2$(**5a**)](PF$_6$) and [Ir(ppy)$_2$(**10**)](PF$_6$)*

Complex	**λ^{abs} / nm**	**λ_{max}^{em} / nm**	**τ (ns)**
[Ru(bpy)$_2$(**5a**)](PF$_6$)$_2$ (**16**)	288, 461	639	229.3
[Ru(bpy)$_2$(**10**)](PF$_6$)$_2$ (**26**)	287, 460	612	7.36
[{Ru(bpy)$_2$}$_2$(**5c**)](PF$_6$)$_4$ (**24**)	288, 459	653	260.6
[Ir(ppy)$_2$(**5a**)](PF$_6$) (**17**)	250, 315, 373, 466	624	
[Ir(ppy)$_2$(**10**)](PF$_6$) (**27**)	253, 310, 389, 468	472, 510	
[{Ir(ppy)$_2$}$_2$(**5c**)](PF$_6$)$_2$ (**25**)	248, 268, 391, 470	590	

The luminescent lifetimes where measured in aerated acetonitrile for all three of the ruthenium complexes **16**, **24** and **26**, and are shown in **Error! Reference source not found.**. Complex **26** has a short lifetime of 7.36 ns consistent with the quenched emission intensity. Complex **16** displays a much longer lifetime of 229.3 ns whereas the dinuclear ruthenium complex **24** has an extended lifetime of 260.6 ns possibly due to the observed sensitisation of the [Ru(bpy)$_3$] domain by the [Ru(bpy)$_2$(pytz)] domain.

6.4 Conclusion

In conclusion we have successfully synthesised and characterised a small library of click derived bridging ligands. We have subsequently prepared two dinuclear ruthenium and iridium complexes of the 4-pyridyl-1-(2,2'-bipyrid-4-yl)-1,2,3-triazole bridging ligand, and carried photophysical studies. From our studies we have shown that the dinuclear species exhibit greater luminescent intensities than mono-nuclear model complexes possibly because the metal centre coordinated to the pyridine-triazole domain acts as a sensitizer for the metal centre coordinated to the bipyridyl domain through a photoinduced energy transfer mechanism. This shows that there is efficient transfer across the bridging ligand.

This therefore presents the potential use of this bridging ligand in functional supramolecular complexes. For example a mixed Ru/Re system could be envisaged for photocatalytic CO_2 reduction [169] and dinuclear complexes of this sort could also be investigated as novel chromophores for dye-sensitised solar cell applications.

7 General Conclusions & Outlook

7.1 General Conclusions

In conclusion we have demonstrated that the CuAAC reaction is a versatile coupling reaction which has a great deal of application within supramolecular and coordination chemistry.

Through our work with rhenium tricarbonyl complexes we have shown that 1,4-disubstituted-1,2,3-triazole ligands can act as either axial monodentate ligands, through the N3 atom of the triazole ring, or as bidentate N^N donor ligands if a pyridyl substituent is incorporated into a chelate ligand framework. The bipyridyltricarbonylrhenium(I) complexes with axial monodentate 1,2,3-triazoles have been shown to slightly better donor ligands than pyridine in these types of complexes. The complexes show long luminescent lifetimes in excess of 500 ns in dichloromethane and therefore may have potential applications as luminescent probes in biological time-gated imaging (Figure 7.1).

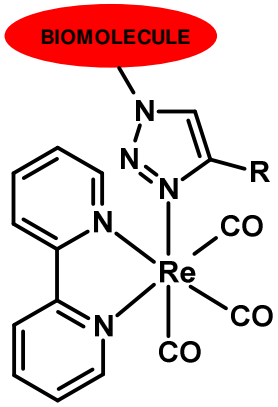

Figure 7.1 Rhenium polypyridine biological imaging agents

The CuAAC reaction can also be used to chemical modify the periphery of a metal complex when an azido substituted ligand is allowed to react with a range of alkynes. We have implemented the CuAAC reaction to introduce a redox active component into ligands by reacting azido bpy with ethynyl ferrocene and investigated the redox behaviour of this ligand. Further, we have successfully prepared and characterised rhenium, ruthenium and iridium complexes incorporating this ligand and investigated the redox behaviour of these complexes. From these investigations we have shown that the luminescent properties of the ruthenium and iridium complexes can be modulated through oxidation of the ferrocene moiety.

Furthermore, complexes of the type $[Ru(p\text{-cymene})(bpy\text{-}N_3)Cl]^+$ have been implemented in CuAAC reactions with bis alkynes and successfully been used as building blocks for metallo-supramolecular structures with greater control of selective metal binding.

We have also demonstrated that the CuAAC reaction can be used as an excellent tool for the preparation of new bidentate ligands incorporating either one or multiple binding sites starting from 4-azido-2,2'-bipyridyl and reacting them with a range of acetylenes.

In a marriage of the two uses of the triazole, as a coordinating donor and linker moiety the CuAAC reaction was used to prepare a small library of ligands with multiple binding sites. The photophysical properties of a dinuclear ruthenium and iridium complex with 4-pyridyl-1-(2,2'-bipyrid-4-yl)-1,2,3-triazole bridging ligand were studied and it was demonstrated that the metal coordinated in the

pyridine-triazole domain has the potential to acts as a sensitizer for the metal in the bpy domain and could have an effect on luminescent intensity when compared to the model mononuclear phenyltriazolyl-bpy analogue.

7.2 Future Work

'Click' chemistry and the CuAAC reaction in particular is a relatively new area of interest within coordination chemistry therefore all the work presented in this thesis has the potential to be extended further.

Our work with rhenium tricarbonyl complexes can be extended by implementing a similar synthetic scheme to that described here to introduce into the 1,2,3-triazole ligand a photophysically active complex, for example $[Ru(bpy)_2(\mathbf{5a})]$ or $[Ir(ppy)_2(\mathbf{5a})]$ (Figure 7.2). Ishitani [219] and co-workers have shown that ruthenium-rhenium polynuclear complexes act as light harvesting supramolecular photocatalysts for the reduction of CO_2.

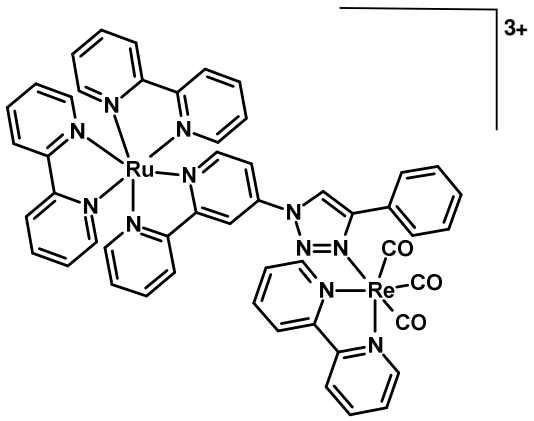

Figure 7.2 Potential ruthenium-rhenium complex as a supramolecular photocatalysts for the reduction of CO_2.

Further work with our ruthenium cymene complexes can be explored, in particular the complex with 4-(pyrid-2-yl)-1-(2,2'-bipyrid-4-yl)-1,2,3-triazole ligand constructed at the coordinated azido-bpy ligand. This provides the basis for incorporating a second metal into the pyridyl-triazole domain and access to selective heteronuclear complexes. This approach would be beneficial as it would allow for absolute control over regiospecificity of metal coordination. Some of the potential applications of mixed metal complexes include

- Mixed Ru/Re complexes again for the photocatalysis of CO_2 reduction.
- Mixed Ru/Ir complexes could be envisaged and have potential applications in water oxidation photocatalysis. [220]
- Dinuclear ruthenium complexes with carboxylic acid derivative of bpy in one site could be used as novel DSSC dyes.

Similarly the multi oligotopic ligands discussed in chapter 6 that have not been utilised as yet in our work will provide the basis of various hetero dinuclear/trinuclear metal complexes for these and other applications.

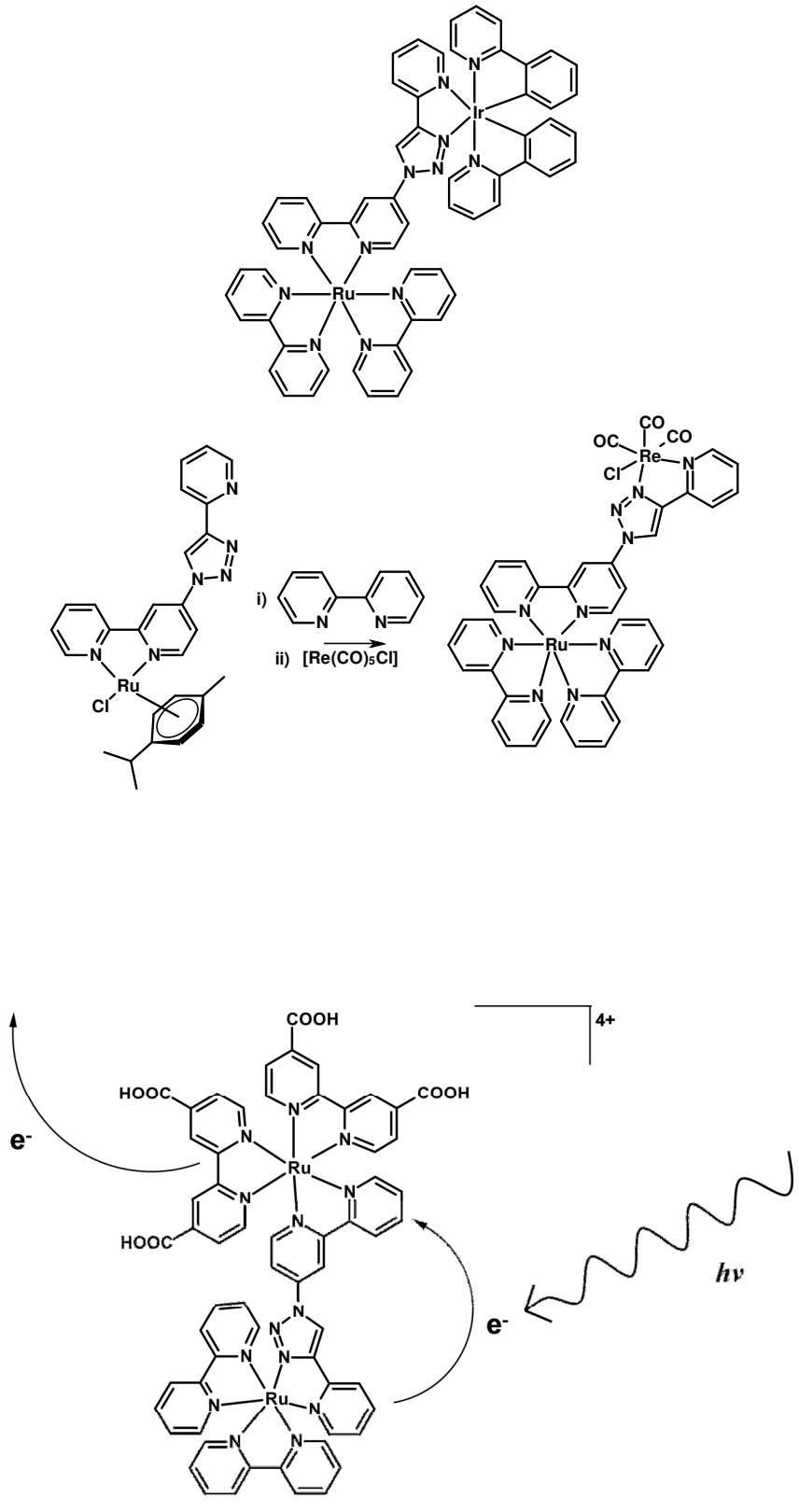

Figure 7.3 Proposed synthesis of mixed metal complexes

The mild and modular Cu(I)-catalyzed 1,3-cycloaddition of terminal alkynes with organic azides allows the ready formation of functionalised 1,4-disubstituted-1,2,3-triazole scaffolds and this has led to an explosion of interest in the coordination chemistry of these heterocycles. A diverse array of mono-, bi-, tri- and polydentate ligands incorporating 1,4-disubstituted-1,2,3-triazole units have been synthesised, characterised and reported during the course of this projec. Easy access to readily functionalised ligand architectures is of crucial importance in a range of different areas and we are exploiting these ligands for the development of new catalysts, metallo-pharmaceuticals, bio-imaging agents, metallosupramolecular architectures, and molecular machines.

Therefore, the work presented in this thesis and the recent explosion of interest in the use of 'click' chemistry, in particular CuAAC reactions for ligand design and as supramolecular linkers has shown that the CuAAC reaction has great potential in inorganic chemistry.

8 REFERENCES

1. H. C. Kolb, M. G. Finn and K. B. Sharpless, *Angewandte Chemie-International Edition*, 2001, **40**, 2004-2021.

2. V. V. Rostovtsev, L. G. Green, V. V. Fokin and K. B. Sharpless, *Angewandte Chemie-International Edition*, 2002, **41**, 2596-2599.

3. M. Meldal and C. W. Tornoe, *Chemical Reviews*, 2008, **108**, 2952-3015.

4. J. A. Prescher and C. R. Bertozzi, *Nature Chemical Biology*, 2005, **1**, 13-21.

5. C. J. Hawker and K. L. Wooley, *Science*, 2005, **309**, 1200-1205.

6. J. E. Moses and A. D. Moorhouse, *Chemical Society Reviews*, 2007, **36**, 1249-1262.

7. D. Fournier, R. Hoogenboom and U. S. Schubert, *Chemical Society Reviews*, 2007, **36**, 1369-1380.

8. R. Schibli, H. Struthers and T. L. Mindt, *Dalton Transactions*, 2010, **39**, 675-696.

9. B. Beyer, C. Ulbricht, D. Escudero, C. Friebe, A. Winter, L. Gonzalez and U. S. Schubert, *Organometallics*, 2009, **28**, 5478-5488.

10. B. Happ, C. Friebe, A. Winter, M. D. Hager, R. Hoogenboom and U. S. Schubert, *Chemistry-an Asian Journal*, 2009, **4**, 154-163.

11. J. D. Crowley and P. H. Bandeen, *Dalton Transactions*, 2010, **39**, 612-623.

12. J. D. Crowley, P. H. Bandeen and L. R. Hanton, *Polyhedron*, 2010, **29**, 70-83.

13. J. D. Crowley and E. L. Gavey, *Dalton Transactions*, 2010, **39**, 4035-4037.

14. A. Michael, *Journal für Praktische Chemie*, 1893, **48**, 94-104.

15. R. Huisgen, *Angewandte Chemie International Edition* 1963, **2**, 565-632.

16. R. Huisgen, *Angewandte Chemie International Edition*, 1963, **2**, 633-696.

17. C. W. Tornoe, C. Christensen and M. Meldal, *Journal of Organic Chemistry*, 2002, **67**, 3057-3064.

18. P. Appukkuttan, W. Dehaen, V. V. Fokin and E. Van der Eycken, *Organic Letters*, 2004, **6**, 4223-4225.

19. P. Wu and V. V. Fokin, *Aldrichimica Acta*, 2007, **40**, 7-17.

20. M. Juricek, P. H. J. Kouwer and A. E. Rowan, *Chemical Communications*, 2011, **47**, 8740-8749.

21. J. F. Lutz and Z. Zarafshani, *Advanced Drug Delivery Reviews*, 2008, **60**, 958-970.

22. J. F. Lutz, *Angewandte Chemie-International Edition*, 2007, **46**, 1018-1025.

23. V. Ganesh, V. S. Sudhir, T. Kundu and S. Chandrasekaran, *Chemistry-an Asian Journal*, 2011, **6**, 2670-2694.

24. Y. Li and C. Z. Cai, *Chemistry-an Asian Journal*, 2011, **6**, 2592-2605.

25. O. Altintas and U. Tunca, *Chemistry-an Asian Journal*, 2011, **6**, 2584-2591.

26. M. Meldal, *Macromolecular Rapid Communications*, 2008, **29**, 1016-1051.

27. P. L. Golas and K. Matyjaszewski, *Chemical Society Reviews*, 2010, **39**, 1338-1354.

28. A. J. Qin, J. W. Y. Lam and B. Z. Tang, *Chemical Society Reviews*, 2010, **39**, 2522-2544.

29. I. Aprahamian, O. S. Miljanic, W. R. Dichtel, K. Isoda, T. Yasuda, T. Kato and J. F. Stoddart, *Bulletin of the Chemical Society of Japan*, 2007, **80**, 1856-1869.

30. O. S. Miljanic, W. R. Dichtel, I. Aprahamian, R. D. Rohde, H. D. Agnew, J. R. Heath and J. F. Stoddart, *Qsar & Combinatorial Science*, 2007, **26**, 1165-1174.

31. K. D. Hanni and D. A. Leigh, *Chemical Society Reviews*, 2010, **39**, 1240-1251.

32. A. C. Fahrenbach and J. F. Stoddart, *Chemistry-an Asian Journal*, 2011, **6**, 2660-2669.

33. J. Hu, J. R. Lu and Y. Ju, *Chemistry-an Asian Journal*, 2011, **6**, 2636-2647.

34. X. C. Li, *Chemistry-an Asian Journal*, 2011, **6**, 2606-2616.

35. J. M. Holub and K. Kirshenbaum, *Chemical Society Reviews*, 2010, **39**, 1325-1337.

36. J. E. Hein and V. V. Fokin, *Chemical Society Reviews*, 2010, **39**, 1302-1315.

37. H. C. Kolb and K. B. Sharpless, *Drug Discovery Today*, 2003, **8**, 1128-1137.

38. E. J. Yoo, M. Ahlquist, S. H. Kim, I. Bae, V. V. Fokin, K. B. Sharpless and S. Chang, *Angewandte Chemie-International Edition*, 2007, **46**, 1730-1733.

39. V. D. Bock, H. Hiemstra and J. H. van Maarseveen, *European Journal of Organic Chemistry*, 2005, 51-68.

40. F. Himo, T. Lovell, R. Hilgraf, V. V. Rostovtsev, L. Noodleman, K. B. Sharpless and V. V. Fokin, *Journal of the American Chemical Society*, 2005, **127**, 210-216.

41. S. Quader, S. E. Boyd, I. D. Jenkins and T. A. Houston, *Journal of Organic Chemistry*, 2007, **72**, 1962-1979.

42. F. Alonso, Y. Moglie, G. Radivoy and M. Yus, *Tetrahedron Letters*, 2009, **50**, 2358-2362.

43. C. Girard, E. Onen, M. Aufort, S. Beauviere, E. Samson and J. Herscovici, *Organic Letters*, 2006, **8**, 1689-1692.

44. D. T. S. Rijkers, G. W. van Esse, R. Merkx, A. J. Brouwer, H. J. F. Jacobs, R. J. Pieters and R. M. J. Liskamp, *Chemical Communications*, 2005, 4581-4583.

45. C. Ornelas, J. R. Aranzaes, E. Cloutet, S. Alves and D. Astruc, *Angewandte Chemie-International Edition*, 2007, **46**, 872-877.

46. T. L. Mindt, H. Struthers, L. Brans, T. Anguelov, C. Schweinsberg, V. Maes, D. Tourwe and R. Schibli, *Journal of the American Chemical Society*, 2006, **128**, 15096-15097.

47. T. R. Chan, R. Hilgraf, K. B. Sharpless and V. V. Fokin, *Organic Letters*, 2004, **6**, 2853-2855.

48. C. L. Merrill, L. J. Wilson, T. J. Thamann, T. M. Loehr, N. S. Ferris and W. H. Woodruff, *Journal of the Chemical Society-Dalton Transactions*, 1984, 2207-2221.

49. M. G. Simmons, C. L. Merrill, L. J. Wilson, L. A. Bottomley and K. M. Kadish, *Journal of the Chemical Society-Dalton Transactions*, 1980, 1827-1837.

50. W. G. Lewis, F. G. Magallon, V. V. Fokin and M. G. Finn, *Journal of the American Chemical Society*, 2004, **126**, 9152-9153.

51. V. O. Rodionov, S. I. Presolski, S. Gardinier, Y. H. Lim and M. G. Finn, *Journal of the American Chemical Society*, 2007, **129**, 12696-12704.

52. S. Diez-Gonzalez, A. Correa, L. Cavallo and S. P. Nolan, *Chemistry-a European Journal*, 2006, **12**, 7558-7564.

53. S. Diez-Gonzalez and S. P. Nolan, *Angewandte Chemie-International Edition*, 2008, **47**, 8881-8884.

54. B. Schulze, C. Friebe, M. D. Hager, A. Winter, R. Hoogenboom, H. Gorls and U. S. Schubert, *Dalton Transactions*, 2009, 787-794.

55. A. K. Feldman, B. Colasson and V. V. Fokin, *Organic Letters*, 2004, **6**, 3897-3899.

56. J. T. Fletcher, B. J. Bumgarner, N. D. Engels and D. A. Skoglund, *Organometallics*, 2008, **27**, 5430-5433.

57. L. Zhang, X. G. Chen, P. Xue, H. H. Y. Sun, I. D. Williams, K. B. Sharpless, V. V. Fokin and G. C. Jia, *Journal of the American Chemical Society*, 2005, **127**, 15998-15999.

58. B. C. Boren, S. Narayan, L. K. Rasmussen, L. Zhang, H. T. Zhao, Z. Y. Lin, G. C. Jia and V. V. Fokin, *Journal of the American Chemical Society*, 2008, **130**, 8923-8930.

59. B. C. Boren, S. Narayan, L. K. Rasmussen, L. Zhang, H. T. Zhao, Z. Y. Lin, G. C. Jia and V. V. Fokin, *Journal of the American Chemical Society*, 2008, **130**, 14900-14900.

60. L. K. Rasmussen, B. C. Boren and V. V. Fokin, *Organic Letters*, 2007, **9**, 5337-5339.

61. G. Aromi, L. A. Barrios, O. Roubeau and P. Gamez, *Coordination Chemistry Reviews*, 2011, **255**, 485-546.

62. J. A. Kitchen and S. Brooker, *Coordination Chemistry Reviews*, 2008, **252**, 2072-2092.

63. M. H. Klingele and S. Brooker, *Coordination Chemistry Reviews*, 2003, **241**, 119-132.

64. U. Beckmann and S. Brooker, *Coordination Chemistry Reviews*, 2003, **245**, 17-29.

65. J. G. Haasnoot, *Coordination Chemistry Reviews*, 2000, **200**, 131-185.

66. S. Fanni, T. E. Keyes, C. M. O'Connor, H. Hughes, R. Y. Wang and J. G. Vos, *Coordination Chemistry Reviews*, 2000, **208**, 77-86.

67. S. Q. Bai, D. J. Young and T. S. A. Hor, *Chemistry-an Asian Journal*, 2011, **6**, 292-304.

68. Y. Angell and K. Burgess, *Angewandte Chemie-International Edition*, 2007, **46**, 3649-3651.

69. D. S. Moore and S. D. Robinson, *Advances in Inorganic Chemistry*, 1988, **32**, 171-239.

70. B. M. J. M. Suijkerbuijk, B. N. H. Aerts, H. P. Dijkstra, M. Lutz, A. L. Spek, G. van Koten and R. J. M. K. Gebbink, *Dalton Transactions*, 2007, 1273-1276.

71. S. Badeche, J. C. Daran, J. Ruiz and D. Astruc, *Inorganic Chemistry*, 2008, **47**, 4903-4908.

72. C. Maeda, S. Yamaguchi, C. Ikeda, H. Shinokubo and A. Osuka, *Organic Letters*, 2008, **10**, 549-552.

73. F. Wang, J. Q. Zhang, X. Ding, S. Y. Dong, M. Liu, B. Zheng, S. J. Li, L. Wu, Y. H. Yu, H. W. Gibson and F. H. Huang, *Angewandte Chemie-International Edition*, 2010, **49**, 1090-1094.

74. V. Aucagne, K. D. Hanni, D. A. Leigh, P. J. Lusby and D. B. Walker, *Journal of the American Chemical Society*, 2006, **128**, 2186-2187.

75. V. Aucagne, J. Berna, J. D. Crowley, S. M. Goldup, K. D. Haenni, D. A. Leigh, P. J. Lusby, V. E. Ronaldson, A. M. Z. Slawin, A. Viterisi and D. B. Walker, *Journal of the American Chemical Society*, 2007, **129**, 11950-11963.

76. M. J. Barrell, D. A. Leigh, P. J. Lusby and A. M. Z. Slawin, *Angewandte Chemie-International Edition*, 2008, **47**, 8036-8039.

77. K. M. Mullen and M. J. Gunter, *Journal of Organic Chemistry*, 2008, **73**, 3336-3350.

78. J. P. Collin, F. Durola, V. Heitz, F. Reviriego, J. P. Sauvage and Y. Trolez, *Angewandte Chemie-International Edition*, 2010, **49**, 10172-10175.

79. M. L. Gower and J. D. Crowley, *Dalton Transactions*, 2010, **39**, 2371-2378.

80. C. Richardson, C. M. Fitchett, R. Keene and P. J. Steel, *Dalton Transactions*, 2008, 2534-2537.

81. C. Nolte, P. Mayer and B. F. Straub, *Angewandte Chemie-International Edition*, 2007, **46**, 2101-2103.

82. D. V. Partyka, L. Gao, T. S. Teets, J. B. Updegraff, N. Deligonul and T. G. Gray, *Organometallics*, 2009, **28**, 6171-6182.

83. E. M. Schuster, M. Botoshansky and M. Gandelman, *Angewandte Chemie-International Edition*, 2008, **47**, 4555-4558.

84. Y. Tulchinsky, M. A. Iron, M. Botoshansky and M. Gandelman, *Nature Chemistry*, 2011, **3**, 525-531.

85. S. P. Nolan, *N-Heterocyclic Carbenes in Synthesis*, Wiley-VCH: Weinheim, 2006.

86. P. Mathew, A. Neels and M. Albrecht, *Journal of the American Chemical Society*, 2008, **130**, 13534-13535.

87. A. Poulain, D. Canseco-Gonzalez, R. Hynes-Roche, H. Muller-Bunz, O. Schuster, H. Stoeckli-Evans, A. Neels and M. Albrecht, *Organometallics*, 2011, **30**, 1021-1029.

88. T. Nakamura, K. Ogata and S. Fukuzawa, *Chemistry Letters*, 2010, **39**, 920-922.

89. A. Prades, E. Peris and M. Albrecht, *Organometallics*, 2011, **30**, 1162-1167.

90. T. Nakamura, T. Terashima, K. Ogata and S. Fukuzawa, *Organic Letters*, 2011, **13**, 620-623.

91. S. Hohloch, C. Y. Su and B. Sarkar, *European Journal of Inorganic Chemistry*, 2011, 3067-3075.

92. K. J. Kilpin, U. S. D. Paul, A. L. Lee and J. D. Crowley, *Chemical Communications*, 2011, **47**, 328-330.

93. J. Bouffard, B. K. Keitz, R. Tonner, G. Guisado-Barrios, G. Frenking, R. H. Grubbs and G. Bertrand, *Organometallics*, 2011, **30**, 2617-2627.

94. A. Seridi, M. Wolff, A. Boulay, N. Saffon, Y. Coulais, C. Picard, B. Machura and E. Benoist, *Inorganic Chemistry Communications*, 2011, **14**, 238-242.

95. A. Boulay, A. Seridi, C. Zedde, S. Ladeira, C. Picard, L. Maron and E. Benoist, *European Journal of Inorganic Chemistry*, 2010, 5058-5062.

96. M. Obata, A. Kitamura, A. Mori, C. Kameyama, J. A. Czaplewska, R. Tanaka, I. Kinoshita, T. Kusumoto, H. Hashimoto, M. Harada, Y. Mikata, T. Funabiki and S. Yano, *Dalton Transactions*, 2008, 3292-3300.

97. C. H. Zhang, X. D. Shen, R. Sakai, M. Gottschaldt, U. S. Schubert, S. Hirohara, M. Tanihara, S. Yano, M. Obata, N. O. Xiao, T. Satoh and T. Kakuchi, *Journal of Polymer Science Part a-Polymer Chemistry*, 2011, **49**, 746-753.

98. M. Felici, P. Contreras-Carballada, Y. Vida, J. M. M. Smits, R. J. M. Nolte, L. De Cola, R. M. Williams and M. C. Feiters, *Chemistry-a European Journal*, 2009, **15**, 13124-13134.

99. B. Happ, D. Escudero, M. D. Hager, C. Friebe, A. Winter, H. Gorls, E. Altuntas, L. Gonzalez and U. S. Schubert, *Journal of Organic Chemistry*, 2010, **75**, 4025-4038.

100. M. Felici, P. Contreras-Carballada, J. M. M. Smits, R. J. M. Nolte, R. M. Williams, L. De Cola and M. C. Feiters, *Molecules*, 2010, **15**, 2039-2059.

101. M. Mydlak, C. Bizzarri, D. Hartmann, W. Sarfert, G. Schmid and L. De Cola, *Advanced Functional Materials*, 2010, **20**, 1812-1820.

102. S. Zanarini, M. Felici, G. Valenti, M. Marcaccio, L. Prodi, S. Bonacchi, P. Contreras-Carballada, R. M. Williams, M. C. Feiters, R. J. M. Nolte, L. De Cola and F. Paolucci, *Chemistry-a European Journal*, 2011, **17**, 4640-4647.

103. O. Fleischel, N. Wu and A. Petitjean, *Chemical Communications*, 2010, **46**, 8454-8456.

104. K. J. Kilpin and J. D. Crowley, *Polyhedron*, 2010, **29**, 3111-3117.

105. K. J. Kilpin, E. L. Gavey, C. J. McAdam, C. B. Anderson, S. J. Lind, C. C. Keep, K. C. Gordon and J. D. Crowley, *Inorganic Chemistry*, 2011, **50**, 6334-6346.

106. A. D'Amora, L. Fanfoni, D. Cozzula, N. Guidolin, E. Zangrando, F. Felluga, S. Gladiali, F. Benedetti and B. Milani, *Organometallics*, 2010, **29**, 4472-4485.

107. D. Schweinfurth, R. Pattacini, S. Strobel and B. Sarkar, *Dalton Transactions*, 2009, 9291-9297.

108. D. Schweinfurth, S. Strobel and B. Sarkar, *Inorganica Chimica Acta*, 2011, **374**, 253-260.

109. I. Stengel, A. Mishra, N. Pootrakulchote, S. J. Moon, S. M. Zakeeruddin, M. Gratzel and P. Bauerle, *Journal of Materials Chemistry*, 2011, **21**, 3726-3734.

110. A. Mattiuzzi, I. Jabin, C. Moucheron and A. Kirsch-De Mesmaeker, *Dalton Transactions*, 2011, **40**, 7395-7402.

111. U. Monkowius, S. Ritter, B. Konig, M. Zabel and H. Yersin, *European Journal of Inorganic Chemistry*, 2007, 4597-4606.

112. C. E. Welby, S. Grkinic, A. Zahid, B. S. Uppal, E. A. Gibson, C. R. Rice and P. I. P. Elliott, *Dalton Transactions*, 2012, **41**, 7637-7646.

113. G. C. Kuang, H. A. Michaels, J. T. Simmons, R. J. Clark and L. Zhu, *Journal of Organic Chemistry*, 2010, **75**, 6540-6548.

114. W. S. Brotherton, H. A. Michaels, J. T. Simmons, R. J. Clark, N. S. Dalal and L. Zhu, *Organic Letters*, 2009, **11**, 4954-4957.

115. D. Urankar, B. Pinter, A. Pevec, F. De Proft, I. Turel and J. Kosmrlj, *Inorganic Chemistry*, 2010, **49**, 4820-4829.

116. Y. Fu, Y. Liu, X. P. Fu, L. Zou, H. Li, M. Li, X. G. Chen and J. G. Qin, *Chinese Journal of Chemistry*, 2010, **28**, 2226-2232.

117. I. Bratsos, D. Urankar, E. Zangrando, P. Genova-Kalou, J. Kosmrlj, E. Alessio and I. Turel, *Dalton Transactions*, 2011, **40**, 5188-5199.

118. D. Urankar, A. Pevec, I. Turel and J. Kosmrlj, *Crystal Growth & Design*, 2010, **10**, 4920-4927.

119. D. Urankar, A. Pevec and J. Kosmrlj, *European Journal of Inorganic Chemistry*, 2011, 1921-1929.

120. B. Pinter, A. Demsar, D. Urankar, F. De Proft and J. Kosmrlj, *Polyhedron*, 2011, **30**, 2368-2373.

121. E. Amadio, M. Bertoldini, A. Scrivanti, G. Chessa, V. Beghetto, U. Matteoli, R. Bertani and A. Dolmella, *Inorganica Chimica Acta*, 2011, **370**, 388-393.

122. J. M. Fernandez-Hernandez, C. H. Yang, J. I. Beltran, V. Lemaur, F. Polo, R. Frohlich, J. Cornil and L. De Cola, *Journal of the American Chemical Society*, 2011, **133**, 10543-10558.

123. Y. Boutadla, D. L. Davies, R. C. Jones and K. Singh, *Chemistry-a European Journal*, 2011, **17**, 3438-3448.

124. E. Orselli, R. Q. Albuquerque, P. M. Fransen, R. Frohlich, H. M. Janssen and L. De Cola, *Journal of Materials Chemistry*, 2008, **18**, 4579-4590.

125. A. Maisonial, P. Serafin, M. Traikia, E. Debiton, V. Thery, D. J. Aitken, P. Lemoine, B. Viossat and A. Gautier, *European Journal of Inorganic Chemistry*, 2008, 298-305.

126. G. F. Manbeck, W. W. Brennessel and R. Eisenberg, *Inorganic Chemistry*, 2011, **50**, 3431-3441.

127. R. J. Detz, S. A. Heras, R. de Gelder, P. W. N. M. van Leeuwen, H. Hiemstra, J. N. H. Reek and J. H. van Maarseveen, *Organic Letters*, 2006, **8**, 3227-3230.

128. T. L. Mindt, C. Muller, M. Melis, M. de Jong and R. Schibli, *Bioconjugate Chemistry*, 2008, **19**, 1689-1695.

129. T. L. Mindt, C. Muller, F. Stuker, J. F. Salazar, A. Hohn, T. Mueggler, M. Rudin and R. Schibli, *Bioconjugate Chemistry*, 2009, **20**, 1940-1949.

130. T. L. Mindt, C. Schweinsberg, L. Brans, A. Hagenbach, U. Abram, D. Tourwe, E. Garcia-Garayoa and R. Schibli, *Chemmedchem*, 2009, **4**, 529-539.

131. T. L. Ross, M. Honer, P. Y. H. Lam, T. L. Mindt, V. Groehn, R. Schibli, P. A. Schubiger and S. M. Ametamey, *Bioconjugate Chemistry*, 2008, **19**, 2462-2470.

132. H. Struthers, B. Spingler, T. L. Mindt and R. Schibli, *Chemistry-a European Journal*, 2008, **14**, 6173-6183.

133. H. Struthers, D. Viertl, M. Kosinski, B. Spingler, F. Buchegger and R. Schibli, *Bioconjugate Chemistry*, 2010, **21**, 622-634.

134. L. Brans, E. Garcia-Garayoa, C. Schweinsberg, V. Maes, H. Struthers, R. Schibli and D. Tourwe, *Chemmedchem*, 2010, **5**, 1717-1725.

135. T. L. Mindt, H. Struthers, B. Spingler, L. Brans, D. Tourwe, E. Garcia-Garayoa and R. Schibli, *Chemmedchem*, 2010, **5**, 2026-2038.

136. F. Tinnis and H. Adolfsson, *Organic & Biomolecular Chemistry*, 2010, **8**, 4536-4539.

137. S. J. Gu, H. Xu, N. Zhang and W. Z. Chen, *Chemistry-an Asian Journal*, 2010, **5**, 1677-1686.

138. Y. J. Li, J. C. Huffman and A. H. Flood, *Chemical Communications*, 2007, 2692-2694.

139. R. M. Meudtner, M. Ostermeier, R. Goddard, C. Limberg and S. Hecht, *Chemistry-a European Journal*, 2007, **13**, 9834-9840.

140. M. Ostermeier, M. A. Berlin, R. M. Meudtner, S. Demeshko, F. Meyer, C. Limberg and S. Hecht, *Chemistry-a European Journal*, 2010, **16**, 10202-10213.

141. P. Danielraj, B. Varghese and S. Sankararaman, *Acta Crystallographica Section C-Crystal Structure Communications*, 2010, **66**, M366-M370.

142. N. Chandrasekhar and R. Chandrasekar, *Dalton Transactions*, 2010, **39**, 9872-9878.

143. L. Munuera and R. K. O'Reilly, *Dalton Transactions*, 2010, **39**, 388-391.

144. W. W. Yang, L. Wang, Y. W. Zhong and J. N. Yao, *Organometallics*, 2011, **30**, 2236-2240.

145. W. W. Yang, J. N. Yao and Y. W. Zhong, *Organometallics*, 2012, **31**, 1035-1041.

146. L. Wang, W. W. Yang, R. H. Zheng, Q. Shi, Y. W. Zhong and J. N. Yao, *Inorganic Chemistry*, 2011, **50**, 7074-7079.

147. D. G. Brown, N. Sanguantrakun, B. Schulze, U. S. Schubert and C. P. Berlinguette, *Journal of the American Chemical Society*, 2012, **134**, 12354-12357.

148. B. Schulze, D. Escudero, C. Friebe, R. Siebert, H. Gorls, U. Kohn, E. Altuntas, A. Baumgaertel, M. D. Hager, A. Winter, B. Dietzek, J. Popp, L. Gonzalez and U. S. Schubert, *Chemistry-a European Journal*, 2011, **17**, 5494-5498.

149. W. S. Brotherton, P. M. Guha, H. Phan, R. J. Clark, M. Shatruk and L. Zhu, *Dalton Transactions*, 2011, **40**, 3655-3665.

150. E. C. Constable, *Coordination Chemistry Reviews*, 2008, **252**, 842-855.

151. G.-L. Xu and T. Ren, *Organometallics*, 2005, **24**, 2564-2566.

152. W.-Z. Chen and T. Ren, *Organometallics*, 2005, **24**, 2660-2669.

153. X. Y. Wang, A. Kimyonok and M. Weck, *Chemical Communications*, 2006, 3933-3935.

154. B. Baeza, L. Casarrubios, P. Ramirez-Lopez, M. Gomez-Gallego and M. A. Sierra, *Organometallics*, 2009, **28**, 956-959.

155. A. Chakraborty, S. Dey, S. Sawoo, N. N. Adarsh and A. Sarkar, *Organometallics*, 2010, **29**, 6619-6622.

156. E. C. Constable, C. E. Housecroft, M. Neuberger and P. Rosel, *Chemical Communications*, 2010, **46**, 1628-1630.

157. S. Bedeche, J.-C. Daran, J. Ruiz and D. Astruc, *Inorganic Chemistry*, 2008, **47**, 4903-4908.

158. R. A. Fallahpour and M. Neuburger, *Helvetica Chimica Acta*, 2001, **84**, 715-721.

159. R. A. Fallahpour, M. Neuburger and M. Zehnder, *Synthesis-Stuttgart*, 1999, 1051-1055.

160. A. Winter, A. Wild, R. Hoogenboom, M. W. M. Fijten, M. D. Hager, R.-A. Fallahpour and U. S. Schubert, *Synthesis*, 2009, 1506-1512.

161. A. Baron, C. Herrero, A. Quaranta, M.-F. Charlot, W. Leibl, B. Vauzeilles and A. Aukauloo, *Chemical Communications*, 2011, **47**, 11011-11013.

162. E. C. Constable, C. E. Housecroft, J. R. Price, L. Schweighauser and J. A. Zampese, *Inorganic Chemistry Communications*, 2010, **13**, 495-497.

163. J. V. Caspar and T. J. Meyer, *Journal of Physical Chemistry*, 1983, **87**, 952-957.

164. B. P. Sullivan, D. J. Salmon and T. J. Meyer, *Inorganic Chemistry*, 1978, **17**, 3334-3341.

165. S. Sprouse, K. A. King, P. J. Spellane and R. J. Watts, *Journal of the American Chemical Society*, 1984, **106**, 6647-6653.

166. D. Wenkert and R. B. Woodward, *Journal of Organic Chemistry*, 1983, **48**, 283-289.

167. R. A. Fallahpour, *Helvetica Chimica Acta*, 2000, **83**, 384-393.

168. G. Maerker, *Journal of American Chemical Society*, 1958, **80**, 2745-2748.

169. H. Hori, J. Ishihara, K. Koike, K. Takeuchi, T. Ibusuki and O. Ishitani, *Journal of Photochemistry and Photobiology a-Chemistry*, 1999, **120**, 119-124.

170. K. Koike, H. Hori, M. Ishizuka, J. R. Westwell, K. Takeuchi, T. Ibusuki, K. Enjouji, H. Konno, K. Sakamoto and O. Ishitani, *Organometallics*, 1997, **16**, 5724-5729.

171. H. Hori, F. P. A. Johnson, K. Koike, O. Ishitani and T. Ibusuki, *Journal of Photochemistry and Photobiology a-Chemistry*, 1996, **96**, 171-174.

172. H. Hori, O. Ishitani, K. Koike, K. Takeuchi and T. Ibusuki, *Analytical Sciences*, 1996, **12**, 587-590.

173. O. Ishitani, M. W. George, T. Ibusuki, F. P. A. Johnson, K. Koike, K. Nozaki, C. J. Pac, J. J. Turner and J. R. Westwell, *Inorganic Chemistry*, 1994, **33**, 4712-4717.

174. N. J. Lundin, A. G. Blackman, K. C. Gordon and D. L. Officer, *Angewandte Chemie-International Edition*, 2006, **45**, 2582-2584.

175. Z. J. Si, J. Li, B. Li, F. F. Zhao, S. Y. Liu and W. L. Li, *Inorganic Chemistry*, 2007, **46**, 6155-6163.

176. S. Ranjan, S. Y. Lin, K. C. Hwang, Y. Chi, W. L. Ching, C. S. Liu, Y. T. Tao, C. H. Chien, S. M. Peng and G. H. Lee, *Inorganic Chemistry*, 2003, **42**, 1248-1255.

177. A. J. Amoroso, R. J. Arthur, M. P. Coogan, J. B. Court, V. Fernandez-Moreira, A. J. Hayes, D. Lloyd, C. Millet and S. J. A. Pope, *New Journal of Chemistry*, 2008, **32**, 1097-1102.

178. A. J. Amoroso, M. P. Coogan, J. E. Dunne, V. Fernandez-Moreira, J. B. Hess, A. J. Hayes, D. Lloyd, C. Millet, S. J. A. Pope and C. Williams, *Chemical Communications*, 2007, 3066-3068.

179. M. P. Coogan, V. Fernandez-Moreira, J. B. Hess, S. J. A. Pope and C. Williams, *New Journal of Chemistry*, 2009, **33**, 1094-1099.

180. V. Fernandez-Moreira, F. L. Thorp-Greenwood and M. P. Coogan, *Chemical Communications*, 2010, **46**, 186-202.

181. S. S. Sun and A. J. Lees, *Organometallics*, 2001, **20**, 2353-2358.

182. A. Coleman, C. Brennan, J. G. Vos and M. T. Pryce, *Coordination Chemistry Reviews*, 2008, **252**, 2585-2595.

183. K. Oshin, A. M. Landis, B. W. Smucker, D. M. Eichhorn and D. P. Rillema, *Acta Crystallographica Section E-Structure Reports Online*, 2004, **60**, M1126-M1127.

184. W. B. Connick, A. J. DiBilio, M. G. Hill, J. R. Winkler and H. B. Gray, *Inorganica Chimica Acta*, 1995, **240**, 169-173.

185. H. Tsubaki, S. Tohyama, K. Koike, H. Saitoh and O. Ishitani, *Dalton Transactions*, 2005, 385-395.

186. P. J. Stephens, F. J. Devlin, C. F. Chabalowski and M. J. Frisch, *Journal of Physical Chemistry*, 1994, **98**, 11623-11627.

187. D. Andrae, U. Haussermann, M. Dolg, H. Stoll and H. Preuss, *Theoretica Chimica Acta*, 1990, **77**, 123-141.

188. R. Krishnan, J. S. Binkley, R. Seeger and J. A. Pople, *Journal of Chemical Physics*, 1980, **72**, 650-654.

189. M. F. Guest, I. J. Bush, H. J. J. Van Dam, P. Sherwood, J. M. H. Thomas, J. H. Van Lenthe, R. W. A. Havenith and J. Kendrick, *Molecular Physics*, 2005, **103**, 719-747.

190. M. Valiev, E. J. Bylaska, N. Govind, K. Kowalski, T. P. Straatsma, H. J. J. Van Dam, D. Wang, J. Nieplocha, E. Apra, T. L. Windus and W. de Jong, *Computer Physics Communications*, 2010, **181**, 1477-1489.

191. M. W. George, F. P. A. Johnson, J. R. Westwell, P. M. Hodges and J. J. Turner, *Journal of the Chemical Society-Dalton Transactions*, 1993, 2977-2979.

192. G. DeSantis, L. Fabbrizzi, M. Licchelli, N. Sardone and A. H. Velders, *Chemistry-a European Journal*, 1996, **2**, 1243-1250.

193. R. Bergonzi, L. Fabbrizzi, M. Licchelli and C. Mangano, *Coordination Chemistry Reviews*, 1998, **170**, 31-46.

194. F. Zapata, A. Caballero, A. Espinosa, A. Tarraga and P. Molina, *Journal of Organic Chemistry*, 2008, **73**, 9196-9196.

195. F. Zapata, A. Caballero, A. Espinosa, A. Tarraga and P. Molina, *Dalton Transactions*, 2009, 3900-3902.

196. A. Baron, C. Herrero, A. Quaranta, M. F. Charlot, W. Leibl, B. Vauzeilles and A. Aukauloo, *Inorganic Chemistry*, 2012, **51**, 5985-5987.

197. K. P. Chitre, E. Guillen, S. Y. Audri and E. Galoppini, *European Journal of Inorganic Chemistry*, 2012, **33**, 5461–5464

198. T. Romero, A. Caballero, A. Tarraga and P. Molina, *Organic Letters*, 2009, **11**, 3466-3469.

199. F. Zapata, A. Caballero, A. Espinosa, A. Tarraga and P. Molina, *Journal of Organic Chemistry*, 2008, **73**, 4034-4044.

200. J. W. Steed, *Supramolecular Chemistry*, John Wiley and Sons, West Sussex, 2000.

201. J. P. Sauvage, *Transition metals in supramolecular chemistry*, John Wiley and sons, west sussex, 1999.

202. J. M. Lehn, *Supramolecular Chemistry*, VHC: Weinheim, Germany, 1995.

203. V. Balzani, G. Bergamini, F. Marchioni and P. Ceroni, *Coordination Chemistry Reviews*, 2006, **250**, 1254-1266.

204. V. Balzani, A. Juris, M. Venturi, S. Campagna and S. Serroni, *Chemical Reviews*, 1996, **96**, 759-833.

205. T. J. Meyer, *Pure and Applied Chemistry*, 1986, **58**, 1193-1206.

206. A. Juris, V. Balzani, F. Barigelletti, S. Campagna, P. Belser and A. Vonzelewsky, *Coordination Chemistry Reviews*, 1988, **84**, 85-277.

207. F. S. Han, M. Higuchi, T. Ikeda, Y. Negishi, T. Tsukuda and D. G. Kurth, *Journal of Materials Chemistry*, 2008, **18**, 4555-4560.

208. J. P. Sauvage, J. P. Collin, J. C. Chambron, S. Guillerez, C. Coudret, V. Balzani, F. Barigelletti, L. Decola and L. Flamigni, *Chemical Reviews*, 1994, **94**, 993-1019.

209. F. Barigelletti, L. Flamigni, V. Balzani, J. P. Collin, J. P. Sauvage, A. Sour, E. C. Constable and A. M. W. C. Thompson, *Journal of the American Chemical Society*, 1994, **116**, 7692-7699.

210. F. Barigelletti, L. Flamigni, J. P. Collin and J. P. Sauvage, *Chemical Communications*, 1997, 333-338.

211. F. Barigelletti, L. Flamigni, M. Guardigli, A. Juris, M. Beley, S. ChodorowskiKimmes, J. P. Collin and J. P. Sauvage, *Inorganic Chemistry*, 1996, **35**, 136-142.

212. G. Denti, S. Campagna, S. Serroni, M. Ciano and V. Balzani, *Journal of the American Chemical Society*, 1992, **114**, 2944-2950.

213. M. D. Ward, *Journal of the Chemical Society-Dalton Transactions*, 1993, 1321-1325.

214. D. A. Bardwell, F. Barigelletti, R. L. Cleary, L. Flamigni, M. Guardigli, J. C. Jeffery and M. D. Ward, *Inorganic Chemistry*, 1995, **34**, 2438-2446.

215. R. L. Cleary, K. J. Byrom, D. A. Bardwell, J. C. Jeffery, M. D. Ward, G. Calogero, N. Armaroli, L. Flamigni and F. Barigelletti, *Inorganic Chemistry*, 1997, **36**, 2601-2609.

216. H. Takeda, K. Koike, H. Inoue and O. Ishitani, *Journal of the American Chemical Society*, 2008, **130**, 2023-2031.

217. H. Tsubaki, A. Sugawara, H. Takeda, B. Gholamkhass, K. Koike and O. Ishitani, *Research on Chemical Intermediates*, 2007, **33**, 37-48.

218. A. Baron, C. Herrero, A. Quaranta, M. F. Charlot, W. Leibl, B. Vauzeilles and A. Aukauloo, *Chemical Communications*, 2011, **47**, 11011-11013.

219. B. Gholamkhass, H. Mametsuka, K. Koike, T. Tanabe, M. Furue and O. Ishitani, *Inorganic Chemistry*, 2005, **44**, 2326-2336.

220. R. Lalrempuia, N. D. McDaniel, H. Muller-Bunz, S. Bernhard and M. Albrecht, *Angewandte Chemie-International Edition*, 2010, **49**, 9765-9768.

9 APPENDIX

9.1 X-ray crystallography

Single crystal X-ray diffraction data were collected on a Bruker Apex Duo diffractometer equipped with a graphite monochromated Mo(Ka) radiation source (0.071073 nm) and a cold stream of N_2 gas. Preliminary scans were employed to assess crystal quality, lattice symmetry, ideal exposure time etc. prior to collecting a full sphere of diffraction intensity data using SMART operating software. Intensities were then integrated from several series of exposures, merged and corrected for Lorentz and polarisation effects using SAINT software. Solutions were generated by conventional heavy atom Patterson or direct methods and refined by full-matrix non-linear least squares on all F_2 data, using SHELXS-97 and SHELXL software respectively (as implemented in the SHELXTL suite of programs). Empirical absorption corrections were applied based on multiple and symmetry-equivalent measurements using SADABS. All structures were refined until convergence (max shift/esd < 0.01) and in each case, the final Fourier difference map showed no chemically sensible features.

Complex	**[Re(bpy)(CO)$_3$(1a)](PF)$_6$**
Formula	$C_{22}H_{17}F_6N_5O_3PRe$
M_r / g mol^{-1}	730.58
T/K	103
Space group	C2/*c*
a / Å	36.1896(14)
b / Å	8.5518(3)
c / Å	17.3133(7)
α (°)	90
β (°)	116.081(1)
γ (°)	90
V / Å^3	4812.6(3)
D_c / g cm^{-1}	2.017
Z	8
μ_{Mo} / mm^{-1}	5.199
'*T*'$_{min, max}$	0.430,0.620
$2\theta_{max}$	69.94
N_{ref}	10543
R_1	0.0210
wR_2	0.0484
S	1.031

Complex	**$[Re(bpy)(CO)_3(1b)](PF)_6$**
Formula	$C_{24}H_{21}F_6N_5O_3PRe$
M_r / *g mol*$^{-1}$	758.63
T/*K*	110
Space group	*Pbca*
a / Å	13.5102(5)
b / Å	19.4031(6)
c / Å	20.6142(7)
α (°)	90
β (°)	90
γ (°)	90
V / Å^3	5403.8(3)
D_c / g cm^{-1}	1.865
Z	8
μ_{Mo} / mm^{-1}	4.634
'T'$_{min, max}$	0.330,0.710
$2\theta_{max}$	60.06
N_{ref}	7884
R_1	0.0376
wR_2	0.1145
S	0.947

Complex	**$[Re(bpy)(CO)_3(1c)](PF)_6$**
Formula	$C_{28}H_{21}F_6N_5O_3PRe$
M_r / *g mol*$^{-1}$	806.67
T/K	100
Space group	*P-1*
a / Å	10.2372(7)
b / Å	12.2663(8)
c / Å	12.4058(8)
α (°)	76.3200(10)
β (°)	81.8120(10)
γ (°)	69.9900(10)
V / Å^3	1419.03(16)
D_c / g cm^{-1}	1.888
Z	2
μ_{Mo} / mm^{-1}	4.418
'T'$_{min, max}$	0.351,0.472
$2\theta_{max}$	60.06
N_{ref}	8262
R_1	0.0214
wR_2	0.0452
S	1.088

Complex	**[Ru(*p*-cymene)(4b)Cl](PF$_6$)**
Formula	$C_{20}H_{20}ClF_6N_8PRu$
M_r / g mol^{-1}	653.93
T/K	150
Space group	*P-1*
a / Å	8.8409(10)
b / Å	14.1712(16)
c / Å	19.682(2)
α (°)	81.279(3)
β (°)	86.805(2)
γ (°)	87.935(3)
V / Å^3	2432.7(5)
D_c / g cm^{-1}	1.785
Z	4
μ_{Mo} / mm^{-1}	0.894
'*T*'$_{min, max}$	0.856, 0.991
$2\theta_{max}$	52.94
N_{ref}	9885
R_1	0.1104
wR_2	0.2580
S	1.249

9.2 Atomic Coordinates of the optimised geometries of the S_0 ground states and T_1 excited states of complexes

To view molecular structures copy and paste portion between # marks into notepad, save as a .xyz file and open molecular viewing program such as Mercury.

9.2.1 Atomic coordinates for calculated S_0 state of [Re(bpy)(CO)$_3$Cl]

#
28
Re 12.6254245418 -9.91988245522 -0.587361492846
C 9.19983528015 -6.43833256705 0.396865128406
C 8.98751846087 -7.78101209912 0.67440296002
C 9.94168798728 -8.72795269728 0.297707730475
N 11.0800458237 -8.3511571887 -0.333811042971
C 11.2655020418 -7.05348654177 -0.625650941364
C 10.3545777594 -6.06586032872 -0.282756046011
C 8.64968101594 -10.7437605078 1.12131616739
C 8.55237700754 -12.1211736836 1.25567071512
C 9.57355140194 -12.9202688426 0.753028978281
C 10.6671966923 -12.3016131979 0.166631593011
N 10.7813417588 -10.9678579713 0.0603763439796
C 9.77587947617 -10.182252169 0.517024132689
C 13.8263326343 -11.4479030036 -0.546766314303
C 14.1346040077 -8.74956386262 -0.95187623204
Cl 12.8820767627 -9.57358870892 1.90106302781
O 14.500991028 -12.3787215894 -0.498934904874
O 14.9989977564 -8.01772355476 -1.15404909866
C 12.3057077578 -10.1664521609 -2.4753312529
O 12.111958807 -10.3130531873 -3.60548181863
H 8.47004669736 -5.69939070385 0.702739912111
H 8.0882970337 -8.08991425153 1.18753743009
H 12.1807819271 -6.80962040142 -1.14671872718
H 10.5573021872 -5.03300419328 -0.537425334817
H 7.85775186597 -10.1085342145 1.49085560095
H 7.68808851209 -12.5590831559 1.73873787723
H 9.53559946251 -14.0005263253 0.81795878451
H 11.4883779531 -12.8821427511 -0.230051763095
#

9.2.2 Atomic coordinates for calculated T_1 state of [Re(bpy)(CO)$_3$Cl]

#
28
Re -0.0003172 -0.85829331 0.04383135
C 2.88364937 3.15939279 -0.19496315
C 1.51878074 3.24650364 -0.22718674
C 0.71090023 2.07927123 -0.15008624
N 1.33470056 0.83200288 -0.04991423
C 2.68812101 0.77795738 -0.00884221
C 3.4969303 1.88397486 -0.07787974
C -1.51262239 3.24986953 -0.22811579
C -2.87770718 3.16519772 -0.1962238
C -3.49321725 1.89135473 -0.07854224
C -2.68623754 0.78379638 -0.0085773
N -1.33326862 0.83578347 -0.04957717
C -0.70712313 2.08105125 -0.15012066
C -1.3488216 -2.31442935 0.17061182
C 1.34655251 -2.31376434 0.17497826
Cl -0.00871899 -0.6298173 2.45747972
O -2.12215445 -3.15449379 0.24175705
O 2.11956247 -3.15409646 0.24863774
C -0.00133365 -0.91961989 -1.95211822
O -0.00283221 -0.9537998 -3.09306255
H 3.49065465 4.05650595 -0.25200434
H 1.04469789 4.21663987 -0.30681753
H 3.11511383 -0.21231264 0.0906567
H 4.57280187 1.77142466 -0.03522275
H -1.03646008 4.21883768 -0.30800992
H -3.48274882 4.06346089 -0.25417957
H -4.56913669 1.78081995 -0.03618527
H -3.11510406 -0.20563926 0.09158748
#

9.2.3 Atomic coordinates for calculated S_0 state of [Re(3a')$(CO)_3$Cl]

#
28

Re	12.2276270565	-10.0580080241	-0.665848337555
C	13.2213020801	-11.5435580964	-1.41964271745
C	12.8898641843	-10.47535643	1.09964494046
N	9.68336705966	-6.86322555526	0.631143163611
C	8.77135082056	-7.86336706895	0.565558395009
C	9.50168540818	-8.9770501227	0.209033646421
N	10.7996442449	-8.56865047031	0.0783776225771
N	10.9136341037	-7.29975588655	0.334047743843
C	7.91793749456	-10.9228823714	0.0771559116372
C	7.72335815914	-12.2675610813	-0.205437994541
C	8.82003240576	-13.0395527998	-0.5769796222
C	10.0684796961	-12.4372195138	-0.654740012725
N	10.2667161737	-11.135682541	-0.391908168694
C	9.1962399987	-10.3799165005	-0.0382809816862
C	13.721890769	-8.85155690843	-0.97491866241
O	13.7722642918	-12.4604900724	-1.8465347247
O	13.2819461877	-10.721650064	2.15941776983
O	14.5798850215	-8.1077486277	-1.14581933795
C	9.48281379217	-5.45476942792	0.952174423279
Cl	11.1928515431	-9.47426890657	-2.8976569389
H	7.72385833724	-7.70643137444	0.758658363207
H	7.08973400208	-10.2953967734	0.380399786051
H	6.73488192907	-12.7054511329	-0.136974132635
H	8.71996588174	-14.0919467851	-0.809758287294
H	10.9460407444	-13.0022439692	-0.93986137409
H	10.4512023575	-4.9700294844	0.862833258698
H	9.11020746039	-5.34579103405	1.97116162331
H	8.78260371655	-5.00713521689	0.246823393098

#

9.2.4 Atomic coordinates for calculated T_1 state of [Re(3a')$(CO)_3$Cl]

#
28

Re	-0.14231111	-0.86426357	0.06778034
C	0.82440758	-2.54895528	0.31436723
C	-0.12343055	-1.08837918	-1.90409506
N	-2.10492203	2.91826216	-0.04290307
C	-0.81280051	3.33420079	-0.09719666
C	-0.05780196	2.16228353	-0.08796617
N	-0.98059723	1.13536717	-0.02641633
N	-2.21093436	1.59558207	-0.00078419
C	2.38230024	2.72601994	-0.13721878
C	3.68475454	2.29083892	-0.18325624
C	3.93119992	0.87692755	-0.21969403
C	2.87715268	0.01420287	-0.18412886
N	1.56445762	0.41031446	-0.11152124
C	1.31584652	1.81363424	-0.12160552
C	-1.91309962	-1.82632582	0.12079541
O	1.4001172	-3.52799637	0.47284459
O	-0.11679359	-1.22937532	-3.03944108
O	-2.92795975	-2.34720563	0.13723733
C	-3.30925339	3.73680465	-0.02841311
Cl	-0.31387518	-0.60569068	2.48734101
H	-0.54477794	4.37557047	-0.14219348
H	2.15817953	3.78819236	-0.11296293
H	4.50648773	2.99677545	-0.19408512
H	4.93968425	0.48444645	-0.26548767
H	3.03826032	-1.05665267	-0.19775937
H	-4.16265982	3.06382945	-0.02379922
H	-3.34170559	4.36707919	-0.91821437
H	-3.32931423	4.36003625	0.86659519

#

9.2.5 Atomic coordinates for calculated S_0 state of [Re(3b)$(CO)_3$Cl]

#
28

Re	12.3057444298	-10.731141806	-0.569495789395
C	13.7451410601	-9.49533290289	-0.121307953385
C	12.7506000382	-10.6131968254	-2.44604231139
C	7.99228225922	-11.7069323933	-0.965419723589
C	7.89774568777	-13.090472645	-1.00856595861
C	9.06336248981	-13.8518565343	-0.981544910969
C	10.2838234607	-13.2001559026	-0.917638533057
N	10.3941262259	-11.8598078186	-0.871472814071
C	9.25945648855	-11.1399927935	-0.883337385753
C	13.4970341482	-12.2489278595	-0.360675983401
O	14.5620515449	-8.73713264821	0.148399593242
O	13.0076070194	-10.541367874	-3.56986519023
O	14.1572513016	-13.186768042	-0.261842388876
Cl	11.5383487193	-10.8606622689	1.83114969719
N	9.44342820642	-9.74374557327	-0.812970920861
N	10.7072643872	-9.2519378359	-0.73624464803
N	10.6588079669	-7.96210699915	-0.704679822075
C	9.35175416503	-7.56853568006	-0.755831129249
C	8.56690651459	-8.69723137947	-0.822571937925
C	8.98139752343	-6.12133347737	-0.726734278986
H	7.11004947753	-11.0821908956	-0.992568038302
H	6.92557726406	-13.5629828318	-1.06513804914
H	9.03419012599	-14.9329580014	-1.00753670935
H	11.2146583981	-13.747966389	-0.894777081221
H	7.50080393453	-8.83038247286	-0.866969517801
H	8.30185392636	-5.89926942942	0.0978590092436
H	9.88538424241	-5.52958457801	-0.593394798576
H	8.50198073011	-5.80572548818	-1.65572392328

9.2.6 Atomic coordinates for calculated T_1 state of [Re(3b)$(CO)_3$Cl]

#
28

Re	-0.16867924	0.8679123	0.02497743
C	-1.86368941	1.81177884	0.32313779
C	-0.36678898	1.08393577	-1.93229687
C	2.19518424	-2.87228249	-0.17352268
C	3.52063026	-2.5133017	-0.17722709
C	3.87345715	-1.14700685	-0.1178327
C	2.86484254	-0.21027433	-0.07202588
N	1.55178094	-0.52388794	-0.08380588
C	1.21704768	-1.8566051	-0.11624787
C	0.87015669	2.5885905	0.04165665
O	-2.86347578	2.33060299	0.51761988
O	-0.48527612	1.23531698	-3.06098627
O	1.48596156	3.55042744	0.03572333
Cl	0.23174064	0.81322065	2.44707011
N	-0.12221021	-2.1103466	-0.08580563
N	-1.00772542	-1.02600602	-0.05665366
N	-2.27774973	-1.49702173	-0.07631125
C	-2.21702457	-2.82249226	-0.08092385
C	-0.87907518	-3.25695135	-0.08496985
C	-3.45089955	-3.66424426	-0.08169125
H	1.89604453	-3.91217575	-0.21508617
H	4.28911918	-3.27686179	-0.22296441
H	4.90780913	-0.82923195	-0.10473159
H	3.09131417	0.84713951	-0.01952368
H	-0.44631365	-4.24124974	-0.05498523
H	-3.49476732	-4.30960865	0.80008945
H	-4.33096737	-3.02166659	-0.08075153
H	-3.4930571	-4.30905057	-0.96425939

#

9.2.7 Atomic coordinates for calculated S_0 state of [Re(3c)$(CO)_3$Cl]

#
28

Re	10.4610690743	-6.1087415519	-0.857243562047
C	10.1270482127	-5.65927570052	-2.7079661406
C	11.4535435541	-7.6975222563	-1.37182718333
C	7.98017336651	-2.89059157926	0.859060015018
N	7.19314111466	-3.96620124747	0.861711668047
N	7.92850960433	-4.92111172751	0.295855346387
N	9.15462573109	-4.5242953363	-0.0769324931078
C	9.2133249544	-3.24386273598	0.267907921486
C	6.26263056275	-6.68717768087	0.475760656513
C	5.92772438798	-8.0045411736	0.20160908144
C	6.84721281799	-8.82370314785	-0.45234235172
C	8.0797106077	-8.29653045866	-0.801680559142
N	8.42421234901	-7.02138978709	-0.542373351437
C	7.51892136748	-6.24818831698	0.0779281396333
C	12.0983585347	-5.07150361924	-0.872150372302
O	9.9186027994	-5.38480841844	-3.81038089932
O	12.0205398289	-8.65609564662	-1.65703813436
O	13.0312238714	-4.3994878825	-0.854397118964
C	7.5531232941	-1.57325433372	1.42214329044
Cl	10.6917073772	-6.67198342167	1.58797794289
H	10.1024285173	-2.65922994434	0.0993620835944
H	5.59086406838	-6.00544810654	0.97541884051
H	4.95734183081	-8.38888057658	0.490442672378
H	6.62095107349	-9.85513971306	-0.691280584175
H	8.82999776119	-8.89559914595	-1.2991382135
H	7.19415014937	-1.6902792343	2.44656238654
H	8.39052150154	-0.874529922518	1.43348228353
H	6.74500286254	-1.12883540214	0.834739463439

#

9.2.8 Atomic coordinates for calculated T_1 state of [Re(3c)$(CO)_3$Cl]

#
28

Re	0.183963	0.89558152	0.01413156
C	0.36001533	1.03862184	1.98459562
C	-0.882627	2.60230409	0.0750112
C	2.0803109	-2.99150765	0.00181689
N	0.74556406	-3.28028837	0.01926214
N	0.14724137	-2.07334881	0.04079799
N	1.03884223	-1.01221178	0.01989601
C	2.27187827	-1.63101418	0.00979363
C	-2.14888457	-2.86132176	0.09061761
C	-3.47747193	-2.51681586	0.09660208
C	-3.84514819	-1.1506927	0.0800418
C	-2.85172797	-0.19963986	0.06439769
N	-1.53218066	-0.4998416	0.07031236
C	-1.19107965	-1.8275262	0.07034974
C	1.86669585	1.86568464	-0.23923989
O	0.45978078	1.14983334	3.11888964
O	-1.51161826	3.553748	0.12397405
O	2.87267137	2.38721699	-0.40708493
C	3.09576032	-4.08430713	-0.02954155
Cl	-0.20581893	0.95986254	-2.40082551
H	3.17806754	-1.04923809	-0.0108402
H	-1.80593799	-3.88728874	0.09477148
H	-4.23879915	-3.2890105	0.10901849
H	-4.88272035	-0.842999	0.07173569
H	-3.09255492	0.85590019	0.04257671
H	2.98942542	-4.69231953	-0.93218218
H	4.10688453	-3.67526947	-0.01157784
H	2.98032214	-4.75148455	0.82902045

#